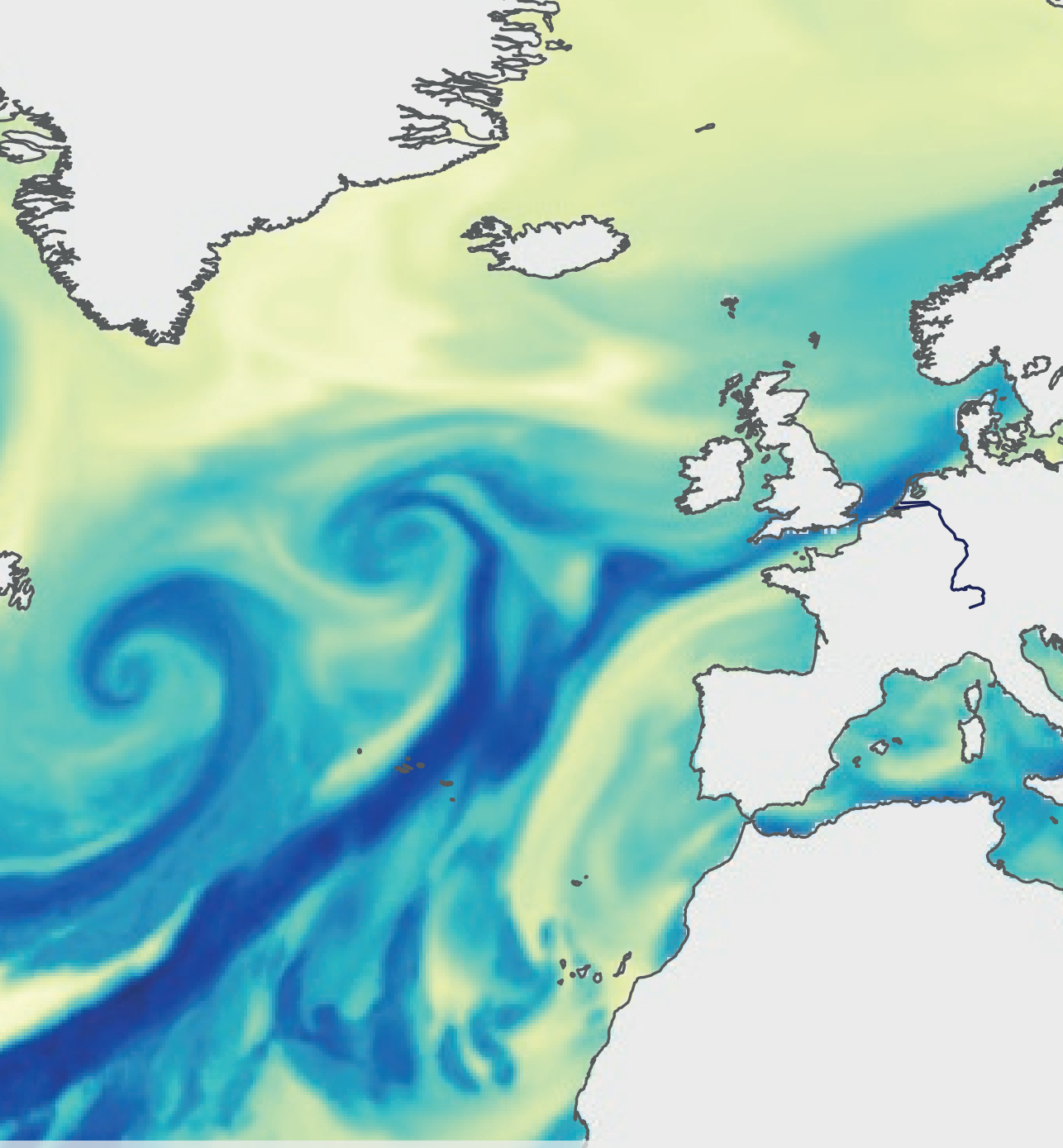

Atmospheric moisture transport and river runoff in the mid-latitudes

Imme Bo Benedict

Propositions

1. The road to better global simulations via higher spatial resolution is less bumpy in atmospheric modelling than in hydrological modelling (this thesis)

2. Rainfall in the Rhine basin depends more on local evaporation during summer drought than during normal conditions (this thesis)

3. Journals with an open-access review process should release all referee reports simultaneously to ensure independent reviews

4. One can learn more about the future from advancing our understanding of the present, rather than from simulating the uncertain future

5. Communication of science is more powerful through attractive metaphors (such as an atmospheric river) than through physically correct descriptions

6. The imposed quest of formulating propositions increases the stress level of a nearly finished PhD student

Propositions belonging to the thesis, entitled
Atmospheric moisture transport and river runoff in the mid-latitudes

Imme Bo Benedict
Wageningen, 20 November 2020

Atmospheric moisture transport and river runoff in the mid-latitudes

Imme Bo Benedict

Thesis committee

Promotors:
Prof. Dr Wilco Hazeleger
Special professor Climate Dynamics
Wageningen University & Research
Professor of Climate System Science
Utrecht University

Prof. Dr Albrecht H. Weerts
Special professor of Hydrologic Predictability
Wageningen University & Research

Co-promotor:
Dr Chiel C. van Heerwaarden
Assistant professor, Meteorology and Air Quality group
Wageningen University & Research

Other members:
Prof. Dr F. Ludwig, Wageningen University & Research
Dr D. Coumou, Vrije Universiteit Amsterdam
Prof. H. Cloke, University of Reading, UK
Dr K. L. Findell, NOAA/GFDL, USA

This research was conducted under the auspices of the Graduate School for Socio-Economic and Natural Sciences of the Environment (SENSE)

Atmospheric moisture transport and river runoff in the mid-latitudes

Imme Bo Benedict

Thesis
submitted in fulfilment of the requirements for the degree of doctor
at Wageningen University
by the authority of the Rector Magnificus
Prof. Dr A.P.J. Mol,
in the presence of the
Thesis Committee appointed by the Academic Board
to be defended in public
on Friday, 20 November 2020
at 1.30 p.m. in the Aula.

Imme Bo Benedict
Atmospheric moisture transport and river runoff in the mid-latitudes
180 pages.

PhD thesis, Wageningen University, Wageningen, NL (2020)
With references, with summary in English

ISBN: 978-94-6395-501-0
DOI: 10.18174/529303

Atmospheric moisture transport and river runoff in the mid-latitudes

Imme Bo Benedict

Summary

Hydrometeorological extremes such as floods and droughts are the result of anomalous transport of water in the atmosphere, impacting the land. Recent examples are the devastating floods in southern Louisiana (United States) in 2016 and drought over Western Europe in 2018. In this thesis the water cycle and its extremes are investigated for the mid-latitudes, on various temporal and spatial scales, encompassing climate science, meteorology and hydrology. The main focus is on the Rhine and Mississippi river basins, two socially, economically and ecologically relevant study areas. From a scientific point of view, studying their different climatic drivers provides insight in different transport mechanisms, and the ability to simulate those. Additionally, anomalous moisture transport associated to extreme precipitation over the coast of Norway is studied. In the Introduction of this thesis two key scientific challenges concerning the water cycle and its extremes are identified. The first challenge is to increase process understanding of the water cycle and its extremes, and the second addresses how these are regionally affected by climate change. This is done with a global modelling approach, making use of reanalysis data, simulations from a global climate model, a moisture tracking tool, and a global hydrological model (all described in Chapter 2). Observational products are used to verify the model results.

In Chapter 3 we study anomalous transport of moisture and its relation to extreme precipitation events for three regions (North, South and West) along the coast of Norway. As part of mid-latitude cyclones, excess moisture is transported to higher latitudes in narrow corridors, so-called atmospheric rivers. When these filaments of moisture in the lower troposphere encounter a mountain range, such as the fjords in Norway, forced lifting can result in extreme precipitation. We show a climatology (1979 to 2014) of cold season (October to March) precipitation events based on the 99th percentile of daily precipitation, of which more than 85% is related to an atmospheric river. Furthermore, those selected precipitation events are associated with a positive phase of the North Atlantic Oscillation (NAO) for all three regions. Two characteristic patterns conducive to anomalous moisture transport can be identified with significant time before the event (5 days), which is helpful for forecasting. When the event approaches, regional differences become apparent, with for the North and West regions zonal flow impinging upon the south-north oriented

coastline, while for the South region a significant southerly flow was found. To predict the precise location and impact of subsequent extreme precipitation events, higher resolution models are needed to capture the exact orography.

The relation between precipitation and moisture transport is further explored in Chapter 4 for the Mississippi river basin. We determine the origin of precipitation over the Mississippi basin for present and future climate (RCP4.5), using high resolution (~25 km) climate simulations. Precipitation falling over the Mississippi basin is tracked backward in time using an Eulerian offline moisture tracking tool, to determine the moisture sources. We find that the most important continental sources are the Mississippi basin itself, and the area southwest of it, while the most relevant oceanic sources are the Gulf of Mexico/Caribbean and the Pacific. Those sources vary per season, with more transport from the oceans to land in winter, and more recycling of moisture within the basin in summer. We conclude that the moisture sources of the Mississippi River basin in the future 1) enhance over the oceans in winter, due to future increased evaporation over the oceans, resulting in more future winter precipitation, and 2) show a relative decline over terrestrial areas in summer. The latter conclusion indicates that potential land-use changes will have relatively little impact on precipitation over the Mississippi basin in the future, compared to present climate.

The moisture sources of the Rhine basin are investigated in Chapter 5, specifically for the recent summer (May to August) droughts of 2003 and 2018. During those summers persistent blocking prevented moisture to be transported from the oceans towards the Rhine basin, as we found that the contribution in moisture source from the Atlantic was much lower in 2003 and 2018 compared to an average summer. These anomalous moisture sources in 2003 and 2018 were mostly a result of anomalous wind, and not so much due to anomalous moisture advection. In 2018, moisture was transported from the east towards the basin, due to the anticyclonic flow around the Scandinavian blocking. The large-scale circulation in 2018 was especially favorable for dry conditions over the Rhine. Although blocking also occurred in the summer of 2003, conditions were less favorable for dryness over the Rhine basin. In 2003 the recycling of moisture within the basin was lower than average (and lower than 2018), especially in August, suggesting drying out of the soils, and explaining the enhanced drought in August in 2003 through positive land-atmosphere feedbacks. The unique character of both extreme events indicates that hydrometeorological extremes should be investigated in detail to enhance our understanding of these extremes, and of the complex processes ranging from the larger-scale circulation to interactions with the land-surface.

To study the global hydrological cycle and its response to climate change, it is common to force a hydrological model with meteorological data from a climate model. In Chapter 6, we assess and compare the benefits of an increased resolution of a global climate model (GCM) and global hydrological model (GHM) in simulating the hydrogical cycle for two

basins with long observational records: the Rhine and Mississippi basins. Increasing the resolution of a GCM (1.125° to 0.25°) results in an improved precipitation budget over the Rhine basin, attributed to a more realistic large-scale circulation. These improvements with increased resolution are not found for the Mississippi basin, possibly because precipitation is strongly dependent on the representation of still unresolved convective processes. The (improved) monthly-averaged precipitation from the GCM is reflected in (improved) monthly-averaged actual evaporation and discharge from the GHM, although an increase in resolution in the GHM does not lead to significant changes in discharge. A straightforward resolution increase in the GHM is thus most likely not the best method to improve discharge predictions, which emphasizes the need for better representation of processes and improved parameterizations that go hand in hand with resolution increase in a GHM.

In the Synthesis (Chapter 7) we reflect back on the two scientific challenges identified in the Introduction concerning the water cycle and its extremes. The first challenge on enhanced process understanding is addressed in all Chapters, as different moisture transport mechanisms are investigated for distinct geographical areas, on different temporal and spatial scales. In Chapter 5, the second challenge on regional projections is addressed, by investigating the moisture sources of the Mississippi basin in present and future climate. In my vision, enhanced understanding of the future climate can be mostly gained from an increased understanding of the present, rather than from simulating the uncertain future. In the case of understanding the water cycle and its extremes in present climate, combined efforts from climate science and the fields of hydrology and meteorology are needed.

Contents

1

Introduction

1.1 Motivation

Water is an integral part of our weather and the earth's climate system. An illustrative example is how precipitation determines our day-to-day weather, and via the runoff from rivers the availability of our freshwater resources. In this thesis I study how water vapour flows through the atmosphere, driven by the regional circulation, and results in precipitation which affects society. The uneven distribution of water vapour in the atmosphere can result in extreme precipitation and subsequent flooding, while a long-lasting lack of precipitation can cause drought. Floods and droughts are hydrometeorological extremes, resulting from the interactions between atmospheric and hydrological processes at different time and spatial scales. These processes need to be better understood in present climate to make predictions for the future. Impacts of hydro-meteorological extremes are well-known. I give three recent examples of events to illustrate their relevance, and as basis for the research conducted within this thesis.

In August 2016, when I just started my PhD research, a stationary low-pressure system brought prolonged rainfall over the state of Louisiana and Mississippi in the United States. It rained for almost two days in a row, which resulted in river flooding in following days. Because of this natural disaster over 30 000 people had to be rescued from their flooded homes and cars, and 13 people were killed due to the flood (van der Wiel et al., 2016a). Where low pressure systems or tropical cyclones result in moisture transport towards south-eastern US, extratropical cyclones transport moisture north eastwards over the Atlantic towards Europe. This moisture transport over the Atlantic is characterized by long narrow filaments of water. As these corridors of moisture look like rivers on satellite images, the term atmospheric river was suggested (Zhu and Newell, 1998). The amount of moisture that atmospheric rivers transport is equivalent to about 10 times the average daily discharge of the Mississippi river (Ralph and Dettinger, 2011). Once these atmospheric rivers experience orographic lifting, when reaching steep cliffs of the European continent, extreme precipitation can occur. This was the case over the West Coast of Norway, where in October 2014 locally up to 300 mm of rain fell in less than 5 days, causing floods and damages in several valleys (Lussana et al., 2018). In contrast, conditions characterized by prolonged absence of precipitation, were found over Scandinavia and western Europe in the last few summers, resulting in droughts and record-breaking warmth. Especially the spring and summer of 2018 were exceptionally dry and hot over England, The Netherlands, Belgium, Germany and Scandinavia (Rosner et al., 2019). The rainfall-deficit and extreme heat had major impacts on water supply and agriculture, and induced wildfires. In 2019, a heatwave impacted western Europe, with temperatures in The Netherlands first measured above 40°C. At the time of writing, summer of 2020, a very dry spring is a concern for many farmers and local water managers.

What all those extremes have in common is that there is a large-scale driver (e.g. Sillmann et al. 2017), a synoptic circulation, resulting in anomalous moisture transport and anomalous precipitation. For the United States, the large-scale driver relates to subtropical dynamics, as excess moisture is transported from the Caribbean and Gulf of Mexico towards the US in hurricanes or a low level jet, depending on the season. For the case of the local flood in Norway, the large-scale driver was an extratropical cyclone transporting high amounts of moisture to the coast of Norway, where it was forced over the local topography and resulted in extreme rainfall. Opposite, a lack of moisture transport over longer time scales of weeks, when the large-scale driver is a persistent high-pressure system, can result in a drought or heatwave impacting several countries. Besides the large-scale drivers, regional feedbacks with the land surface can strengthen extremes (Sillmann et al., 2017).

These examples of hydrometeorological extremes show the complex processes at play, acting at different time and spatial scales (Figure 1.1), in different geographical locations (Figure 1.2) and different seasons. To understand such events we need a multidisciplinary approach encompassing climate science, meteorology and hydrology. Further understanding of the large-scale driving processes and local surface feedbacks is needed, as many processes are not yet fully understood. For example, the synoptic circulation during hydrometeorological events is often tightly coupled to the variability of the storm-track, the region where most storms occur. Related to the storm-track, one of the four emerging questions concerning clouds, circulation and climate posed by Bony et al. (2015) is: "What controls the position, strength and variability of storm tracks?" Deepening our process understanding is crucial to improve forecasts and projections, not only for extreme situations but also for the water cycle in general.

In this thesis, I identify process understanding of the water cycle and its extremes as the first key scientific challenge. More specifically, I quantify moisture transport and how it impacts the land surface in two climatologically different regions, North America and north western Europe. I do so from the global perspective as regional moisture transport is tightly coupled to the global atmospheric circulation. The second key scientific challenge addresses how the water cycle and its extremes are affected by climate change. Anthropogenic climate change is unprecedented, and this already affects and will continue to affect the global water cycle on regional scales (Stocker et al., 2013). The weather is chaotic by nature with non-linear dynamics that lead to internal variations in the system. This internal variability is especially large in the mid-latitudes, and it poses the challenge to detect trends from the background 'noise' (Stott et al., 2013; Woollings, 2010). Moreover, the dynamical changes due to climate change are uncertain, which makes regional projections extra challenging (Marotzke et al., 2017; Shepherd, 2014).

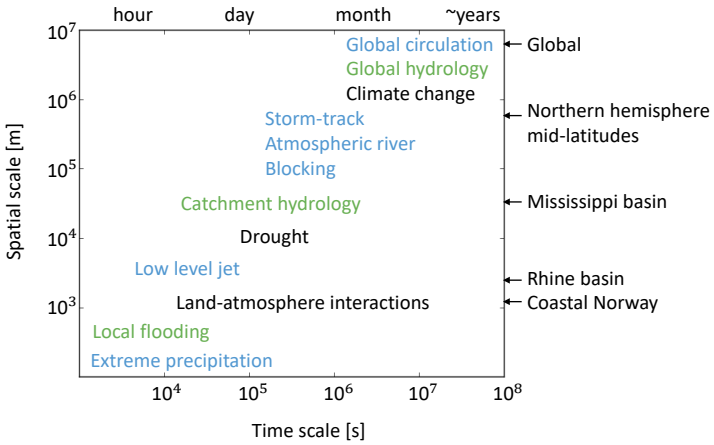

Figure 1.1: Time and spatial scales of hydrometeorological processes that are relevant in this thesis. Blue colours indicate meteorological processes, green colours hydrological processes, and black colours concern both meteorology and hydrology.

In summary, my thesis deals with improving our current understanding of the essential processes that govern the water cycle and hydrometeorological extremes, and their regional future projections. In the following sections I will explain fundamental concepts and describe modelling tools which set the stage for the specific research questions outlined in the last section of this Introduction, and which are answered in the subsequent Chapters.

1.2 Moisture transport in the atmosphere

1.2.1 Physical background

The atmospheric general circulation of the earth, and therefore atmospheric moisture transport, is foremost a result of differential solar heating. This means that the sun heats the tropics more than the poles, thereby creating a meridional temperature gradient in the mid-latitudes. As a result of this gradient, and the rotation of the earth, zonal geostrophic wind increases with height (vertical shear) up to the tropopause. This consequence of the thermal wind balance is called the *jet stream*: a 'river' of high wind speeds up in the troposphere whirling eastwards around the globe. Due to the meridional temperature gradient and the vertical shear, *baroclinic instabilities* form in the mid-latitudes. It is these instabilities that relate to storms that grow, and lead to mixing of warm humid

air masses from the tropics and dry cold air masses from the poles, causing a reduced gradient. The speed and direction of storms (i.e. mid-latitude cyclones) are determined by the strength and waviness of the jet stream. The preferred region where mid-latitude cyclones occur is termed the storm-track (Blackmon, 1976; Hoskins and Valdes, 1990). Fronts associated to mid-latitude cyclones, govern the day-to-day variability of weather in the mid-latitudes, bringing precipitation and unsettled weather. As the temperature gradient from equator to pole is larger in winter, baroclinicity and the jet stream are more intense in this season (Shaw et al., 2016). Therefore, mid-latitude cyclones are the main cause of precipitation over Europe in winter. In summer, the meridional temperature gradient weakens, so does baroclinic instability. Increased solar heating results in enhanced land evaporation and triggers convective, more locally generated, precipitation over mid-latitude continents. The relative contribution between terrestrial and oceanic sources of terrestrial precipitation is highly variable over space and time, also because of internal climate variability. There is a growing need to further understand those sources (Gimeno et al., 2020; Trenberth et al., 2003), and how these are affected by climate change on a regional scale (Gimeno et al., 2020).

Three mechanisms of anomalous moisture transport in and towards the mid-latitudes are shown in Figure 1.2 and discussed further, as they are relevant for the research conducted in this thesis.

Atmospheric rivers. The first mechanism is that of moisture transport as part of mid-latitude cyclones. High amounts of moisture can be found in the warm conveyor belt, along the cold front of a mid-latitude cyclone. These regions of intense poleward moisture fluxes are often quite narrow, and referred to in literature as *Atmospheric River* (AR; Ralph et al. 2004; Zhu and Newell 1998), although this name has been debated (Dacre et al., 2015; Wernli, 1997). In fact, those atmospheric rivers are continuously fuelled by evaporation of the relatively warm ocean (Dacre et al., 2015), while travelling north eastward over the Atlantic, as well as the Pacific. When these high amounts of moisture in the lower troposphere encounter a mountain range, forced lifting can result in heavy precipitation. Earlier work mainly focused on this mechanism for the east coast of the United States. Over recent years, however, the relationship between ARs and (extreme) precipitation received increased attention for coastal regions over Europe (Knippertz and Wernli, 2010; Lavers et al., 2011; Lavers and Villarini, 2013; McTaggart-Cowan et al., 2017; Ummenhofer et al., 2017). We investigate if there is a robust relationship between ARs and extreme precipitation over coastal regions in Norway, and what the large-scale pre-conditioning of such events is (Benedict et al., 2019a).

Low level jet. The second mechanism of moisture transport is specifically important for the precipitation budget over the Mississippi basin. The Great Plains Low Level Jet (GPLLJ) transports moisture from the relatively warm Caribbean and Gulf of Mexico towards central United States (Figure 1.2). This low level jet should not be confused with

the jet stream, as it is a maximum of wind speed in the lower troposphere, often occurring during the night, and for the case of the GPLJJ mainly present in spring and summer. The GPLLJ is the most significant circulation feature of the central US linking large-scale atmospheric circulation with the regional climate (Tang et al., 2017). Although multiple mechanisms have been suggested to cause this wind maxima at night, a full theory explaining the observations is still missing. Suggested mechanisms are related to the slope of the Great Plains, inertial oscillations, complicated radiative heating and cooling of the terrain, and a combination of the subtropical high and the blocking effect of the Rocky mountains. Besides the GPLLJ, another important phenomenon to bring (extreme) precipitation to central and eastern US are tropical cyclones, which we do not elaborate on here, as they are not studied within this thesis.

Blocking. In contrast to enhanced moisture transport, a lack of moisture transport can lead to droughts and heatwaves, as was the case over Western Europe in 2003 and 2018. This lack of transport, resulting in lesser-than-normal precipitation, is caused by a so-called *blocking*. Blocking is a persistent weather pattern, generally an anticyclone, that blocks the prevailing westerlies and mid-latitude storms (Rex, 1950; Woollings, 2010). It is the result of a very wavy jet stream, which in turn is the result of amplified or breaking *Rossby waves* (Pelly and Hoskins, 2003). Land regions situated below a blocking are often related to bright weather conditions, generating cold spells in winter, while leading to droughts and heatwaves in summer, if the blocking persist long enough. The lack of moisture transport towards the Rhine basin, and relation to blocking conditions is investigated in Chapter 5.

In general, when assessing moisture transport in the atmosphere, the atmospheric water balance is a starting point for analysis:

$$\frac{\partial S}{\partial t} + \text{moisture convergence} = E - P \tag{1.1}$$

where evaporation E is the source of moisture in the atmosphere, and precipitation P the sink. S is the vertical integral of moisture in the atmosphere, and moisture convergence is the moisture flux vertically integrated over the atmosphere.

A key question is how the atmospheric water balance changes under anthropogenic global warming, and if this affects moisture transport. To answer these questions, changes in the atmospheric water cycle can be disentangled in two components: changes in *thermodynamics* (roughly speaking everything related to heat and moisture) and changes in the *dynamics* (circulation patterns) (Shepherd, 2014). For the first, future changes are quite robust, as the Clausius-Clapeyron relationship tells us that warmer air can hold more moisture, under the assumption that relative humidity is constant. In contrast to the robust changes in the thermodynamics, changes in the dynamical part of the water cycle are much more uncertain. This uncertainty is especially present in the mid-latitude

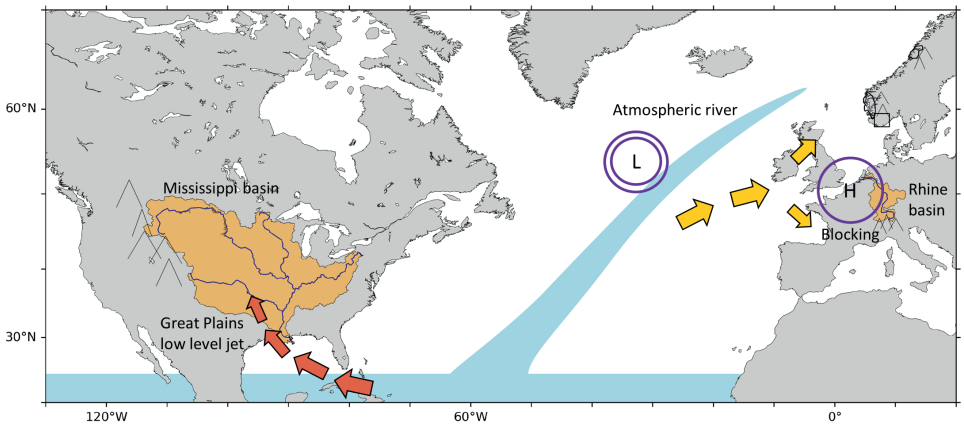

Figure 1.2: Geographical map indicating the Rhine and Mississippi basins, the regions of interest in coastal Norway, and involved topography. The different moisture transport mechanisms are schematically indicated: Great Plains Low level jet (with red arrows), high moisture content (light blue) in form of atmospheric river and a mid-latitude cyclone (low pressure in purple), and Blocking (high pressure in purple, rerouting of moisture indicated with yellow arrows). This Figure is based on Figure 5 from Gimeno et al. (2020).

regions, where the signal from internal variability dominates over the signal of changes due to a warming world (i.e. a low signal-to-noise ratio) (Shepherd, 2014; Woollings, 2010). Projections of changes in the water cycle are therefore most uncertain in these mid-latitude regions.

1.2.2 Modelling

Global climate models. To further understand how the water cycle will be affected by climate change, and to enhance process understanding of past events, one needs to perform simulations. In climate science, the tool to do so are *global climate models* (GCMs), numerical simulations of the basic laws of physics (conservation of mass, energy and momentum), solved spectrally or on a grid covering the earth. The resulting grid consists of a longitudinal, latitudinal and vertical component and provides atmospheric quantities such as temperature, wind and humidity over time. A typical grid cell of a GCM has a size of about 100 km, thereby limiting the amount of details that can be resolved. Atmospheric processes acting on smaller scales than the size of a grid cell, such as turbulence, convection, and cloud processes, cannot be resolved explicitly, and need to be parameterized. Consequently, models do not capture all processes acting in the real world. However, they are useful, and the only tool available to test how the atmosphere behaves under changing initial and boundary conditions.

Before GCMs were developed, numerical models were invented to provide the well-known weather forecast (Bauer et al., 2015). These *numerical weather prediction* (NWP) models are based on the same physical laws as a climate model, and also incorporate the land-surface and (sometimes) the ocean and sea ice. In this thesis we make use of the global climate model EC-Earth (Hazeleger et al., 2010, 2012). This model is based on the NWP system (Integrated Forecasting System IFS) of the European Centre of Medium-Range Weather Forecasts (ECMWF), but performs free simulations of the climate system. In this thesis we use simulations from the EC-Earth model at two different spatial resolutions, and with initial and boundary conditions of current and future climate. With these simulations, we can test if increased model resolution results in improved water transport trough the atmosphere-land continuum, and how this may look like in the future.

Moisture tracking models. In this thesis we focus on the atmospheric water cycle, and specifically on moisture transport within and towards the mid-latitudes. To further understand this moisture transport and the contributions of oceanic and terrestrial evaporation to terrestrial precipitation, one can track moisture (water vapour) as it flows through the atmosphere and determine the source (evaporation) and sink (precipitation). Or reversed, when moisture is tracked backward in time, precipitation will be the source and evaporation the sink. Forward tracking can be performed while the weather model is running, what we call 'online' moisture tracking. The 'offline' option allows tracking of moisture forward and backwards in time, as the tracking is applied to the output of NWP models, GCMs, or reanalysis products (discussed in the next section). Furthermore, two approaches can be taken: *Lagrangian* and *Eulerian* moisture tracking. In the Lagrangian approach many parcels are released in the atmosphere and while dispersing their trajectories are simulated, ideally from source to sink. Eulerian approaches are based on solving the water balance for every grid cell. When a certain region is selected as source or sink, the moisture there is tagged and accounted for when transported from grid cell to grid cell. In this thesis we determine moisture sources using the Eulerian offline moisture tracking model WAM-2layers (Van der Ent et al., 2010, 2014). The details of this model are given in Chapter 2.

1.2.3 Observations

To verify how well models perform in simulating the atmospheric water balance, results are compared to observations. In the case of this thesis, we use observational datasets where measurements are interpolated to a consistent gridded field. Observational products of precipitation are least accurate over data sparse regions, such as oceans and mountainous regions like the Alps (Hofstra et al., 2009; Van Osnabrugge et al., 2017). Observational products of evaporation are more uncertain, as measurements on larger scales are still limited (Wang and Dickinson, 2012). Alternatively, blended products of evaporation appear, combining information from multiple sources such as satellite remote sensing and potential evaporation estimates from observations of near-surface air temperature and net

radiation (Martens et al., 2016). Where precipitation and evaporation are observed at the surface, quantifying moisture transport higher up in the atmosphere is more challenging. The only observations available are those from aircraft measurements, satellites and radiosondes. These sources provide crucial information on the vertical structure of the atmosphere. However, they do not provide a consistent gridded product of the whole atmosphere. For that, we have to rely on *reanalysis* products. These products are the result of forecast models simulating the past weather again, while constrained with observations. This process is called data assimilation and involves complex mathematical techniques (Bauer et al., 2015). The result is a physically consistent dataset describing the history of the atmosphere, land surface and ocean. A widely used reanalysis product from the ECMWF was the ERA-Interim reanalysis dataset (Dee et al., 2011). Halfway my PhD, a new reanalysis dataset named ERA5 (Hersbach et al., 2020) was produced, with higher temporal and spatial resolution and improved parameterizations and data assimilation techniques. These reanalysis datasets are relevant for climate analysis of the past, when it comes to dynamic processes in the atmosphere. In this thesis, I use reanalysis datasets to investigate past events and climatologies of anomalous moisture transport impacting the land surface.

1.3 Impact: hydrology

Climate model output is used to assess and understand a broad range of impacts, from flood frequency to wind power potential, and from heat stress in cities to agricultural disasters, and so on. Although the focus of this thesis is mostly on atmospheric moisture transport, we also assess the impact of atmospheric moisture on the terrestrial water cycle. The moisture fluxes that are studied in this thesis are indicated in Figure 1.3.

1.3.1 Physical background

Precipitation and evaporation are the shared components between the atmospheric water balance and the terrestrial water balance. Where evaporation acts as a source and precipitation as a sink for the budget in the atmosphere, this is exactly opposite for the terrestrial water balance:

$$\frac{ds}{dt} = P - E - Q \tag{1.2}$$

where $\frac{ds}{dt}$ is the change of water in the soil continuum and Q is river discharge. This terrestrial water balance holds when integrated over a river catchment, and on a global scale. Besides the terrestrial water balance, the surface energy balance plays an important role in partitioning fluxes at the earth surface, and interaction with the atmosphere above. The characteristics of the land-surface influence the partitioning of the available energy at

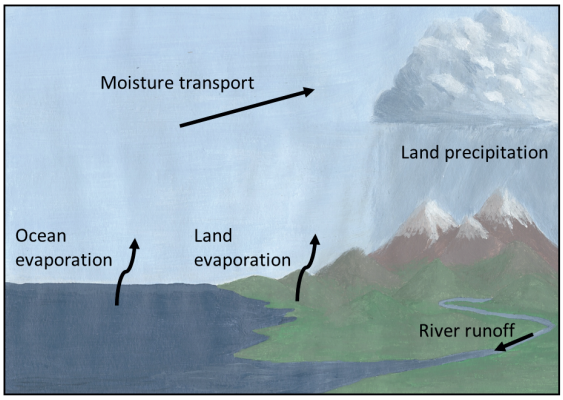

Figure 1.3: Fluxes of the water cycle that are considered in this thesis: ocean and land evaporation, moisture transport in the atmosphere, land precipitation and river runoff.

the surface into sensible and latent heat fluxes (Koster et al., 2004). Dry soils, for example, can lead to an enhanced sensible heat flux and via the positive *soil-moisture temperature feedback* intensify a heatwave (Fischer et al., 2007b; Seneviratne et al., 2010).

1.3.2 Modelling

Hydrological models use meteorological forcing to compute the water flow from land areas to oceans. The quantification (modelling) of spatially and temporally resolved water fluxes results in further understanding of the terrestrial part of the water cycle (Döll et al., 2016). Moreover, hydrological models are also used for, among others, water use assessments, understanding human interventions, and flood and drought forecasting. Eagleson (1986) advocated that the processes involved in the terrestrial water cycle demand knowledge, and need to be addressed, on the global scale. Global models simulating the water cycle on land can be roughly divided into *land-surface models* (LSMs) and *global hydrological models* (GHMs). LSMs originate from atmospheric science, where they were developed to represent the land surface as part of weather and climate models. Consequently, LSMs solve both the energy- and water balance, and often incorporate many soil layers. Most LSMs describe evapotranspiration and snow melt in a more physically consistent manner than GHMs, but often lack groundwater reservoirs, human impacts and lateral routing (Döll et al., 2016). In contrast, global hydrological models were traditionally designed to simulate (sub-)surface water flows. GHMs are based on solving the water balance, and simulating water resources and lateral transfer of water (Bierkens et al., 2015; Haddeland et al., 2011).

Compared to climate models, where flow phenomena are partly resolved between grid cells, most hydrological models fully depend on parameterizations. Inherently, these pa-

rameterizations introduce uncertainties. In fact, many parameters do not represent physical quantities (Melsen et al., 2016), partly due to model calibration. Uncertainties also arise from model structure (Döll et al., 2016), and model resolution limits the description of heterogeneities in topography, soil, and vegetation. Those uncertainties also arise in global climate models. The spatial resolution of GHMs is around 50 km, which is higher compared to GCMs (~100 km). Yet to date, there is a plethora of GHMs and LSMs (and GCMs) available, all slightly different in model structure, land-surface description, and parameterizations. The global climate model EC-Earth, which is used in this thesis, includes the land-surface model H-TESSEL (Balsamo et al., 2009; Van den Hurk et al., 2000). In addition, we use the global hydrological model W3RA (Van Dijk, 2010a; van Dijk et al., 2013) to simulate discharge of the Rhine and Mississippi basins. With this hydrological model we perform the same experiments as performed with the EC-Earth climate model, we change the spatial resolution to see if including more details results in better simulations of discharge (Chapter 6).

1.3.3 Observations

One of the most used variables for hydrological model evaluation is discharge, as it represents the integrated response of many hydrological processes occurring at catchment scale (Fekete et al., 2012). Equally important, discharge observations are readily available for many catchments around the world (Hannah et al., 2011). Different performance metrics for evaluating simulated discharge exist, assessing low and high discharge, duration and variability.

1.3.4 Study areas: Rhine and Mississippi river basins, coastal Norway

This thesis studies the water cycle in the mid-latitudes. More specifically, we focus on two major delta regions, the Rhine and Mississippi River basins (Figure 1.2). These are societally, economically and ecologically highly relevant study areas. The scientific interest arises from their different climatic drivers, which allows insights in the ability to simulate various mechanisms of moisture transport impacting hydrology. By using global models to study these regions, different internal model structures do not influence the results. Additionally, the mechanism of excess moisture transport to the coast of Norway is also investigated.

Rhine River Basin. The River Rhine originates in the Swiss Alps and flows through Switzerland, Germany, and the Netherlands, where it discharges into the North Sea. In this thesis, we analyse discharge at Lobith, which is the location where the Rhine enters the Netherlands. Therefore, the basin is defined upstream of Lobith. The average discharge at Lobith is 2200 $m^3\ s^{-1}$ (Table 1.1) and the highest discharges occur in late winter and spring. The precipitation budget of the Rhine basin is mainly determined by the Atlantic storm-track. In winter and spring, large-scale rainfall events, associated with

Table 1.1: Basin characteristics of the two study basins including basin area, used gauge station and its average discharge there.

Basin	Basin area [km^2]	Gauge station	Average discharge [$m^3\ s^{-1}$]
Rhine	165 000	Lobith	2 200
Mississippi	2 981 100	Vicksburg	16 500

storms, occur over saturated soils, which can lead to extreme flood events. Snowmelt, in combination with frozen soils, can occasionally lead to extreme flood events as well (Hegnauer et al., 2014). About 65% of the available fresh water in the Netherlands is supplied by discharge from the Rhine (Kramer et al., 2019).

Mississippi River Basin. The Mississippi River basin covers almost half of the United States, and is in size 16 times larger than the Rhine basin (Figure 1.2 and Table 1.1). This makes it the fourth-largest river basin in the world. The Mississippi River originates at Lake Itasca, Minnesota, from where it flows south towards the Gulf of Mexico. The two largest tributaries of the Mississippi are the Missouri and Ohio rivers. In this thesis, we study discharge of the Mississippi basin at Vicksburg, where the average discharge is 16500 $m^3\ s^{-1}$ (Table 1.1). In contrast to the Rhine basin, the precipitation budget of the Mississippi is influenced by moisture input from multiple drivers: moisture is advected from the Pacific, from the Caribbean, and from the Gulf of Mexico, and extreme precipitation occurs within tropical cyclones. In addition, convective precipitation plays an important role over the Mississippi basin (Iorio et al., 2004). Precipitation amounts vary widely over the basin, and so does temperature. Most flood events occur in winter and spring due to heavy (excess) precipitation, snowmelt, and rain-on-snow events (Berghuijs et al., 2016; Van der Wiel et al., 2018).

1.4 Outline and research questions

At the start of this Chapter I illustrated the societal relevance of studying anomalous moisture transport, by giving three examples of extreme hydrometeorological events. In addition, two key scientific challenges related to the water cycle and its extremes in the mid-latitudes were identified: enhanced process understanding and regional projections. Thereafter, theory and tools were introduced for further understanding of the specific research questions posed in this thesis, which we introduce here. In Chapter 2 we give specific details on the datasets and models we use to conduct the research in this thesis.

The first study of this thesis concerns atmospheric rivers. Anomalous moisture transport over the Atlantic is most pronounced in winter and can result in heavy precipitation and flood events along the coast of Norway. I investigate the relationship between atmospheric rivers and extreme precipitation for three regions in coastal Norway. In addition, the

large-scale pre-conditioning of these atmospheric rivers is investigated, to see if there are favourable patterns which result in these extreme precipitation events. This is potentially useful information for forecasters. In Chapter 3, the main research question is:
How is extreme precipitation along the coast of Norway linked to Atmospheric Rivers and how is their large-scale pre-conditioning?

Research on moisture transport continues in Chapter 4, although focussing on a different region, the Mississippi River Basin. The precipitation budget of the Mississippi is partly controlled by moisture transported with the Great Plains Low Level Jet, whereas convective precipitation is also important. The moisture sources of the Mississippi River Basin are determined per season, by tracking precipitation backwards in time to see where the moisture was evaporated. Sources under present climate and future climate conditions are compared to understand the impact of climate change. The main research question of Chapter 4 reads as follows:
How is the modeled atmospheric water budget over the Mississippi River basin (with a focus on its moisture sources) projected to change in the future?

In Chapter 5, the moisture sources of the Rhine basin are investigated during the extremely dry summers of 2003 and 2018. With this approach, both the large-scale circulation and the land-atmosphere processes during those droughts are captured. Additionally, the inter-annual variability in Rhine summer precipitation is investigated in relation to large-scale synoptics and local moisture recycling. Chapter 5 answers the main research question:
What are the anomalous moisture sources of the drought over the Rhine basin in summer 2003 and 2018?

In Chapter 6 the effect of model resolution on representing the hydrological cycle of the Rhine and Mississippi River Basin is studied. We use high and low-resolution global climate model output to force a high- and low resolution global hydrological model, and evaluate how well precipitation, evaporation and discharge are simulated. The main research question reads:
Can we improve the simulated hydrological cycle over the Rhine and Mississippi basin by increasing the resolution of climate- and hydrological model?

In the Synthesis, Chapter 7, the findings of this thesis are embedded in the existing literature, and an outlook on further research is provided along the two proposed key scientific challenges.

2

Description of datasets and models

2.1 Introduction

In this Chapter we describe the observations, reanalysis datasets, and models we use in this thesis (Figure 2.1). First, details on the atmospheric and hydrologic observations are given (Section 2.2), followed by a description of the used reanalysis datasets (Section 2.3). Then, the global climate model EC-Earth and global hydrological model W3RA are described in Section 2.4. Last, the derivation of the atmospheric water balance is presented (Section 2.5), together with the moisture tracking tool WAM-2layers.

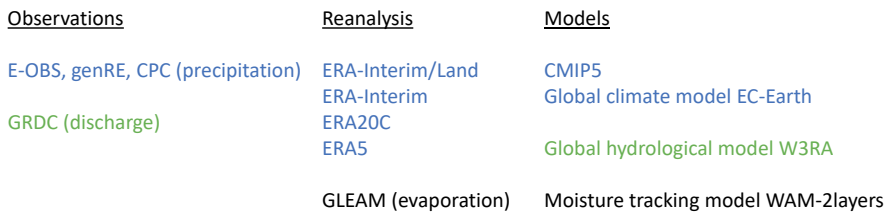

Figure 2.1: Overview of observations, reanalysis data and models used in this thesis. Blue colour indicates atmospheric variables, datasets and models, where green indicates hydrological products. Black colour concerns both meteorology and hydrology.

2.2 Observations

In this thesis, observations are mainly used to validate model results. Thereby the focus is on variables representing the hydrological cycle: precipitation, evaporation and discharge. The dataset used to verify evaporation is discussed in Section 2.3 on reanalysis data.

For precipitation comparison over the Rhine basin, we use the E-OBS dataset version 12.0 (Haylock et al., 2008) with a spatial resolution of 0.25° from 1985 until 2015 (30 years). This high-resolution gridded dataset with daily timestep is based on interpolation of the most complete collection of station data over Europe (Klok and Klein Tank, 2009), and is continuously updated. The E-OBS dataset shows good comparison (high correlations) with existing data, especially in winter, although relative differences in precipitation can be large. Usually, E-OBS shows biases towards lower precipitation values, and performs worse in mountainous areas (Hofstra et al., 2009). For extra verification, we use the genRE precipitation dataset (Van Osnabrugge et al., 2017), which provides hourly data on a grid of 1.2 by 1.2 km over the Rhine basin, and is available from 1996 to 2015, to be updated in real-time. This dataset was produced to meet the need for estimates of precipitation at high temporal and spatial resolution, as input for regional hydrological forecasting models. The genRE dataset interpolates gauge data to near real-time, and matches well with the

E-OBS dataset on daily and yearly time scales (Van Osnabrugge et al., 2017). For the Mississippi basin, the Climate Prediciton Center (CPC) 0.25° Daily US Unified Gauge-Based precipitation dataset version 1.0 (Higgins and Joyce., 2000) is used from 1985 to 2015 (30 years). This dataset is based on the interpolation of gauge observations, and the quality degrades in regions where the network of station observations becomes sparser (Chen et al., 2008). The precipitation datasets described here are used for validation in Chapter 4 and 6.

Daily discharge data for the Rhine at Lobith and the Mississippi at Vicksburg are obtained from the Global Runoff Data Center (GRDC, 2007), which provides quality controlled data. We obtained discharge data from 1985 until 2015 (30 years). Additionally, recent discharge observations (until 2019) at Lobith are obtained from Rijkswaterstaat. Discharge observations are used for the research presented in Chapter 5 and 6.

2.3 Reanalysis data

The idea and concept of reanalysis datasets, a physically consistent gridded product describing the history of the atmosphere, is provided in the Introduction (Section 1.2.3). Reanalysis datasets are widely used in atmospheric and hydrological research, mostly for validation and global to synoptic scale atmospheric studies. First, we provide technical details of the reanalysis datasets, and then we shortly explain how the datasets are used in this thesis.

We make use of the global reanalysis datasets provided by the European Centre for Medium Range Weather Forecast (ECMWF). The ERA-Interim reanalysis dataset (Dee et al., 2011) is based on the integrated forecasting system (IFS) release cy31r2. It includes the land-surface scheme TESSEL (Viterbo and Beljaars, 1995). Data assimilation is based on the 4D-Var system, which assimilates historical measurements (like satellite and weather station observations) with a 12-hourly time step (Dee et al., 2011). ERA-Interim has a spatial resolution of around 80 km and 60 vertical levels (T255L60), however the atmospheric variables are also interpolated to different grid resolutions. Most atmospheric variables are available with a 6-hourly time step, while surface variables such as evaporation and precipitation are accumulated with a 3-hourly timestep. The ERA-Interim dataset is available from 1979 until 2019, and is superseded by ERA5 reanalysis.

The ERA5 dataset (Hersbach et al., 2020) is currently available from 1979 to within 5 days of real time, and will extend further back in time to 1950. ERA5 is based on the IFS cy41r2, and 4D-Var data assimilation, which benefits 10 year of developments. Much more historical observations are assimilated compared to ERA-Interim. The spatial resolution of ERA5 is around 30 km (at the equator), with 137 vertical levels (T639L137). The output frequency of the ERA5 reanalysis data is hourly.

In addition, the ERA-Interim/Land reanalysis (Balsamo et al., 2013) is shortly addressed, where precipitation from ERA-Interim is corrected with satellite data, and an improved land-surface scheme H-TESSEL is used (Balsamo et al., 2009). ERA-Interim/Land is only available until 2010. Lastly, the ERA20C dataset (Poli et al., 2016) is used for extra verification. ERA20C is based on IFS cy38r1 and performs the assimilation on fewer variables than ERA-Interim.

The ERA-Interim and ERA5 reanalysis datasets are extensively used in this thesis. The ERA-Interim dataset is used to investigate the link between atmospheric rivers and extreme precipitation over Norway in Chapter 3. Furthermore, ERA-Interim is used for validation of the moisture tracking tool in Chapter 4, and for validation of the global hydrological model in Chapter 6. In Chapter 6 the ERA-Interim/Land and ERA20C reanalysis datasets are used for extra validation. The newest ERA5 dataset is used to study the moisture sources of the Rhine basin during the extremely dry summers of 2003 and 2018 in Chapter 5.

For the verification of actual evaporation over Europe and North America, we use the GLEAM (Global Land Evaporation: the Amsterdam Methodology) dataset version 3.0a (Martens et al., 2016) from 1985 until 2015 (30 years). The GLEAM dataset is a result of a set of algorithms (models) dedicated to estimate global terrestrial evaporation from satellite data. The product is primarily driven by potential evaporation estimates based on the Priestley-Taylor equation (Priestley and Taylor, 1972) and by passive microwave remote sensing data, but also includes different precipitation products and reanalysis data (Martens et al., 2016). The GLEAM dataset is used for comparison of evaporation in Chapter 4 and 6.

2.4 Models

The models that we use in this thesis are presented here, and outlined in Figure 2.1. First, simulations from the global climate model EC-Earth are described and thereafter details on the global hydrological model are given. The theory on moisture tracking and the tracking tool WAM-2layers are described in Section 2.5.

Besides using the simulations of one climate model, other model simulations from the Atmospheric Model Intercomparison Project (AMIP) CMIP5 (Taylor et al., 2012b) are used in Chapter 4. For present climate, atmosphere only CMIP5 data is taken from 1979 to 2008, and from 2070 to 2100 for future climate based on the Representative Concentration Pathway (RCP) 4.5 emission scenario (Van Vuuren et al., 2011).

2.4.1 EC-Earth global climate model

In this thesis, we make use of global climate simulations performed with the atmospheric global climate model EC-Earth V2.3 (Hazeleger et al., 2010, 2012). The EC-Earth model

is based on the European Centre for Medium-Range Weather Forecasts numerical weather prediction model Integrated Forecasting System (IFS) cy31r1. An improved hydrology scheme (H-TESSEL; Balsamo et al. 2009; Van den Hurk et al. 2000) is implemented in EC-Earth. Actual evaporation is computed by this scheme using a tile approach, such that each grid cell can contain multiple land-use types.

Simulations are performed with a high spatial resolution, with a lower spatial resolution, and both for present and future climate (Haarsma et al., 2013). The high resolution experiments have a horizontal spectral resolution of T799, which corresponds to 25 km (at the equator), and 91 vertical levels (further referred to as High or T799). For comparison in resolution, the same model simulations are performed with a spectral horizontal resolution of T159, corresponding to 120 km (at the equator) and 62 vertical levels (further referred to as Low or T159), which is the common resolution of the current generation of climate models. The parameterization packages of the high and low resolution simulations are the same (Van Haren et al., 2015). The land-surface characteristics are described in the IFS model documentation (2007, IFS Documentation Cy31r1, Book Chapter, ECMWF) and are interpolated to the requested resolutions (T799 and T159).

In the present-day simulations, observed greenhouse gases and aerosol concentrations were applied, while future concentrations were derived from the RCP4.5 scenario (Van Vuuren et al., 2011). Sea surface temperatures (SSTs) were imposed using daily data at 0.25° horizontal resolution from NASA (`http://www.ncdc.noaa.gov/oa/climate/research/sst/oi-daily.php`) for the 2002 to 2006 period. The SSTs for the future were calculated by adding the projected ensemble mean change using the 17 members of the coupled climate model ECHAM5/MPI-OM in the ESSENCE project (Sterl et al., 2008) under the SRES A1B emission scenario (Nakicenovic et al., 2000). This scenario is compatible with the RCP4.5 scenario, but the median global temperature increase by the end of the twenty-first century is about 1° C smaller (Rogelj et al., 2012). Further details on model setup can be found in Baatsen et al. (2015) and Haarsma et al. (2013).

For both resolutions, the experiment consists of 6 members of 5 years for present climate (2002-2006) and future climate (2094-2098), resulting in a data set of 30 years for each period and each resolution. A 10 year spin up run at low resolution (T159) was made for both the present and the future, followed by a 9 month (from January to October) spin up run at T799 resolution. The 6 member ensemble was made by taking the atmospheric state of one of the first 6 days of October as initial state for each member. Thereafter, the model was run for another 3 months until 1st of January before the data were used for the analysis. After this spin up the spread in the atmospheric states was sufficient to treat the 6 runs as independent members (Haarsma et al., 2013).

The atmospheric variables are available at a 6-hourly time interval and on five pressure levels in the atmosphere (850, 700, 500, 300, and 200 hPa). Surface variables are available at a 3-hourly time interval. Precipitation and evaporation are accumulated products.

The high resolution simulations of present and future climate are used in Chapter 4 to investigate the moisture sources of the Mississippi river basin under a changing climate. In Chapter 6 we study the potential of higher spatial resolution simulations in representing the hydrological cycle over the Rhine and Mississippi basins.

2.4.2 W3RA global hydrological model

The global hydrological model W3RA is used to simulate the hydrological cycle of the Rhine and Mississippi basins. This hydrological model is based on the landscape hydrology component model of the AWRA system (AWRA-L; van Dijk et al. 2013; Van Dijk 2010a,c; Van Dijk and Renzullo 2011). AWRA-L can be considered a hybrid between a simplified grid-based land surface model and a non-spatial, or so-called lumped, catchment model applied to individual grid cells. The model consists of two hydrological response units (HRUs); deep-rooted tall vegetation (forest) and shallow-rooted short vegetation (herbaceous), each of them occupying a fraction of a grid cell. Vertical processes are described for each HRU individually. There is no lateral redistribution of water between grid cells. The model consists of three soil layers and runs with a daily time step. Actual evaporation is calculated with the energy balance. For the full technical details about the model algorithm and parameters, we refer to the technical documentation (Van Dijk, 2010c). The main evaluation of the model on global scale is documented in van Dijk et al. (2013). The model does not contain reservoirs.

The global hydrological model W3RA is used in Chapter 6 to determine if increased model resolution leads to a better representation of the hydrological cycle for the Rhine and Mississippi basins.

2.5 Atmospheric moisture tracking

2.5.1 Derivation of the atmospheric water balance

Before a description of the moisture tracking model is given, the atmospheric water balance, which forms the basis of the tracking model, is derived. For completeness, we present the full derivation here. This derivation is based on Seager and Henderson (2013).

The local rate of change of specific humidity (moisture) in the atmosphere (q in kg kg^{-1}) is determined by advection of moisture, and by its sources and sinks (S in kg kg^{-1} s^{-1}):

$$\frac{\partial q}{\partial t} + \frac{\partial (uq)}{\partial x} + \frac{\partial (vq)}{\partial y} + \frac{\partial (\omega q)}{\partial p} = S \tag{2.1}$$

where u,v and ω are the wind components in respectively the zonal, meridional and vertical direction. Equation 2.1 can be written in the mass divergence form as $\nabla \cdot \boldsymbol{u} = 0$ in pressure coordinates, and is valid at every location in the atmosphere. We integrate

Equation 2.1 over the vertical column, from the surface (surface pressure p_s) to the top of the atmosphere (where $p = 0$). We divide each term of the balance by the gravitational constant g and the density of water ρ_w to get the units of m s^{-1}.

$$\frac{1}{\rho_w g}\left(\int_0^{p_s}\frac{\partial q}{\partial t}dp + \int_0^{p_s}\frac{\partial (uq)}{\partial x}dp + \int_0^{p_s}\frac{\partial (vq)}{\partial y}dp + \int_0^{p_s}\frac{\partial (\omega q)}{\partial p}dp\right) = E - P \tag{2.2}$$

where E is surface evaporation and P is surface precipitation, respectively the source and sink. We extend the first three terms on the left hand side (LHS) of Equation 2.2 by applying Leibniz theorem (taking into account a constant pressure 0 at the top):

$$\begin{aligned}
\int_0^{p_s}\frac{\partial q}{\partial t}dp &= \frac{\partial}{\partial t}\int_0^{p_s} q dp - q(p_s)\frac{\partial p_s}{\partial t} \\
\int_0^{p_s}\frac{\partial (uq)}{\partial x}dp &= \frac{\partial}{\partial x}\int_0^{p_s} (uq) dp - u(p_s)q(p_s)\frac{\partial p_s}{\partial x} \\
\int_0^{p_s}\frac{\partial (vq)}{\partial y}dp &= \frac{\partial}{\partial y}\int_0^{p_s} (vq) dp - v(p_s)q(p_s)\frac{\partial p_s}{\partial y}
\end{aligned} \tag{2.3}$$

Where $u(p_s) = u_s$, $v(p_s) = v_s$ and $q(p_s) = q_s$. The vertical advection term, in Equation 2.2 the last term on the LHS, is integrated:

$$\int_0^{p_s}\frac{\partial (\omega q)}{\partial p}dp = \omega(p_s)q(p_s) - \omega(0)q(0) = \omega_s q_s \tag{2.4}$$

We assume that there is no moisture at the top of the atmosphere, thus $q(0) = 0$. And $\omega(p_s) = \omega_s$ is the vertical velocity (in pressure coordinates) at the surface, which we can write as:

$$q_s\omega_s = q_s\frac{Dp_s}{Dt} = q_s\left(\frac{\partial p_s}{\partial t} + u_s\frac{\partial p_s}{\partial x} + v_s\frac{\partial p_s}{\partial y} + \omega_s\frac{\partial p_s}{\partial p}\right) \tag{2.5}$$

The last term on the right hand side (RHS) in Equation 2.5 is zero, because surface pressure does not change with height. Combining Equation 2.4 and 2.5 gives:

$$\int_0^{p_s}\frac{\partial (\omega q)}{\partial p}dp = q_s\frac{\partial p_s}{\partial t} + q_s u_s\frac{\partial p_s}{\partial x} + q_s v_s\frac{\partial p_s}{\partial y} \tag{2.6}$$

Now, the extended terms of Equation 2.3 and 2.6 are implemented into the vertical integrated moisture balance presented in Equation 2.2:

$$\frac{1}{\rho_w g}\left(\frac{\partial}{\partial t}\int_0^{p_s} q dp - q_s\frac{\partial p_s}{\partial t} + \frac{\partial}{\partial x}\int_0^{p_s}(uq)dp - u_s q_s\frac{\partial p_s}{\partial x} + \frac{\partial}{\partial y}\int_0^{p_s}(vq)dp - v_s q_s\frac{\partial p_s}{\partial y} + q_s\frac{\partial p_s}{\partial t} + q_s u_s\frac{\partial p_s}{\partial x} + q_s v_s\frac{\partial p_s}{\partial y}\right) = E - P \tag{2.7}$$

Three terms cancel each other on the LHS of Equation 2.7, and re-writing gives:

$$\frac{1}{\rho_w g}\left(\frac{\partial}{\partial t}\int_0^{p_s} q dp + \frac{\partial}{\partial x}\int_0^{p_s}(uq)dp + \frac{\partial}{\partial y}\int_0^{p_s}(vq)dp\right) = E - P \tag{2.8}$$

Shortly written as:

$$\frac{\partial S}{\partial t} + \frac{\partial F_x}{\partial x} + \frac{\partial F_y}{\partial y} = E - P \tag{2.9}$$

where $S = \frac{1}{\rho_w g}\int_0^{p_s} q\, dp$, $F_x = \frac{1}{\rho_w g}\int_0^{p_s}(uq)\, dp$, $F_y = \frac{1}{\rho_w g}\int_0^{p_s}(vq)\, dp$.

This is the resulting atmospheric water balance as presented in the Introduction, and as used in Chapter 4 and 5.

2.5.2 Description moisture tracking model WAM-2layers

When moisture is tracked from its source (evaporation over a region) to its sink (precipitation), Equation 2.9 can be adapted as follows, indicating forward tracking:

$$\frac{\partial S_m}{\partial t} + \frac{\partial F_{x,m}}{\partial x} + \frac{\partial F_{y,m}}{\partial y} = \delta E + P_m \tag{2.10}$$

where m indicates the tracked moisture, and δ indicates the source area of interest, with $\delta = 1$ inside the region of interest and $\delta = 0$ outside the region of interest.

In this thesis, we are mostly interested in the moisture sources which bring precipitation to a defined region. To determine these moisture sources, moisture is tracked backward in time, which means that precipitation becomes the source and evaporation the sink. Therefore, E and P switch sign compared to the forward tracking:

$$\frac{\partial S_m}{\partial t} + \frac{\partial F_{x,m}}{\partial x} + \frac{\partial F_{y,m}}{\partial y} = -E_m + \delta P \tag{2.11}$$

E_m is the source of the tracked moisture, and is shown throughout this thesis as the resulting moisture source.

We use the Water Accounting Model-2layers (WAM-2layers; Van der Ent et al. 2010, 2014) to track moisture of our interest. WAM-2layers is an Eulerian offline moisture tracking model which solves the atmospheric water balance (Eq. 2.9) for every grid cell. The model can perform both forward and backward moisture tracking. We primarily use backward tracking to determine the moisture sources of the Mississippi and Rhine basins. WAM-2layers performs the tracking on two layers in the atmosphere, hence the atmospheric information is integrated to two layers. The lowest layer (bottom layer) extends from the surface (p_s) to the division (p_{division}). The top layer extends from the division (p_{division}) to the top of the atmosphere where pressure is 0. The division between the two layers depends on the surface pressure: $p_{\text{division}} = 7438 + 0.72 \cdot p_s$ [Pa] (Van der Ent, 2014), which corresponds to about 800 hPa. This level was chosen as the vertical distribution of wind velocities showed that the shear-layer is approximately at this level (Van der Ent and Savenije, 2013). The model assumes well-mixed conditions in both layers: $P_k = P \cdot \frac{S_k}{S}$, where k indicates either the top or bottom layer. Evaporation only contributes to the bottom layer. Transport of moisture between the two layers can occur via vertical component F_v. This vertical transport (F_v) is determined from closing the water balance between the two layers. Furthermore, to take into account the non-closure of the data a sigma term σ_k is added.

$$\frac{\partial S_{m,k}}{\partial t} + \frac{\partial F_{x,m,k}}{\partial x} + \frac{\partial F_{y,m,k}}{\partial y} = \delta P_k - E_{m,k} + F_v + \sigma_k, \tag{2.12}$$

For more information on the model we refer to Van der Ent (2014).

2.5.3 Adaptions made to the WAM-2layers model: WAM-2layers-5pres

Originally, the WAM-2layers model was developed to perform moisture tracking with atmospheric data on multiple model levels from ERA-Interim. However, we modified the WAM-2layers model in order to run it with output from EC-Earth, which provides atmospheric data at five pressure levels (850, 700, 500, 300, 200 hPa). We describe the modifications here, where the validation of these modifications is provided in the next Section 2.5.4.

First, atmospheric data on pressure levels can intersect with topography. We use surface pressure to identify and eliminate levels which are situated below the surface. Thereafter, we perform a spline interpolation on the vertical flux profiles (uq and vq) at pressure levels to better estimate the real vertical wind profiles. A spline interpolation is chosen to better capture the low level jet (LLJ). We perform a linear interpolation for the vertical profiles of specific humidity. Afterwards, the interpolated data is integrated to two layers (bottom and top), which is needed for the tracking model (see previous Section). Second, we apply a linear interpolation of the moisture fluxes ($\frac{\partial F_x}{\partial x}$ and $\frac{\partial F_y}{\partial y}$) over time. Third, when there is a local non-closure of the moisture balance (i.e. on gridcell level) it can

happen that the amount of water vapor in a cell S_k is smaller than the amount of tracked water vapor $S_{m,k}$. We allow this to happen, in order to ensure water conservation. The spatial resolution of the EC-Earth data (~25 by 25 km) is much higher than the spatial resolution of the ERA-Interim data (~150 by 150 km) and therefore we decrease the time step of WAM-2layers from 15 to 6 minutes.

2.5.4 Validation of WAM-2layers-5pres model

This Section provides a validation of the question: Can we apply moisture tracking to atmospheric data at five pressure levels? The validation is two-fold, and with a focus on North America. First, vertical profiles from moisture fluxes obtained with ERA-Interim at multiple model levels are compared to the vertical profiles obtained from ERA-Interim at the five pressure levels available with EC-Earth. Second, we run the adapted version of the WAM-2layers model with ERA-Interim at the pressure levels that are available in the EC-Earth model, and we compare these results with the simulations from the original WAM-2layers code with ERA-Interim at model levels.

First, the vertical profiles of specific humidity and moisture fluxes (uq and vq) from ERA-Interim at model levels and five pressure levels are compared. Hereby we assume that the vertical profiles from the model levels represent the 'truth'. To make a direct comparison between the profiles obtained from model level and pressure levels, the information available at five pressure levels is interpolated to the model levels. Figure 2.2 shows an example of the interpolation of the zonal (uq) and meridional moisture flux (vq) at a random location and time step. Both a linear and a spline interpolation were performed (Figure 2.2). The bias from these interpolated profiles compared to the 'truth' profiles was determined, and we found reduced biases when performing a spline interpolation for the moisture fluxes. The main reason is that the spline interpolation better captures the low level jet, as is illustrated with the spline interpolation in Figure 2.2. For the vertical profiles of specific humidity, we perform a linear interpolation, as the spline interpolation did not substantially reduced the bias, and is computationally more expensive.

However, the question remains if the vertical profiles of specific humidity and the moisture fluxes interpolated from pressure levels represent the 'truth' well enough. To further estimate this, the variance of the 'truth' vertical profiles over time is determined. This variance is compared to the root mean square error (RMSE) between the 'truth' vertical profiles and the newly obtained interpolated profiles. The results are shown in Figure 2.3 for the zonal moisture flux (uq). We find that the variance over time in the 'truth' profiles is an order of magnitude larger than the difference between profiles obtained at model levels ('truth') and pressure levels. In other words, the variance of the 'truth' profile dominates over the difference between the 'truth' and pressure level profiles. Based on this result, we conclude that the interpolated profiles represent the reality well enough to use for moisture tracking.

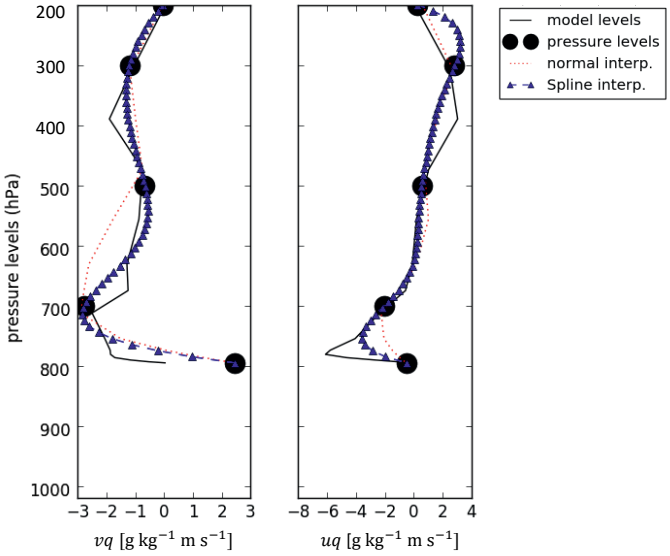

Figure 2.2: Vertical profiles (latitude= 27 °N, longitude = 106 °W) of meridional (vq [g kg^{-1} m s^{-1}]) and zonal moisture fluxes (uq [g kg^{-1} m s^{-1}]) obtained from ERA-Interim at 18 model levels (black line), and five pressure levels (black dots). The blue triangles and red dots show the result of interpolation from the five pressure levels to model levels using respectively a spline and linear interpolation.

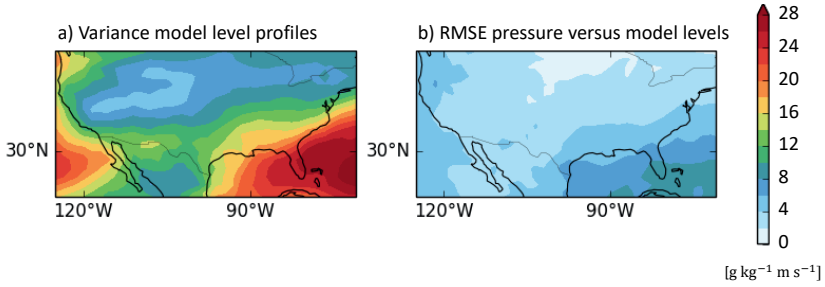

Figure 2.3: a) Variance [g kg^{-1} m s^{-1}] in time of zonal moisture flux profiles (uq) from model levels ('truth') and b) the root mean square error (RMSE [g kg^{-1} m s^{-1}]) of zonal moisture flux from model levels compared to pressure levels.

Second, we run the adapted version of the WAM-2layers model with ERA-Interim at the pressure levels which are available in the EC-Earth model, and we compare these results with the simulations from the original WAM-2layers code with ERA-Interim at model levels (Table 2.1). Validation is done by comparing the moisture sources of the Mississippi river basin for the year 2002. The first row of Table 2.1 indicates the non-closure of the water balance with the WAM-2layers model (i.e. how much water is lost between source and sink), when run with ERA-Interim at model levels (first column) and run with ERA-Interim at 5 pressure levels (second column).

Although we did not assess the closure of the atmospheric water balance using ERA-Interim data, we did study the closure of the atmospheric water balance within the EC-Earth data. We find that over the whole domain, and over the time period of one year (2002) the atmospheric water budget closes almost totally (-0.06%). However, per time step (6-hourly) the local non-closure of the balance per gridcell can be substantial (up to 20 mm d^{-1}). The largest non-closure occurs mostly under large gradients of specific humidity. The non-closure can occur because we use instantaneous 6-hourly atmospheric data (wind and specific humidity), and because we have a coarse representation of the lowest layer of the atmosphere where the highest amounts of moisture occur (between surface pressure and 850 hPa). Furthermore, we do not use the same numerical methods for discretization as were used in the spectral EC-Earth model. Finally, the fact that atmospheric data is transformed from model levels to pressure levels also contributes to the non-closure of the water balance (Seager et al., 2010; Seager and Henderson, 2013; Trenberth, 1991). Nevertheless, the non-closure at local gridcell level does not lead to a non-closure of the water balance over the whole domain in 2002 in the EC-Earth data. As mentioned, we have not assessed the (local non-)closure of the atmospheric water budget in ERA-Interim, but expect similar results as for EC-Earth as both models are based on the same numerical weather prediction model (IFS). ERA-Interim does provide atmospheric variables close to the surface, however due to data assimilation other biases may be introduced (Trenberth et al., 2011). These reasons explain the non-closure as presented in the first row of Table 2.1.

Furthermore, Table 2.1 quantifies the contributions per source region in percentage. The source regions are indicated in Figure 2.4. We find very small differences in using model levels versus 5 pressure levels between sources from continental areas (Mississippi basin and surrounding continental areas) and the Pacific. For the Atlantic, Gulf of Mexico and Caribbean the differences are slightly larger. By using the data at pressure levels we lack information in the lowest layer which leads to an underestimation of the velocities associated with the low level jet, which is an important mechanism in the warm season to transport moisture from these regions towards the Mississippi basin. Note that we do not perform the tracking globally, to reduce computational costs, and therefore some tracked moisture crosses the boundaries of the domain (domain is shown in Figure 2.4). This outflux over the boundaries is indicated in Table 2.1 (East, West, North and South). We

Table 2.1: Relative contribution of moisture sources per region contributing to precipitation over the Mississippi [%] averaged for the year 2002. The column with ERA-Interim model levels indicates the results with the standard version of WAM-2layers and ERA-Interim at model levels. The column with ERA-Interim 5 pressure levels shows the results with the adapted version of WAM-2layers with ERA-Interim data at 5 pressure levels.

Relative source in %		ERA-Interim model levels 2002	ERA-Interim 5 pressure levels 2002
Non-closure in WAM-2layers		100 - 99.6 = 0.4	100 - 99.5 = 0.5
Tracked source	Total	73.4	71.7
	Mississippi basin	12.6	12.4
	Continental (not Mississippi)	18.9	19.0
	Atlantic	8.5	7.0
	Gulf of Mexico/Caribbean	15.6	14.9
	Pacific	17.8	18.2
Outflux over boundaries	East	6.7	6.2
	West	14.1	14.5
	North	0.6	0.3
	South	5.7	7.9

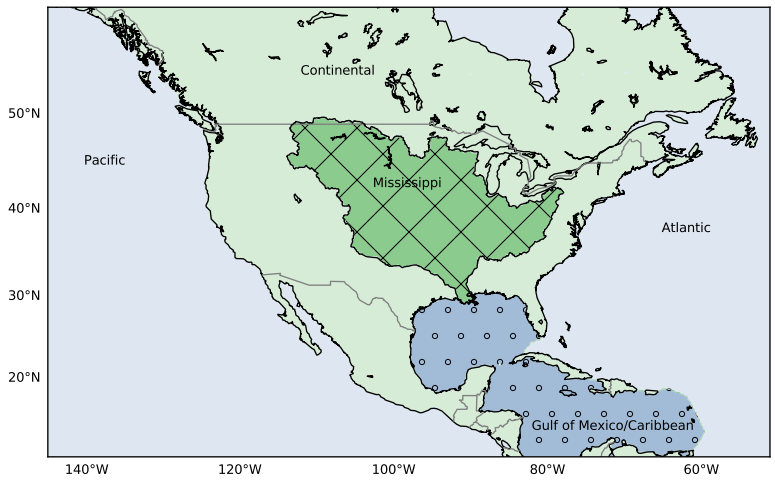

Figure 2.4: Map of the domain on which we performed the moisture tracking, including the source regions used for analyses: continental area outside Mississippi basin (green, not hatched), Mississippi river basin (green, hatched), Pacific (blue left of the continent), Atlantic (blue right of the continent, including Hudson Bay) and Gulf of Mexico/Caribbean (blue dotted).

find the largest outflux at the western boundary.

From this validation we conclude that the moisture sources of the Mississippi basin determined with ERA-Interim at model levels and ERA-Interim at 5 pressure levels are comparable, thus that we can apply WAM-2layers on the available data from EC-Earth. In Chapter 4 the moisture sources of the Mississippi basin are studied for present and future climate using the simulations from EC-Earth. In Chapter 5, the moisture sources of past summers for the Rhine are investigated, using ERA5 reanalysis data as input for the modified version of WAM-2layers. This adapted version is available on Github: `https://github.com/Imme1992/moisture\_tracking\_mississippi/`.

3

Large-scale flow patterns associated with extreme precipitation and atmospheric rivers over Norway

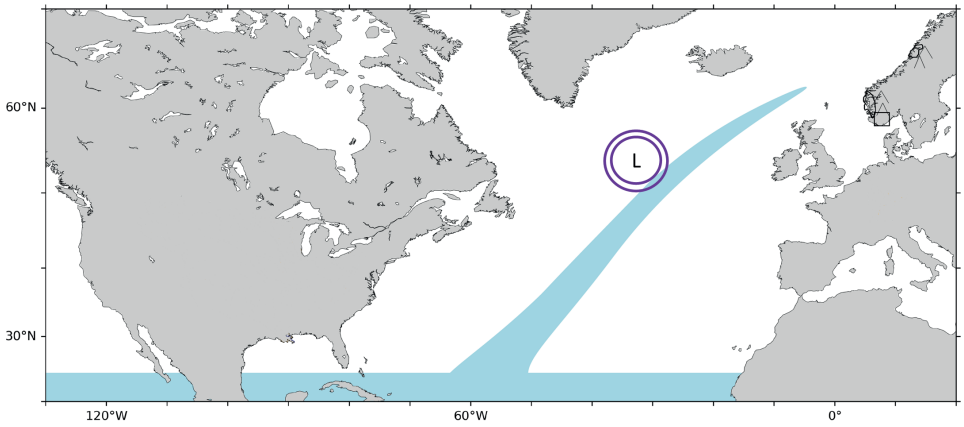

This Chapter is based on:
Benedict, I., Ødemark, K., Nipen, T., and Moore, R.: Large-scale flow patterns associated with extreme precipitation and atmospheric rivers over Norway, Monthly Weather Review, 147, 1415–1428, 2019a

A climatology of extreme cold season precipitation events in Norway from 1979-2014 is presented, based on the 99th percentile of the 24-hour accumulated precipitation. Three regions, termed North, West and South are identified, each exhibiting a unique seasonal distribution. There is a proclivity for events to occur during the positive phase of the NAO. The result is statistically significant at the 95th percentile for the North and West regions. An overarching hypothesis of this work is that anomalous moisture flux, or so-called atmospheric rivers (ARs), are integral to extreme precipitation events during the Norwegian cold season. An objective analysis of the integrated vapor transport illustrates that more than 85% of the events are associated with ARs. An empirical orthogonal function and fuzzy cluster technique is used to identify the large-scale weather patterns conducive to the moisture flux and extreme precipitation. Five days before the event and for each of the three regions, two patterns are found. The first represents an intense, southward-shifted jet with a southwest to northeast orientation. The second identifies a weak, northward-shifted, zonal jet. As the event approaches, regional differences become more apparent. The distinctive flow pattern conducive to orographically-enhanced precipitation emerges in the two clusters for each region. For the North and West regions, this entails primarily zonal flow impinging upon the south-north orientated topography, the difference being the latitude of the strong flow. In contrast, the South region exhibits a significant southerly component to the flow.

3.1 Introduction

Extreme precipitation events in Norway are often the result of anomalously large moisture flux impinging upon the complex mountainous terrain. Azad and Sorteberg (2017); Sodemann and Stohl (2013); Stohl et al. (2008) have shown how so-called atmospheric rivers (ARs), long narrow regions of intense water vapor transport within the lower atmosphere, are integral to the transport of (sub- and extra-) tropical moisture to Norwegian latitudes. Their studies incorporated a variety of techniques (synoptic analyses, clustering, tracer transport), datasets (surface observations, model operational and reanalysis data) and time frames (single events to a century) to imply that the connection of integral water vapour transport and ARs is a robust result and to identify possible large scale structures that are conducive to these events. Using the previous work as a foundation, the overarching goal of this work is to use a cohesive long term dataset (reanalysis data) to identify a large number of extreme precipitation events to better understand the climatology and processes at work.

ARs are a key component to the global water cycle (Zhu and Newell, 1998) and to regional extreme precipitation (Knippertz and Wernli, 2010; Leung and Qian, 2009; Ralph et al., 2006; Stohl et al., 2008). As such, ARs can strongly affect short-term weather and flood prediction, as well as seasonal climate anomalies (Ralph et al., 2004). In regards to the latter, Stohl et al. (2008) note that the large moisture fluxes are relatively more important during the positive phase of the North Atlantic Oscillation in Norway, associated with the increased storminess in general during this phase. This result implies relevance to seasonal predictability. Furthermore, other work has shown that there remains large uncertainties regarding quantitative precipitation forecasts under climate change scenarios, making a better understanding of precipitation processes vital for future climate services to properly predict extreme precipitation events (Dettinger, 2011; Ralph et al., 2010).

An example of a Norwegian extreme precipitation event on 13 September 2005 was examined by Stohl et al. (2008). Vertically integrated water vapor images clearly identify a coherent, narrow plume of moisture extending from the tropics and subtropics to southwestern Norway. The moisture transport along this plume was found to play a critical role in producing orographically-enhanced precipitation resulting in landslides and flooding that caused considerable damage to property and life. Further corroborative work regarding the importance of orographic enhancement can be found here (Bader and Roach, 1977; Browning and Pardoe, 1973; Harrold, 1973).

An intriguing comparison is found in the North Pacific, where moisture plumes have been linked to extreme precipitation in western North America. The apparent dynamical similarity in the two ocean basins implies the North Pacific and North America research is likely relevant for extreme precipitation in Norway. An extensive series of research in this region (Ralph et al., 2004, 2006, 2010; Wick et al., 2013) incorporating some combination

of in-situ aircraft observations, satellite data, coastal wind profilers and GPS meteorological stations, gridded precipitation data, global reanalysis data, and operational ensemble prediction systems can be summarized in the following key findings: i) the overwhelming majority of extreme precipitation events are associated with ARs, ii) forecasts of landfalling ARs and their characteristics are significantly poorer than that of the large-scale patterns related to the AR, and iii) quantitative precipitation forecasts (QPF) improve with shorter forecast length, yet significant biases exist and biases can and do exhibit a strong sensitivity to the local geography. The overarching conclusion can be stated thusly: to properly capture extreme precipitation events, the large-scale flow patterns on scales from planetary to the mesoscale need to be well resolved to provide an accurate forecast of the location and intensity of the extreme precipitation (Ralph and Dettinger, 2011).

The analyses of Azad and Sorteberg (2017), Heikkilä and Sorteberg (2012), Sodemann and Stohl (2013), and Stohl et al. (2008) centered on Norway in conjunction with similar work focusing on Great Britain and Northern Europe (Knippertz and Wernli, 2010; Lavers et al., 2011; Lavers and Villarini, 2013; McTaggart-Cowan et al., 2017; Ummenhofer et al., 2017) provide compelling evidence for the causal link between large-scale moisture transport and extreme precipitation in Norway.

The objectives of this work are to i) systematically identify extreme precipitation events using a cohesive long term dataset of 36 years, ii) explore their seasonal, intraseasonal and geographic variability, iii) test the connection to ARs on the identified dataset of events, and iv) use fuzzy clustering to examine their large-scale patterns. This work will contribute to an improved understanding of the climatology and processes leading to extreme precipitation along the coastline in Norway, which can eventually lead to more accurate forecasts that can mitigate damage to life and property.

The outline of this Chapter is as follows. After a description of the data and methodology (Section 3.2), a climatology of extreme precipitation events will be presented in Section 3.3. Section 3.4 will examine the large-scale atmospheric structures that lead to the anomalous moisture flux that is integral to extreme precipitation in Norway. Finally, study conclusions are presented in Section 3.5.

3.2 Data and Methodology

3.2.1 Data

The primary data source for this study is the European Centre for Medium-Range Weather Forecasts (ECMWF) reanalysis (ERA-Interim; Dee et al. 2011) from 1979 to 2014. The precipitation analysis is performed on a grid of 0.25° latitude by 0.25° longitude over Norway, which is a bilinear interpolated field from the original 0.75° latitude by 0.75° lon-

gitude resolution of ERA-Interim. To examine large-scale dynamic patterns, ERA-Interim data are obtained on a grid of 0.75° latitude by 0.75° longitude over the Atlantic basin (70°W to 20°E, 20°N to 80°N). Relevant variables that are examined are the: i) potential temperature along the dynamic tropopause (defined as the two potential vorticity unit surface), ii) integrated vapour transport, iii) mean sea level pressure, and iv) daily total accumulated precipitation (calculated by summing the 12-hour forecasted precipitation from 0000-1200 and 1200-2400 UTC).

3.2.2 Climatology of extreme precipitation events

A climatology of extreme Norwegian precipitation is constructed based upon the 99th percentile of daily precipitation amounts during the 1979-2014 time period (see Figure 3.1a). Figure 3.1b shows the topography of Norway. Distinct maxima of precipitation are identified in north and southwest Norway via a closed contour of enhanced precipitation (24 and 30 mm d^{-1}, respectively, see black contour lines). A southern region is subjectively identified in the absence of a climatological maximum, based upon an examination of previous extreme storm reports that indicate a different flow pattern for storms in this region. The region is represented by the black box in Figure 3.1 and ranges from 6.5°E to 9°E and from 58°N to 59.5°N. The results of this work make a strong argument for the distinction of this southern region. The three regions will hereafter be referred to as North, West and South Norway, respectively. For each region, all dates with area-averaged daily precipitation exceeding the 99th percentile are selected as extreme precipitation events.

To objectively identify atmospheric rivers, the definition introduced by Rutz et al. (2014) is employed. This definition is based on the vertically integrated horizontal water vapour flux (hereafter, integrated vapour transport, IVT) and is defined as:

$$IVT = \frac{1}{g} \int_{p_{1000\ \mathrm{hPa}}}^{p_{100\ \mathrm{hPa}}} q\mathbf{V} dp \tag{3.1}$$

where g is the gravitational acceleration, q is the specific humidity, $\mathbf{V}$ is the total wind vector and p is pressure. The integration is computed using 50-hPa intervals from 1000 hPa to 500 hPa, and 100 hPa intervals from 500 to 100 hPa.

ARs are identified when the IVT exceeds the threshold of 250 kg m^{-1} s^{-1} for a contiguous length of ≥ 2000 km (Rutz et al., 2014). IVT objects are identified when they intersect the respective precipitation region. If the above criteria are met at any of the four time steps (0000, 0600, 1200 and 1800 UTC) during the day of the event, it is deemed to be associated with an AR.

A primary focus of this work is to study the large-scale patterns related to moisture transport and extreme precipitation events over Norway. Such events are typically char-

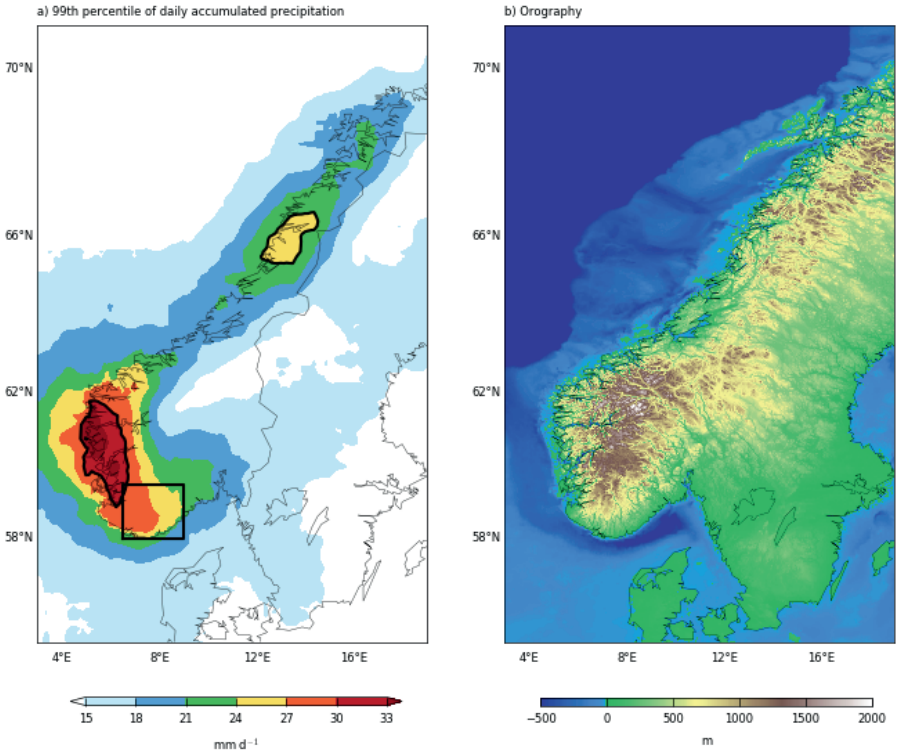

Figure 3.1: In a) we show the 99 percentile of daily accumulated precipitation over Norway in mm d^{-1}. Regions defined as West and North Norway are defined with respectively the 30 mm d^{-1} and 24 mm d^{-1} contour line. South Norway is defined with the indicated black box. In b) we show the elevation of our study area in m.

acterized by a persistent flow (on the order of 24-72 hours) of warm moist air impinging on mountainous terrain. To avoid including warm season, convective events (on the order of one to a few hours) only cases occurring during the cold season (defined here as September to March) are used for further analysis. Furthermore, to avoid 'counting' a multi-day event more than once, events that occur on consecutive days are parsed to solely the day of the most extreme precipitation. The rationale is that the multi-day events are associated with a similar large-scale pattern.

3.2.3 Statistical and composite analysis

To study the variability in the large-scale pre-conditioning of the events, a two-step procedure is employed. Step one is an empirical orthogonal function (EOF) analysis of the potential temperature on the dynamic tropopause (defined as the two potential vorticity

unit surface) over the large domain (70°W to 20°E, 20°N to 80°N). The EOF analysis will detect the underlying structure that best explains the variability in a multivariate dataset (Richman, 1986). Information on the dynamic tropopause was chosen due to the fact that AR structure and evolution are tightly coupled to the predominant circulation patterns on the synoptic scale, including the location, strength and shape of the upper-level flow at tropopause level (Sodemann and Stohl, 2013).

In step two a fuzzy cluster analysis is incorporated, based on the first two principal components of the EOF analysis, to partition events into groups with similar large-scale structure. The analyses are conducted separately for each of the three regions and for different timesteps ahead of the event (24-hour intervals beginning 120 hours before the event, including the day of the event itself). All analyses are performed at 1200 UTC.

This method is thoroughly described and has been successfully applied by Harr et al. (2008) with respect to the extratropical transition of the West North Pacific Typhoon Nabi (September 2005). Their goal was to examine the predictability of the event in ECMWF ensemble forecast data. Here, in contrast, ERA-Interim data are used to determine the variability between the large-scale atmospheric patterns of many events as opposed to ensemble members for a singular event.

For the fuzzy cluster analysis, the number of clusters is a subjective choice based on the level of precision or detail desired (Harr et al., 2008). This analysis incorporates the first two principal components (PCs) from the EOF analysis. The clustering procedure randomly places centers of the number of clusters chosen in the PC1-PC2 phase space, as a first guess. Each event member is also placed in the PC1-PC2 phase space, and thus represented by the pair of PC values. Every event member is attributed to the nearest cluster center. To find the solution with shortest distances between members and cluster centers, the analyses iterates and calculates new cluster centers. Each point is evaluated again in every iteration. When the distance to the cluster centers is minimized a stable solution is found and the iteration ceases.

Here, both two and three-cluster solutions for all regions at the different times before the event were created. After an in-depth examination of the data, we believe that the two-cluster solution is more appropriate for this study because: i) the detail added by the three-cluster solution is deemed insufficient to justify the increase in complexity, ii) cluster members were more coherent over time with the two-cluster solution, in that the majority of events remained in the same cluster for the 120 hours leading to the event, and iii) the choice of a two-cluster solution allows for a direct comparison with the work of Sodemann and Stohl (2013) wherein they identified two moisture transport configurations for the month of December 2006; a month characterized by well above average temperature and precipitation in Norway. The latter is especially appealing in that Sodemann and Stohl (2013) equated the two patterns to the known characteristic life cycles of baroclinic waves (Thorncroft et al., 1993), providing a valuable dynamical distinction.

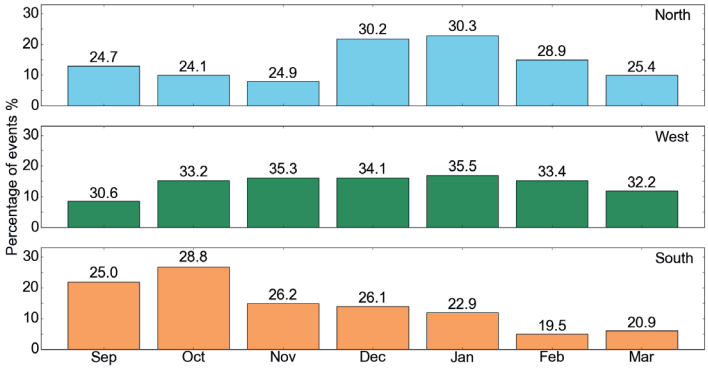

Figure 3.2: Histogram with monthly climatology for the selected events for every region, the y-axis indicates the fraction of events in that month compared with the total amount of events. Value above each bar indicates the 99 percentile of extreme precipitation for that specific month in mm d^{-1}.

Subsequent to the cluster analysis, the composite structure of the clustered members are constructed. These composites can be created for any meteorological variable of interest. Finally, the cluster members are established at 120 hours before the event and remain the same until the event itself. We believe this is justifiable based on point ii) above.

3.3 Extreme precipitation climatology

The results of the climatological analysis of extreme precipitation are presented in this Section. With the omission of multi-day events, the total cold season event counts are 101, 118, and 101 for the North, West and South regions, respectively. The fraction of events per month for the three regions is presented in Figure 3.2. The area-averaged value of the 99 percentile for each month and region is provided on top of the bars in Figure 3.2.

Each of the three regions exhibit a characteristic seasonal variability, providing further motivation for the selection of three distinct regions. For North Norway, a maximum fraction of event counts is found in December and January (22% and 23%), and thereafter in February and September (15% and 13%). There is a remarkable consistency of event counts in West Norway from October through February with no clear maximum (all around 16%). In contrast, a fall maximum (September, 22% and October, 28%) and a minimum in late winter (February, 5% and March, 6%) are observed in South Norway.

To investigate the hypothesis that different flow patterns can be identified for each region, the anomalies of mean sea level pressure (MSLP) at 1200 UTC and daily accumulated precipitation anomaly for all events in each region are presented in Figure 3.3, for the day of the events. The anomalies are calculated from the average MSLP at 1200 UTC of all the events compared to the cold season average MSLP at 1200 UTC, and accordingly for daily accumulated precipitation. The stippling indicates regions where the anomaly is statistically significant at the 0.05 level according to the independent samples t-test. Figure 3.4 shows the composites of the selected events of MSLP and precipitation for the three regions.

A distinct similarity exists for all regions: the presence of a low and high pressure couplet resulting in strong inferred low-level flow oriented in such a way as to result in enhanced orographic uplift (Figure 3.3 b), d) and f)). The fundamental difference between the regions is in the position of the pressure centers. For North Norway, the couplet is meridionally-aligned, leading to strong zonal flow. Southwesterly flow is observed for West Norway due to a southwestward (northeastward) shift in the low (high) pressure centers. The pattern for South Norway exhibits a low-pressure center shifted to the southwest and the high pressure center located far to the southwest. The result is a significant southerly component to the inferred low-level flow. The difference in flow pattern between West and South Norway supports the decision to include the subjectively defined South region.

The precipitation anomalies in each region are apparent. Moreover, a secondary positive anomaly over Great Britain is observed for West and South Norway. The implication is that the very same moisture flux leading to extreme precipitation in South-Western Norway is conducive to enhanced precipitation in Great Britain, a result consistent with the study of Lavers et al. (2011) who linked winter flooding in Britain to atmospheric rivers.

Also of note is the overlap of precipitation between the three regions (see Figure 3.4). A clear secondary anomaly in West Norway is found in the North analysis (15 mm d^{-1} in West while 30 mm d^{-1} in North). For the West analysis, enhanced precipitation is observed in the North region (10 mm d^{-1} in North while $>$ 25 mm d^{-1} in West). Additionally, there is a significant overlap between the West and South regions. An examination of the overlap of the events between the regions reveals that only two events are identical for the North and West region. However, there is an overlap of 15 events between the West and South regions, which is roughly 15% of the total number of selected events. While this is a significant fraction, we believe the different flow patterns observed in Figure 3.3 and 3.4 provide compelling evidence to consider the regions separately.

3.3.1 Inter region correlation

To further examine the association between regions, the inter region correlation, the correlation of monthly event totals (number of events occurring per month) for regional

couplets (South/West, South/North, and West/North) was computed. Using the 0.05 threshold, the results show there is a statistically significant correlation of monthly event totals for all three couplets. The correlation was strongest for West/North (0.28) and South/West (0.27), but weaker for South/North (0.11). As seen in Figure 3.3, the flow patterns for the North and West regions are most similar, which explains the strongest correlation. Less similar flow patterns are found for the couplets including the South region, especially the South/North couplet.

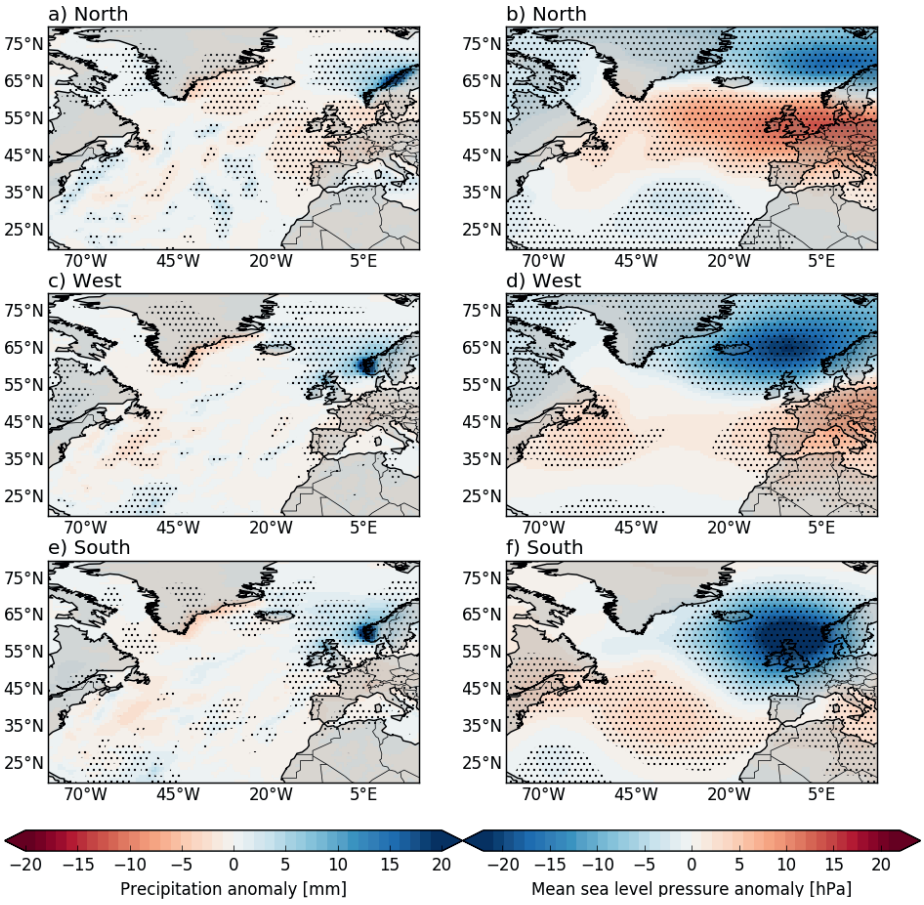

Figure 3.3: Left figures: Precipitation anomalies (mm) for all extreme precipitation events for a) the North region, c) West region, and e) South region at the day of the events. Right figures: Mean sea level pressure anomaly (hPa) for all the events for b) the North region, d) West region and f) South region. For all figures holds that dotted regions indicate where the anomaly is statistical significant.

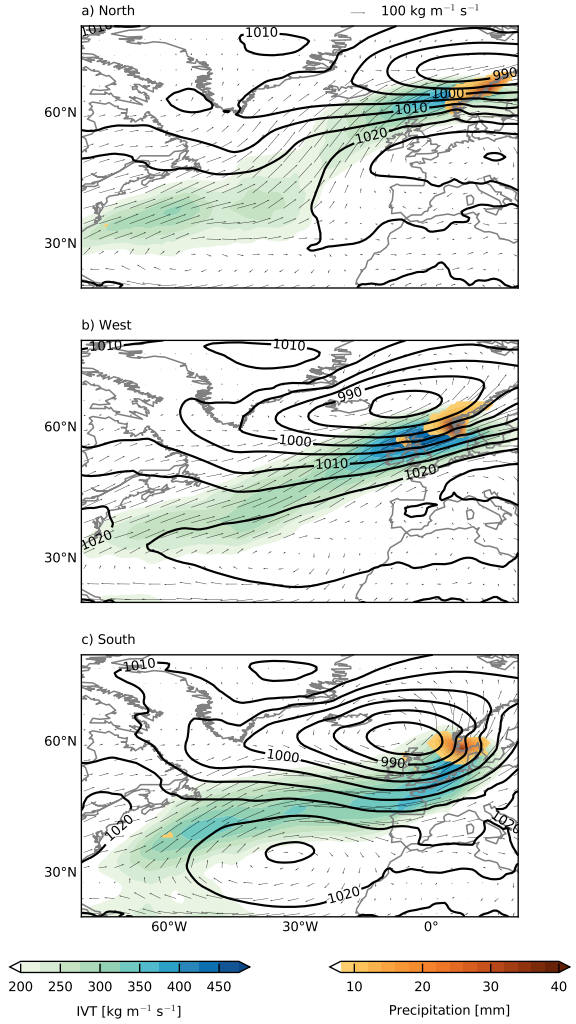

Figure 3.4: Composites of mean sea level pressure (hPa) in contours and total precipitation (mm) in orange/red shading and IVT vectors and magnitude (kg m^{-1} s^{-1}) in green/blue shading at the day of the events for a) the North region, b) the West region and c) the South region.

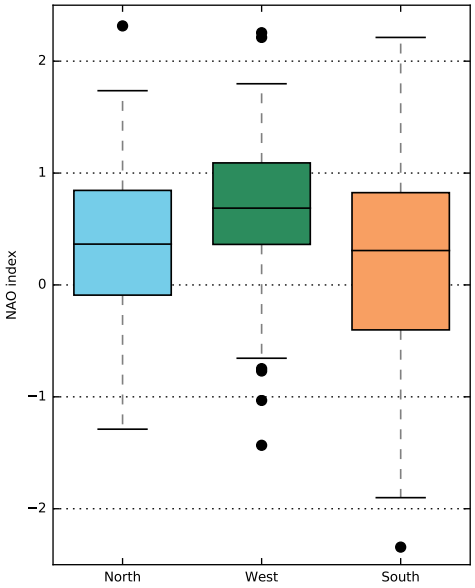

Figure 3.5: Box and whisker plot of the NAO index of the North, West and South region selected events. The boxplot shows the median, the upper quartile ($Q1$, 75%) and lower quartile ($Q3$, 25%), the upper whisker ($Q1 - 1.5 \cdot (Q1 - Q2)$) and the lower whisker ($Q3 + 1.5 \cdot (Q1 - Q2)$), and the outliers (in black dots).

3.3.2 Intra-seasonal variability

Previous work has illustrated that extreme precipitation events are more likely during the positive phase of the NAO (Uvo, 2003; Stohl et al., 2008; Brands et al., 2017). The phase and magnitude of the daily NAO index (data from the Climate Prediction Center) for the events are presented in the form of box and whisker plots in Figure 3.5. The median value is positive for all regions.

To establish the statistical significance of this result (i.e. a positive NAO index is more likely for event days as opposed to non-event days), an independent samples t-test is incorporated. The test is based on the average index value for each region as well as the standard deviation and number of events. Since the NAO index is heavily correlated in time, the number of independent data points is reduced. To account for this 'serial correlation', a so-called effective sample size is introduced. The effective sample size is calculated for non-events and events by:

$$\hat{n} = n\frac{(1-\rho)}{1+\rho} \tag{3.2}$$

Table 3.1: Table with significance test (independent samples t-test) for North, West and South region.

	North	West	South
Number of non-events	13048	13031	13048
Number of events	101	118	101
Mean NAO index of non-events	0.046	0.043	0.047
Mean NAO index of events	0.383	0.684	0.205
Autocorrelation non-events	0.871	0.871	0.873
Autocorrelation events	0.263	0.104	0.058
Effective number of non-events	900	902	887
Effective number of events	58	95	89
p-value	4.97e-04	1.90e-14	0.114
Significant (0.05 level)	Yes	Yes	No

where n is the number of events and ρ is the auto-correlation. The results are presented in Table 3.1. For non events, the effective sample size is reduced by roughly a factor of 15. The reduction is much less for events, as the NAO index is less correlated between individual events.

A significance test at the 0.05 level indicates that the positive phase of the NAO during the selected extreme events (Figure 3.5) is statistically significant for the North and West regions. In contrast, the significance threshold is not met for the South region.

3.3.3 Link to Atmospheric Rivers

An overarching hypothesis of this work is that extreme precipitation in Norway can be directly linked to anomalously large moisture transport (Lavers and Villarini, 2013). The composite magnitude and direction of IVT on the day of the extreme precipitatoin events are presented in Figure 3.4. The AR-like structure is evident as a relatively narrow and elongated region of enhanced IVT for all regions. Concomitantly, the regional differences in the inferred low-level flow discussed above are apparent in the IVT vector field.

Given the climatology of events, we objectively calculate what fraction of the identified events are associated with ARs. Based on the criteria of Rutz et al. (2014), the majority of cold-season events are linked to ARs: 87, 97 and 88% of events were associated with an AR for respectively the North, West and South regions. To test the robustness of this result, we examine the sensitivity to the IVT threshold value chosen by Rutz et al. (2014). The above analysis is repeated by successively increasing the IVT threshold from 250 to 500 kg m^{-1} s^{-1} with steps of 50 kg m^{-1} s^{-1}. As the threshold increases, the fraction of events attributable to ARs lowers (Figure 3.6a). More specifically, a 40% increase in IVT threshold (from 250 to 350 kg m^{-1} s^{-1}) results in a 25% decrease in identified ARs in the South region but only a 5% decrease in identified ARs in the West region. With a

threshold value of 350 kg m^{-1} s^{-1}, approximately 71% of the events in the North and 61% in the South remain associated with ARs, while the number for the West exceeds 92%. We believe these findings illustrate the results are not overly sensitive to the threshold value from the study by Rutz et al. (2014), and that the West region inhibits largest IVT fluxes (also seen in Figure 3.4).

Figure 3.6b further illustrates the sensitivity of IVT magnitude for ARs detected in the three regions. The figure shows the density of IVT values for all ARs (above the 250 kg m^{-1} s^{-1} threshold) for each region. The IVT values in the detected ARs is lower in the North compared to the South and the West region, consistent with the fact that on average less moisture is transported to higher latitudes. The IVT in the West region is on average higher than in the South region, even though South is lower in latitude than West. However, the West region is the region with highest precipitation extremes (Figure 3.1).

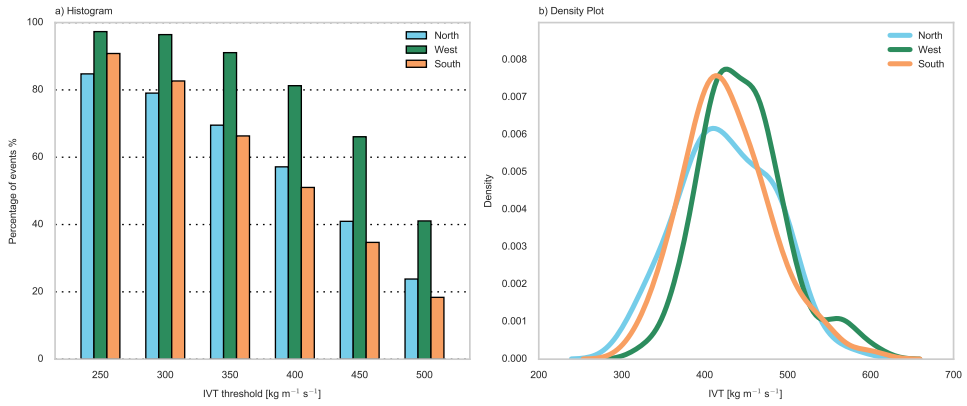

Figure 3.6: a) Percentage of identified atmospheric rivers compared to total events for the three regions (north, west, and south) by changing the IVT threshold from default (250 kg m^{-1} s^{-1}) to 500 kg m^{-1} s^{-1} with increasing steps of 50 kg m^{-1} s^{-1}. b) Density plot of IVT values for ARs detected (above 250 kg m^{-1} s^{-1}) in each region.

3.4 Large-scale pre-conditioning

The EOF and fuzzy cluster analyses are performed to define characteristic large-scale patterns that pre-condition the atmosphere for anomalous moisture transport and extreme precipitation in Norway.

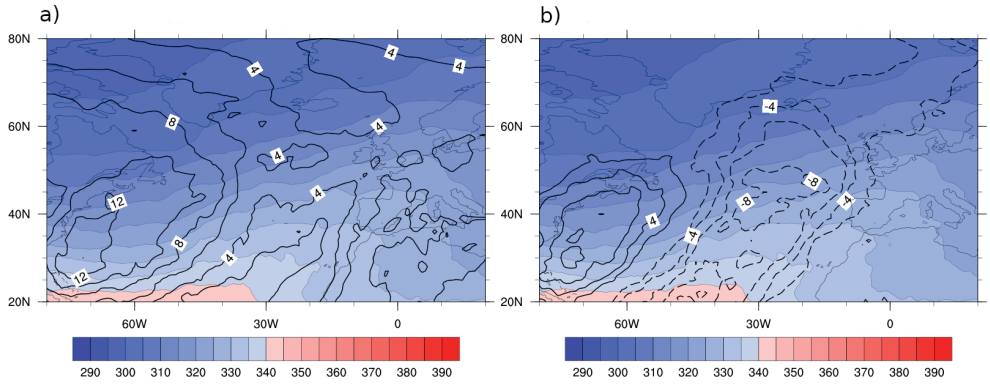

Figure 3.7: Spatial EOF patterns (contoured at an interval of 1.0 K, negative contours are dashed) for potential temperature on the 2-PVU surface for the West region 120 hours prior to the actual event for a) EOF 1 (which explains 18.6% of the variability) and b) EOF 2 (wich explains 6.9% of the variability). The average potential temperature (K) is shaded.

3.4.1 EOF / Fuzzy cluster analysis

As an illustration of the method, the results of the EOF analysis for the West region 120 hours prior to the event are presented in Figure 3.7. The colours represent the average potential temperature (PT) on the dynamic tropopause for all events. The first two principal components are shown as PT anomalies (black contours). Principal component one (PC1) explains the largest variability in the dataset (18.58%) and principal component two (PC2) the second largest variability (6.94%).

The PC anomalies observed in Fig. 3.7 are largely similar in structure, with two centers of enhanced variability identified in the western and central Atlantic basin. The primary difference between the PC1 and PC2 patterns is in the sign and the magnitude of the anomalies: a positive-positive and a positive-negative couplet for PC1 and PC2, respectively. PC1 represents a meridional displacement in the PT gradient, while PC2 is associated with a meridionally-amplified flow pattern.

The first two principal components provide a framework for the fuzzy cluster analysis. Figure 3.8 shows the clustering of the events in the PC1-PC2 phase space, where each event is represented by a unique PC1-PC2 value. The primary difference between the two clusters are the values of PC1. Please note that not all events are placed in a cluster. These events will not be included in the subsequent analyses.

The composite structure of potential temperature (PT) on the dynamic tropopause for the clustered events is presented in Figure 3.9 for both clusters. Cluster one is characterized by an intense southward shifted jet (large PT gradient of 70 K over 30° latitude) over North America and the western Atlantic. The jet exhibits a southwest to northeast orientation

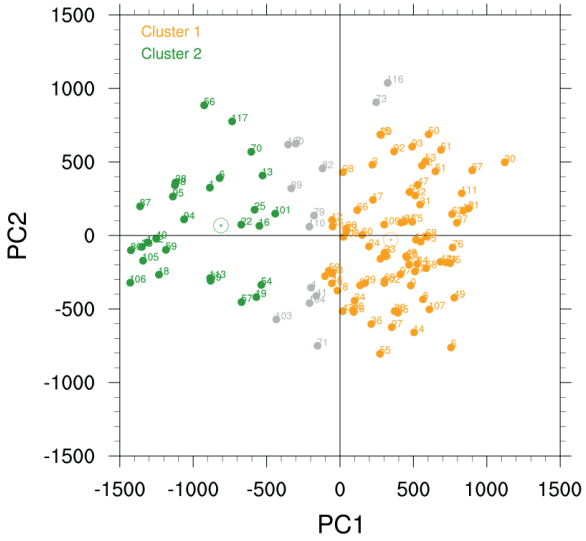

Figure 3.8: The first and second principal component phase space with the two-cluster solution for the events selected for the West region 120 hours prior to the actual event. Each dot represents a selected event. The light gray points define events that do not belong to any cluster. The circles with the small dots are the cluster centers.

towards western Europe and Norway, with a weakening of the jet going eastward (smaller PT gradient of 30 K over 30° latitude over England, Figure 3.9a). Although we cannot confirm this from the composite plot, the observed structure in the eastern Atlantic is consistent with the presence of anticyclonic wave breaking. The reversal of the meridional gradient of PT is not immediately evident, likely due to the compositing of a number of wave breaking events; however an analysis of individual events lends credence to the veracity of the statement. In contrast to cluster one, cluster two is characterized by a weak northward shifted jet (smaller PT gradient of 45 K over 30° latitude). This jet is primarily zonal in nature, with very little undulation across the Atlantic basin (Figure 3.9b).

3.4.2 Composite Analyses

We will primarily focus on West Norway, as this region exhibits both the largest precipitation amounts and the highest fraction of ARs. The cluster composites of MSLP, daily precipitation and IVT magnitude and vector are presented for the time steps 120, 72, 24, and 0 hours before the event (Figure 3.10).

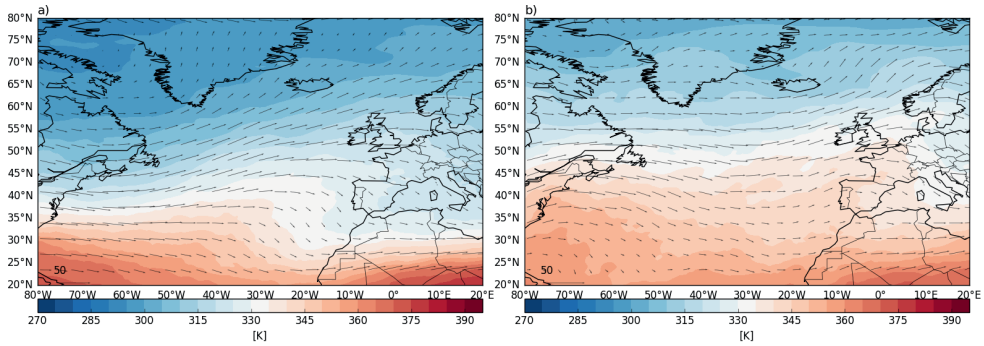

Figure 3.9: Composite analysis of potential temperature at the tropopause in K and wind vectors for the West region 120 hours prior to the actual event for a) cluster one and b) cluster two.

For both clusters and all time steps, the MSLP pattern exhibits a similar couplet with a negative anomaly to the north inferring low-pressure and a positive anomaly to the south inferring high pressure. The result is inferred low-level flow across the Atlantic basin which is conducive to moisture transport towards western Europe and Norway in particular. The primary difference between the two cluster composites is in the orientation of the pressure centers. At 120 hours, a low-pressure center is located off the east coast of Greenland in both clusters. A high pressure center is located in the eastern (western) Atlantic for cluster one (two). Consistent with the dynamic tropopause analysis (Figure 3.9), cluster one exhibits inferred low-level flow from the southwest to the northeast, whereas cluster two is characterized by westerly flow.

As the time before the events occur decreases, the two clusters converge to a similar structure in the eastern Atlantic / western Europe, with a low-pressure center between Iceland and Norway and a high pressure center over western Europe. At the time of the event, both clusters exhibit strong flow with a southwesterly component impinging upon the mountainous terrain of southwestern Norway. Given the moisture convergence resulting in extreme precipitation that defines the events and consistent with case study analyses, it is logical to assume an orographic enhancement of precipitation due to the conducive flow pattern.

There are minor differences between the clusters, even on the day of the event. The inferred low-level flow is both more westerly and stronger (larger pressure gradient force) for cluster one. In contrast, cluster two exhibits a more southerly component and weaker flow. Both flow patterns are reminiscent of a positive NAO, however, the more meridional and weaker flow observed in cluster two may indicate a larger fraction of negative NAO events for cluster two. Further work would be needed to confirm this result.

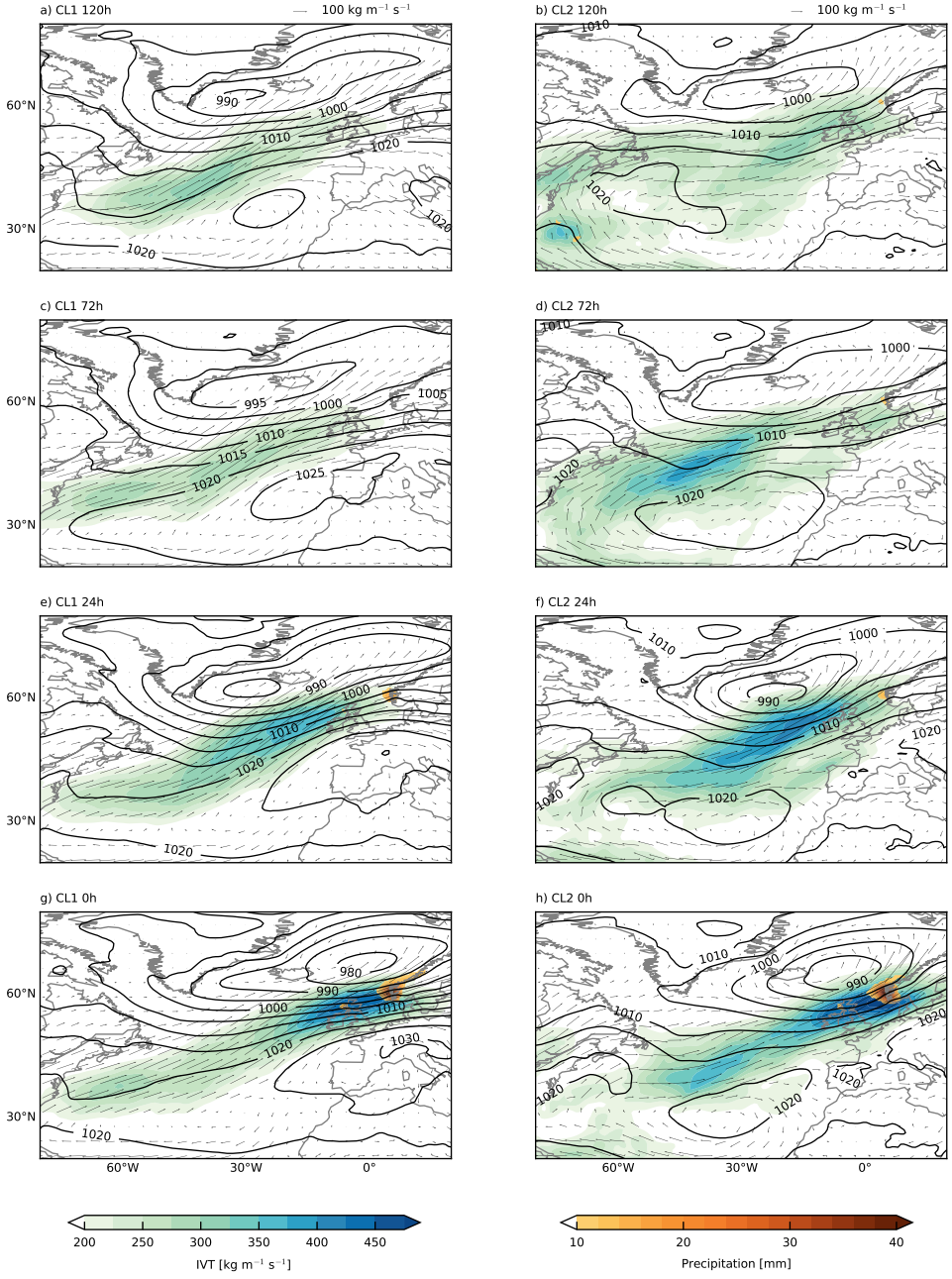

Figure 3.10: Composites of mean sea level pressure (hPa) in contours and total precipitation (mm) in orange/red shading and IVT vectors and magnitude (kg m^{-1} s^{-1}) in green/blue shading at 120 hours, 72 and 24 hours before the event and at the actual event itself (0 hours) for the two clusters (CL1 and CL2) for the West region (cluster one in left figures and cluster two in right figures).

In addition, the cluster composites of MSLP, daily precipitation and IVT magnitude and vectors for the North and South regions at time steps 120 and 24 hours before the event are presented in Figure 5.3. At 120 hours, the qualitative structure of the composites are similar to those for the West region. A low-pressure center is observed to the east of Greenland and high pressure to the south. The placement of the high pressure system is also comparable, with a tendency for the highest pressure to be in the eastern (western) Atlantic for cluster one (two). Both cluster patterns result in significant moisture transport across the Atlantic basin.

Given the clear link between extreme precipitation in Norway and ARs and the context of previous work on the topic of AR dynamics and predictability, the similarity of the cluster analyses for the three regions 120 hours before the event is expected. The large scale structure must be conducive to anomalous moisture transport towards Norway for an extreme event to occur. That there are two relatively distinct patterns is consistent with Sodemann and Stohl (2013) and the known characteristic life cycles of baroclinic waves. This point will be raised in further detail in the following Section.

At 24 hours before the event, regional differences are more pronounced and, as also observed in the West composites, the two clusters for each region become more similar. The North region composites show southwesterly flow between Iceland and Great Britain. The South region composites exhibit a southerly component to the flow towards southern Norway. Both regional patterns are consistent with moisture transport towards the area of extreme precipitation. Logically, as the flow pattern during events for each region must be similar to result in extreme precipitation in that region.

The EOF/ fuzzy cluster/ composite results highlight previously reported facets of the predictability of extreme precipitation associated with ARs. The presence and general location of ARs are well predicted in today's numerical weather prediction systems as they are directly tied to the large scale flow patterns which are inherently more predictable (Dettinger, 2011). While this study incorporates a reanalysis dataset rather than forecast data, we believe the synoptic scale indicators out to 120 hours identified herein will be reasonably consistent with today's state-of-the-art global forecast models.

3.5 Discussion and conclusions

This study presents a climatology of cold season extreme precipitation events for Norway from 1979 to 2014, based on the the 99th percentile of area-averaged precipitation from ERA-Interim. Three regions are identified: North and West regions exhibit a climatological maxima in precipitation, and a South region is based upon previous cases of extreme weather. The performance of ERA-Interim in simulating precipitation over Norway is not studied in detail here, as we focus on the large-scale processes related to these extreme precipitation events. We have not assessed trends.

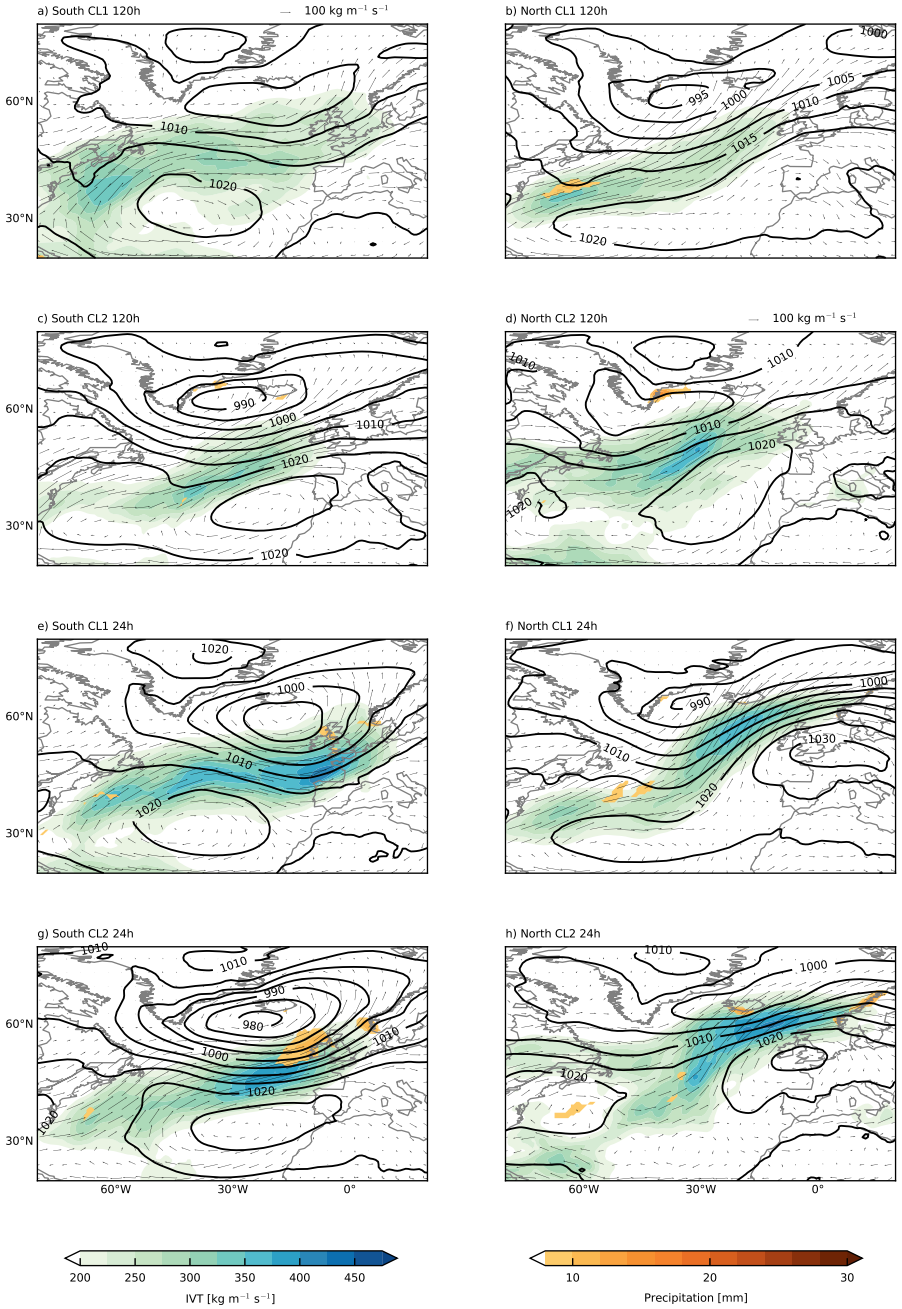

Figure 3.11: Composites of mean sea level pressure (hPa) in contours and total precipitation (mm) in orange/red shading and IVT vectors and magnitude (kg m^{-1} s^{-1}) in green/blue shading at 120 hours (upper Figures) and 24 hours (lower Figures) before the event, for the two clusters (CL1 and CL2) for the South region (left Figures) and North region (right Figures).

Consistent with previous work, we found that extreme precipitation events are more frequent during the positive phase of the NAO. These results are statistically significant at the 0.05 threshold for the North and West regions, while no statistical significance was found for the South. Additionally, there is a statistically significant correlation of monthly events (number of events occurring per month) for all three couplets (West/North, West/South, North/South). This indicates an increased likelihood of an event in a region during a month wherein an event occurs in another region.

An overarching hypothesis of this work is that anomalous moisture transport, or so-called atmospheric rivers (ARs), are critical to cold season extreme precipitation in Norway. An objective analysis illustrates that more than 85% of events are linked to ARs, and that the causal link is not overly sensitive to the subjective threshold of 250 kg m^{-1} s^{-1} integrated vapour transport provided by Rutz et al. (2014).

EOF and fuzzy cluster analyses are performed to define the characteristic synoptic scale patterns that lead to extreme precipitation over Norway. Multiple days before the event (120 hours), two patterns are identified, for all regions. The first represents an intense, southward shifted jet that exhibits a southwest to northeast orientation. The second identifies a weak, northward shifted jet that is zonal in structure. This finding can be directly compared to the results of Sodemann and Stohl (2013), who examined the month of December 2006 which was characterized by well above average temperature and precipitation in Norway. They subjectively identified two moisture transport configurations associated with the characteristic life cycles of baroclinic waves: i) anticyclonic wave breaking associated with a meridional jet, and ii) cyclonic wave breaking associated with a zonal jet. The objective patterns found herein are consistent with their schematic representation. It would be of interest to further explore the link between anomalous moisture transport and wave breaking (Hu et al., 2017). Momentum fluxes associated with wave breaking are important to the jet strength and structure and are typically conducive towards maintaining the orientation of the jet and, hence, the type of wave breaking. These fluxes can imply some measure of predictability that may be exploited.

As the time before the events occur decreases, the similarity of the two patterns for each region lessens. The distinctive flow pattern conducive to orographically-enhanced precipitation emerges in the two clusters for each region. For the North and West regions, this entails primarily zonal flow impinging upon the south-north orientated topography, the difference being the latitude of the strong flow. In contrast, the South region exhibits a significant southerly component to the flow.

Taken as a whole, the results of this work confirm that similar large-scale flow patterns as identified in the Pacific basin and North America are relevant to Norwegian extreme precipitation events. The overwhelming majority of events (more than 85%) are associated with ARs. Characteristic patterns conducive to anomalous moisture transport can be identified with significant time before the event (5 days), which is helpful to and can

improve forecasting. However, the identification of large-scale patterns 5 days before the event is insufficient to predict the precise location of subsequent extreme precipitation. Given the limited resolution of the reanalysis data employed, little can be said regarding the sensitivity of the mesoscale structure of precipitation, which ultimately defines the sensible weather impact. Future work will attempt to explore the direct link between ARs and flooding, landslides and avalanches associated with extreme precipitation in Norway.

Acknowledgements. We would like to thank Patrick Harr and Julian Quinting for providing the EOF/ fuzzy cluster script and Anne Fouilloux for her significant contributions regarding data acquisition and analysis. Funding has been provided by the Research Council of Norway in association with the FlomQ project under the ENERGIX program.

4

Decline in terrestrial moisture sources of the Mississippi River Basin in a future climate

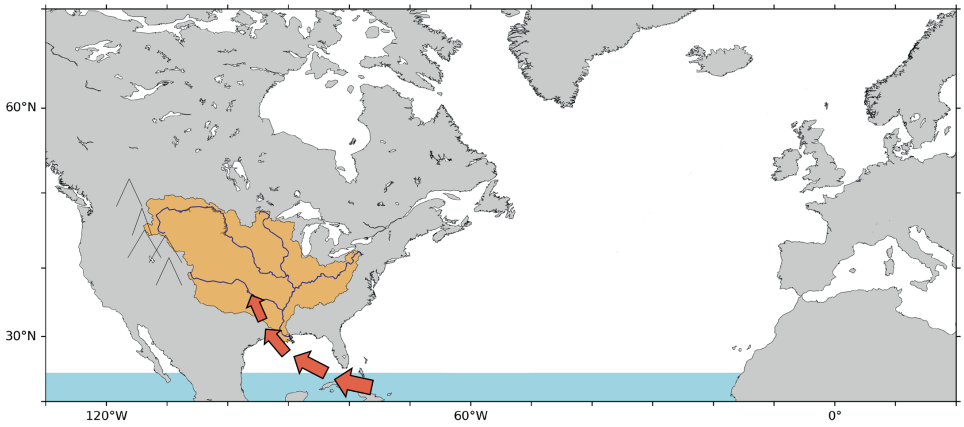

This Chapter is based on:
Benedict, I., van Heerwaarden, C. C., van der Ent, R. J., Weerts, A. H., and Hazeleger, W.: Decline in Terrestrial Moisture Sources of the Mississippi River Basin in a Future Climate, Journal of Hydrometeorology, 21, 299–316, 2020

Assessment of the impact of climate change on water resources over land requires knowledge on the origin of the precipitation and changes therein towards the future. We determine the origin of precipitation over the Mississippi basin using high resolution (~25 km) climate model simulations for present and future climate (RCP4.5). Moisture resulting in precipitation over the Mississippi basin is tracked back in time using Eulerian offline moisture tracking, in order to find out where this water originally evaporated (i.e. the moisture sources). We find that the most important continental moisture sources are the Mississippi basin itself and the area southwest of the basin. The two most relevant oceanic sources are the Gulf of Mexico/Caribbean and the Pacific. The distribution of sources varies per season, with more recycling of moisture within the basin during summer and more transport of moisture from the ocean towards the basin in winter. In future winters, we find an increase in moisture source from the oceans (related to higher sea surface temperatures), resulting in more precipitation over the Mississippi basin. In future summers, we find an approximately five per cent decrease in moisture source from the basin itself, while the decrease in precipitation is smaller (i.e. lower recycling ratios). The results here are based on one climate model, and we do not study low-frequency climate variability. We conclude that Mississippi's moisture sources will become less local in a future climate, with more water originating from the oceans.

4.1 Introduction

The atmospheric water budget is affected by climate change. Precipitation is expected to increase at high latitudes and around the equatorial band (Gimeno et al., 2012; Trenberth, 2011), and a reduction is expected in sub-tropical subsidence regions (Allen and Ingram, 2002). Changes in mean annual evaporation follow the changes in temperature (Held and Soden, 2006), with increasing evaporation rates over most of the oceans (Gimeno et al., 2012). Higher temperatures in a future climate also result in more atmospheric water vapor in the lower troposphere following Clausius-Clapeyron, amplifying the atmospheric water cycle (Held and Soden, 2006). Besides thermodynamic effects, changes in circulation patterns can affect the atmospheric water budget on a regional level. Both dynamic (circulation) and thermodynamic effects are relevant when considering moisture sources of a region, i.e. the evaporative sources resulting in precipitation over a defined area.

Hydrological basins are often used as study areas on a regional level, since changes in the atmospheric water cycle also influence discharge and soil moisture characteristics, which are important for water management. In addition, the origin of the precipitation, being continental or oceanic, can indicate the vulnerability of a basin to ongoing and future land-use changes. Furthermore, the location of the sources can also indicate whether there is a greater need to improve the model representation of ocean or land evaporation.

So far, moisture source regions are mostly determined for present climate (Algarra et al., 2019; Bosilovich and Chern, 2006; Bosilovich and Schubert, 2001; Brubaker et al., 2001; Dirmeyer and Brubaker, 1999; Knoche and Kunstmann, 2013; Sodemann et al., 2008; Stohl and James, 2005). Consequently, one of the remaining questions in atmospheric moisture transport was stated in the review by Gimeno et al. (2012): "How will climate change alter the location and significance of source regions and the transport of moisture from these toward continental areas in the future?" Here, we focus on the atmospheric water budget and the moisture sources of the Mississippi basin and how these are affected by climate change.

The Mississippi basin is the fourth-largest river basin in the world, and it contains one of the world's most productive agricultural regions (the Corn Belt). In addition, it is an important source of water to millions of people, as well as industry. Therefore, it is important to understand its hydrological cycle and the local variations therein. The precipitation budget of the Mississippi basin is influenced by moisture input from multiple drivers. Moisture is advected from the Pacific over the Western boundaries of the Mississippi basin, resulting in high precipitation amounts and snow over the Rocky Mountains, mainly in winter. At the southern boundary, moisture is advected from the warm tropical Atlantic, Caribbean and the Gulf of Mexico resulting in relatively wet conditions in the southeast. A large set of climate models indicates that in the future those wet regions (southeast and Rocky Mountains) get wetter (CMIP3; Seager et al. 2010 and CMIP5;

Seager et al. 2013). In summer time, moisture transport is related to the Great Plains low level jet, ranging from the Gulf of Mexico inlands (Algarra et al., 2019; Helfand and Schubert, 1995; Higgins et al., 1997). This supply of moisture, together with large surface fluxes results in convective precipitation in summer over the Mississippi basin.

In present climate, moisture sources and moisture recycling of the Mississippi basin is widely studied. First research was conducted by Benton et al. (1950), who studied the different (continental and maritime) air masses bringing precipitation over the river basin. Benton et al. (1950) concluded that 10% or less of the precipitation over the Mississippi had its evaporative sources from within the basin, where Brubaker et al. (1993) found recycled fractions ranging between 20% and 30% depending on the season. Later, Brubaker et al. (2001) determined from a long climatology (36 years) of warm-season precipitation that 32% of the moisture source originated from the Mississippi basin itself and about 20% from the Gulf of Mexico. Further, the establishment of anti-cyclonic flow around the Bermuda High, a high pressure system over the Atlantic during summer, lengthens the fetch of moisture sources from the Gulf of Mexico/Atlantic ocean into the Caribbean and Tropical Atlantic. In the project by Dirmeyer et al. (2009), a climatology of moisture sources per basin, including the Mississippi, were determined and visualized. Over time, other moisture tracking methods were suggested and applied to the Mississippi basin, for example the use of passive tracers (Bosilovich and Schubert, 2002; Bosilovich and Chern, 2006) and a Lagrangian tracking method (Stohl and James, 2005). The latter found similar moisture sources for the Mississippi basin as Brubaker et al. (2001). Recently, a moisture tracking model was used to explore the role of reduced moisture transport in drought propagation over North America (Herrera-Estrada et al., 2019).

All studies mentioned above assess the moisture sources and moisture recycling of the Mississippi basin/North America for present climate, because moisture tracking is mostly applied to atmospheric reanalysis datasets. However, reanalyses do not provide information on the future. As a consequence, one of the open questions in the field of atmospheric moisture transport is how moisture sources are affected by climate change (Gimeno et al., 2012; Guo et al., 2019). Findell et al. (2019) studied continental precipitation under rising temperatures on a global scale, and emphasised the need to further study regions such as the corn producing regions of North America, given their importance for agriculture. Gimeno et al. (2013) detected regions of continental precipitation which are vulnerable to changes in oceanic moisture sources (i.e. changes in evaporation). They selected regions where climate change will likely lead to an increase in evaporation minus precipitation (so-called hot spot regions) and performed forward tracking of moisture to identify which continental regions were affected by these hot spot source regions. Ideally, a tracking algorithm should be applied directly to simulations of future climate using a global climate model (Gimeno et al., 2013), which is what we do in this study.

We use 30-year high spatial resolution (~25 km) simulations of a global climate model for present and future climate (RCP4.5, Van Vuuren et al. 2011). We choose to use high-resolution global simulations as this benefits the representation of, amongst others, El Niño-Southern Oscillation (Shaffrey et al., 2009), the global water cycle (Demory et al., 2014), storm tracks (Hodges et al., 2011), and cyclones (Strachan et al., 2013). At the expense of the high resolution, the simulations have a limited simulation length (6 members of 5 years per period), and therefore we cannot study multi-decadal variability. We focus on the mean change of the different terms of the atmospheric water budget, and Mississippi's moisture sources. Our two main research questions are stated as follows: 1) How is the modelled atmospheric water budget over the Mississippi basin projected to change in the future? 2) How will climate change alter the relative contribution of the oceanic and terrestrial moisture source regions of the Mississippi basin?

We structure the Chapter as follows: Theory on atmospheric water vapor tracking is provided in Chapter 2. In the methodology (Section 4.2), we shortly describe the data from the climate model EC-Earth, the tracking model WAM-2layers and in the experimental set-up the evaporation recycling ratio is introduced. In Section 4.3, we validate precipitation and evaporation from EC-Earth and analyse how it is changing towards the future. In Section 4.4, we show and discuss the moisture sources of the Mississippi basin in present and future climate, and their seasonal variation. Finally, we discuss the methodology, and we end with a summary and conclusion.

4.2 Methodology

4.2.1 Model data: EC-Earth

We use simulations with high spatial resolution (Haarsma et al., 2013) from the atmospheric global climate model EC-Earth V2.3 (Hazeleger et al., 2010, 2012). More details on the simulations is given in Chapter 2 (Section 2.4.1). Here, the high resolution (T799) simulations are used for present (2002-2006) and future climate (2094-2098; RCP4.5).

We obtain the following variables: evaporation E(t,x,y), precipitation P(t,x,y), surface pressure p_s(t,x,y), the two horizontal wind components at 10 m u_{10}(t,x,y) and v_{10}(t,x,y), dewpoint temperature at 2 m T_d(t,x,y), specific humidity in the atmosphere q(t,x,y,p) and the two wind-components in the atmosphere u(t,x,y,p) and v(t,x,y,p). Specific humidity at the surface is derived from dewpoint temperature at 2 m and surface pressure. Surface data is available at a 3-hourly time interval and atmospheric data at a 6-hourly time interval. One important constraint of the EC-Earth data compared to reanalysis data is that the atmospheric variables are only saved at five pressure levels in the atmosphere, namely 850, 700, 500, 300 and 200 hPa.

4.2.2 Validation data: ERA-Interim, CMIP5 and observations

We compare E and P from EC-Earth with other model simulations of the Atmospheric Model Intercomparison Project (AMIP) CMIP5 (Taylor et al., 2012b) from 1979 to 2008 for present climate, and from 2070 to 2100 for future climate based on the RCP4.5 scenario. This project also includes simulations with EC-Earth, although with a different set-up and lower resolution than the climate runs we perform the tracking for. Furthermore, we use reanalysis data from ERA-Interim (1985-2014; Dee et al. 2011) and ERA-Interim/Land (1985-2010; Balsamo et al. 2013). We also include observational data of the Climate Prediction Center (CPC) 0.25° Daily US Unified Gauge-Based dataset version 1.0 (1985-2014; Higgins and Joyce. 2000) for precipitation and the GLEAM dataset (1985-2014; Martens et al. 2016) for evaporation. Details of the datasets are given in Chapter 2.

4.2.3 Tracking method: WAM-2layers

We use the Water Accounting Model-2layers (WAM-2layers; Van der Ent et al. 2010, 2014) to determine the moisture sources of the Mississippi basin. Information on the Eulerian WAM-2layers offline moisture tracking models is given in Chapter 2 (Section 2.5.2). The WAM-2layers model is modified in order to run it with input data from EC-Earth, which provides atmospheric data at five pressure levels. The validation of the adapted version of WAM-2layers applied to EC-Earth data is provided in Chapter 2 (Section 2.5.4).

4.2.4 Experimental set-up

Here we describe the analyses in the same order as we discuss the results. First, we compare monthly basin-averages of daily evaporation and precipitation from EC-Earth with CMIP5 model simulations, reanalyses, and observations. We indicate the inter-annual variance per model by showing the standard deviation of the monthly means per month, where we take the average of the standard deviations over all models for the CMIP5 ensemble. Variance between models, for the CMIP5 ensemble, is determined as standard deviation between each year for the different models and then averaging over the years.

Secondly, we quantify the spatial changes of E, relative humidity (RH) and P towards the future over Northern America. We determine if the change is statistically significant by bootstrapping the monthly averages per season (3 months per season times 30 years) to a sample of 1000. Then we calculate the 95% confidence intervals. If there is no overlap between the confidence intervals of the present and future variable, the change is deemed significant.

In this study, we are mostly interested in the moisture sources which result in precipitation over the Mississippi basin. To determine these moisture sources, moisture is tracked backward in time (Equation 2.12 in Chapter 2). We analyse the moisture sources per

season (DJF, MAM, JJA, SON), for present climate, future climate and the difference (Δ fu -pr). We determine the statistical significant differences in absolute moisture sources per season using bootstrapping and 95% confidence intervals (as described before). For further quantification, we determine the contribution of moisture source per geographical region. These regions are defined as follows: Mississippi basin itself, continental areas outside the basin, Pacific ocean, Gulf of Mexico/Caribbean and the Atlantic ocean (see Figure 4.1). To allow a fair comparison between present and future moisture sources, the sources are normalized with the area-averaged precipitation falling over the Mississippi basin in the respective period. We indicate the robustness of the relative sources with error bars, which show the 95% confidence intervals after bootstrapping 1000 realizations (Efron and Tibshirani, 1994) of the monthly average sources over the regions.

When tracking moisture backwards in time, we can determine the ratio between evaporation moisture source summed over the region (A) and the total evaporation summed over the region, which we call the evaporation recycling ratio ϵ_r:

$$\epsilon_r = \frac{\int_A \delta E_m \, dA}{\int_A \delta E \, dA} \tag{4.1}$$

The averaged evaporation recycling ratio is shown per month for present and future climate. To support the results, we include an extra analysis where we perform forward tracking to determine the moisture sinks (precipitation) from a selected source region (evaporation over the southern Great Plains and northeast Mexico). These results are discussed in Section 4.4.2.

4.3 Evaporation and precipitation in present and future climate

4.3.1 Comparison of EC-Earth with CMIP5 model results and observations

We first compare monthly basin-averages of daily evaporation and precipitation from EC-Earth with other model results (CMIP5 model means and ensemble mean), reanalyses and observational data (Figure 4.2).

For evaporation, we find a pronounced yearly cycle with smallest rates (~0.5 mm d^{-1}) and inter-annual variances in winter and largest rates (~3 mm d^{-1}) and inter-annual variances in summer. The variability among the CMIP5 models (black thin errorbars) is largest in summer, when absolute values are largest. We find higher evaporation values in October-May in EC-Earth compared to most other CMIP5 models, the CMIP5 ensemble mean, and observations. For all months (shown for April, July and October), the spread

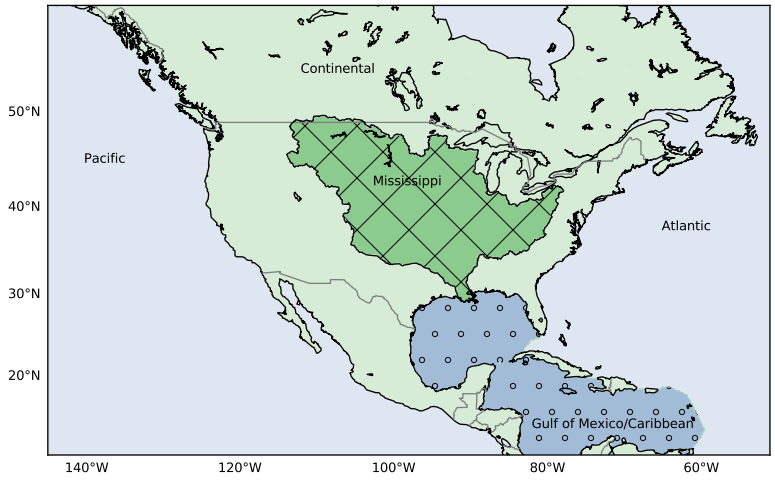

Figure 4.1: Map of the domain on which we performed the moisture tracking, including the source regions used for analyses: continental area outside Mississippi basin (green, not hatched), Mississippi basin (green, hatched), Pacific (blue left of the continent), Atlantic (blue right of the continent, including Hudson Bay) and Gulf of Mexico/Caribbean (blue dotted).

because of inter-annual variability in EC-Earth falls within the possibilities of CMIP5 output given by the model means (grey dotted lines).

In a future climate, we find increased values of evaporation in winter and spring (~0.2 mm d^{-1}) using EC-Earth. Increased evaporation rates in spring and summer are found by comparing the ensemble mean of historical AMIP CMIP5 simulations with the ensemble mean of future (RCP4.5) AMIP CMIP5 simulations. Ferguson et al. (2018) performed a similar analysis using the coupled runs from CMIP5 and the future simulations based on the RCP8.5 scenario, and found significant increases for evaporation in every month of the year except for July and August.

Furthermore, we compared the spatial pattern of evaporation simulated by EC-Earth over the whole domain with the reanalysis product ERA-Interim (the GLEAM product only provides evaporation over land, and is therefore not useful to do a spatial comparison). Over land, EC-Earth and ERAI are very comparable, with a similar spatial distribution (not shown). Over the ocean, evaporation in EC-Earth is higher over the Gulf of California, Gulf of Mexico and the Gulf Stream. It should be noted that EC-Earth has fixed SSTs and only simulates from 2002-2006, which makes the comparison non-trivial. Within all models, we find high daily precipitation values in the beginning of summer, which is mainly related to convective precipitation, and lower values of daily precipitation in winter (Figure 4.2b). There is a large variability in precipitation within the model means of CMIP5, in summer ranging from 1.5 mm d^{-1} to 4 mm d^{-1} (grey dotted lines). Precipi-

tation simulated by EC-Earth falls mostly within this spread of model means, except for April and October. We find the peak in precipitation in May and June for CMIP5, CPC, and ERA-Interim/Land whereas precipitation from EC-Earth peaks in April and May, falling outside the variability. However, the inter-annual variance from EC-Earth always overlaps with the inter-annual variance and model variance around the CMIP5 ensemble mean. The higher values for precipitation in winter and spring in EC-Earth compared to most other models were also found for evaporation. The model mean precipitation of the EC-Earth AMIP CMIP5 runs shows a similar pattern in precipitation, and evaporation, as the high-resolution simulations used in this study (not shown).

In a future climate with EC-Earth, higher precipitation amounts over the Mississippi are simulated in winter and spring (an increase of ~0.5 mm d^{-1}). In July and August a decrease in precipitation over the basin is found towards the future. Precipitation from the ensemble mean of the CMIP5 future simulations is in every month higher than the ensemble mean from CMIP5 for the present (Figure 4.2b). The study by Ferguson et al. (2018) found a significant increase in precipitation over the Mississippi basin from November to May using the coupled runs from CMIP5 and the RCP8.5 scenario for future simulations.

Despite the biases in precipitation in EC-Earth, the changes towards the future still contain valuable information, as studies show that there is a weak or non-existent relation between obvious metrics of observable quantities and projections (Knutti et al., 2010). In the next Section, we will focus on the spatial changes of components of the atmospheric water balance towards the future.

4.3.2 Spatial changes in evaporation and precipitation in EC-Earth

In simulations of future climate with EC-Earth (2094-2098; RCP4.5) we find an increase in 2 m temperature of 2.5°C to 3°C over the ocean, and 3°C to 4°C over land, with the largest increases in the northern parts of the domain (not shown). Because of these higher temperatures, and an increase in evaporation in general, larger amounts of column integrated water vapor (S) are found over the whole domain and again especially in the northern parts.

We show the spatial distribution of the change in evaporation, relative humidity and precipitation towards the future for winter (DJF) and summer (JJA) in Figure 4.3. Over the oceans, a general increase in evaporation is projected for the future, with locally increases up to 50 mm $month^{-1}$, for example over the Gulf Stream. Especially in winter (DJF) and autumn (SON, not shown) evaporation also increases over the southern parts of the domain, including the Gulf of Mexico (Figure 4.3a). This increase in evaporation over the ocean is the result of an increase in saturated vapor pressure, which is driven by an increase in SST, and a relative humidity that significantly but unsubstantially changes towards the future (0-2 %, Figure 4.3b).

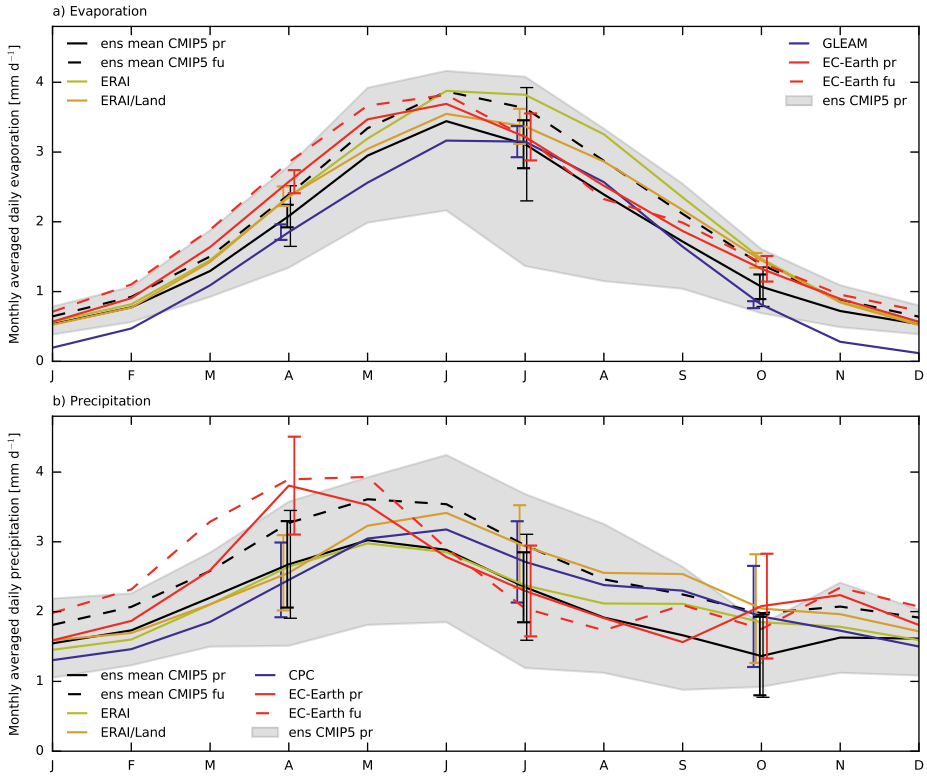

Figure 4.2: Monthly averages of a) basin-averaged daily evaporation [mm d^{-1}] and b) basin-averaged daily precipitation [mm d^{-1}] over the Mississippi basin. The grey shading denotes the AMIP CMP5 1979-2008 coverage of model means around the ensemble mean (black line). Additional plotted data includes: ensemble mean from CMIP5 future RCP4.5 (2070-2100; black dashed), CPC 1985-2014 precipitation and GLEAM 1985-2014 evaporation (blue), ERA-Interim 1985-2014 (yellow), ERA-Interim/Land 1985-2010 (brown), EC-Earth present (6 x 2002-2006; red solid line) and future climate (6 x 2094-2098; red dashed line). The errorbars indicate the standard deviation between the monthly values (inter-annual variance), in the corresponding color. We only show the errorbars for the present day datasets (observations, EC-Earth pr, AMIP CMIP5 pr and ERAI/Land) for the months April, July and October. The variance around ERAI is comparable to ERAI/Land and not shown. The thin black errorbar around the ens mean of AMIP CMIP5 present indicates the standard deviation in the model spread.

In contrast to oceans which provide an infinite source of water to evaporate, land evaporation is limited by soil moisture and a rise in temperature does not automatically imply an increase in evaporation. We find that soil moisture availability limits evaporation in winter, as the change in evaporation and relative humidity are spatially correlated, both positive in the North and both negative in the South-West (Figure 4.3a and b). In the North (over the Mississippi basin), an increase in evaporation combined with an enhancement in relative humidity points to an increase in the supply of water (Van Heerwaarden et al., 2010), thus an increase in soil moisture. In the South-West, a decrease in evaporation leads to an increase in sensible heat flux, which heats up the boundary layer and which decreases the relative humidity. It should be noted that other aspects like frozen ground, snow cover and vegetative seasonality can also influence the relation between soil moisture and evaporation in winter, but are not assessed in this study.

The same signal with decreased evaporation rates and decreased relative humidity is found in spring and summer over Mexico (Figure 4.3d and e). This decrease in evaporation towards the future is also found by Seager et al. (2007), using a large suite of climate models. In summer (JJA) over the Mississippi basin, except for the north-western corner, an increase in evaporation corresponds with a decrease in relative humidity. Here, soil moisture may not be the limiting factor and the increase in evaporation could be mainly related to an increase in temperature (highest increases of temperature were also found in the northern parts). If increases in temperature dominate over increases in humidity, relative humidity will decrease (Figure 4.3e).

For precipitation, we find an increase in winter and spring over the Mississippi basin (Figure 4.3c and 4.2b), especially in the central and eastern part of the basin. The strongest increase in precipitation in winter outside the Mississippi basin occurs along the North-West coast and the strongest decrease outside the Mississippi basin over the South Pacific and southeastern North America and Mexico. In summer, we find a slight decrease in precipitation over the Mississippi basin (Figure 4.2b and 4.3f). The most obvious positive change in summer (JJA) is found over the tropical Pacific with much higher precipitation rates in future, while over the Caribbean a negative change of precipitation to the future is found.

Additionally, we also find a clear dipole of positive and negative changes in $\boldsymbol{E}$ and $\boldsymbol{P}$ over the Northern Atlantic ocean. This has been attributed to a too far North location of the Gulf Stream in the ECHAM5/MPI-OM model (Sterl et al., 2008), which is used to determine the SST projections of the EC-Earth future simulations. Furthermore, the changes in circulation (wind) over North America to the future are very small (not shown), except for JJA where we find a strengthening of the circulation over central North America, which is discussed further in Section 4.4.2.

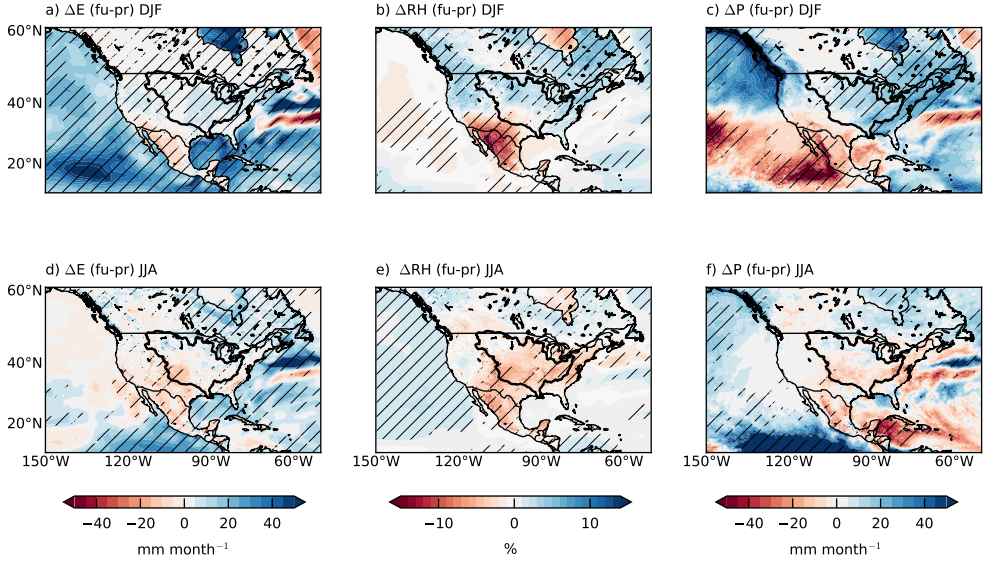

Figure 4.3: Spatial patterns of the change in EC-Earth RCP4.5 (a,d) evaporation ΔE (future - present) in mm month^{-1}, (b,e) relative humidity ΔRH (future - present) in %, and (c,f) precipitation ΔP (future - present) in mm month^{-1} for (a-c) DJF and (d-f) JJA. Significant differences are indicated with hatching.

4.4 Moisture sources of the Mississippi basin in present and future climate

4.4.1 Seasonal variability of the moisture sources in present climate in EC-Earth

We show the moisture sources (E_m) of the Mississippi basin in present climate averaged per season in Figure 4.4 (left column). The amount of precipitation occurring over the river basin is indicated in the titles. We find that the most important continental moisture sources are the Mississippi basin itself and the continental area southwest of the basin. The most important oceanic sources are the Gulf of Mexico and Caribbean and the (South) Atlantic and (East) Pacific. In the (East) Pacific ocean, the sources are mainly found around the Gulf of California.

There is a large seasonal variation in the moisture sources. In winter (DJF), the moisture sources are mostly located over the oceans, because evaporation over the oceans is much larger than over land during winter. Moisture is transported with the westerlies from the Pacific towards the Mississippi basin, and with an anti-cyclonic flow (Bermuda high)

and LLJ from the Atlantic and Gulf of Mexico and Caribbean towards the Mississippi basin. In spring (MAM), the moisture sources over land increase as the increasing solar radiation drives the evaporation. This increase in sources over land, together with supply of moisture from the oceans, results in high precipitation amounts in spring over the Mississippi basin (~100 mm month^{-1}), although spring precipitation is overestimated in EC-Earth compared to observations and other simulations (Fig. 4.2b). In the summer (JJA), the Pacific (Gulf of California) moisture sources substantially decrease, resulting in less precipitation over the Mississippi basin. The source contribution from the Gulf of Mexico is similar in MAM as in JJA. During this warm season, the Bermuda High is shifted westward enhancing the Great Plains LLJ which results in large amounts of moisture being transported from the Gulf of Mexico as far as the northeast USA (Algarra et al., 2019).

Dirmeyer and Kinter (2010) studied the moisture sources of the Midwestern region of the United States during late spring and summer (May-June-July). The spatial distribution of moisture sources (Fig. 4 in Dirmeyer and Kinter 2010) is comparable to our study. However, their contribution of continental sources is larger, which could be caused by their study region which is smaller and located more land-inwards. Evaporation rates over land peak during summer and most precipitation in the Mississippi basin is convectively driven (Benedict et al., 2019b), i.e. moisture is recycled within the river basin. The evaporation recycling ratio as defined in Equation (4.1) is around 20% in summer (compared to 10% in winter), which means that 20% of the evaporation occurring over the Mississippi basin results in precipitation within the same basin. In SON, sea surface temperatures are still high, resulting in high oceanic evaporation rates. However, land evaporation decreases compared to summer, and therefore the main source of moisture for precipitation over the Mississippi basin in SON is the Gulf of Mexico (Figure 4.4j).

To summarize, we find that the moisture sources are varying throughout the seasons, with high recycling rates over land during MAM and JJA, and a dominant role of advection of moisture from the oceans to the Mississippi basin during SON.

4.4.2 Moisture sources in a future climate

The projected moisture sources of the Mississippi basin in a future climate are shown per season in Figure 4.4 (middle column) and the difference between present and future in the right column, where significant differences are indicated with hatching. The future seasonal spatial patterns of moisture sources are similar to the spatial patterns in present climate, but there are differences in the strength of the sources, especially in winter (DJF) and summer (JJA). Over the Gulf of Mexico and the Gulf of California, the moisture source is strongly increased in winter from maximum source values in present climate of 20 mm month^{-1} to values of 30 mm month^{-1} in a future climate (Figure 4.4c). This is related to an increase in evaporation over the oceans in winter (Figure 4.3a), and results

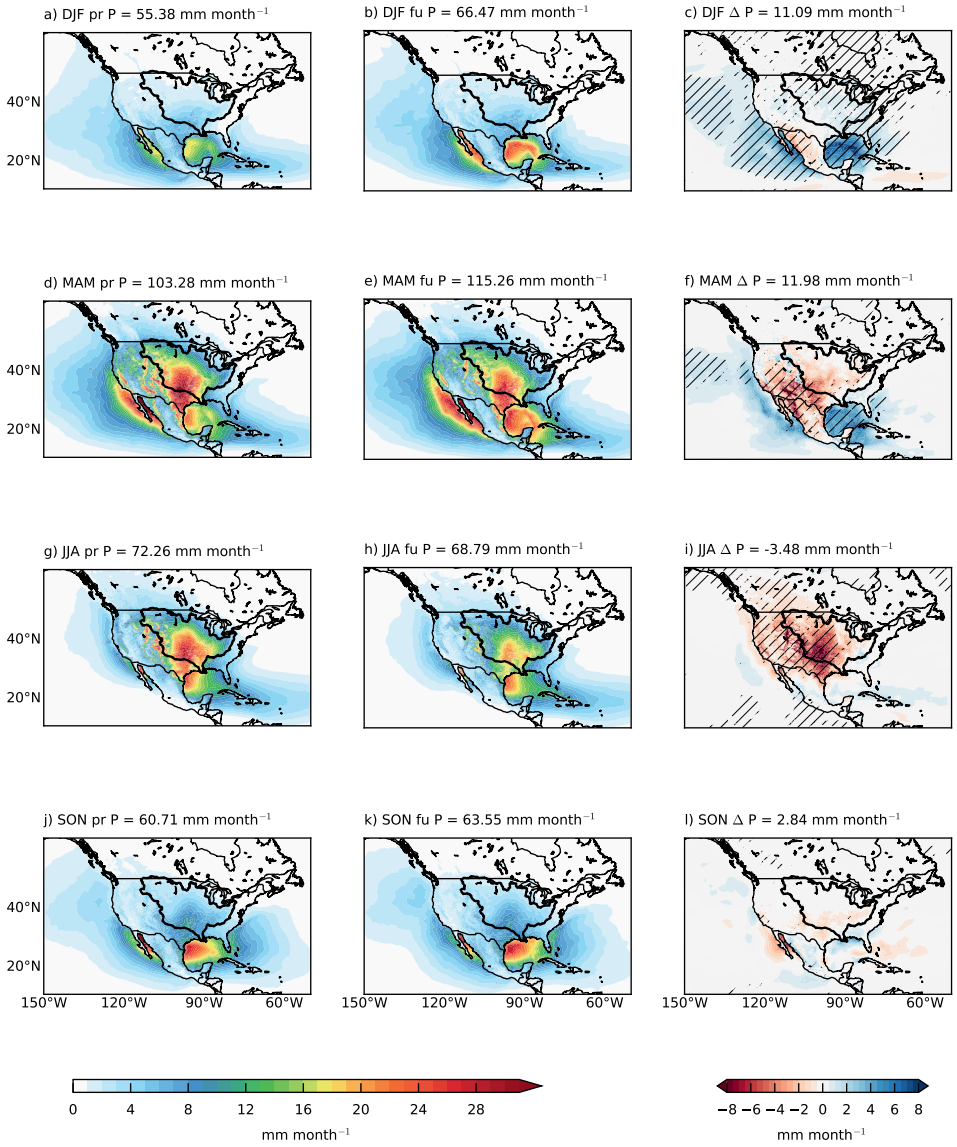

Figure 4.4: The absolute moisture sources, E_m, of precipitation over the Mississippi basin (basin indicated with thick black line) in present and future climate for (a-c) DJF, (d-f) MAM, (g-i) JJA and (j-l) SON in mm month^{-1} from EC-Earth. Left figures show the sources for present climate (pr), middle figures for future climate (fu), and right figures for the difference (Δ) fu-pr. The statistically significant differences are indicated with hatching in the (Δ) fu-pr plots. The monthly averaged precipitation over the Mississippi basin is indicated in the subplot titles.

in an increase in precipitation over the Mississippi basin in winter of 10 mm month^{-1}. In MAM, an increase in moisture source of 8 mm month^{-1} over the Gulf of Mexico is found, which can also be related to an increase in precipitation over the Mississippi basin. In summer (JJA), we find a decrease of moisture source over continental areas of around 10 mm month^{-1}, both within the Mississippi basin and south and west from the river basin. However, we do not find such a large decrease in evaporation in this period (Figure 4.3b). In autumn (SON), there are no large differences in moisture source and precipitation between present and future climate.

If in a future climate more or less precipitation over the Mississippi basin occurs, more or less moisture will be tracked. Therefore, we normalize the absolute sources with precipitation over the Mississippi basin ($\frac{\int_A \delta E_m \, dA}{\int_{dA} \delta P dA}$) and show the relative contribution per region and season in Figure 4.5, and the robustness with 95% confidence intervals obtained after bootstrapping (Efron and Tibshirani, 1994) the monthly average sources over the regions. We also show the yearly averaged relative contribution of all land regions and all ocean regions, and thereby we include the yearly average relative moisture sources which leave the domain over the four boundaries (North, East, South, West).

Averaged over all seasons (Figure 4.5f and 4.5g and Table 4.1), we find a significant decrease of relative moisture sources over land from 33% in present climate to 27% in a future climate. The relative contribution of oceanic moistures sources slightly increases from 44% to 47% (Figure 4.5g). The rest of the moisture is transported out of the domain. If we focus on the different seasons (Figure 4.5), we find that in DJF and MAM the relative moisture source contribution from the Gulf of Mexico and Gulf of California (Pacific) is slightly increased. These slight increases in moisture sources over the ocean lead to an increase in precipitation over the Mississippi basin. The contribution of terrestrial moisture sources over land is declined for all seasons. For the continental areas outside the Mississippi basin this decrease can be mostly attributed to MAM and JJA, and for a lesser extent to DJF. For the Mississippi basin the largest decline in relative moisture source is found in MAM and JJA.

A different way to show the contribution of sources over land (Mississippi basin) to precipitation over the Mississippi basin is the evaporation recycling ratio. Figure 4.6 shows the monthly-averaged evaporation recycling ratio, as defined in Equation (4.1), for the present and future climate. This evaporation recycling ratio is not directly comparable to the recycled precipitation fractions mentioned in the Introduction, which are determined using forward moisture tracking. We find a lower yearly averaged evaporation recycling ratio in future (0.12) compared to present (0.14). For both periods, we find larger evaporation recycling ratios in summer compared to winter. In summer, land evaporation is highest and triggers local convective precipitation, and therefore recycling of moisture within the basin, while in winter relatively more moisture is advected into the Mississippi basin. In the simulations of future climate, we find that the evaporation recycling ra-

Table 4.1: Relative contribution of moisture sources per region contributing to precipitation over the Mississippi basin [%] from EC-Earth averaged over 30 years (6 members from 2002-2006 for present climate and 6 members from 2094-2098 for future climate).

Relative source in %		EC-Earth pr 6 x 2002-2006	EC-Earth fu 6 x 2094-2098
Terrestrial	Mississippi basin	13.2	10.9
	Continental (not Mississippi)	20.0	16.4
Oceanic	Atlantic	8.1	8.1
	Gulf of Mexico/Caribbean	14.5	15.5
	Pacific	21.6	23.1
Outflux over boundaries	East	5.2	5.6
	West	13.4	15.9
	North	0.3	0.4
	South	3.6	3.8

tios are significantly lower in April to July and October compared to present conditions, consistent with our previous results (Figure 4.5).

There are two hypotheses that can explain the decrease in (relative) terrestrial moisture source over land. Either there is less moisture to evaporate over land (drier soils in a future climate), or the evaporated water rains out downstream of the Mississippi basin. For the first hypothesis, we expect less evaporation in a future climate in the months (JJA) where the moisture source over land has decreased. We do find a decrease in evaporation in JJA over the Mississippi basin (a decrease of 0.92 mm month^{-1} averaged over the basin), but this decrease is smaller than the decrease in moisture source over the Mississippi basin (3.39 mm month^{-1}). Therefore, the decrease in evaporation cannot explain the decrease in moisture source.

To evaluate the second hypothesis, we use forward tracking to determine the precipitation sinks related to the land region where we find a decrease in JJA moisture source (southwest Mississippi basin and southwest of the Mississippi basin, see Fig. 4.4i). We performed forward tracking from May to September, as these are the months during which we find the (largest) decrease in moisture source from land. Figure 4.7 shows the precipitation sinks, for both present and future climate, and the difference between future and present. We find a decrease in tracked precipitation south of 40° north, which was also found in the spatial changes of precipitation in Figure 4.3d. We also find a small increase in tracked precipitation in the north within the Mississippi basin and north of the river basin, and also in the region of Florida (Figure 4.7f). This can be related to an increase in the moisture fluxes over mid North America in the future (integrated moisture fluxes indicated with arrows in Figure 4.7def). We also find an increase in southerly winds at

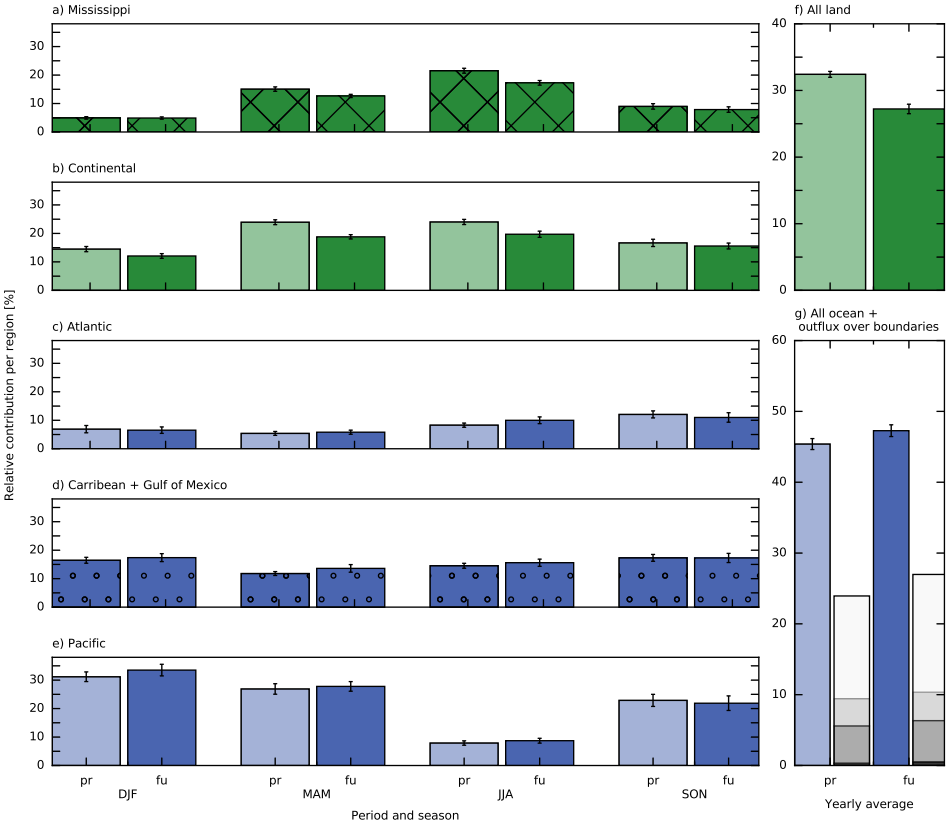

Figure 4.5: Relative contribution of moisture sources per region contributing to precipitation over the Mississippi basin ($\frac{\int_A \delta E_m \, dA}{\int_{dA} \delta P dA}$). Seasonal Mississippi basin precipitation totals are included as subplot titles in Fig. 4.4. The moisture source contribution per region is shown for each season (DJF, MAM, JJA and SON) for present and future climate from EC-Earth. The area covering the Gulf of Mexico and Caribbean is indicated in Figure 4.1. We also show the yearly average relative contribution for (f) all land and (g) all oceans and the fluxes over the boundaries of the domain for North-East-South-West from black to white colors. These numbers are also presented in Table 4.1. The errorbars indicate the 95% confidence intervals after bootstrapping the monthly averages.

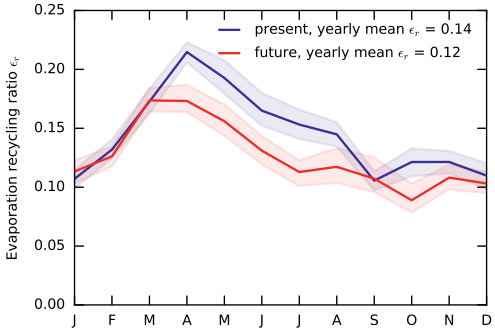

Figure 4.6: The monthly averaged evaporation recycling ratio $\epsilon_r = \frac{\int_A \delta E_m \, dA}{\int_A \delta E \, dA}$ for the Mississippi basin in present and future conditions according to EC-Earth. The shaded bands indicate the 95% confidence intervals after bootstrapping the monthly average ratios.

10m and at 850 hPa in the same area in the future (not shown), indicating a strengthening of the circulation in the summer. The Great Plains LLJ is the most important moisture transport mechanism in summer in mid North America, and previous studies reported a strengthening of the Great Plains LLJ because of a westward shift of the Bermuda high in April-May-June in the future (Cook et al., 2008; Seager et al., 2014). To summarize, our second hypothesis is confirmed as we find that more moisture is transported out of the river basin in the future.

4.5 Discussion on methodology

We used the Eulerian water tracking model WAM-2layers (Van der Ent et al., 2010, 2014) to determine the moisture sources of the Mississippi basin. There are also other approaches to determine the moisture sources of a region, such as online water vapor tracers (Knoche and Kunstmann, 2013; Singh et al., 2016) and Lagrangian tracking (Stohl and James, 2005; Sodemann et al., 2008; Dirmeyer and Brubaker, 2007). Online tracking will provide the most realistic moisture sources as the tracking is performed on full model resolution, but it is computationally very expensive and backward tracking is impossible. The performance of offline Lagrangian tracking depends on the amount of parcels that are tracked, which relates to the computational expense of the tracking, with longer time series being computationally more expensive. This is also the case for Eulerian tracking. In the study by Van der Ent and Savenije (2013) the three approaches mentioned were compared for moisture recycling over the Volta region (West Africa). They found only one percent difference in recycling ratio determined with the online method and the WAM-2layers method with ERA-Interim data (Table 2 in Van der Ent and Savenije 2013). We show in Chapter 2 that WAM-2layers can also be applied to global climate

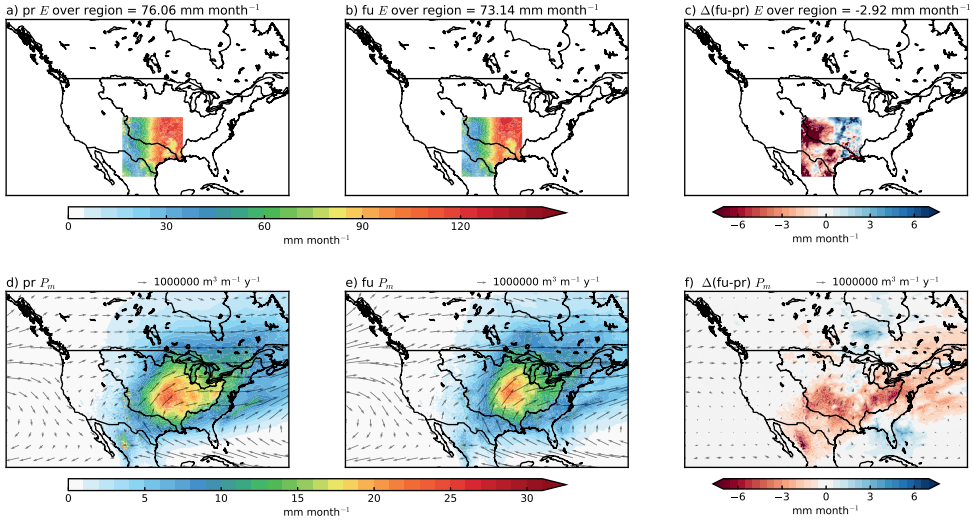

Figure 4.7: Forward tracking of the May-September evaporation over the tracked subdomain (107° to 95° west, 25° to 40° north, land-only) for a) present, b) future and c) Δ fu-pr. The monthly area-averaged evaporation over the tracked domain is indicated in the titles in mm month^{-1}. Lower figures show in shading the tracked precipitation P_m and in arrows the moisture fluxes for d) present, e) future and f) Δ fu-pr. The arrows indicate the integrated moisture fluxes over the whole atmosphere.

simulations with higher horizontal resolution, but less information in the vertical, compared to ERA-Interim (Table 2.1 in Chapter 2). By performing a spline interpolation on the moisture fluxes we found an overall better representation of the seasonally varying Great Plains LLJ. We conclude that an Eulerian approach is an appropriate method to perform moisture tracking for climate simulations, over longer time periods (2 x 30 years), and over a large region (North America) using high-resolution data. Nevertheless, a comparison of moisture sources determined with different datasets and tracking approaches is recommended, for example such as done by Hoyos et al. (2018).

The horizontal resolution of the data used here is ~ 25 km, and there are only a few climate models which have run simulations for both present and future climate at such a high spatial resolution, and for a time period of 30 years (Murakami et al., 2015). However, for present climate only, studies have been performed at such high resolution to assess the atmospheric water transport, however without moisture tracking. Demory et al. (2014) found an increase in transport of water from oceans to land with higher spatial resolution simulations (from 135 to 25 km and from 270 to 60 km), as more precipitation will occur over land than over the ocean, indicating that the partitioning of moisture sources changes from local to more non-local moisture sources. Nevertheless, in spectral models such as

EC-Earth, it was found that the moisture advection to land increases less with resolution (Vannière et al., 2018). We use similar high resolution simulations as the study from Demory et al. (2014) and Vannière et al. (2018) but expand the sensitivity of the moisture sources towards the future for the Mississippi basin, concluding that moisture sources over the ocean increase and moisture sources over land decrease. This indicates that both increased spatial resolution, as well as future projections, will lead to an increase in moisture transport from oceans to land, affecting the water resources of river basins. Findell et al. (2019) performed moisture tracking on low resolution earth system model simulations of historical and future climate and found also an increase in oceanic sources resulting in continental precipitation. The robustness of this increase in oceanic sources can be assessed when more high-resolution simulations for future climate are available, for example within the Horizon 2020 project PRIMAVERA (`https://www.primavera-h2020.eu/`) and the CMIP6-endorsed HighResMIP (Haarsma et al., 2016).

The results presented in this study are based on one model and 30-years of simulations for both present and future climate. Due to this finite length we do not study multi-decadal variabilities, but focus instead on the mean change in moisture sources under climate change.

The EC-Earth model is constrained with sea surface temperature, limiting the variability of the simulations. While we capture some inter-annual variability (6 x 5 years), we do not analyse this in detail. From previous studies we know that the moisture sources and/or regional recycling can differ substantially from year to year (Dirmeyer and Brubaker, 1999; Bosilovich and Schubert, 2001), and that multi-decadal and inter-decadal (such as El Niño) variability can produce large variations in the precipitation over the Mississippi basin. It would be of interest to further study the variability in moisture sources in combination with these large-scale inter-annual variations, to better predict and project the moisture sources of the Mississippi. However to do so, longer simulations and more ensembles are needed, which are currently unavailable at the spatial resolution of our dataset. Simulations covering a longer time period can also be used to understand moisture sources under extreme or compound events (such as compound fluvial and coastal flooding), and especially how these sources of extreme events are affected by climate change. Lastly, although this study focuses on the moisture sources of the Mississippi basin, the methodology used in this study can also be applied to other regions of interest.

4.6 Summary and conclusions

We study the changes in moisture sources, resulting in precipitation over the Mississippi basin, under climate change. To do so, we make use of a set of high spatial resolution (~25 km) simulations of 30-year present and 30-year future climate from EC-Earth. We use the output of one climate model and only focus on the mean change towards the future.

We first validate precipitation and evaporation from EC-Earth with model simulations and observations. Evaporation from EC-Earth falls within the variability of CMIP5 model mean simulations, where precipitation from EC-Earth is positively biased in spring. Secondly, we study the local spatial changes of evaporation, relative humidity and precipitation over North America under climate change (Figure 4.3). Evaporation is increasing over large parts of the domain, and especially over the southern part of the oceans. This increase is related to an increase in SST and an almost constant relative humidity. In summer, we find a decrease in evaporation over southwest North America, probably because of drier soils. This also results in lower relative humidity and less precipitation in this region. Precipitation over the Mississippi basin increases towards the future in winter and decreases in summer (Figure 4.2 and 4.3).

Thirdly, we determine the moisture sources of the Mississippi basin under present and future climate conditions using an adapted version of the Eulerian WAM-2layers tracking model which fits the EC-Earth climate simulations, and which was validated using ERA-Interim reanalysis data (Table 2.1 in Chapter 2). Averaged over the 30 years of present climate, we find a contribution of moisture sources from continental (land) origin of 33% and from oceanic origin of 44%, where the rest is transported out of the domain. The most important continental moisture sources are the sources within the Mississippi basin itself and the continental area southwest of the basin. The most important oceanic sources are the Pacific and Gulf of Mexico and Caribbean (Figure 4.4 and 4.8). The sources are seasonally varying, with more recycling of moisture within the river basin in summer and more transport of moisture from the ocean towards the Mississippi basin in winter. In the future, the moisture source contribution from oceanic origin increases from 44% to 47%, and the contribution from continental origin decreases from 33% to 27%. The increase in moisture source from the ocean is small and mainly found in winter (higher SST leads to higher evaporation rates), especially over the Gulf of Mexico, and results in more precipitation over the Mississippi basin in winter (Figure 4.4). In summer, we find a significant decrease in moisture sources from the basin itself (i.e. lower recycling ratios within the basin, Figure 4.6) and from the continental areas outside the basin (Figure 4.8), although precipitation is not decreasing. We find that higher moisture fluxes over mid North America in the future result in a larger transport of moisture outside of the basin.

We conclude that the moisture sources of the Mississippi basin in the future 1) enhance over the oceans in winter, resulting in more future winter precipitation and 2) show a relative decline over terrestrial areas in summer, indicating that land-surface properties will have relatively less impact on precipitation over the Mississippi basin in the future.

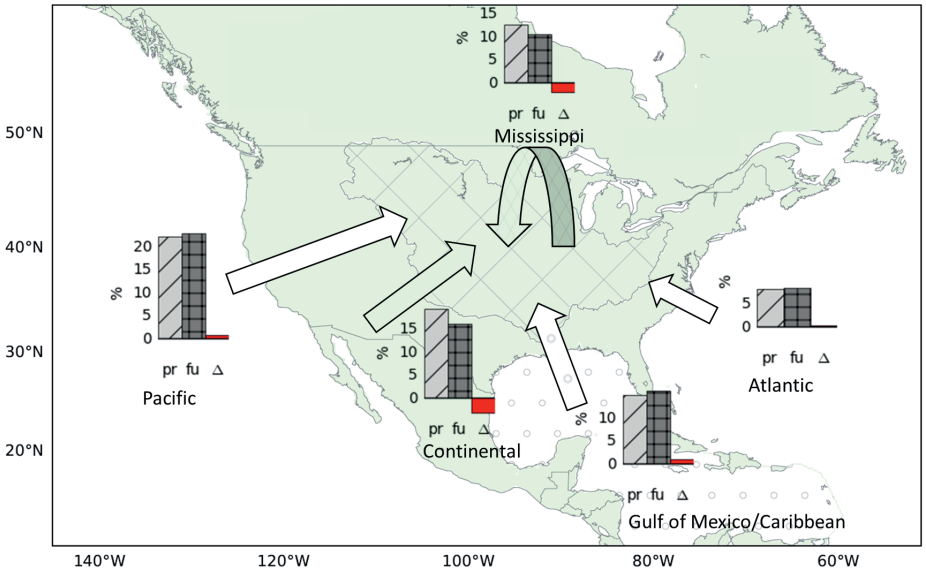

Figure 4.8: Mean annual moisture transport to the Mississippi basin indicated with arrows (drawn to scale). The arrow indicates if the origin is oceanic (white) or continental (green). The barplots indicate the relative contribution of evaporation to precipitation over the Mississippi basin for present (pr), future (fu), and the difference between present and future (Δ fu-pr). The numbers in these figures are also given in Table 4.1. The differences between present and future are significant for the terrestrial sources, but not significant for the oceanic sources.

Acknowledgements. We acknowledge ECMWF for supplying ERA-Interim data through their server at `http://www.ecmwf.int`. The EC-Earth data is available upon request by the author. The original WAM-2layers code is available on Github (`https://github.com/ruudvdent/WAM2layersPython`), as well as the adapted version used in this study (`https://github.com/Imme1992/moisture\_tracking\_mississippi`). The simulations are performed on the Cartesius supercomputer from SURFsara (project number SH-312-15). Imme Benedict and Ruud van der Ent both acknowledge funding from the Netherlands Organization for Scientific Research (NWO), for respectively project number 869.15.004 and 016.Veni.181.015.

5

Anomalous moisture sources of the Rhine basin during the extremely dry summers of 2003 and 2018

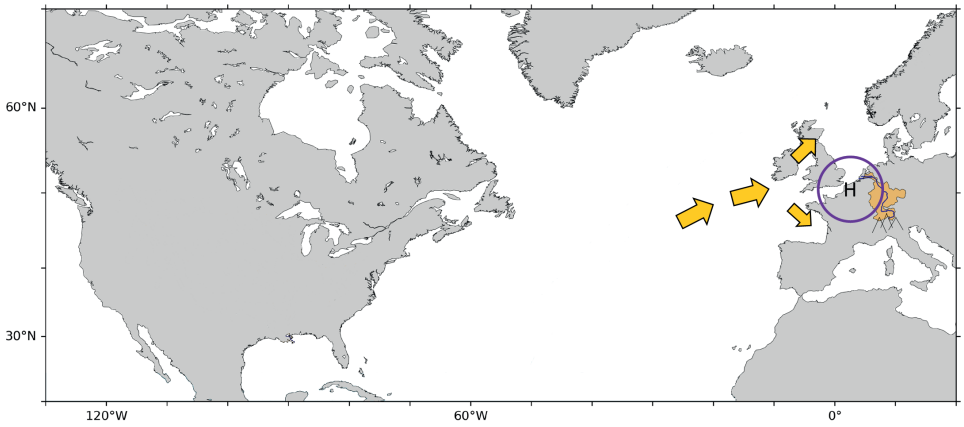

This Chapter is based on:
Benedict, I., van Heerwaarden, C. C., van der Linden, E. C., Weerts, A. H., & Hazeleger, W.: Anomalous moisture sources of the Rhine basin during the extremely dry summers of 2003 and 2018. *Under review.*

Droughts can be studied from an atmospheric perspective by analysing large-scale dynamics and thermodynamics, and from a hydrological perspective by analysing interaction of precipitation, evaporation, soil moisture and temperature at the land-surface. Here, we study it from both perspectives, and assess the moisture (evaporative) sources of precipitation in the Rhine basin during the exceptionally dry summers of 2003 and 2018. We use ERA5 re-analysis data (1979-2018) and the Eulerian moisture tracking model WAM-2layers in order to determine the moisture sources of the Rhine basin. During an average summer, these evaporative sources are mostly located over the Atlantic Ocean, and there is a large contribution from continental evaporation, mostly from regions west of the Rhine basin. Both in 2003 and 2018 the absolute moisture source contribution declined over the ocean. In both years the anomalous moisture fluxes over the boundaries of the Rhine basin are mainly a result of anomalous wind and not because of anomalous moisture advection by the mean wind. Due to high pressure (blocking) over Europe, moisture is transported from the ocean with anticyclonic flow around the Rhine basin, but not into the basin. In 2018, unlike 2003, moisture is transported from the east towards the basin as a result of the anticyclonic flow around the Scandinavian blocking. The large-scale synoptic situation during the summer of 2018 was exceptional, and very favourable for dry conditions over the Rhine basin. Although blocking also occurred in 2003, the exact synoptic conditions were less favourable to dryness over the Rhine basin. In 2003 however, the recycling of moisture within the basin was much lower than the climatology and 2018, especially in August, possibly indicating the drying out of the soil resulting in the second heatwave in August 2003. To conclude, although the summer of 2003 and 2018 were both exceptionally dry, their characteristics in terms of moisture sources and recycling, and thereby their dependence on the large-scale circulation and land-atmosphere interactions, were found to be very different. It is therefore imperative that droughts are also studied as individual events to advance understanding of complex interactions between the large-scale atmospheric processes and the land surface.

5.1 Introduction

Drought is a multidisciplinary problem with large societal and economic impact. Recent examples are the drought in 2003 in western Europe resulting in reduced crop yields, forest fires, overheated power plants, and most striking, excess death (Fischer et al., 2007b; Schär and Jendritzky, 2004). During the dry summer of 2018 52% of the agricultural region over western Europe suffered from severe-to-extreme drought (Toreti et al., 2019).

The multidisciplinary aspect of drought is highlighted when explaining different drought perspectives. The climate perspective, to start with, focuses on synoptic situations such as atmospheric blocking conditions or other large-scale dynamic features (e.g. weather regimes, blocking indices, wave patterns), in relation to the climatology. The meteorological view on drought is a lack of (or less-than-normal) precipitation, or a large imbalance between precipitation and evaporation. A hydrologist will describe drought as a lack of water in the soil-vegetation system, or as low river discharge. Lastly, drought from an ecological and agricultural perspective would focus on affected nature areas, forest fires, and reduced crop yields. These perspectives can be studied on a global scale, but are often also analysed for specific regions. The selection of these regions depends, again, on the different perspectives. Where a hydrologist probably focuses on a river catchment, an ecologist would rather look to an area with similar vegetative conditions.

Here, we aim to combine the view of the climate/meteorologist and the hydrologist. We do so, by analysing the anomalous moisture sources, which are evaporative sources of precipitation over a region, of the Rhine river basin during the extremely dry summers of 2003 and 2018. We focus on the Rhine basin as hydrological catchment, which was clearly affected in 2003 and 2018, and where the lack-of-precipitation can also be translated to river runoff. By determining moisture sources of a basin, both large-scale dynamic and thermodynamic effects are captured, as well as land-atmosphere interactions. In addition, evaporative sources, either continental (local) or oceanic (non-local) can give an indication of the vulnerability of the Rhine basin to ongoing and future land-use changes.

Moisture sources in relation to drought events are often studied for the US (Bosilovich and Schubert, 2001; Brubaker et al., 2001; Dirmeyer and Brubaker, 1999; Dominguez et al., 2006; Herrera-Estrada et al., 2019; Roy et al., 2018; Zangvil et al., 2001, 2004), while only few studies focus on central western Europe (Bisselink and Dolman, 2009; Rosner et al., 2019; Stojanovic et al., 2018), and none specifically for the Rhine catchment. On the other hand, the droughts of 2003, and to lesser extend 2018, are studied extensively in terms of large-scale circulation (Black et al., 2004; Black and Sutton, 2007; Cassou et al., 2005; Drouard et al., 2019; Kornhuber et al., 2019), land-atmosphere interactions (Ferranti and Viterbo, 2006; Fischer et al., 2007b), and future projections (Beniston, 2004; Schär and Jendritzky, 2004; Stott et al., 2004; Vogel et al., 2019; Wehrli et al., 2019). Related to future projections, there is relatively high confidence and understanding in the ther-

modynamics aspects of drought under climate change (Shepherd, 2014), where increases in temperatures will result in more heatwaves and droughts in the future (Schär et al., 2004), as is also concluded specifically for the 2018 drought (Vogel et al., 2019; Wehrli et al., 2019). Differently, future changes in dynamics are very uncertain and not yet well understood (Shepherd, 2014; Woollings, 2010). For example, changes in frequency and persistence of blocking conditions are uncertain, especially because western Europe has a low signal-to-noise ratio (Woollings, 2010), and simulating blocking with high-resolution models remains challenging (Schiemann et al., 2016). Furthermore, soil moisture temperature and soil moisture precipitation feedbacks are shown to be important in droughts (Seneviratne et al., 2010), however the suggestion that droughts intensify and propagate via land-atmosphere feedbacks is not yet well understood (Miralles et al., 2019). To summarize, multiple aspects of droughts need further investigation, starting with understanding and simulating the current climate before projecting it towards the future. Here we take the approach by comparing two individual recent extreme drought events in terms of moisture sources, whereby we can combine the perspectives from the larger-scale circulation and the land-atmosphere interactions. Such an event-approach is consistent with developing physical storyline approaches (Hazeleger et al., 2015; Shepherd, 2016), where understanding is advanced by studying complex physical, and potentially socio-economic and ecological interactions of individual climatological relevant events.

The objectives of this study are to (I) characterize and compare the 2003 and 2018 summer droughts in the Rhine basin in terms of moistures sources, (II) explain the differences and similarities in patterns of the moisture sources by analysing anomalies in wind and specific humidity separately and (III) put the dry summers further in context, by studying the inter-annual variability of summer precipitation over the Rhine in relation to large-scale circulation (blocking) and moisture recycling within the basin.

5.2 Methodology

5.2.1 ERA5 data

We use the latest reanalysis dataset ERA5 data (Hersbach et al., 2020) from the European Centre for Medium Range Weather Forecast (ECMWF). The dataset is described in Chapter 2. We obtain specific humidity and zonal and meridional wind at multiple levels in the atmosphere (850, 700, 500, 300, 200 hPa; Table 5.1). Further, we obtain zonal and meridional wind, precipitation, evaporation, surface pressure, and dewpoint temperature at or near the surface (Table 5.1). We use dewpoint temperature and surface pressure to obtain specific humidity at the surface. Further characteristics of the obtained variables are given in Table 5.1. We obtain the variables from 1979 until 2018 (40 years) over the following domain: 10° to 75° N, and -105° E to 30° W (Figure 5.1).

Table 5.1: Obtained variables from ERA5, including the levels in the atmosphere, time step and unit.

Variable	Level(s) in the atmosphere	Time step	Unit
Zonal (east-west) wind u	10m + 850, 700, 500, 300, 200 hPa	6-hourly	m s^{-1}
Meridional (north-south) wind v	10m + 850, 700, 500, 300, 200 hPa	6-hourly	m s^{-1}
Specific humidity q	850, 700, 500, 300, 200 hPa	6-hourly	kg kg^{-1}
Evaporation E	Surface	hourly	m
Precipitation P	Surface	hourly	m
Surface pressure p_s	Surface	6-hourly	Pa
Dewpoint temperature T_d	2m	6-hourly	K

5.2.2 Theory and tracking method WAM-2layers

To determine the moisture sources of the Rhine basin we use the Eulerian moisture tracking method Water Accounting Model on 2-layers (WAM-2layers; Van der Ent et al. 2010, 2014). More details on this model are given in Chapter 2. Here, we use the adapted version of WAM-2layers to determine the moisture sources of the Rhine basin with ERA5 data on five pressure levels. The validation to perform tracking with atmospheric data on five pressure levels instead of multiple model levels is provided in Chapter 2.

We tracked precipitation falling in the Rhine basin back in time during May-June-July-August. The model runs with a time step of six minutes over the same domain as the variables were obtained: 10° to 75° N, and -105° E to 30° W.

In addition to analysing the moisture sources, another interesting variable to quantify is the amount of moisture recycled within a basin. The precipitation recycling ratio of a basin is the amount of precipitation occurring in a basin that is generated locally by evaporation (P_{local}), versus the total amount of precipitation occurring in a basin ($P = P_{\text{local}} + P_{\text{advected}}$). Thereby we assume that on monthly timescales almost all tracked evaporation within the basin results in local precipitation, the implications of these assumptions are in the discussion section. Hence the precipitation recycling ratio is defined as:

$$\rho_r = \frac{\int_A E_m \, dA}{\int_A P \, dA} \tag{5.1}$$

where A is the area of the Rhine basin.

5.2.3 Experimental set-up

The analyses are focused on the Rhine basin, indicated in Figure 5.1, and on the Northern Hemisphere summer period, here defined as May-June-July-August. We perform the

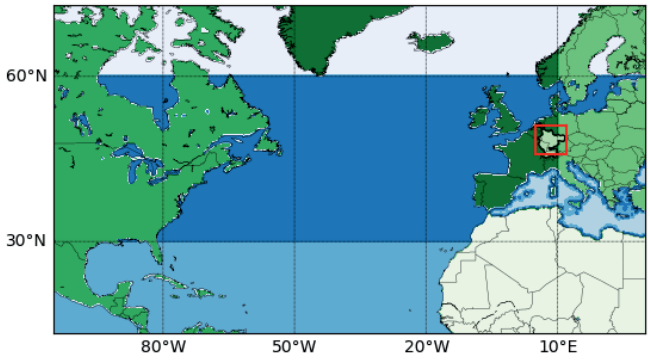

Figure 5.1: Domain on which we perform the tracking, with the defined continental regions (America, Africa, western Europe, Rhine basin, eastern Europe) and oceanic regions (tropical, extratropical, high latitudes, Mediterranean Sea) in different colours of respectively green and blue. We also indicated the Rhine basin and the box surrounding it is used to analyse the moisture fluxes over those boundaries.

analyses on a 40-year time period (1979-2018), with a focus on the summer of 2003 and 2018. Data is not detrended.

First, precipitation and discharge averages over May-June-July-August are analysed, to get a better overview of the anomalous events of 2003 and 2018 within the whole time series 1979-2018. We analyse monthly averaged daily observed discharge at Lobith (Rijkswaterstaat). In addition, we use temperature from ERA5 averaged over the Rhine basin to further elaborate on the events (not shown). Precipitation is obtained from the ERA5 re-analysis data, as will be used later for the moisture source analysis. We show the yearly cycle of daily precipitation and evaporation amounts, compared to the climatology. We apply a 20-day smoothed window on the daily time series, and we visualise one standard deviation around the climatological values.

Second, absolute moisture sources in mm month^{-1} are visualised spatially, together with the 500 hPa geopotential height obtained from ERA5. We also show anomalies compared to climatology (summers 1979-2018). Normalized moisture sources (absolute moisture sources divided by the amount of precipitation occurring over the basin) are shown averaged over May-June-July-August and averaged over different regions. These regions are either continental or oceanic (Figure 5.1): high latitude ocean (north of 60° N), extratropical ocean (between 30° and 60° N), tropical ocean (south of 30° N), Mediterranean Sea, America, Africa, western Europe (west of 10° E) and eastern Europe (east of 10° E).

Third, to further explore the results of the moisture sources, we take one step back and further analyse the moisture fluxes (F_x and F_y) over the boundaries of the Rhine basin.

We simplified the boundaries of the catchment with a box (47° to 52° N and 5° to 12° W; Figure 5.1), which makes the analyses on the moisture fluxes more straightforward and easier to interpret. For 2003 and 2018, we study the anomaly in moisture flux compared to the climatological flux per month, and whether this anomaly is a result of an anomaly in moisture (q') or in wind (u' or v'). With this analysis, we can further enhance our understanding which processes (dynamics or thermodynamics) played an important role during those anomalous events.

The zonal moisture flux F_x (uq) is studied over the eastern and western boundary of the box over the Rhine basin, and can be obtained as hourly values per month in 2003 and 2018:

$$uq = (u_c + u') \cdot (q_c + q') = u_c q_c + u' q_c + u_c q' + u' q' \tag{5.2}$$

Where uq is the hourly flux in 2003 and 2018, u_c and q_c are the climatological monthly means, and u' and q' are the anomalies with respect to the climatological monthly mean. As we want to know the average flux over a boundary per month, we average over time (month), and over latitude (47° to 52° N) and height (900, 850, 700 and 500 hPa) along the boundary:

$$\langle uq \rangle = \langle (u_c + u') \cdot (q_c + q') \rangle = \langle u_c q_c \rangle + \langle u' q_c \rangle + \langle u_c q' \rangle + \langle u' q' \rangle \tag{5.3}$$

Rewriting gives:

$$\langle uq \rangle - \langle u_c q_c \rangle = \langle u' q_c \rangle + \langle u_c q' \rangle + \langle u' q' \rangle \tag{5.4}$$

where the left hand side (LHS) indicates the total anomaly of a specific year and month over the boundary $\langle uq \rangle$ compared to the climatology $\langle u_c q_c \rangle$, and the right hand side (RHS) the contributions to the total anomaly from anomalies in wind $\langle u' q_c \rangle$, moisture $\langle u_c q' \rangle$, and combined wind and moisture $\langle u' q' \rangle$.

The same method is applied to separate the anomalies for the meridional moisture flux $F_y(vq)$ over the North-South boundaries, where we average over the same height (900, 850, 700 and 500 hPa) and over longitude (5° to 12° W), resulting in:

$$\langle vq \rangle - \langle v_c q_c \rangle = \langle v' q_c \rangle + \langle v_c q' \rangle + \langle v' q' \rangle \tag{5.5}$$

where the LHS indicates the total anomaly of a specific year and month over the boundary $\langle vq \rangle$ compared to the climatology $\langle v_c q_c \rangle$, and the RHS the contributions to the total anomaly from anomalies in wind $\langle v' q_c \rangle$, moisture $\langle v_c q' \rangle$, and combined wind and moisture $\langle v' q' \rangle$.

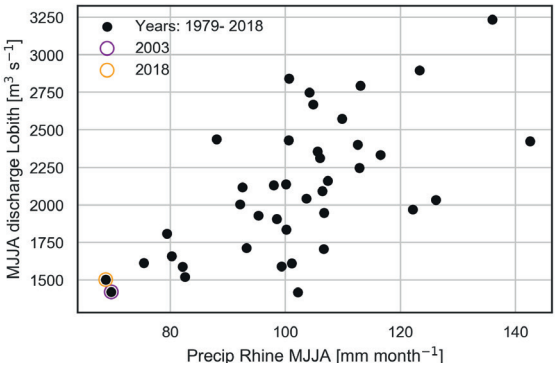

Figure 5.2: May-June-July-August averages of precipitation over the Rhine basin in mm month^{-1} against May-June-July-August averages of discharge in Lobith in m^3 s^{-1} for every year from 1979 to 2018. The years 2003 and 2018 are indicated with respectively an orange and purple circle

5.3 Quantifying the 2003 and 2018 summer droughts

Averaged over the Rhine basin, the summers of 2003 and 2018 have the lowest amount of precipitation of the last 40 years (Figure 5.2). More precisely, the monthly average precipitation is 69.7 mm month^{-1} for 2003 and 68.8 mm month^{-1} for 2018, both deviating two standards from the mean (102 mm month^{-1}). By fitting a Gumbel distribution to the summer precipitation anomalies, we find a return time of 20 and 40 years, for respectively the summer of 2003 and 2018. We find an expected, positive correlation between precipitation over the Rhine basin and discharge at Lobith, with a correlation coefficient of 0.64. This correlation likely increases if evaporation is subtracted from precipitation, according to the hydrological water balance. The average discharge in Lobith over MJJA in 2018 (1501 m^3 s^{-1}) and 2003 (1419 m^3 s^{-1}) falls within the range of two standard deviations from the mean (2103 m^3 s^{-1}). Lowest discharge averaged over four summer months occurred in 2011. In 2003 and 2018, high temperatures presumably also resulted in more snow melt from the Alps and therefore less exceptional values for discharge as we found for precipitation. However, later in the season exceptionally low discharges of 810 m^3 s^{-1} occurred in October to November 2018, compared to a climatology of 1809 m^3 s^{-1} in October to November. In this season, groundwater level and soil moisture content was probably still very low from the previous dry months, and snow melt does not play a role anymore. The year 2003 was not so exceptionally dry in October-November, however discharge was still on the low side (1214 m^3 s^{-1}) compared to the mean.

5.3.1 Month-to month description of dry summer 2003

Figure 5.3 shows the smoothed daily variations of precipitation and evaporation for the year 2003 and 2018, and also for the climatology. Although 2003 started in January with enormous discharge amounts reaching 9500 m^3 s^{-1}, precipitation in the winter of 2003 was already quite dry, except for the beginning of February (Figure 5.3b). In March and April, daily precipitation values around 1 mm day^{-1} were found, while climatological values are around 2 mm day^{-1} (1 mm day^{-1} falls outside one standard deviation from the mean). During this period, a high-pressure system developed over western Europe, resulting in dry conditions. These dry conditions continued into May 2003, while the month ended rather wet. June shows the opposite signal, with a wet start and a dry ending of the month in terms of precipitation. Moreover, June was very warm with a positive temperature anomaly of 4.3°C over the Rhine basin. Evaporation was much higher than average (more than one standard deviation) at the end of June, due to high temperatures. In that period, probably enough water was present in the soils and plants to evaporate. Thereafter, daily evaporation values dropped below the climatology in July and even lower in August. The same signal is found for precipitation which is low in July, and even lower in August. Especially the middle-to-end of August was very dry. In addition, a second heatwave occurred in August 2003 affecting whole of southwestern Europe, with positive temperature anomalies of 4°C over the Rhine basin.

5.3.2 Month-to month description of dry summer 2018

The winter of 2018 started with daily precipitation rates above 5 mm day^{-1} (Figure 5.3b), while end of February and beginning of March were rather dry. From May 2018 onwards high pressure over Scandinavia and western Europe resulted in fewer clouds, more incoming radiation and therefore higher evaporation rates. The latter is clearly visible from Figure 5.3a with in May 2018 daily evaporation rates above one standard deviation from the climatology. Similarly, though opposite, less precipitation occurred from May onwards. The high-pressure system remained persistent until July, but disappeared shortly in June. During this blocking period, temperature was high and precipitation rates low. Precipitation rates were often more than one standard deviation less than the climatology, especially and consistently in July and August (Figure 5.3). Evaporation over the Rhine basin was below climatology from July onwards. In contrast to 2003, where whole of Europe was dry, in 2018 north western Europe was dry while the south of Europe was relatively wet.

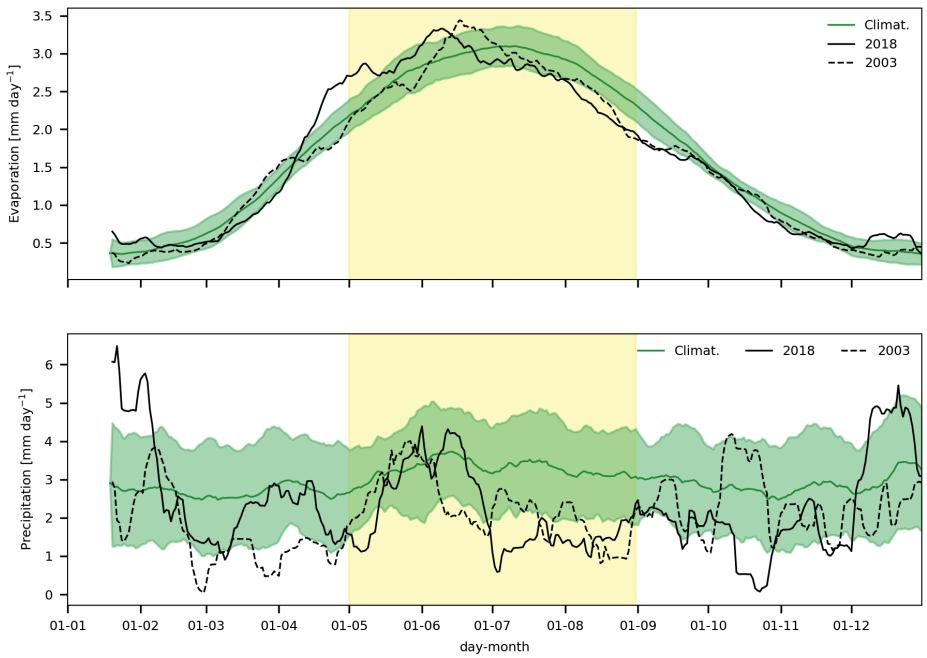

Figure 5.3: a) Evaporation and b) precipitation over the Rhine basin and over time in mm day^{-1} using a 20-day smoothed window, for the climatology (1979-2018) in green, and the year 2018 and 2003 in black straight and dotted respectively, all based on ERA5 reanalysis data. The green shading indicates one standard deviation of the 20-day smoothed window.

5.4 Moisture sources during the summer of 2003 and 2018

The climatological moisture sources (averaged over 40 years) for the months May, June, July and August are shown in the left column of Figure 5.4, together with the geopotential at 500 hPa in meter, and the integrated moisture fluxes derived from the tracking model WAM-2layers. The amount of precipitation over the Rhine basin is indicated in the subtitles. Figure 5.6 shows the normalized moisture sources averaged per region (upper plot ocean region, and lower plot land regions). We first discuss the climatological moisture sources and fluxes, and then the sources specific for the two dry summers.

In all summer months the climatological moisture sources cover a large oceanic area, including the Caribbean Sea, Gulf of Mexico and the North Atlantic Ocean. Although the local contributions per grid cell appear small, a normalized average over the tropical

and extra tropical North Atlantic (between 30° and 60° N) region results in about 50% of the precipitation in the Rhine basin (Figure 5.6). Much smaller ocean contributions (~1-5%) come from the polar North Atlantic and Mediterranean Sea. Because of the pre-dominantly western winds, most (oceanic) moisture sources are located west of the Rhine basin. Over land, we find small contributions from North America, even smaller contributions from North Africa, and as expected larger contributions from west and eastern Europe, with increasing sources for decreasing distance to the basin. The largest moisture sources (~6 mm month^{-1}) are found in the Rhine basin itself, indicating high recycling of moisture over this region in summer. These large moisture sources over land happen because evaporation is highest in summer time over land (Figure 5.3). The recycling of precipitation is around 8% in summer over the Rhine basin, and much lower in winter. When analysing the climatological moisture sources per summer month, only small differences between months appear, while the overall pattern is similar.

5.4.1 Description of the monthly moisture sources in 2003 compared to climatology

2003 was the second driest summer over the Rhine basin in our 40-year time series, based on precipitation averages over May, June, July and August (see Figure 5.2). Here, we discuss the moisture sources of the dry summer of 2003 (absolute sources in middle column and anomalies in right column Figure 5.4) and in the next section for 2018, and thereafter we compare the sources for the two dry summers. The normalized sources per region are indicated in Figure 5.6 for 2003.

In May 2003 the precipitation over the Rhine basin is only 6 mm month^{-1} less than the climatology of about 100 mm month^{-1}. May 2003 is characterized by larger than normal moisture fluxes over the Atlantic Ocean, over the Netherlands and northern Germany towards the Baltic States. In this month, higher than normal pressure occurred over southern and eastern Europe and lower than normal pressure over Iceland (Figure 5.4c), inducing stronger flow over the Netherlands (Black et al., 2004), as is also visible from the geopotential heights being closer together. The higher than normal pressure over the Iberian peninsula 'blocks' the moisture transport those regions towards the Rhine basin, resulting in negative anomalies of absolute moisture sources from the Iberian peninsula.

In June 2003, there is a clear dipole in geopotential over the Atlantic and western Europe, with lower than normal pressure over the ocean and higher pressure over the continent, indicating an Atlantic Low weather regime (Cassou et al., 2005). The high pressure system over the Rhine basin induces a strong anti-cyclonic transport of moisture around/northward of the Rhine basin (Figure 5.4e and f). As a result, only half of the precipitation compared to normal falls within the basin, 55.5 mm month^{-1} in 2003 whereas 102.4 mm month^{-1} precipitates in the climatology. Normalized, still more mois-

ture came from western Europe and the Rhine basin itself (in this month primarily from Spain/southwest France), and there is also a small positive normalized contribution from the extratropical oceanic region (Figure 5.6).

In July 2003 the high pressure system over western Europe weakens, but it is still present. The moisture fluxes are close to normal in this month, however the anomaly in absolute and normalized moisture source is negative over the entire ocean and land domain. There is also a negative anomaly in evaporation (1 mm day^{-1}, not shown) over the South of France, which indicates dry soils. The pattern persists into August, with a negative anomaly in absolute moisture source over land, and half of the precipitation amounts (45 mm month^{-1}) compared to the climatology (97.3 mm month^{-1}). In this month we find lower moisture fluxes and the hypothesized dry soils could still persist. This is further discussed in Section 5.5.2 on the connection between recycling and precipitation within the basin.

5.4.2 Description of the monthly moisture sources in 2018 compared to climatology

In the second column of Figure 5.5 we show the absolute moisture sources of May, June, July and August 2018, and in the third column the anomalies in absolute moisture sources, with a focus on the Rhine basin. In Figure 5.6 the normalized moisture sources per region are indicated for 2018 with a purple cross.

In May 2018, we find much smaller moisture fluxes over the Netherlands, UK, France and Germany compared to climatology. Anomalous northward directed moisture fluxes are found along the coast of Scandinavia, and anomalous southward directed moisture fluxes at the coast of France and Spain. Hence, in May 2018, little moisture is transported from the west towards the Rhine basin, explaining the low amounts of moisture source contribution from the land region west of the Rhine basin, and from the Atlantic Ocean (Figure 5.5b and c). From the normalized moisture sources (Figure 5.6), we find that the contribution from the extra tropical ocean region is almost half of its climatological contribution in May (18% in 2018 compared to 35% in climatology). In contrast, a large positive contribution in moisture source was found in May from eastern Europe, with a normalized contribution of 34% compared to the climatology where this amounts to 9%. This anomalous contribution of moisture source from eastern Europe is also clearly visible from Figure 5.5b and c, and is explained by the moisture fluxes from east to west (to the Rhine basin) over Poland. This anomalous moisture transport in May 2018 is related to a high-pressure system which was located over southern Scandinavia, resulting in a blocking of the westward flow towards western Europe and an enhancement of the anti-cyclonic flow from eastern Europe towards the Rhine.

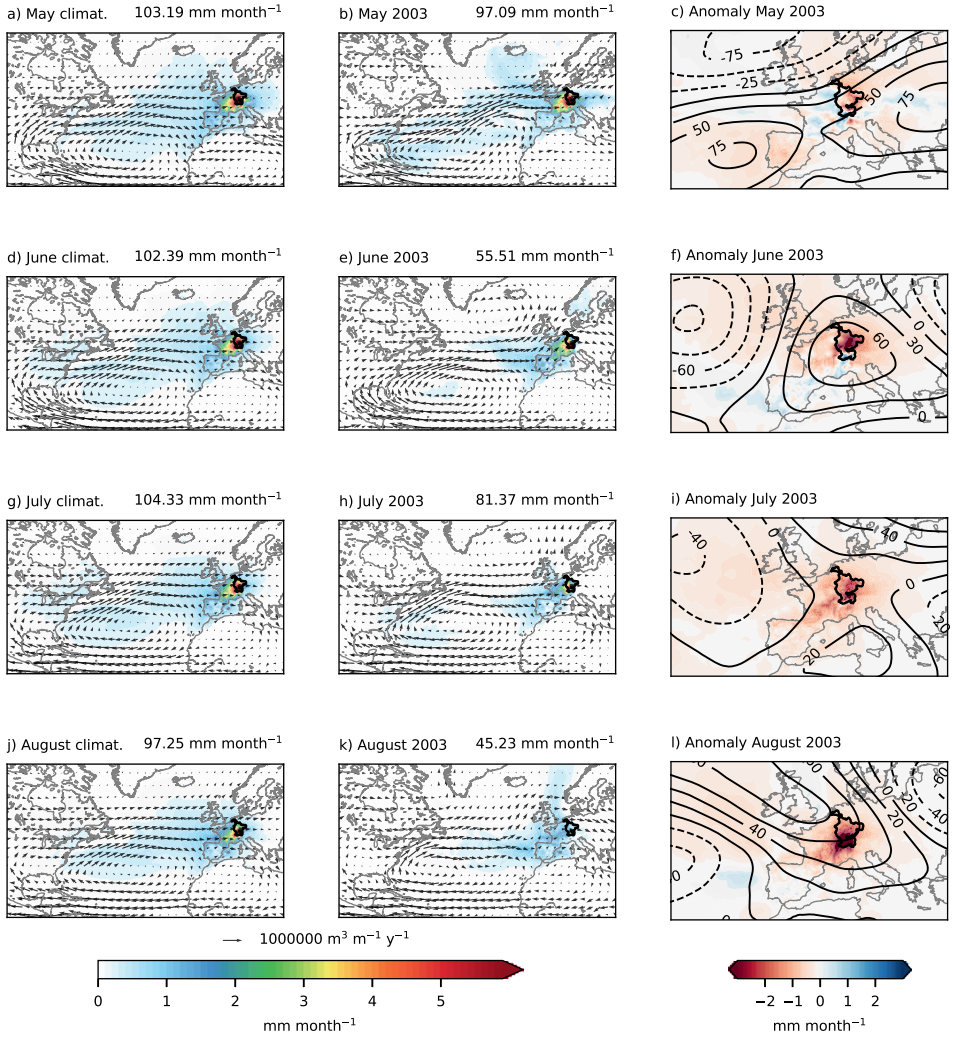

Figure 5.4: Absolute moisture sources (colours, mm month^{-1}) and vertically integrated moisture fluxes for May June July and August for the climatology (1979-2018), and 2003. The anomalous moisture sources are zoomed on the Rhine basin and the 500 hPa geopotential height anomalies (m) are also shown. Titles show the average precipitation over the Rhine basin in mm month^{-1}.

In June 2018 the high-pressure system persisted and expanded over the United Kingdom and Ireland (Figure 5.5f). The absolute moisture source anomalies show a similar pattern as in May 2018, with a negative anomaly west of the Rhine basin (Figure 5.5f), which is in line with the small moisture fluxes west of the basin, and a positive anomaly east of the Rhine basin, although smaller than in May. The negative anomaly in terms of moisture sources from the extratropical ocean is also clearly visible from the normalized contributions (Figure 5.6), where the contribution of June 2018 falls outside one standard deviation of the distribution. The normalized positive anomaly in moisture source contribution from eastern Europe falls outside one standard deviation as well, but is not as anomalous as in May. Together, the smaller contribution from the East, and the still negative anomaly from the Atlantic, leads to anomalously low precipitation in the Rhine in June 2018 (~70 mm month^{-1}) compared to the climatology (102 mm month^{-1}).

July was the driest month over the Rhine basin with precipitation amounts less than half of the climatological values (~48 mm month^{-1} in 2018 compared to 104 mm month^{-1} averaged over 40 years). The high-pressure anomaly persisted over Europe in July 2018, and expanded towards northern Scandinavia, resulting in strong Northwards moisture fluxes over the North Sea and along the coast of Norway (Figure 5.5h). The moisture fluxes over the Netherlands and the Rhine basin, and thereby the contribution of absolute moisture sources over the Atlantic, North America and West Europe, are still small, similar as for May and June 2018. The only exception is the mid-southern part of France, where the moisture sources are enhanced, as is clearly visible from Fig. 5.5i. In this dry month in July, we do find that the normalized sources over land are equal or higher than average, except for North America and Africa. Thus, in this exceptional dry month, there is relatively more moisture recycled locally over land. The relation between dryness and recycling is further investigated for all summers in the 40-year study period in Section 5.2. Besides, the large moisture fluxes found in the south of Europe in July 2018 likely explain the positive moisture source anomaly over the South of France, and can additionally explain the high precipitation amounts in southern Europe in July 2018 (Toreti et al., 2019), although that should be studied in more detail and is beyond the scope of this study.

In August 2018 the high-pressure anomaly (blocking) moved eastward into eastern Europe. As a result, moisture was transported further land inwards over western Europe compared to the previous months. Although more moisture could reach the Rhine basin, the absolute moisture sources are still anomalously low over the largest part of Europe and the Atlantic Ocean. However, the normalized moisture source contributions from land are higher compared to the average, except for Africa. Over land, negative anomalies in soil moisture, because of the preceding drought, could be an explanation of the low moisture sources. If we analyse evaporation from ERA5 for August 2018 compared to the climatology we find over western Europe negative anomalies of evaporation of 3 mm day^{-1} (not shown), indicating dry soils.

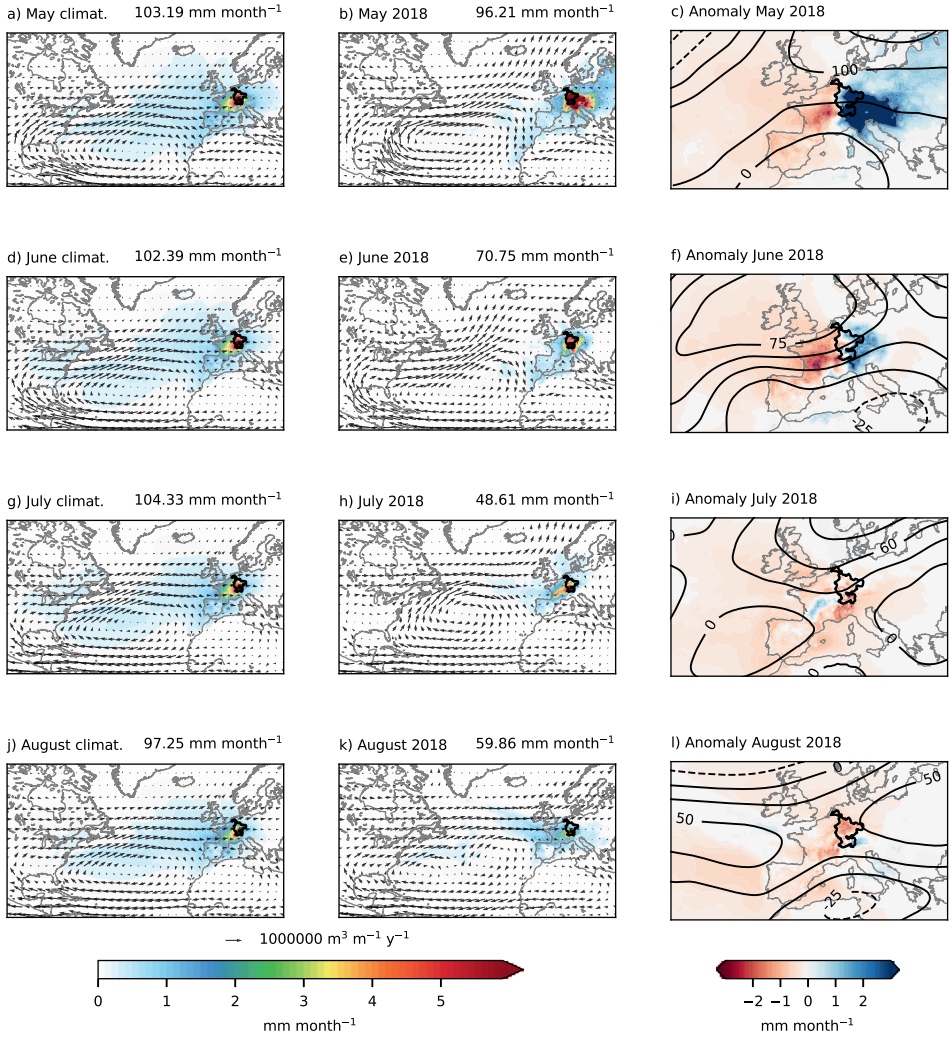

Figure 5.5: Absolute moisture sources (colours, mm month^{-1}) and vertically integrated moisture fluxes for May June July and August for the climatology (1979-2018), and 2018. The anomalous moisture sources are zoomed on the Rhine basin and the 500 hPa geopotential height anomalies (m) are also shown. In the titles we indicate the average precipitation over the Rhine basin in mm month^{-1}.

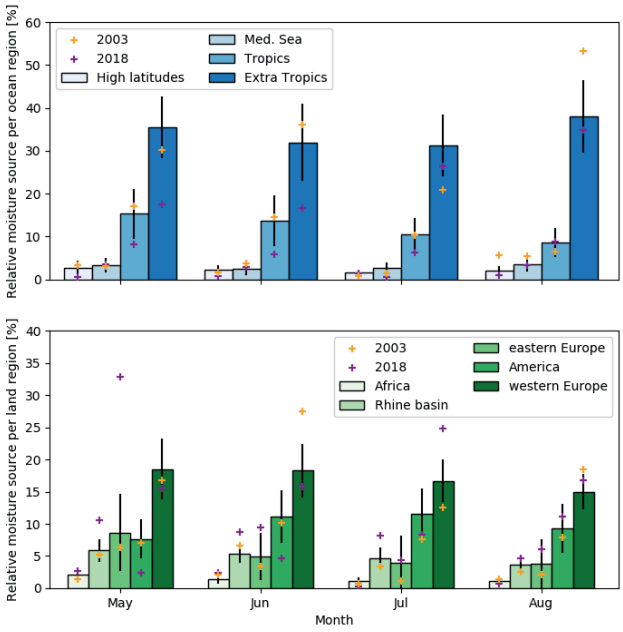

Figure 5.6: Normalized moisture source contribution averaged over 40-years per ocean region (upper plot) and land region (lower plot) for the months May, June, July and August. The error bars indicate one standard deviation around the mean. Normalized moisture sources for 2003 and 2018 are indicated with orange and purple crosses. Regions are indicated in Figure 5.1

5.4.3 Mechanisms of anomalous moisture fluxes – effects of wind and humidity

In the previous sections we found that during the drought of 2003 and 2018 moisture fluxes into the Rhine basin were anomalous, both in size and direction, resulting in anomalous moisture sources (Figure 5.4 to 5.6). The moisture fluxes, and sources, give us a combined picture of changes in thermodynamics (i.e. moisture contribution to moist static energy) and changes in dynamics (wind speed and direction) during those extreme summers. Here, we will separate the contributions from anomalous moisture and anomalous wind, as described in the methodology, to quantify their contributions to the total moisture fluxes over the boundaries of the Rhine basin in 2003 and 2018. We first discuss the climatological fluxes and then the anomalies for 2003 and 2018, and which component contributed to these anomalies. The zonal moisture fluxes are indicated in Table 5.2, and

the meridional moisture fluxes in Table 5.3 (LHS of Equation 5.4 and 5.5). The total anomalies in 2003 and 2018, and the different anomalies contributing are shown in Figure 5.7 and 5.8.

We find that in May, June, July and August the climatological zonal moisture fluxes increase over the course of summer from 8.55 and 6.34 kg kg^{-1} m s^{-1} in May to 22.25 and 18.78 kg kg^{-1} m s^{-1} in August, over the west and eastern boundary respectively. These zonal moisture fluxes increase over summer, as more moisture is available for transport due to higher temperatures and more evaporation. The climatological zonal moisture flux over the eastern boundary is always smaller than over the western boundary, as wind speeds decrease over land. The climatological meridional (north-south) moisture fluxes (Table 5.3), are much smaller than the zonal moisture fluxes (Table 5.2), as the flow is predominantly westerly. The largest meridional fluxes are found in May and August, and the meridional fluxes over the northern boundary are always larger than the fluxes over the southern boundary. The latter is related to lower windspeeds in the south, as moisture levels are higher in the south because of higher temperatures.

Contributions to anomalous moisture fluxes in 2003. In May 2003 we find a doubling of the zonal moisture flux, both over the western and eastern boundary (see also Figure 5.4b). Nevertheless, there is still divergence of moisture within the marked region, as the flux over the north boundary is remarkably large as well (see next Section). The anomalous zonal moisture flux is a result of anomalous zonal wind (green bar Figure 5.7a and 5.7b). This positive anomaly in zonal moisture flux is still present although much smaller in June, where the anomaly is a result of both anomaly in moisture and wind. In July, the zonal moisture fluxes are comparable with the climatology. In contrast, August shows a negative anomaly in zonal moisture flux over the western boundary and almost no anomaly over the eastern boundary. In that month, the western boundary is located in the middle of the high-pressure system, with very low winds, and the eastern boundary is located on the edge of the high-pressure, with higher windspeeds comparable to the climatology.

The meridional flux in May 2003 over the northern boundary is remarkably large. Due to the high pressure over Germany/Poland (Figure 5.4c) all moisture is transported northwards over this boundary. The meridional moisture flux over the northern boundary is also in June (7.36) and July (7.97) much larger than the climatology (1.03 and 2.04), indicating much more transport of moisture northwards, and thus out of the Rhine basin. Not more moisture is transported into the basin over the southern boundary in these months, thus resulting in divergence of moisture. In August, we find fluxes of opposite sign, with negative flows of moisture over the northern boundary (thus into the Rhine basin) and south boundary (thus out of the Rhine basin), still leading to divergence of moisture. The southward moisture fluxes are related to the high pressure occurring in August 2003, with northerly winds on the east side of the highest pressure. This anomaly

in moisture flux can almost totally be related to an anomaly in the wind compared to the climatology.

Contributions to anomalous moisture fluxes in 2018. In May 2018 we find negative zonal moisture flux over both the eastern and the western boundary, indicating eastern winds. Furthermore, the zonal moisture flux is more negative over the eastern than over the western boundary. The contribution of the anomaly in wind also results in this negative anomaly. In June 2018 we still find slightly eastern winds over the western boundary, while we find slight positive values, thus western wind over the eastern boundary, resulting in large divergence of moisture in this month. From July onwards positive zonal moisture fluxes dominate, although much smaller than the climatology. In August, the zonal moisture fluxes are closest to climatology compared to the rest of the months.

For the meridional moisture fluxes over the northern and southern boundary we find negative values in all months except for the northern boundary in May and August. Thus, instead of the climatological southerlies we have mostly northerlies in 2018, related to the Scandinavian blocking. In August we have the expected southerlies, though double the size as normal. In all months with large anomalies in the moisture flux, we find that this is a result of anomalous wind. In June and July, we find that for both the south and northern boundary the contribution from the multiplied wind and moisture anomaly is opposite in direction of the total anomaly (Figure 5.8c and d).

Overall, we can see from the absolute and normalized moisture sources, that the behavior of the dry summer in 2003 and 2018 are quite different. In 2018, the lack of moisture transport from the Atlantic Ocean and western Europe is very clear, while in 2003 this is not the case, except for August 2003. In May and June 2018, we also find enhanced moisture sources east of the Rhine basin, which are not observed for 2003. Thus, slightly different synoptic situations, with a blocking system located a bit more north or eastwards, can already lead to very different sources, as is found when we compare 2003 and 2018.

Furthermore, we quantified the anomalies in moisture fluxes over the boundaries of the Rhine basin during the summer of 2003 and 2018. We find in both summers anomalous conditions in terms of moisture fluxes, although 2018 is more persistent in the anomalies compared to 2003. In addition, we find that the anomalies in moisture fluxes are mostly related to anomalies in the wind (dynamics). We therefore conclude that the exceptional dynamical situation played an important role in both droughts.

Table 5.2: Climatological moisture flux $\langle u_c q_c \rangle$ and moisture flux occurring in 2003 $\langle u_{2003} q_{2003} \rangle$ and 2018 $\langle u_{2018} q_{2018} \rangle$ averaged over month and boundary (east and west) in kg kg^{-1} m s^{-1}. These are the components of the LHS of Equation 5.4, when subtracted resulting in the yellow bars in Figure 5.7.

	$\langle u_c q_c \rangle$		$\langle u_{2003} q_{2003} \rangle$		$\langle u_{2018} q_{2018} \rangle$	
	west	east	west	east	west	east
May	8.55	6.34	19.19	12.16	-7.53	-12.66
June	16.15	15.04	22.62	18.67	-0.42	3.19
July	21.44	19.54	22.63	17.45	4.84	5.18
August	22.25	18.78	13.76	18.53	19.52	12.25

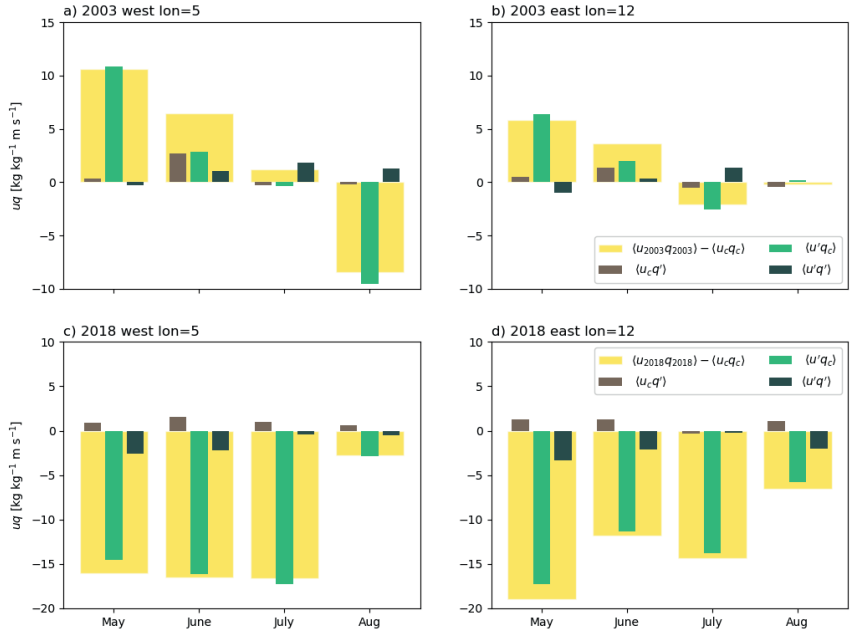

Figure 5.7: Contribution of anomaly in zonal wind $\langle u'q_c \rangle$, humidity $\langle u_c q' \rangle$ and both $\langle u'q' \rangle$ to the monthly anomaly of (c-d) 2018 and (a-b) 2003 compared to the climatology of 1979-2018. Flux contributions are shown for the western (a,c) and eastern boundary (b,d), and all four summer months. Location of the boundaries is shown in Figure 5.1.

Table 5.3: Climatological moisture flux $\langle v_c q_c \rangle$ and moisture flux occurring in 2003 $\langle v_{2003} q_{2003} \rangle$ and 2018 $\langle v_{2018} q_{2018} \rangle$ averaged over month and boundary (north and south) in kg kg^{-1} m s^{-1}. These are the components of the LHS of Equation 5.5, when subtracted resulting in the yellow bars in Figure 5.8.

	$\langle v_c q_c \rangle$		$\langle v_{2003} q_{2003} \rangle$		$\langle v_{2018} q_{2018} \rangle$	
	north	south	north	south	north	south
May	3.84	2.68	12.41	4.08	4.93	-0.33
June	1.03	0.74	7.36	1.24	-6.21	-6.17
July	2.04	1.0	7.97	0.52	-3.46	-5.16
August	4.99	2.34	-3.45	-0.93	9.94	-0.33

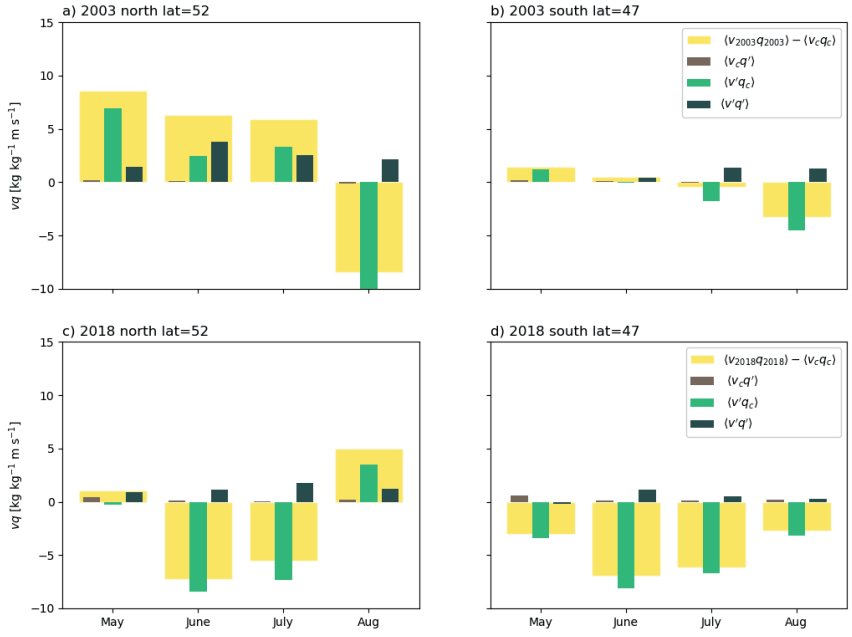

Figure 5.8: Contribution of anomaly in zonal wind $\langle v' q_c \rangle$, humidity $\langle v_c q' \rangle$ and both $\langle v' q' \rangle$ to the monthly anomaly of (c-d) 2018 and (a-b) 2003 compared to the climatology of 1979-2018. Flux contributions are shown for the northern (a,c) and southern boundary (b,d), and all four summer months. Location of the boundaries is shown in Figure 5.1.

5.5 Inter-annual variability

Finally, the two driest summers in the Rhine basin of (at least) the last 40 years are put into a longer time perspective by evaluating inter-annual variability in summer precipitation in relation to large-scale synoptics (Section 5.5.1) and local moisture recycling (Section 5.5.2).

5.5.1 Inter-annual variability in Rhine precipitation related to large-scale synoptics

Figure 5.9 shows the correlation per grid cell between monthly anomalies of geopotential height at 500 hPa (Z500) and monthly precipitation time series over the Rhine basin. The correlation is performed for summer months May, June, July and August for the entire 40-year time series. Similar results were obtained when the correlation was performed with geopotential height at 850 hPa instead of 500 hPa.

Strong negative correlations are found over western Europe (Figure 5.9a), indicating that positive anomalies in Z500 relate to lower-than-normal precipitation values. In other words, high pressure over the Rhine basin relates to dry conditions over this same basin. Values of -0.78 are found just west of the Rhine basin, and are the strongest absolute correlations over the domain, implying that Rhine precipitation is mostly sensitive to its local Z500 value. The negative correlation region is located over the Rhine basin and west of it, indicating that a blocking occurs over the Netherlands, blocking moisture to be transported with the prevailing westerlies from the North Atlantic towards the Rhine basin. The pattern visible in Figure 5.9a clearly resembles the positive phase of the summer North Atlantic Oscillation (NAO), sometimes also called "Blocking" pattern. This summer NAO, is one of the four weather regimes occurring over the North Atlantic during summer (Cassou et al., 2005; Folland et al., 2009), and is associated to dry and warm conditions over western Europe (Cassou et al., 2005; Folland et al., 2009; Lavers et al., 2013; Meehl and Tebaldi, 2004; Pfahl and Wernli, 2012). From a hydrological point of view, Fleig et al. (2011) shows that high-pressure systems centred over respective regions in western Europe were frequently associated with droughts in daily streamflow.

Around western Europe, we find a wave like pattern in the correlation, with positive correlations over southeast Greenland and the Labrador Sea and negative correlations over northeast North America (Figure 5.9a). Furthermore, there are positive correlations over the Mediterranean Sea. This 'wave-train' of positive and negative correlations suggest a strongly meandering jet stream (e.g. high amplitude waves). High amplitude waves, with wavenumber 7, are often associated with persistent surface weather conditions, such as dry conditions over western Europe (Kornhuber et al., 2017), together with dry conditions over other parts of the world. This wave-7 pattern occurred throughout the summer of 2018 (mid-June to early July) and at the start of August 2003 (Korn-

huber et al., 2019; Petoukhov et al., 2013). In addition, Drouard and Woollings (2018) shows the significant contribution of summer North Atlantic Oscillation by amplifying the wavenumber 7-pattern in extreme summer conditions in Europe from end of June until mid-July 2018.

The correlation pattern in Figure 5.9a implies the favourable large-scale conditions for dry summers over the Rhine basin, with a strongly meandering jet and blocking located west of the Rhine basin. For comparison, we show the Z500 anomalies during the dry summers 2003 and 2018 (Figure 5.9b and 5.9c). To further investigate if the large-scale conditions in 2003 and 2018 were indeed very similar to the correlation pattern, and how it compares to other summers we correlate each summer Z500 anomaly with the favourable large-scale conditions for dry summers over the Rhine basin (Figure 5.9a). Or differently phrased, is the Z500 anomaly during the 40 years on the location where it reduces the precipitation over the Rhine basin? The results are shown per summer in Figure 5.10.

From comparing Figure 5.9a and 5.9c, we already find that the Z500 anomaly in 2018 is very comparable with the correlation pattern, as is now quantified with a correlation value of 0.6 (Figure 5.10). This correlation for 2018 is highest in the 40-year time series, indicating the exceptional conditions for a dry summer. In addition, when performing the correlation per month (not shown), all months show a positive correlation, which did not happen in all other 40 years. Nevertheless, it should be noted that from the Z500 anomaly in 2018 the clear wave-train signal with high amplitude waves is less pronounced. The wave-7 pattern only occurred over two weeks during this summer, and therefore is probably averaged out in this MJJA average. As we have not removed trends here, it might be that we already observe the effect of a northward displacement of the jet in response to climate change (De Vries et al., 2013; Lorenz and DeWeaver, 2007).

The correlation value is positive as well for 2003 (Figure 5.10), however not as high as for 2018. The correlations per month show a negative correlation for July 2003, where the other months show clear positive correlations. In addition, we find a clear wave-train (high amplitude wave) in the Z500 anomaly, although the location of the anomalies is shifted compared to the correlation pattern. For 2003 the wave-7 pattern was observed at the start of August (Petoukhov et al., 2013), during the second heatwave of that summer. Other remarkable years with high correlation values are 1992, 1989 and 1994, but in these years the positive Z500 anomalies were shifted or not as strong and therefore not resulting in dry conditions for the Rhine (Z500 anomalies for 1992, 1989 and 1994 not shown).

5.5.2 Inter-annual variability in Rhine precipitation related to moisture recycling

The precipitation recycling ratio is defined in the methodology, and applied to the Rhine basin. It is a common indicator for the amount of moisture recycling within a region. It is the ratio of local precipitation, precipitation related to evaporation which occurred

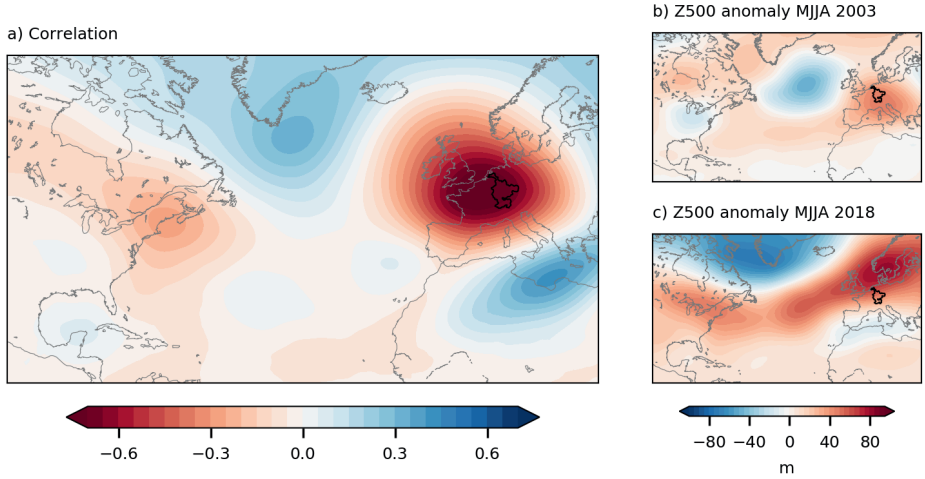

Figure 5.9: a) Spatial correlation of 500 hPa geopotential height anomaly fields (Z500) and precipitation averaged over the Rhine basin. Correlation is performed on 40 years of monthly summer data (May, June, July, August), b) anomaly of geopotential height at 500 hPa averaged over MJJA 2003 and c) 2018.

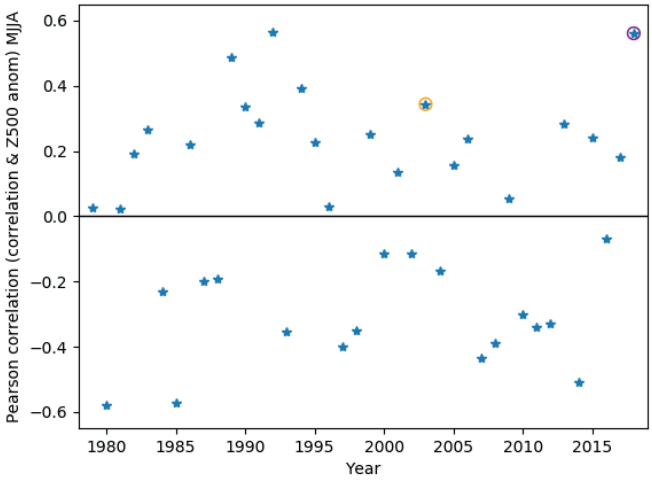

Figure 5.10: Pattern correlation of the pattern in Figure 5.9a (correlation of precipitation Rhine with Z500 anomaly) with the Z500 anomalies averaged over MJJA per year, with an orange and purple circle for respectively 2003 and 2018.

in the basin itself, over total precipitation. Differently formulated; the amount of locally generated precipitation in a region versus the total precipitation (locally generated precipitation and precipitation due to convergence of moisture fluxes by the large-scale flow) in a region. In the summer period this ratio is higher compared to winter, as more evaporation over land takes place in summer, thus the local contribution to precipitation in the Rhine basin is higher. Precipitation recycling indicates the dependence of a basin on its local processes, and thus the local land-atmosphere interactions.

In Figure 5.11 we show monthly precipitation averaged over the Rhine basin against the monthly precipitation recycling ratio per summer month (May, June, July and August; indicated with different symbols). We find a negative correlation of -0.33, indicating that in dry summer months usually more recycling of moisture takes place compared to wet summer months. This negative relationship between precipitation and precipitation recycling was also found by Bisselink and Dolman (2008), who show for central Europe (including the Rhine basin) that local evaporation contributes more to precipitation in dry summers. Additionally, in the previous section we find a positive correlation of dry summers for the Rhine basin with high pressure over western Europe. And high pressure (e.g. blocking) results in a decrease of moisture advected into the basin, which will lead to an increase in the precipitation recycling ratio. If only the amount of local precipitation decreases, a decrease in precipitation recycling should be observed. When correlating precipitation and precipitation recycling per month, we find the strongest correlation in May, while it decreases into summer, with lowest correlation in August. Related to this, we find on average higher recycling ratios at the start of summer (0.059 in May and 0.054 in June) and lower recycling ratios at the end of summer (0.046 in July and 0.037 in August). The high ratios in May are related to a relatively small contribution from advection (see Table 5.2) in this month, while the lower ratios at the end of summer can be related to a general decrease in evaporation, and thus a decrease in precipitation generated by local evaporative fluxes.

In 2003, the recycling ratios in May and June are almost twice as high as in July and August (orange circles in Figure 5.11). In June 2003, when the first heatwave occurred, recycling is above average (0.067 in June 2003 compared to 0.054 as climatology). The second heatwave occurred in August 2003, however, the recycling ratio is very low in this particular month (0.025 in 2003 compared to 0.037 in climatology). This indicates that the local precipitation decreased, probably because of dry soils at that point in time, indicating the importance of land-atmosphere feedbacks. For the summer months in 2018, we find high recycling ratios in combination with low precipitation, especially in May, June and July when the high pressure system was persistent (Figure 5.5), and the moisture fluxes did not reach the Rhine catchment (e.g. moisture was not advected into the Rhine basin). In August 2018, precipitation was still low but the advected amount of moisture increased (see Figure 5.5k) resulting in a similar precipitation recycling ratio as in the climatology.

It is interesting to see the different characteristics of the recycling ratio in the two dry summers. Much higher recycling ratios are found in May, June and July in 2018 compared to 2003. This indicates the effect of the blocking pattern in 2018, which was more persistent and/or effective in blocking moisture advection into the basin. In addition the strong easterly flow in May and June 2018 contributed to recycling, which did not take place in 2003. Bisselink and Dolman (2009) studied the recycling of moisture over Europe in very wet and dry years, they found that in the dry months June 2003 and July 2006 precipitation recycling is enhanced, which we also found for the Rhine basin (Figure 5.11). We conclude that a similar, and stronger, relationship is present for the dry summer of 2018.

Precipitation recycling has been a common approach in the 1990s to study land-atmosphere interactions (Seneviratne et al., 2010), although mainly covering the United States. More specifically, over the Mississippi River basin wet and dry years were studied in terms of moisture recycling, and higher recycling over the Mississippi basin was found during the drought year of 1988 (Bosilovich and Schubert, 2001; Dirmeyer and Brubaker, 1999). Intuitively, it makes sense that more moisture inflow into a region is blocked during dry conditions. As a consequence, it also indicates that a basin during dry conditions depends more on local evaporation, which can decrease substantially during droughts (as in 2003), indicating the importance of land-atmosphere feedbacks.

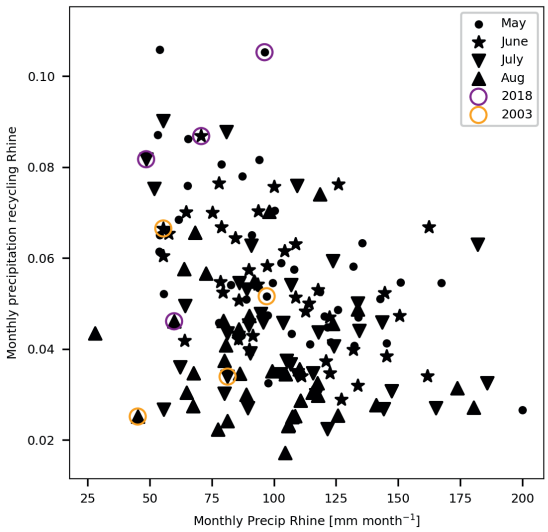

Figure 5.11: Scatter plot with monthly precipitation over the Rhine basin in mm month^{-1} against monthly precipitation recycling ratios for the months May, June, July and August, using different symbols to indicate the months. 2003 and 2018 are encircled with respectively orange and purple.

5.6 Discussion on methodology

To determine the moisture sources of the Rhine basin over a long time period, we use the new re-analysis dataset ERA5 and an adapted version of the Eulerian moisture tracking model WAM-2layers. The ERA5 product is state-of-the-art when it comes to data assimilation and high temporal and spatial resolution and provides all needed variables at multiple levels in the atmosphere to perform the tracking. The performance of ERA5 in simulating precipitation over the Rhine basin is not studied in detail, yet Beck et al. (2019) found that ERA5 performed remarkably better in representing precipitation and land surface variables linked to the terrestrial hydrological cycle (Albergel et al., 2018; **?**) across North America compared to the previous re-analysis dataset ERA-Interim. We use the Eulerian tracking model WAM-2layers as this model is cost effective, and the adapted version used in this study is validated and shown to perform well for tracking moisture over the Mississippi river basin (Benedict et al., 2020). The largest assumptions in the model are the mixed layer approach, and the vertical transport between the two layers, which is determined from closing the water balance between the two layers (Van der Ent, 2014).

Here, we study the normalized moisture sources of the Rhine basin per month and region. As the tracking is performed on a limited domain (shown in Figure 5.1), moisture sources originating outside of this domain are not accounted for. In addition there is a loss term of water, as the water balance does not close on a daily timescale (Benedict et al., 2020; Findell et al., 2019). Those two factors combined form a residual term, which is 10% on average over MJJA 1979-2018, and 10% and 15% for respectively 2003 and 2018. The larger residual term in 2018 is explained by the anomalous sources from east of the Rhine basin where the domain is relatively limited in extend. The residual term can be higher per individual month as the lifetime of (tracked) moisture in the atmosphere is about 5-10 days (Van der Ent and Tuinenburg, 2017; Läderach and Sodemann, 2016; Trenberth, 1998), and thus moisture related to precipitation in the first days of a month can be accounted for in the preceding month (keep in mind we track moisture backwards in time). This residual term also impacts the precipitation recycling ratio where we assume that all tracked moisture within the Rhine basin in a certain month results in precipitation within that same month.

5.7 Conclusions and outlook

We studied the similarities and differences in the drought of the summer 2003 and 2018 in terms of Rhine's moisture sources. By analysing moisture sources, evaporative regions which result in precipitation over the Rhine basin, we could study both large-scale processes as local land-atmosphere interactions, and both dynamics and thermodynamics. We determined the moisture sources of the Rhine basin from 1979 to 2018 with a focus

on May, June, July and August using ERA5 reanalysis data and an adapted version of the Eulerian moisture tracking model WAM-2layers (Benedict et al., 2020; Van der Ent, 2014). During an average summer, Rhine's moisture sources are mostly located over the Atlantic Ocean, together with a large contribution from continental evaporation, mostly from regions west of the Rhine basin (Figure 5.6).

The droughts of 2003 and 2018 stand out as the driest summers in the 40-year time series in terms of precipitation over the Rhine basin. Both are two standard deviations below the mean precipitation over May, June, July and August. In both summers we find a decrease in absolute moisture sources from oceanic regions, although the normalized contributions are different between the two years (Figure 5.6). The anomalous moisture fluxes over the boundaries of the Rhine basin in 2003 and 2018 are a result of anomalies in wind, thus anomalous dynamics (Figure 5.7 and 5.8). The differences in normalized sources are due to the different locations and persistence of the high-pressure systems, blocking moisture to be transported to the Rhine basin. We find that 2018 is most favourable in terms of large-scale conditions to result in dry conditions over the Rhine basin, while this is to a lesser extent the case for 2003 (Figure 5.9 and 5.10). When focusing on land-atmosphere interactions, we found in general higher recycling of moisture within the basin under drier conditions. This relationship was observed for 2018, as a decrease in moisture advected into the basin resulted in higher recycling. In August 2003 however, recycling was lower than normal, although it was very dry, indicating a smaller contribution of local precipitation in this month probably due to drying out of the soils, which enhanced the heatwave (Fischer et al., 2007b).

Here, we have analysed two past drought events in terms of moisture sources. Using this methodology, there is also potential to study droughts in seasonal prediction, as is currently relevant seeing the dry conditions for Western Europe in the spring of 2020, and under future projections, for example to indicate vulnerability to land-use changes. By studying moisture sources and recycling during droughts, we capture both the large-scale circulation and land-atmosphere interactions. To further enhance our understanding on these processes we need case specific studies, as by analysing composites and statistics, important processes playing a role cannot be distinguished. This study highlights the unique nature of the two droughts of 2003 and 2018 that we studied.

Acknowledgements. We would like to acknowledge ECMWF and Copernicus Services for supplying ERA5 data through their server at `https://cds.climate.copernicus.eu`. The adapted version of the WAM-2layers code used in this study is available on Github (`https://github.com/Imme1992/moisture\_tracking\_mississippi`). The simulations are performed on the Cartesius supercomputer from SURFsara (project number SH-312-15). Imme Benedict acknowledge funding from the Netherlands Organization for Scientific Research (NWO) for project 869.15.004. Imme Benedict would like to acknowledge Janno Heger for the inspiration for this study.

6

The benefits of spatial resolution increase in global simulations of the hydrological cycle evaluated for the Rhine and Mississippi basins

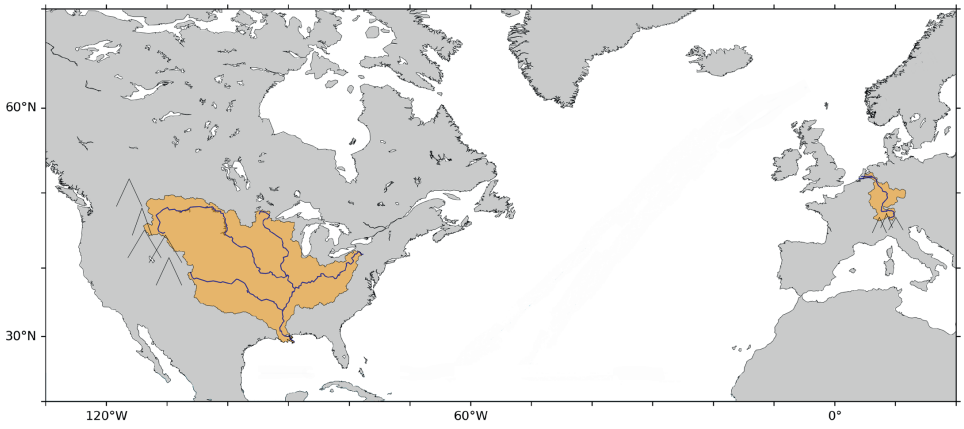

This Chapter is based on:
Benedict, I., van Heerwaarden, C. C., Weerts, A. H., and Hazeleger, W.: The benefits of spatial resolution increase in global simulations of the hydrological cycle evaluated for the Rhine and Mississippi basins, Hydrol. Earth Syst. Sci., 23, 1779–1800, 2019b

To study the global hydrological cycle and its response to a changing climate, we rely on global climate models (GCMs) and global hydrological models (GHMs). The spatial resolution of these models is restricted by computational resources and therefore limits the processes and level of detail that can be resolved. Increase in computer power therefore permits increase in resolution, but it is an open question where this resolution is invested best: in the GCM or GHM. In this study, we evaluated the benefits of increased resolution, without modifying the representation of physical processes in the models. By doing so, we can evaluate the benefits of resolution alone. We assess and compare the benefits of an increased resolution for a GCM and a GHM for two basins with long observational records; the Rhine and Mississippi basins. Increasing the resolution of a GCM (1.125° to 0.25°) results in an improved precipitation budget over the Rhine basin, attributed to a more realistic large-scale circulation. These improvements with increased resolution are not found for the Mississippi basin, possibly because precipitation is strongly dependent on the representation of still unresolved convective processes.Increasing the resolution of the GCM improved the simulations of the monthly averaged discharge for the Rhine, but did not improve the representation of extreme streamflow events. For the Mississippi basin, no substantial differences in precipitation and discharge were found between the two resolutions input GCM and the two resolutions GHM. Increasing the resolution of parameters describing vegetation and orography in the high resolution GHM (from 0.5° to 0.05°) shows no significant differences in discharge for both basins. A straightforward resolution increase in the GHM is thus most likely not the best method to improve discharge predictions, which emphasizes the need for better representation of processes and improved parameterizations that go hand in hand with resolution increase in a GHM.

6.1 Introduction

Hydrometeorological extremes present a combination of atmospheric and hydrological processes. On a global scale, these processes are simulated by forcing global hydrological models (GHMs) with global climate models (GCMs). With these, we can forecast and generate future projections of the hydrological cycle and its extremes. However, the spatial resolution of climate and hydrological models limits the details that can be resolved in a numerical simulation. With higher spatial resolution, and therefore better resolved flows and better represented landscapes, we expect more accurate results when modelling the impact of climate on hydrological processes. However, computer capabilities are limited. Currently, the common horizontal resolution of GCMs in the Coupled Model Intercomparison Project Phase 5 (CMIP5) is around 150 km (Taylor et al., 2012b). For GHMs in the Inter-Sectoral Impact Model Intercomparison Project (ISI-MIP), this resolution is around 50 km (Haddeland et al., 2011; Schellekens et al., 2016; Beck et al., 2016).

To improve the detail level at catchment scale, it is a dilemma whether to use high resolution global models or regional downscaling. High resolution global climate models lead to better resolved large-scale processes (Scaife et al., 2011; Jung et al., 2012; Demory et al., 2014; Hodges et al., 2011), cyclones (Strachan et al., 2013; Manganello et al., 2012) and more pronounced small-scale extremes. For hydrological modelling, an increase in resolution leads to improved spatial representation of topography, soil, and vegetation (Wood et al., 2011) and therefore can result in more realistic surface runoff and evaporation. However, increasing the resolution of a GHM also results in increasing unknown, and often not easily quantifiable, model parameters. This brings in large uncertainties when modelling hydrology across multiple spatial scales. There are multiple ongoing initiatives that assess the benefits of global models with very high spatial resolution for both the atmosphere (High Resolution Model Intercomparison Project; Meehl et al. 2014; Haarsma et al. 2016), and in hydrology (Wood et al., 2011; Bierkens et al., 2015).

In parallel to the research on global modelling, hydrological studies often use downscaled weather and climate variables to study regional climate variations and their hydrological impact (Jacob et al., 2014), as the spatial resolution of a basin can be substantially increased compared to a global model. Although dynamical downscaling has many benefits, it is not able to reduce biases that are related to errors in large-scale circulation patterns (Maraun et al., 2017; Van Haren et al., 2015), which are related to the low-resolution GCMs used as boundary conditions for the downscaled products (Hazeleger et al., 2015; Fowler et al., 2007; Wood et al., 2004).

Here, we study the effect of resolution in global models on the hydrological cycle at the basin scale. The hypothesis of this study is that with higher resolution climate and hydrological models the hydrological cycle will be better simulated. We focus on two contrasting large river basins, the Rhine and Mississippi basins. To study the effect of

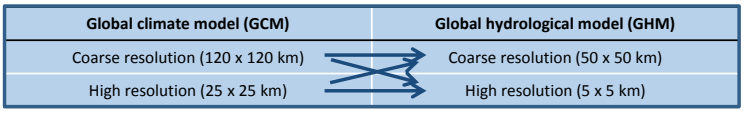

Figure 6.1: Two spatial resolution simulations of the GCM are used to force the GHM with two different spatial resolutions. Note that this set-up was tested for two large river basins; the Rhine and Mississippi basins.

an increased spatial resolution, we compare low- and high-resolution simulations of a global climate model, as well as of a global hydrological model over these two basins. By comparing all cross-combinations of resolutions (Figure 6.1), we aim to answer our main research question: what are the benefits of an increased resolution global climate and global hydrological model is simulating the hydrological cycle over the Rhine and Mississippi basins?

We analyse three main components of the hydrological cycle: precipitation, evaporation and discharge. We have chosen the Rhine and Mississippi basins as long measurement records are available for validation, and because their climatic drivers are different (Figure 6.2), which can contribute to our understanding of the processes resolved with increased spatial resolution. The precipitation budget of the moderately sized Rhine basin is determined by the mid-latitude storm-track, which is shown to be better represented with higher resolution models (e.g. Davini et al., 2017a; Van Haren et al., 2015; Zappa et al., 2013). On the other hand, the precipitation budget of the Mississippi is influenced by moisture input from multiple drivers; moisture is advected from the Pacific, from the Caribbean, and from the Gulf of Mexico and extreme precipitation occurs within tropical cyclones (Figure 6.2). In addition, convective precipitation plays an important role over the Mississippi basin (Iorio et al., 2004). Although the Rhine and Mississippi are two contrasting basins, they do not represent the full diversity of catchments on a global scale. It would be computationally too expensive to study more regions.

This Chapter is structured as follows: more details about the basins are given in Chapter 1. In Section 6.2 the models, data and methods are described. We first present the results for the Rhine basin and thereafter for the Mississippi basin. The methodology of this study, as well as the broader implications, are discussed in Section 6.5 and we end with a conclusion and summary (Section 6.6).

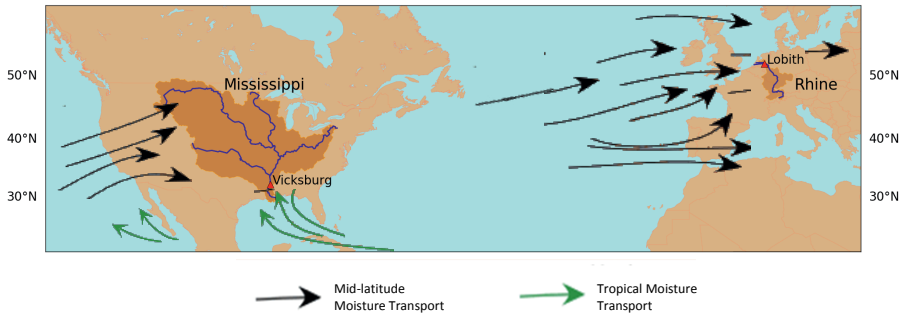

Figure 6.2: Map indicating the Rhine and Mississippi basins, the rivers, the used gauge stations (Lobith and Vicksburg) and the climatological location of mid-latitude moisture transport (black arrows) and tropical moisture transport (green arrows). Figure adapted from: http://www.physicalgeography.net/fundamentals/7s.html.

6.2 Data and methodology

6.2.1 Global climate model EC-Earth

We use high resolution experiments (Haarsma et al., 2013) from the state-of-the-art atmospheric global climate model EC-Earth V2.3 (Hazeleger et al., 2010, 2012). More information on the model is given in Chapter 2. In this study we compare the high resolution and low resolution simulations of present climate. The high resolution experiments have a horizontal spectral resolution of T799, which corresponds to 25 km, and 91 vertical levels (further referred to as high and T799). For comparison in resolution, the same model simulations are performed with a spectral horizontal resolution of T159, corresponding to 120 km and 62 vertical levels (further referred to as low and T159). The parameterization packages of the high and low resolution simulations are the same (Van Haren et al., 2015). The land-surface characteristics are described in the IFS model documentation (2007, IFS Documentation cy31r1, Book Chapter, ECMWF) and are interpolated to the requested resolutions (T799 and T159). For both resolutions, six members of five years (2002-2006) are created, resulting in 30 years of data representing present climate. It should be noted that the fixed boundary conditions (SST and greenhouse forcing) decrease the independency of the members and that this research could also be performed with fewer longer simulations. More information on the experiment and the spin-up can be found in Chapter 2 and in Haarsma et al. (2013).

6.2.2 Global hydrological model W3RA

W3RA is the global hydrological model that we use in this study. It is based on the landscape hydrology component model of the AWRA system (AWRA-L; van Dijk et al. 2013; Van Dijk 2010a,c; Van Dijk and Renzullo 2011). Model details are given in Chapter 2 (Section 2.4.1).

Although W3RA is a global model, in this study we only perform the simulations for the Rhine and Mississippi basins. We run the model at the original horizontal resolution of 0.5° (~50 km) and at a higher horizontal resolution of 0.05° (~5 km). The parameters in W3RA at 0.5° resolution are determined with a regionalization approach (Van Dijk, 2010b). The list of parameters can be found in the documentation (Van Dijk, 2010c). Most of these parameters are not physically based and are difficult to determine at multiple spatial scales. To allow a fair comparison between the two model resolutions, we remapped these parameters from the 0.5° to the 0.05° resolution using area-weighted interpolation. Our approach is verified by Melsen et al. (2016), who conclude that parameters can to a large extent be transferred across the spatial resolution (on regional scales from 1 km^2 to 100 km^2). We only make an exception for orography and vegetation, as these parameters are known at high resolution. Therefore, maps of orography and vegetation (division of HRU per grid cell) are used at the 0.05° resolution. The model algorithm is not adapted for the higher resolution.

The resolution of the GHM does not perfectly coincide with the resolution of the GCM (see Figure 6.1). Therefore, we remap the climate variables in between using closest distance interpolation. Runoff is translated towards discharge using the wflow routing scheme (Schellekens, 2012), which is based on the kinematic wave approximation. For the 0.5° resolution GHM, routing is performed at 0.5°. For the 0.05° resolution GHM, routing is performed at 0.083° as the maps of the river network are available at this resolution from the PCR-GLOBWB model (Sutanudjaja et al., 2018). We use closest distance interpolation to remap the runoff data from 0.05° towards 0.083°. For each member, we perform a spin-up cycle of five years to generate the initial conditions for the simulations of five years, from which we use the last four years for the analysis. With a soil depth of 5 m, we expect that the land-surface is in equilibrium after 6 years. When using the last four years of the simulation, hardly any effect of the initial conditions is found (results not shown). To summarize, we have 24 years of discharge simulations per combination of resolutions.

6.2.3 Observational datasets for model verification

We use the following datasets (described in Chapter 2) for the verification of precipitation; the E-OBS dataset version 12.0 (Haylock et al., 2008) at 0.25° from 1985 until 2015 (30 years) and the genRE hourly precipitation dataset (Van Osnabrugge et al., 2017) (1996-2015) for precipitation comparison over the Rhine basin. For the Mississippi basin,

the Climate Prediciton Center (CPC) 0.25° Daily US Unified Gauge-Based precipitation dataset version 1.0 (Higgins and Joyce., 2000) is used from 1985-2015 (30 years). For the verification of actual evaporation, we use the GLEAM (Global Land Evaporation: the Amsterdam Methodology) dataset version 3.0a (Martens et al., 2016) from 1985 until 2015 (dataset described in Chapter 2. Daily discharge data for the Rhine at Lobith and the Mississippi at Vicksburg are obtained from the Global Runoff Data Center (GRDC, 2007) from 1985 until 2015 (30 years).

In addition to the observational datasets, we verify our model results with reanalysis data from the ECMWF. ERA-Interim (Dee et al. 2011; further referred to as ERAI), is used from 1985 up to 2014 (30 years), and model specifications are given in Chapter 2. ERA-Interim has a spatial resolution of around 80 km and 60 vertical levels (T255L60) and is based on IFS release Cy31r2 (comparable to Cy31r1 used in the EC-Earth simulations), which includes the land-surface TESSEL scheme (Viterbo and Beljaars, 1995). In addition, the ERA-Interim/Land reanalysis (Balsamo et al., 2013) is shortly addressed, where precipitation from ERA-Interim is corrected with satellite data and an improved land-surface scheme H-TESSEL is used (Balsamo et al., 2009). ERA-Interim/Land is only available until 2010 and therefore we analyse the time series from 1985 until 2010. Lastly, the ERA20C dataset (Poli et al., 2016) is used for extra verification of the precipitation budget over the Mississippi (1985-2010). ERA20C is based on IFS cy38r1 and performs the assimilation on fewer variables than ERA-Interim.

6.2.4 Experimental set-up

We use the low and high resolution GCM EC-Earth to force the low and high resolution GHM W3RA (Figure 6.1). To test the GHM without the uncertainty of a free-running GCM, we also force the GHM with ERAI data. The forcing of the GHM with the GCM is illustrated in Figure 6.3. We use the following variables from the GCM: total precipitation ($\boldsymbol{P}$), mean sea level pressure (MSL), temperature and dewpoint temperature at 2m ($\boldsymbol{T}$ and $\boldsymbol{T_d}$), wind at 10m (u_{10} and v_{10}), and surface solar and thermal radiation (SSR and STR). In the pre-process phase, potential evaporation (Epot) is calculated using Penman-Monteith (Monteith et al., 1965). Then we use potential evaporation, precipitation, temperature, mean sea level pressure and wind to force the GHM. We do not perform a bias correction on the GCM output.

In this study, we analyse the three main components of the hydrological cycle: precipitation, evaporation and discharge. First, we analyse precipitation from the GCM, because it is the main and most uncertain forcing variable for hydrological applications (Biemans et al., 2009; Fekete et al., 2004). To get a first impression, we compare simulated and observed spatial distributions of 30-year average daily precipitation sums over the basins. Figure 6.2 indicates the basin areas. With the monthly averages of basin averaged precipitation, we compare the seasonal cycle of the observations with the two resolution GCMs

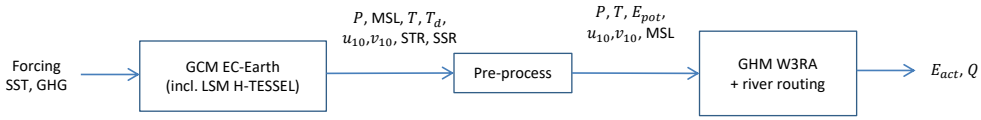

Figure 6.3: Flowchart illustrating the methodology of this study including the global climate model, the global hydrological model and the related variables: total precipitation (P), mean sea level pressure (MSL), temperature at 2 meter (T), dewpoint temperature at 2 meter (T_d), wind component x-direction at 10 meter (u_{10}), wind component y-direction at 10 meter (v_{10}), surface solar radiation (SSR), surface thermal radiation (STR), potential evaporation (E_{pot}), actual evaporation (E_{act}) and discharge (Q).

and ERAI. The robustness of these results is indicated by 95 % confidence intervals which are obtained after bootstrapping the daily data (Efron and Tibshirani, 1994), assuming all years to be independent. We perform an extra analysis over the Mississippi basin to better understand the precipitation patterns. We focus on the Mississippi, as extensive analysis has already been performed for the Rhine (Van Haren et al., 2015). We analyse the large-scale circulation patterns over the basin and we quantify the convective part of precipitation, which plays an important role in the Mississippi.

Furthermore, we statistically assess precipitation extremes by calculating the return time of annual maximum 10-day precipitation sums (van Haren et al., 2013; Shabalova et al., 2003; Kew et al., 2011). We have chosen to analyse 10-day precipitation sums, as multi-day precipitation extremes are mostly connected with extreme discharge (Disse and Engel, 2001; Ulbrich and Fink, 1995). The maxima are rank-ordered and an empirical distribution is applied to determine their return time T: $T = m/(N+1)$, where m is the rank-ordered maxima and N is the number of years in the data (30 years). Gumbel plots show the seasonal 10-day precipitation maxima as a function of the Gumbel variate $x = -\ln(-\ln(T))$, which can be translated into a return time T in years. The plots are made for annual maxima in every season (DJF, MAM, JJA and SON). These Gumbel plots are only based on 30 data points, which should be taken into account during the interpretation of these plots.

Second, we analyse actual evaporation which couples the physical climate system and hydrology as it can constitute a feedback between the atmosphere and the land surface. Therefore, actual evaporation (Eact) is calculated within the global climate and global hydrological model, which allows us to compare the two models. We derive monthly averages of basin-averaged actual evaporation over the basins. We only show Eact results from the 0.5° resolution GHM.

Table 6.1: Four different discharge measures: $\overline{Q}_{\mathrm{mean_h}}, \overline{Q}_{\mathrm{max_h}}, \overline{Q}_{\mathrm{min_h}}$ are respectively the mean, maximum and minimum daily discharge of year number h, ranging from 1 to 24. The total number of years (H) is 24.

Measure	Explanation	Calculation
$\overline{Q}_{\mathrm{mean}}$	24-year average mean annual discharge [$\mathrm{m^3\ s^{-1}}$]	$\overline{Q}_{\mathrm{mean}} = \frac{1}{H} \sum_{h=1}^{24} Q_{\mathrm{mean_h}}$
$\overline{Q}_{\mathrm{max}}$	24-year average annual maximum discharge [$\mathrm{m^3\ s^{-1}}$]	$\overline{Q}_{\mathrm{max}} = \frac{1}{H} \sum_{h=1}^{24} Q_{\mathrm{max_h}}$
$\overline{Q}_{\mathrm{min}}$	24-year average annual minimum discharge [$\mathrm{m^3\ s^{-1}}$]	$\overline{Q}_{\mathrm{min}} = \frac{1}{H} \sum_{h=1}^{24} Q_{\mathrm{min_h}}$

Third, we compare monthly-averaged discharge from the GHM with observations at Lobith (Rhine) and Vicksburg (Mississippi). In addition, we compare three discharge measures as defined in Table 6.1: $\overline{Q}_{\mathrm{mean}}, \overline{Q}_{\mathrm{max}}$ and $\overline{Q}_{\mathrm{min}}$. Finally, we determine the return times of annual maximum discharge per season, by using the same Gumbel distribution as described for precipitation. It should be noted that these results are based on 24 years of discharge simulations.

In addition, we aim to better understand the relation between precipitation and discharge. Therefore, we show scatterplots of daily discharge against previous 10-day precipitation sums for both basins, the high- and low-resolution GCM, and the observations. For the simulations, we only show the discharge results from the 0.5° GHM but the results from the 0.05° GHM were analysed and will be discussed where appropriate. The correlations are calculated for each season (DJF, MAM, JJA and SON) and we also include the annual maxima in discharge and 10-day precipitation sums.

All above-described methods compare observations with model simulations in a statistical way. However, individual high-impact weather events, hydrometeorological extremes, are also relevant. Realistic simulations of individual events are important in forecasts, impact studies and when assessing the potential effect of anthropogenic climate change. In particular, the emerging field of event attribution requires that events are plausibly simulated with numerical models (Stott et al., 2013; Hazeleger et al., 2015). In addition, single cases are often used as narratives to illustrate the complexity and linkage between components in the hydrometeorological system (Moezzi et al., 2017; Zappa and Shepherd, 2017). Therefore, the performance of this model set-up in describing hydrometeorological extremes is assessed by showing the rainfall-runoff response and synoptic pattern of a selected extreme event for each basin. This serves as an illustration of how the modelling results can be used for studying events. We show the results of the high-resolution GCM forcing the low-resolution GHM for the two basins.

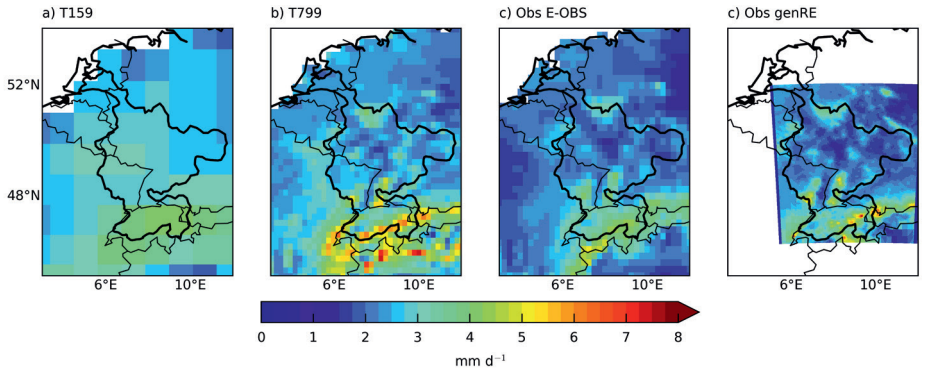

Figure 6.4: 30-year average of daily precipitation sums [mm d^{-1}] over the Rhine basin for the a) low resolution EC-Earth simulations (T159), b) high resolution EC-Earth simulations (T799), c) E-OBS dataset (Obs E-OBS) and the d) genRE precipitation dataset (Obs genRE).

6.3 Results and discussion: Rhine

6.3.1 Precipitation in the Rhine basin

The EC-Earth simulations and the observations (E-OBS and genRE) show a similar spatial distribution of precipitation over the Rhine basin (Figure 6.4), with more precipitation over the Alps (4-5 mm d^{-1}) than downstream over western Germany (1-2 mm d^{-1}). The high-resolution model shows, as expected, a more detailed distribution. A higher resolution orography reveals spatial structures such as the Alps, Ardennes and Black Forest. At the locations with large precipitation amounts, slight overestimations are found with the high resolution model (Figure 6.4b). It is unclear whether these overestimations are related to model performance or to underestimation of precipitation in the E-OBS dataset (Turco et al., 2013; Van Osnabrugge et al., 2017), as E-OBS is based on a sparse gauge network in mountainous areas (Hofstra et al., 2009) and no correction for undercatch is applied (Prein and Gobiet, 2017). The genRE precipitation dataset shows locally also higher precipitation values compared to E-OBS. Besides, it should be noted that not all Alpine, or other topographical, structures are kept within the high-resolution grid of 25 by 25 km.

From the basin-averaged precipitation sums in Figure 6.5a, we find that both resolutions GCM overestimate the observed precipitation amounts. From March until July the high-resolution model outperforms the low-resolution one. Van Haren et al. (2015), who used the same EC-Earth simulations, found similar improvements in high-resolution precipitation for the region that spans the Rhine and Meuse basins. They attributed this to the better represented storm tracks over Europe in the high-resolution simulations and therefore a more accurate horizontal moisture transport (Figure 9 in Van Haren

et al. (2015)). Nevertheless, despite the improvement with resolution, precipitation is still overestimated from January until June in T799 compared to the observations and ERAI (Figure 6.5a).

Figure 6.6 (left panels) shows the influence of resolution on the return time of annual 10-day precipitation maxima per season. During all seasons, and particularly in DJF and MAM, there is a distinct overestimation of precipitation by EC-Earth at lower return times (smaller than two years). This is in agreement with the overestimation in the monthly averages of precipitation (Figure 6.5a). At higher return times (larger than two years), we find an underestimation of precipitation in the GCM data in DJF (Figure 6.6a). The extremes in the storm-track season (SON) are quite well reproduced by the model. By comparing the two model resolutions, we find that in MAM and JJA the high-resolution model outperforms the low-resolution one for all return times, which suggests that with an increased resolution the right large-scale conditions are present to activate convection.

6.3.2 Actual evaporation in the Rhine basin

In Figure 6.5b we show actual evaporation from GLEAM, EC-Earth, ERAI and the 0.5° GHM forced with EC-Earth and ERAI. Actual evaporation (Eact) is overestimated in all simulations compared to the reference GLEAM, especially in winter (0.5 mm d^{-1}). This can be related to an overestimation of precipitation in winter, as an increase in precipitation can lead to larger evaporation rates. Actual evaporation from the high-resolution shows a smaller bias with observations than the low-resolution, which is consistent with our precipitation results. We also find an overestimation of Eact from ERAI compared to GLEAM (Figure 6.5b), though precipitation in ERAI is not overestimated (Figure 6.5a). These high evaporation amounts in ERAI can explain the large underestimation of simulated discharge at Lobith, discussed in the next Section 6.3.3.

There is a large difference between actual evaporation directly from ERAI and actual evaporation indirectly from the GHM forced with ERAI. This difference is smaller for the EC-Earth simulations. Possibly, this is because of an improved land-surface scheme in EC-Earth (H-TESSEL), while ERAI is based on the old scheme (TESSEL) that does not contain a seasonal cycle in leaf area index and has a global uniform soil texture (Balsamo et al., 2009).

The yearly-averaged Eact values from the climate and hydrological model are comparable, but there are seasonal differences (Figure 6.5b). As both models (GCM and GHM) solve actual evaporation from the energy balance, these differences are related to the vegetation and soil characteristics of the models. Actual evaporation from the GHM is higher in the beginning of the year (January until June) and peaks earlier in the season compared to the GCM (Figure 6.5b). Overall, it seems that the Eact from the GCM is in better agreement with the reference GLEAM dataset.

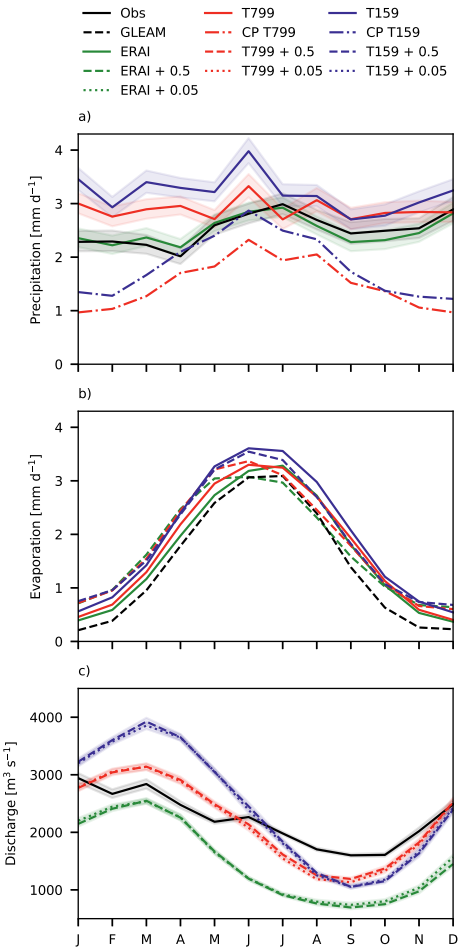

Figure 6.5: Monthly averages of a) basin-averaged daily precipitation sums [mm d^{-1}], b) basin-averaged daily evaporation sums [mm d^{-1}] and c) daily discharge [m^3 s^{-1}] at Lobith for the Rhine basin. Black lines are observations, green is ERAI. The red and blue lines are respectively the high resolution (T799) and low resolution (T159) GCM. The dash-dotted lines indicate convective precipitation, dashed lines output from the 0.5° GHM and dotted lines from the 0.05° GHM. The shaded bands indicate the 95 % confidence intervals.

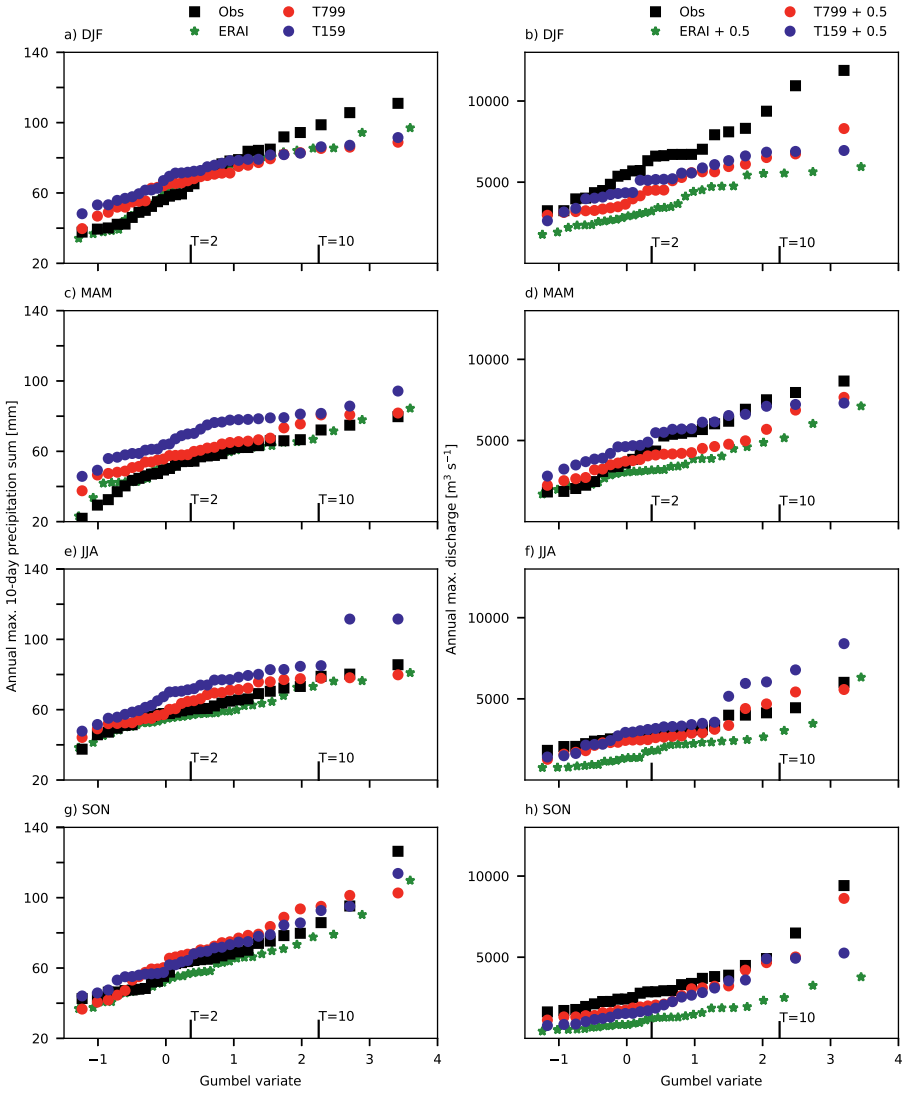

Figure 6.6: Gumbel plots of seasonal (DJF, MAM, JJA and SON) maximum 10-day precipitation sums [mm] over the Rhine (left panels) and maximum discharge [m^3 s^{-1}] at Lobith (right panels) and their related return times T expressed in standardized Gumbel variate $x = -\ln(-\ln(T))$. Observed discharges are shown in black, high resolution forcing (T799) in red, low resolution forcing (T159) in blue and forcing with ERA-Interim in green. The discharge results are output from the 0.5° GHM.

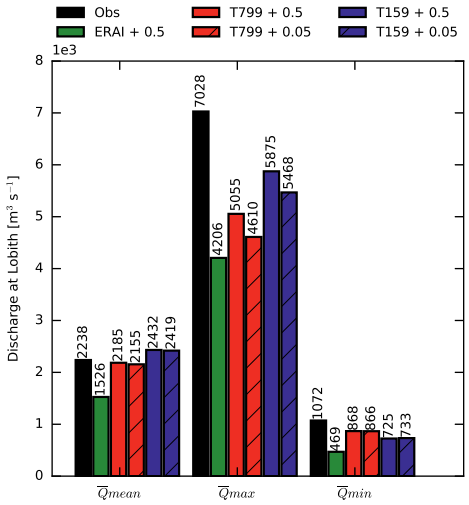

Figure 6.7: $\overline{Q}_{\text{mean}}, \overline{Q}_{\text{max}}$ and $\overline{Q}_{\text{min}}$ in m^3 s^{-1} at Lobith for the observations and the different combinations of simulations.

6.3.3 Discharge in the Rhine

In Figure 6.5c we show monthly-averaged discharge at Lobith from the 0.5° and 0.05° GHM, forced with EC-Earth T799, EC-Earth T159 and ERAI. Observed discharge is also shown. Figure 6.7 shows the discharge measures in a barplot.

The discharge simulated with ERAI forcing largely underestimates the observed discharge (~700 m^3 s^{-1}), in particular from June until December (Figure 6.7 & 6.5c). Photiadou et al. (2011) and Szczypta et al. (2012) present similar results, which they relate to an underestimation of precipitation in ERAI (Balsamo et al., 2010). However, our results show good estimates of basin-averaged precipitation from ERAI, except for a slight underestimation from August to November (Figure 6.5a). Therefore, we conclude that the GHM is too dry in the summer months for the Rhine basin, introducing a negative bias in discharge. We also find lower discharges in the end of summer with EC-Earth forcing, possibly related to the dry bias of the GHM. From February until May, the overestimations in precipitation from both resolutions GCM are reflected in overestimations of discharge, with the largest bias for the low-resolution forcing (Figure 6.5c & $\overline{Q}_{\text{max}}$ in Figure 6.7).

For the discharge extremes, we show similar Gumbel plots to those for precipitation, now for annual maximum discharges per season (right panels in Figure 6.6). The differences found in the return times of 10-day precipitation sums between the high and low resolution simulations are reflected in the differences found in the return values for the discharge,

in every season. However, the differences between simulations and observations are not consistent from precipitation to discharge. Firstly, this is because the hydrological model has a large influence on the discharge results, which was already seen from the monthly average discharge plots. For example, the dry bias of the model results in lower discharge extremes in SON (Figure 6.6h). Secondly, there is no one-to-one correlation between precipitation sums and discharge, as is shown more extensively in the next Section 6.3.4. Lastly, the River Rhine is highly regulated which affects the observations but not the simulations.

Overall, we can conclude that with the high-resolution EC-Earth forcing the seasonal cycle and the monthly averaged discharges are better represented compared to the low-resolution forcing, mainly because of improvements in precipitation. The difference in precipitation between the model resolutions is clearly reflected in discharge, although biases in the hydrological model also influence these results. The discharge extremes ($\overline{Q}_{\min}$ and $\overline{Q}_{\max}$) are not consistently improved with high-resolution forcing. It is not clear from these analyses whether that is related to the forcing or to the performance of the hydrological model. The results are robust based on our modelling system.

We also tested the resolution sensitivity of the global hydrological model. We find small but not significant differences in the discharge (measures) between the 0.5° and 0.05° model; the high resolution GHM (0.05°) gives slightly lower annual mean discharge results. With the 0.05° model, the peak flows are less extreme and the low-flows are similar to the low-flows from the 0.5° model. Because of a higher resolution orography, a more detailed river network is present in the high resolution model. Due to the presence of extra tributaries the response of precipitation to the main river may be damped, leading to a decrease in the peak flow.

6.3.4 Outlook on the extremes for the Rhine

In previous Sections, we showed that, compared to observations, the mean (monthly) statistics of precipitation, actual evaporation and discharge are improved with high-resolution modelling. We show the correlation between 10-day precipitation sums and daily discharge in Figure 6.8. It should be noted that by applying a moving window over the 24-year time series, individual events are reflected in multiple subsequent data points. We find the highest correlations during winter and the lowest correlations during summer. In summer, more evaporation occurs which decreases the correlation between precipitation and discharge. In winter, precipitation amounts are large and there is almost no evaporation, leading to higher discharges. In spring (MAM), fast surface runoff can be generated by rain occurring over saturated soils and rain-on-snow events (McCabe et al., 2007). We also find that the difference in correlations between the seasons is better represented in the high-resolution than low-resolution, compared to observations (Figure 6.8). In addition, the distribution of discharge and precipitation values of the

high-resolution forcing compares better to observations. The low discharge values, which occur in JJA with the low-resolution forcing, can be related to two events in two members of the simulations, and are unrealistic. The correlations of precipitation and discharge from the high-resolution GHM are not shown here, as these distributions are similar to the distributions with the low-resolution GHM (Figure 6.8a and b), except that less high peak flows are found with the higher resolution model (Figure 6.7).

To illustrate how the models simulate a high-impact event, we show here an event for the Rhine basin. The selected event is indicated with an open circle in Figure 6.8b and is an annual maximum in precipitation, occurring at the end of November. The average precipitation sum in SON is 30 mm. In this case the sum is 103 mm, resulting in a discharge of almost 9 000 m^3 s^{-1}. Figure 6.9a shows the rainfall-runoff distribution from 20 days before, until 10 days after the selected event. In addition, the synoptic situation is shown with 10-day averaged mean sea level pressure, vertical integrated moisture fluxes and the 10-day precipitation sums (Figure 6.9b). From the mean sea level pressure and moisture fluxes, we can infer that there is a low-pressure system (mid-latitude cyclone) situated over the North Atlantic, before the coast of Norway, bringing moisture from the Atlantic over Europe leading to extreme precipitation over the Alps.

This single case is an example of the linkage between components in the hydrometeorological system; large-scale circulation associated with extreme precipitation and high discharges for the Rhine basin. In this case, the high-resolution GCM is able to simulate patterns that better correspond to observations. This does not mean that the low-resolution GCM is not able to simulate such circulation patterns but previous studies have shown common biases among low-resolution GCMs, such as a too zonal storm track (Chang et al., 2012; Van Haren et al., 2015; Zappa et al., 2013).

6.4 Results and discussion: Mississippi

6.4.1 Precipitation in the Mississippi basin

While precipitation over the Rhine is dominated by the storm-track, the Mississippi basin has multiple climatic drivers (Figure 6.2). Moisture is advected from the Pacific resulting in high precipitation amounts over the Rocky Mountains (4-5 mm d^{-1}). The Great Plains, which are situated on the lee side of the Rockies, are relatively dry (1-2 mm d^{-1}), whereas the South-East of the USA is relatively wet (3-4 mm d^{-1}) because of convection and advection of moisture from the warm tropical Caribbean and Gulf of Mexico. Figure 6.10 shows the distribution of seasonal averaged precipitation over the Mississippi basin for the two resolutions of the GCM and the observations (CPC). There are clear improvements in the distribution of precipitation for the high resolution GCM over mountain ranges attributed to better representation of orography, such as over the Rockies, the Cascades, and the Sierra Nevada, which is in line with previous resolution studies with

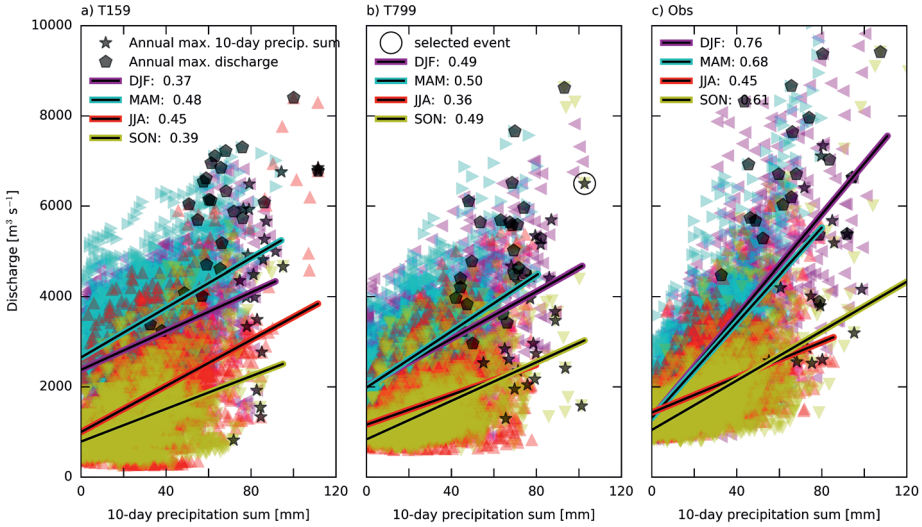

Figure 6.8: Scatterplot for the Rhine basin of daily discharge [m^3 s^{-1}] with previous 10-day precipitation sums [mm] for a) the low resolution forcing (T159), b) the high resolution forcing (T799) and c) the observations (Obs.). The discharge results shown here are obtained with the 0.5° GHM. The different seasons are indicated with the colours and regression line and correlation value. The annual maxima of both 10-day precipitation sums and discharge are indicated with respectively the black stars and hexagons.

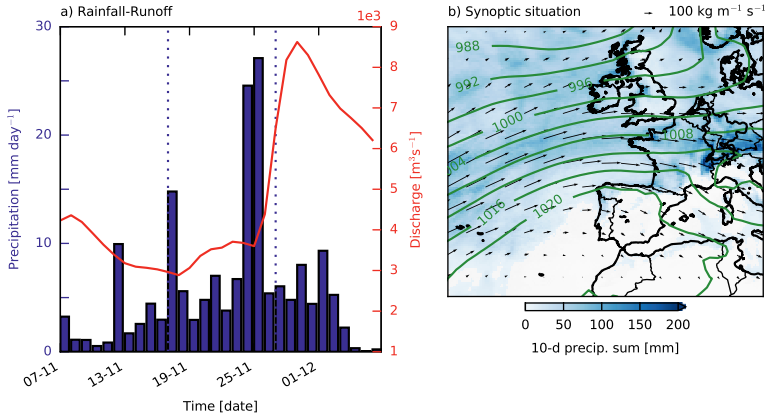

Figure 6.9: In a) precipitation (in blue) and discharge (in red) for the Rhine are shown 20 days before and 10 days after the selected event. The vertical dotted lines indicate the 10 day period, which is spatially summed in b). The contour lines in b) indicate the 10-day averaged mean sea level pressure in hPa and the arrows the 10-day averaged vertical integrated moisture fluxes in kg m^{-1} s^{-1}.

an atmosphere-only GCM (Duffy et al., 2003) and a coupled ocean-atmosphere GCM (van der Wiel et al., 2016b). Comparison of the simulations with observations reveals an overestimation of precipitation in the north-east of the catchment in DJF and MAM (Figure 6.10). In SON, in the south of the Mississippi basin, the high-resolution model shows higher precipitation amounts, comparable to the observations. These are not found in the low-resolution model. This could possibly indicate that cyclones which bring precipitation along the coast are better captured in the high resolution model.

Monthly and basin averaged daily precipitation sums of both simulations show a shift of one to two months in the seasonal cycle, where the highest monthly values occur in April/May instead of in June (Figure 6.11a). Moreover, the amount of precipitation in this shifted peak is overestimated (Figure 6.11a). The increase in precipitation in October-November is not observed but occurs, most pronounced, in the high-resolution simulations. A similar peak in October-November is found in the convective part and suggests a bias in convection in the high-resolution model. Similar precipitation biases are found in the EC-Earth simulations for the sub-basin averages (Missouri and Arkansas-Red, not shown). In contrast to the EC-Earth simulations, precipitation from ERAI shows the correct seasonal cycle (Figure 6.11a). EC-Earth and ERAI are based on the same atmospheric model (IFS), albeit different versions. Therefore we hypothesize that the precipitation bias found with EC-Earth is not present in the ERAI reanalysis, because of the data assimilation process. The precipitation budget from the ERA20C reanalysis data, where assimilation is performed on fewer variables than ERAI, shows a larger bias with observations compared to ERAI, supporting our hypothesis (ERA20C data not shown).

Apart from the precipitation bias between EC-Earth simulations and observations, no substantial differences in basin-averaged precipitation between the low and high resolution simulations were found (Figure 6.11a). This similarity between the two resolutions GCM could be explained by the convective component of precipitation, which is modelled at the sub-grid scale (i.e. parameterized) for both resolutions. We will further discuss convection in the next Section (6.4.2). Thereby, we will also assess the sensitivity of resolution to the large-scale circulation over the Mississippi basin.

The bias between observations and simulations is also reflected in the Gumbel plots of 10-day precipitation sums per season over the basin (left panels Figure 6.12). In MAM, there is an overestimation of the extremes for all the return times and in JJA an underestimation for all the return times. In SON, there are much larger precipitation extremes in the high resolution compared to the low resolution (Figure 6.12). This could possibly be related to the improved simulation of tropical cyclones with higher resolution, although this should be investigated further. In DJF, we find larger biases with the high-resolution compared to the low-resolution, although previous studies show improvements of extreme precipitation with increased resolution (Iorio et al., 2004; Wehner et al., 2010; van der Wiel et al., 2016b; Duffy et al., 2003). In the winter season moisture advection from the Pacific plays a large

role. A more detailed orography in the high-resolution simulations could trigger more precipitation leading to overestimations. In addition, "observed" precipitation products, like the CPC dataset, severely underestimate precipitation over the western mountain ranges (Lundquist et al., 2015; Henn et al., 2017).

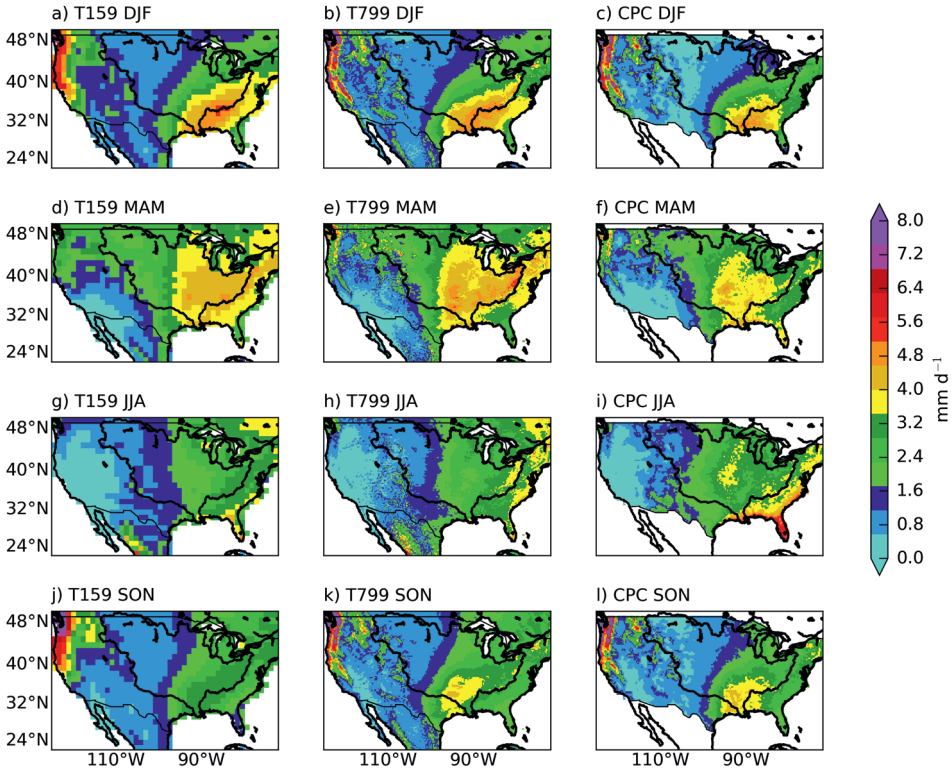

Figure 6.10: Seasonal means (DJF, MAM, JJA and SON) of daily precipitation sums [mm d^{-1}] from the low resolution EC-Earth simulations (T159, left columns) the high resolution EC-Earth simulations (T799, middle columns) and the observations (CPC, right columns).

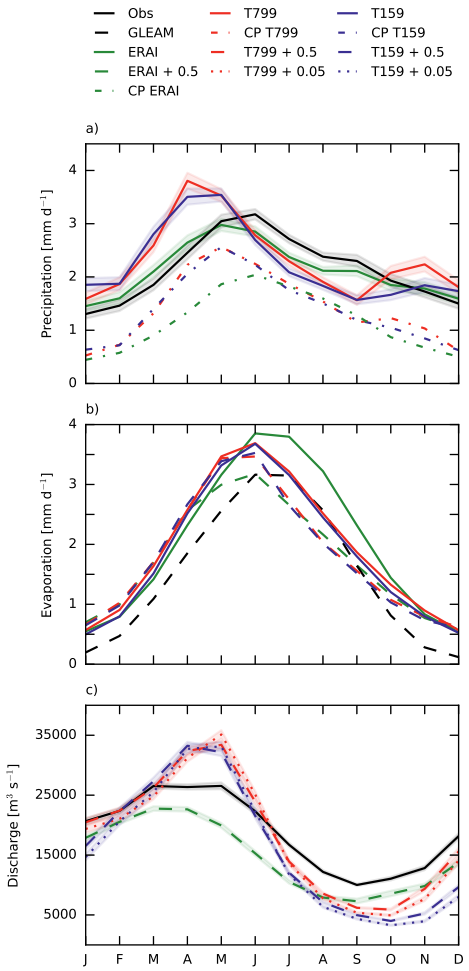

Figure 6.11: Monthly averages of a) basin-averaged daily precipitation sums [mm d^{-1}], b) basin-averaged daily evaporation sums [mm d^{-1}] and c) daily discharge [m^3 s^{-1}] at Vicksburg for the Mississippi basin. Black lines are observations, green is ERAI. The red and blue lines are respectively the high resolution (T799) and low resolution (T159) GCM. The dash-dotted lines indicate convective precipitation, dashed lines output from the 0.5° GHM and dotted lines from the 0.05° GHM. The shaded bands indicate the 95 % confidence intervals.

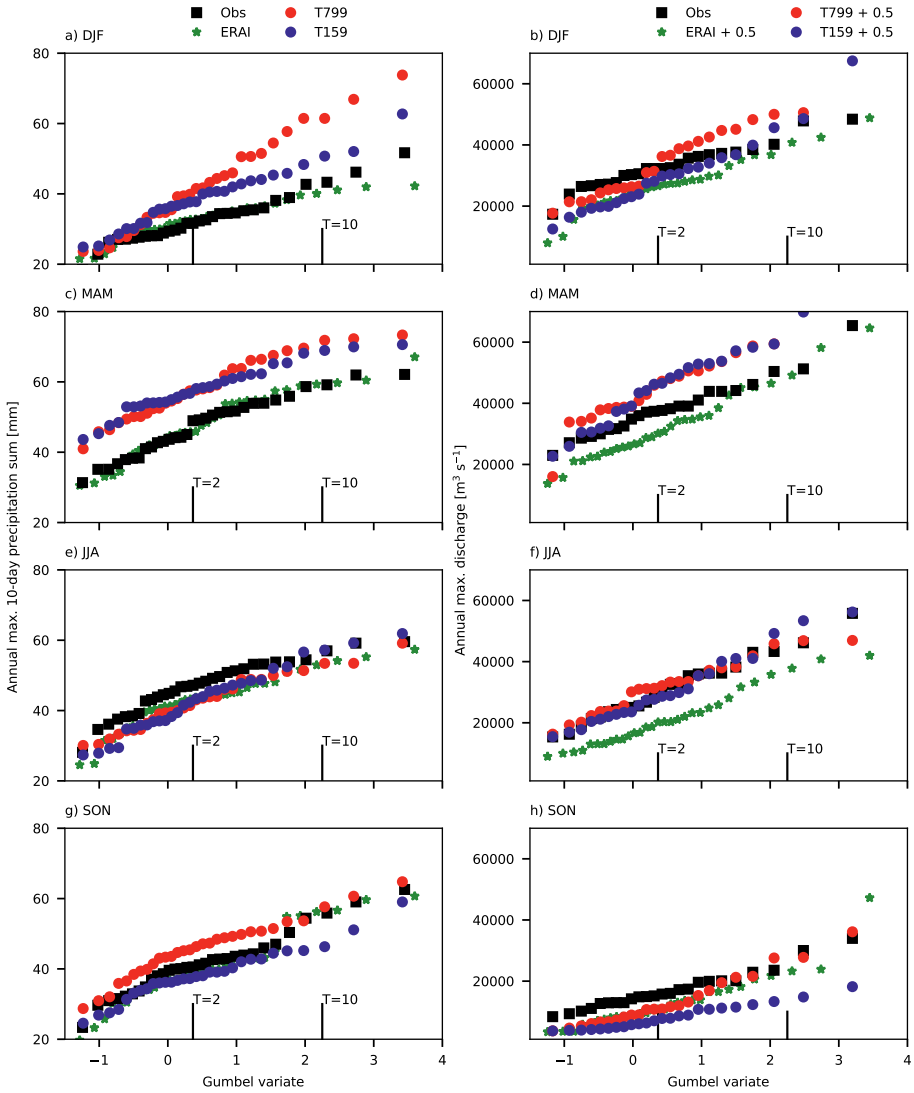

Figure 6.12: Gumbel plots of seasonal (DJF, MAM, JJA and SON) maximum 10-day precipitation sums [mm] over the Mississippi (left panels) and maximum discharge [m^3 s^{-1}] at Vicksburg (right panels) and their related return times T expressed in standardized Gumbel variate $x = -\ln(-\ln(T))$. Observed discharges are shown in black, high resolution forcing (T799) in red, low resolution forcing (T159) in blue and forcing with ERA-Interim in green. The discharge results are output from the 0.5° GHM.

6.4.2 Resolution analysis of the Mississippi basin

In the previous Section 6.4.1, our results show that a bias exists between simulated and observed basin-averaged precipitation for the Mississippi, especially in MAM (~0.5- 1 mm d^{-1}, Figure 6.11a). Moreover, no substantial differences in precipitation are found between the low and high resolution simulations, except for SON (Figure 6.11a). This is in contrast with our results for the Rhine basin, where better precipitation estimates are found with the high resolution GCM, because of better resolved large-scale circulation patterns (Van Haren et al., 2015). Here, we will shortly assess the resolution sensitivity of large-scale circulation and the role of convection over the Mississippi basin.

We show the precipitation generated by the convective parameterization as monthly averages in Figure 6.11a. The monthly averages of convective precipitation are very similar for the two resolutions GCM. Convective precipitation from ERAI shows a different seasonal cycle, with a peak later in the season (Figure 6.11a). This suggests that the bias in total precipitation in EC-Earth is mainly related to a bias in convective precipitation. The large contribution of convective precipitation to total precipitation in the model likely explains why we do not find differences in basin-averaged precipitation between the two resolutions in MAM and summer (Figure 6.11a), as convective cloud systems are smaller than both model resolutions grid size and therefore parameterized. This is confirmed by Iorio et al. (2004) who found no improvements in precipitation over the USA in MAM and JJA with increased resolution, which was related to the dominance of convective precipitation in these two seasons. Balsamo et al. (2010) mentioned that large-scale weather systems in winter are easier to simulate in numerical weather predictions than convective systems in summer. There are also studies which show that the link between soil moisture and precipitation is incorrect in models that parameterize convection (Hohenegger et al., 2009; Taylor et al., 2012a). Recently, convection-permitting simulations over the USA were performed (Liu et al., 2017), which show good performance in capturing the seasonal precipitation climatology, except for a dry bias in summer. In addition, the main characteristics of mesoscale convective systems were well captured in these new simulations (Prein et al., 2017).

Besides convection, large-scale structures bring moisture from the Pacific over the Rockies and from the Caribbean and Gulf of Mexico with the low level jet to the Mississippi. The resolution dependency of these large-scale processes is assessed by analysing geopotential height at 500 hPa (data not shown) and 850 hPa (Figure 6.13). We find that these patterns are very similar between EC-Earth T799, EC-Earth T159 and ERAI. In addition, we also show moisture convergence, as defined under steady state: $P - E = -\frac{1}{g}\nabla \cdot \int_0^{p_s} Vqdp$ (steady state version of Equation 2.9), where P is precipitation, E is evaporation, g is the gravitational constant, V represents the horizontal wind components and q is specific humidity. We define moisture convergence as positive and derive it from evaporation and precipitation. The overall patterns of moisture convergence are similar for EC-Earth T799,

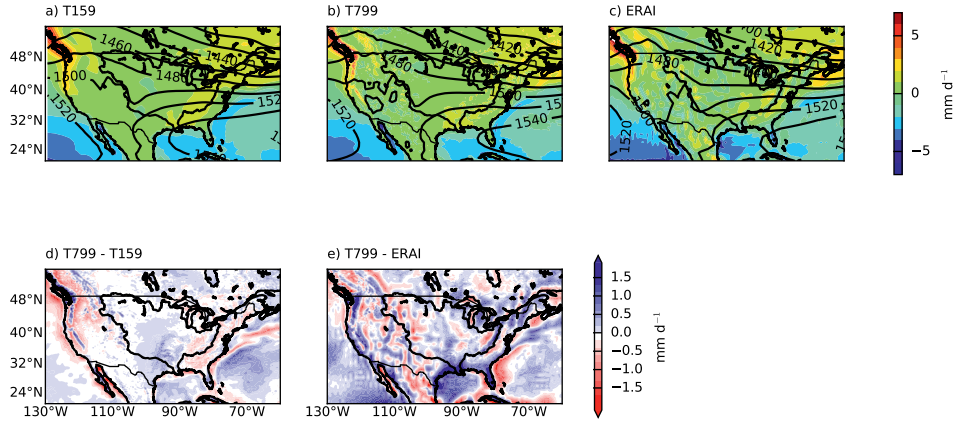

Figure 6.13: 30 year averages of geopotential height [m] at 850 hPa and moisture convergence [mm d^{-1}] over the Mississippi basin for a) the low-resolution GCM (T159), b) high-resolution GCM (T799), c) ERAI, and the difference between d) high and low resolution GCM (T799-T159) and e) high resolution GCM and ERAI (T799-ERAI).

EC-Earth T159 and ERAI. Differences on the local scale can be related to differences in resolution and therefore the representation of orography. From the difference plots (Figure 6.13 d & e) we find that the moisture convergence is more similar between the two resolutions EC-Earth than between the high-resolution EC-Earth and ERAI. This is in line with the precipitation patterns we found (Figure 6.11a), which are similar between the two resolutions but quite different in ERAI. There is more convergence in the high-resolution GCM compared to ERAI, which also results in more precipitation in the high-resolution GCM. There is also slightly more convergence in the high resolution EC-Earth compared to the low resolution, and we also found slightly higher monthly average precipitation in SON.

To summarize, this resolution analysis suggests that the positive bias in precipitation in EC-Earth is mainly related to the convective part of precipitation. A first analysis of the geopotential fields (500 and 850 hPa) shows that the large-scale patterns are very similar between the resolutions of EC-Earth and ERAI. We do find that the difference in moisture convergence between the two resolutions GCM is smaller than between the GCM and ERAI. This possibly indicates that the triggering of convection is different between the GCM and ERAI. However, we recommend further analysis to confirm these results.

6.4.3 Actual evaporation in the Mississippi basin

A consistent pattern between evaporation and precipitation is found in the simulations for the Mississippi basin. The shift in seasonal cycle in the EC-Earth precipitation budget is reflected in a similar shift in the Eact budget (Figure 6.11b). Furthermore, there are no substantial differences found in Eact between the two resolutions GCM. Nevertheless, we find large overestimations (~0.5 mm d^{-1}) of Eact in winter (NDJF) in the simulations compared to the GLEAM dataset. In November and December, these overestimations can not be related to the precipitation budget. These high amounts of evaporation in winter are also found for the Rhine and are therefore possibly related to the performance of the GHM.

The largest overestimations of actual evaporation are from the ERAI data, which was also shown by (Betts et al., 2009). The land-surface scheme of ERAI (TESSEL) has a fixed leaf area index (Van den Hurk et al., 2003) and a global uniform soil texture leading to low amounts of surface runoff (Balsamo et al., 2009), which could induce smaller amounts of interception and open water evaporation resulting in overestimations of evaporation. Moreover, there are large differences in actual evaporation from ERAI directly and from the GHM forced with ERAI (Figure 6.11b). These differences are larger for ERAI than for EC-Earth, which was also observed for the Rhine basin.

The actual evaporation from the GHM decreases faster from June onwards compared to the actual evaporation from the GCM. A similar sudden decrease was found in the discharge at Vicksburg. In other words, there occurs a quick drying in the GHM from May to June. This should be mainly related to the vegetation and soil characteristics of the GHM, as the GCM does not show the quick drying. Overall, it is hard to judge whether the evaporation product from the GCM or the GHM performs better in comparison with the observations as the seasonal bias in precipitation is also influences the evaporation budget.

6.4.4 Discharge in the Mississippi

We show the monthly averaged discharge at Vicksburg in Figure 6.11c and the different discharge measures in Figure 6.14. We find an underestimation of the ERAI forced discharge during the whole year compared to the observed discharge. We can only partly explain this with the underestimation of ERAI precipitation in JJA (Figure 6.11a). Precipitation from the ERAI/Land product agrees very well with the observations, however, discharge is still underestimated (data not shown). Therefore, we conclude that most of the underestimation in discharge is related to an overestimation of actual evaporation, which was shown in Section 6.4.3.

Annual mean discharge is underestimated (~2000 m^3 s^{-1}) with the low-resolution forcing and well simulated with the high-resolution forcing ($\overline{Q}_{\text{mean}}$ in Figure 6.14). The

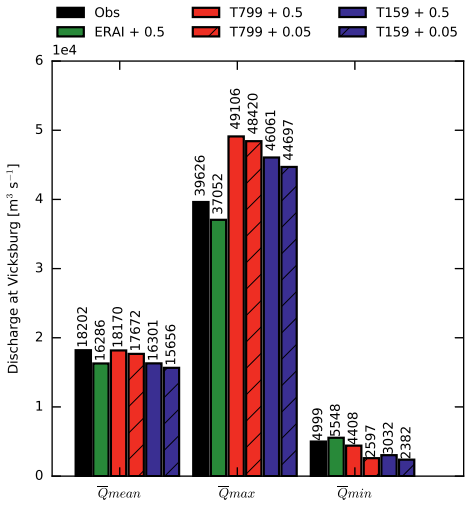

Figure 6.14: $\overline{Q}_{\text{mean}}, \overline{Q}_{\text{max}}$ and $\overline{Q}_{\text{min}}$ in $\text{m}^3\ \text{s}^{-1}$ at Vicksburg for the observations and the different combinations of simulations.

monthly-averaged discharge forced with EC-Earth is too high in spring, because of too high precipitation values (Figure 6.11). In January and February, precipitation (including snow) is also overestimated in EC-Earth leading to increased discharges in April and May when the temperature rises. From May onwards the discharge decreases more rapidly in the model than observed. During the rest of the year, there is a clear discharge response to the precipitation budget. It is possible that in October-November the improvements in discharge for the high-resolution exist for the wrong reason, as the second precipitation peak in the high-resolution is not seen in the observations.

For the extremes in SON, we also find a clear difference between the high and low resolution forcing (Figure 6.12g & h). With high-resolution forcing larger extremes are found, although discharge is still underestimated for lower return values, which was also found for the monthly averages. In DJF, there is a clear difference between the two resolutions for the largest return values in precipitation and this is also reflected in the return values for discharge, which are larger with high resolution forcing. In MAM, precipitation (extremes) is largely overestimated in EC-Earth, which is reflected in slight overestimations of discharge in the lower return values but large overestimations for the higher return values (Figure 6.12 c & d). As the GHM does not take into account reservoirs, a faster response of discharge on precipitation in the model simulations is expected compared to the observations. In the summer months (JJA), the discharge extremes are quite well represented by the model. Nevertheless, the ERAI forced discharge underestimates the extremes in these months.

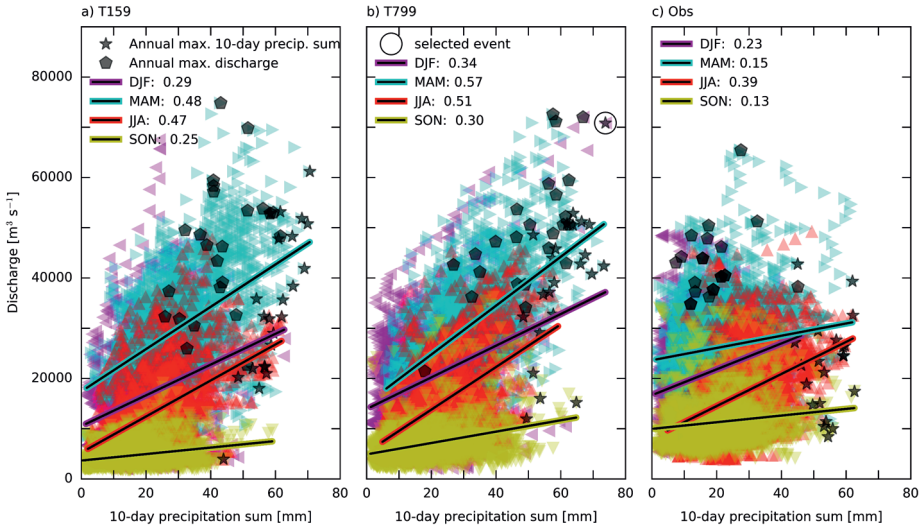

Figure 6.15: Scatterplot for the Mississippi basin of daily discharge [m^3 s^{-1}] with previous 10-day precipitation sums [mm] for a) the low resolution forcing (T159), b) the high resolution forcing (T799) and c) the observations (Obs). The discharge results shown here are obtained with the 0.5° GHM. The different seasons are indicated with the colours and regression line and correlation value. The annual maxima of both 10-day precipitation sums and discharge are indicated with respectively the black stars and hexagons.

In general, for the monthly averages and lower return values, the dry bias of the GHM is clearly reflected in the results. For the extremes with higher return values, we find that the signal of the precipitation extremes is reflected in the discharge extremes and the model performance plays a less important role. There are no substantial differences in discharge between the 0.5° and 0.05° resolutions, as was also found for the Rhine.

6.4.5 Outlook on the extremes for the Mississippi

Figure 6.15 shows the correlations between 10-day precipitation sums and discharge for the two resolution simulations and the observations over the Mississippi basin. For the simulations (Figure 6.15 a & b), we find the highest correlations in summer and the lowest correlations in winter, which is similar to what we found for the Rhine basin. For every season, correlations are lower with the observations compared to the simulations, especially in MAM. As this is the cropping period, irrigation requires a lot of water and reduces substantially the observed streamflow. Irrigation is currently not included in the hydrological model. This result shows the importance of including human activities in hydrological models.

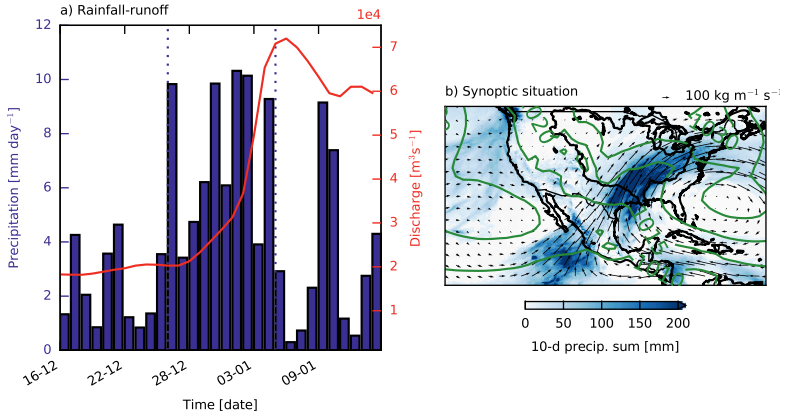

Figure 6.16: In a) precipitation (in blue) and discharge (in red) for the Mississippi are shown 20 days before and 10 days after the selected event. The vertical dotted lines indicate the 10 day period, which is spatially summed in b). The contour lines in b) indicate the 10-day average mean sea level pressure in hPa and the arrows the 10-day averaged vertical integrated moisture fluxes in kg m^{-1} s^{-1}.

The selected event over the Mississippi basin (open circle Figure 6.15b) occurs in January and corresponds to both an annual maximum in the 10-day precipitation sum (66.8 mm) as well to an annual maximum in discharge (72 000 m^3 s^{-1}). In addition, the selected event is the second most extreme event in the DJF Gumbel plot for precipitation (Figure 6.12a). From the synoptic situation and the vertical integrated moisture fluxes in Figure 6.16b we conclude that moisture is mainly transported from the Pacific and the Gulf of Mexico leading to precipitation over the south-east of the Mississippi basin, which is a region prone to extreme precipitation (Wehner et al., 2010). Berghuijs et al. (2016) show that (multiple) large precipitation events mainly occur over the south-east of the USA during winter. As the precipitation falls very close to Vicksburg, the response in discharge is relatively quick and leads to an exceptionally high discharge (72 000 m^3 s^{-1}), with a return period of 30 years.

6.5 Discussion

In this study, we have combined the EC-Earth GCM with the W3RA GHM in order to investigate the benefits of spatial resolution increase, without modification to the process representation within the models. Due to the large computational costs and the large amount of data involved, our study is constrained to one combination of GCM and GHM each run at two resolutions (Figure 6.1), for two river basins: the Rhine and Mississippi. In this section, we evaluate our experiment and put our approach and results in perspective

compared to other work and initiatives. We will discuss i) the importance of GCM resolution in the context of other studies, ii) the relevance of resolution increase in the GHM in comparison to a better process representation and the choice for using a global hydrological model instead of catchment-calibrated models, and iii) the extrapolation of the results for our two basins to the global scale and the limitations thereof.

6.5.1 Increased resolution of the global climate model

We examined the effect of increased resolution on precipitation using an atmosphere-only set-up of the EC-Earth global climate model. By comparing two different resolutions with the same process representation, we were able to estimate the benefits of increased spatial resolution alone. As the spatial scales of atmospheric motions span the entire range from the global to the viscous scales, a resolution increase will always reveal more detailed flow characteristics. This is because the flow characteristics of a non-linear dynamical system such as the atmosphere will change when numerical resolution increases and viscosity and diffusivity decrease. Hence, we found that a resolution increase led to better precipitation simulations in the Rhine basin (Section 6.3.1), where precipitation is dominated by large-scale weather systems.

There are currently only a few global climate model simulations available at such high resolution as the EC-Earth T799 runs used in this study (Davini et al. 2017b; Delworth et al. 2012; Schiemann et al. 2018; and more references within Haarsma et al. 2016). Other global modelling experiments at high resolution similar to ours, such as Schiemann et al. (2018), who used a resolution ~25 km with the HadGEM model, also found improved winter precipitation over Europe. While we found that better representation of weather systems was the main driver of the improvement (Van Haren et al., 2015), they attributed the improvement mainly to a better resolved orography. The varying response to resolution increase among GCMs is one of the main themes of the HighResMIP project, where the robustness of climate simulations at high resolution of ~25 km is examined (Haarsma et al., 2016). While this model intercomparison will likely reveal many new insights into the robustness of numerical model simulations, the studied models will still have insufficient resolution to capture all relevant atmospheric processes, such as convective precipitation and flow phenomena driven by small-scale orography. Hence further studies on the effect of resolution increases will be needed.

6.5.2 Process presentation versus increased resolution in global hydrological modelling

While for an atmospheric numerical model the main benefit of a horizontal resolution increase is the better representation of flow phenomena, such as weather systems, the main benefit of the GHM is found in the representation of details at the land surface, i.e. improved spatial heterogeneities in topography, soil and vegetation. For this reason, to

simulate the land-surface hydrology, we have chosen to calculate actual evaporation with the higher resolution GHM rather than the GCMs land-surface model (LSM). Besides, most GCMs (including EC-Earth) do not have a detailed routing module.

In a GHM, all processes are parameterized. No new phenomena are simulated by just increasing resolution. Increasing the resolution of a GHM potentially requires the addition of different process representations (and thus parameterizations) that become more relevant at finer resolution, such as lateral groundwater flow (Wood et al., 2011; Bierkens et al., 2015; Van Dijk, 2010c). Next to the potential need for additional processes to be included, acquiring the necessary parameters to run the GHM becomes increasingly complex at high spatial resolution. Many parameters are uncertain, especially because most are non-physical and difficult to determine across scales (Melsen et al., 2016).

Different approaches are taken to develop models that are robust over a range of spatial scales for the application in global hydrological modelling. For example, several studies apply parameter regionalization techniques to adapt parameters across scales (Samaniego et al., 2010). Gao et al. (2014a, 2016a) suggest that, when physical processes are connected to the correct landscape indicators, regionalization can be applied without further calibration. The root-zone storage capacity is such a scale-independent parameter (Gao et al., 2014b). This approach has a potential for resolution comparison studies, and it can be applied globally (Wang-Erlandsson et al., 2016).

We believe that different approaches to deal with scale interactions, among the ones we mention here, deserve rigorous study. In this study, we followed probably the most simple approach, namely testing from a 'global modelling perspective' if enhancing the resolution of the GHM will improve modelled discharge (going from 0.5° to 0.05°). We simply remapped the parameters from the low 0.5° to the high 0.05° resolution model, except for vegetation and orography which are known at high resolution (see Section 6.2.2). This allows comparison of the outcome of the models in a transparent way, which would not be possible or be very difficult otherwise, because the model itself would change. With this technique, we find no consistent improvements in discharge with the higher resolution GHM. This could be related to the choice of our GHM, as we only use one model, or to the need for more elaborated process representation (e.g. subsurface lateral flow). Our results therefore indicate that only increasing the resolution of the GHM has limited effect on simulating discharge. This conclusion is in line with the achievements/challenges of prediction in ungauged basins as summarized in Hrachowitz et al. (2013).

Besides the discussion on process presentation versus high-resolution modelling, we would like to note that we have performed the simulations with W3RA from the viewpoint of 'global hydrology', i.e. using a global hydrological model not specifically designed for the two basins. Often global hydrological models are used in a climate context, while not being optimized for individual basins. If we want to obtain the best results in modelling the hydrological balance over the Rhine and Mississippi basins, we should have chosen specific

regional calibrated models built for the specific basins (calibrated-catchment models), which is not in line with our viewpoint here.

Furthermore, we have only carried out a limited performance analysis of W3RA. The study by Beck et al. (2017) compares daily runoff from multiple GHMs, including W3RA, and finds pronounced inter-model differences in the performance. This underlines the importance of hydrological model uncertainty. W3RA obtained moderate to good scores (Beck et al., 2017). Our results show that W3RA overestimates actual evaporation in comparison to GLEAM which possibly results in an underestimation of discharge in both the Rhine and the Mississippi basins.

6.5.3 Extrapolation of results to other basins

This study focuses on the effect of resolution of a GCM and a GHM in modelling the hydrological cycle for the Rhine and Mississippi basins. These two well-measured basins only represent a subsample of the global diversity of catchments. Nonetheless, the conclusions from this study could be used as a guideline when assessing the benefits of resolution increases in modelling the hydrological cycle of other basins with comparable characteristics.

Our conjecture is that the improvements in the simulated hydrological cycle that is found in the Rhine basin will be valid for basins situated along mid-latitude storm-track extensions, where precipitation related to large-scale synoptic weather systems dominates total precipitation. Therefore, for those basins improvements in the hydrological cycle can be expected when higher resolution GCMs are used. For the Mississippi basin, no clear improvements in precipitation were found with increased resolution. This is possibly due to the representation of atmospheric convection. We may expect large improvements in the coming decades, when running convection-permitting GCMs becomes feasible for climate studies (Liu et al., 2017; Prein et al., 2017).

6.6 Summary and Conclusions

We study the benefits of increased spatial resolution in global simulations of the hydrological cycle. In our set-up, we force a global hydrological model (GHM) with output from a global climate model (GCM). The GHM is run at 0.5° (low) and 0.05° (high) resolution, whereas the GCM is run at 1.125° (low) and 0.25° (high) resolution. This yields four combinations that are thoroughly compared in this study. We do not modify the representation of physical processes in the models when increasing the spatial resolution, in order to be able to compare the effects of resolution alone. We analyse three main components of the hydrological cycle: precipitation, actual evaporation and discharge. We focus on two river basins with contrasting climatic drivers and for which enough verification data exist: the Rhine and Mississippi basins.

By increasing the resolution of the EC-Earth GCM from ~120 km^2 to ~25 km^2, precipitation over the Rhine basin improves significantly, caused by the better represented large-scale circulation patterns (Van Haren et al., 2015). Therefore, we suggest using high resolution simulations on a global scale when studying climatic impacts on the Rhine basin. The climatic drivers of the Mississippi basin are related to local convective events, large-scale weather systems from the Pacific and moisture transport from the Caribbean, possibly associated with tropical storms. Our results show that the increased resolution GCM (~25 km^2) hardly affects precipitation over the Mississippi basin. Likely this is because the spatial scales involved in convective precipitation are still too small to be resolved, and the model therefore relies on the same parameterizations for convection at low and high resolutions. For a good representation of the hydrological cycle over the Mississippi basin, we therefore recommend using convection-permitting models to explicitly resolve moist convective processes.

The (improved) monthly averaged precipitation from the GCM is reflected in (improved) monthly averaged actual evaporation and discharge from the GHM. Thus, the monthly averaged discharge of the Rhine is better simulated with high-resolution GCM input, although we did not find improvements in the representation of extreme streamflow events. For the Mississippi basin, no substantial differences in precipitation and discharge were found between the two resolutions input GCM and the two resolutions GHM.

To increase the model resolution of the GHM, we have remapped the parameters from the 0.5° to the 0.05° resolution, except for orography and vegetation where we used high resolution information. With these settings for the high resolution GHM (~5 km^2), no significant changes in discharge were found for both basins. Improvements in discharge are expected with high resolution GHMs when hydrological processes and parameters are better understood and described. Based on the results of our study, we conclude that due to the clearly distinct response of the chosen river basins to resolution increase, the route from improved resolution to better results is a challenging one. Our study, however, provides new and valuable insights on what to expect from spatial resolution increase when modelling the hydrological cycle for basins in the mid-latitude storm tracks or in convection-dominated regions.

Code and data availability The observational data (precipitation from E-OBS and CPC, actual evaporation from GLEAM and discharge from GRDC) used in this study are stored in a repository: `https://doi.org/10.4121/uuid:b7b988fc-f5c8-4ce1-8e33-47f31d04a99d`. A description on how to process the data to obtain the results of this Chapter is presented in the README file `https://data.4tu.nl/repository/uuid:c3b6e367-8215-4640-81d2-9f74994e65f4`. The parameter fields of the hydrological model and the routing module are also stored in this repository, together with the executables of these models. The main description of the global hydrological model W3RA code and parameters is given in Van Dijk (2010c). The model code

is also open source and online available on Github: `https://github.com/openstreams/wflow/blob/master/wflow-py/wflow/wflow\_w3ra.py`. The EC-Earth data and the output of the hydrological model are available upon request to the authors.

7

Synthesis

7.1 Introduction

Water and weather are intrinsically connected. To explain hydrometeorological events, such as flood and drought, one first needs to understand the anomalous circulation of water (vapour) in the atmosphere. In this thesis we combine the field of climate science, meteorology and hydrology to study the water cycle in the mid-latitudes. Atmospheric moisture transport is considered for three distinct geographical regions, where different mechanisms play a role, over multiple time and spatial scales (Figure 1.1). We do so with a modelling approach, using climate and hydrological models to simulate the water cycle and analyse future projections. Observational products are used for validation of model simulations.

In the Introduction of this thesis, two key scientific challenges on the water cycle and its hydrometeorological extremes were identified. The first challenge is to increase process understanding of the water cycle and its extremes, and the second is how these are regionally affected by climate change. In this Synthesis we reflect on these two key scientific challenges, organized along the research conducted within this thesis. In the first part, we discuss two mechanisms of anomalous moisture transport in the mid-latitudes: atmospheric rivers and blockings. These mechanisms are studied for present climate (Chapter 3 and 5), and we reflect upon their possible future changes. Moreover, we embed our conducted research in the broader field, and give an outlook on further research possibilities. The embedding of this research in the existing literature is angled towards the studies that are closely related to my expertise or somehow got my attention, and does not cover all literature that is available within the field. In the second part of this Synthesis we take a wider perspective on global modelling practice and simulating the seasonal water cycle in the mid-latitudes (Chapter 4 and 6), first with a focus on atmospheric moisture tracking, then a focus on atmospheric modelling, and last addressing hydrological modelling. Finally, I end this Chapter with some closing remarks, sharing my vision on how to continue in the field of hydrometeorology.

7.2 Moisture transport mechanisms

7.2.1 Atmospheric rivers

In Chapter 3, we increased our process understanding of the relation between atmospheric rivers and extreme precipitation along the coast of Norway by answering the question: **How is extreme precipitation along the coast of Norway linked to Atmospheric Rivers and how is their large-scale pre-conditioning?** A climatology of winter extreme daily precipitation events was presented, where more than 85% was associated with an atmospheric river. Similar relations between ARs and extreme precipitation were found for other coastal regions in Europe (Lavers and Villarini, 2013), such as Portugal

(Ramos et al., 2015) and the UK (Lavers et al., 2011). Recently, Ionita et al. (2020) showed that past major floods in the lower Rhine basin were associated with atmospheric rivers reaching further inland. This implies that inland mountain ranges such as the Alps might trigger orographic precipitation when atmospheric rivers, or excess moisture, reaches inland, and thereby result in flood. Further research is needed to investigate if this is a robust relationship.

In general, the regions where atmospheric rivers make landfall are mountainous areas with a complex topography. To be able to simulate the local impact of precipitation and flooding over complex terrain, more spatial details on orography are needed (Payne et al., 2020; Schaller et al., 2020). Otherwise, when using a global model in steep terrain with highly varying precipitation amounts, errors may arise. Furthermore, to simulate the impact of floods in local valleys, besides the high spatial resolution to capture the area of a catchment in multiple grid cells, a high temporal resolution is required (Schaller et al., 2020). To provide this information a modelling chain is needed starting from a global climate model, through downscaling with a regional model, which is used as input for a hydrological or operational flood-forecasting model (Hegdahl et al., 2020). Besides the ability of the model chain to capture the process from atmospheric circulation to local impact on hydrology, antecedent soil moisture and snowpack conditions also play a role in determining the local impact of a large-scale feature as an AR (Payne et al., 2020).

In the Introduction we indicated that atmospheric rivers are part of mid-latitude cyclones. The other way around, only half of the mid-latitude cyclones are linked to an atmospheric river (Payne et al., 2020), indicating the complex relationship. Besides, atmospheric rivers have also been linked to the lifetime of multiple cyclones, occurring in temporal sequence (Sodemann and Stohl, 2013). This serial clustering of cyclones occurs more frequently than expected by chance (Pinto et al., 2014). Different mechanisms are proposed to link baroclinicity and cyclone clustering, such as wave breaking and diabatic heating (Hu et al., 2017; Pinto et al., 2014; Weijenborg and Spengler, 2020). The next step is to link those mechanisms to the occurrence of atmospheric rivers. In Chapter 3 we investigate the large-scale preconditioning of atmospheric rivers affecting Norway and find two distinct patterns. One pattern constitutes an intense southward shifted jet with a southwest to northeast orientation. A second pattern is characterized by a more zonal weak northward shifted jet. These findings were in line with the two configurations suggested by Sodemann and Stohl (2013), who studied excess moisture transport in the wet month of December 2006 in Norway. Further investigation is needed to establish the relationship between the jet, individual/clustering of mid-latitude cyclones, and long lasting atmospheric rivers. Potential ways to move forward, are to track the moisture within ARs (Sodemann and Stohl, 2013) to determine to which cyclones they are connected, and get a better understanding where the moisture originates from, and how moisture is related to baroclinicity. Besides moisture tracking, where uncertainties arise related to the moisture tracking model (Box 7.2), more in-situ observations within atmospheric

rivers are needed for increased understanding of the moisture transport mechanism as part of (multiple) mid-latitude cyclones. With aircraft measurements vertical profiles can be collected, which give essential information on the spatial structure and time evolution. Field campaigns such as the NAWDEX campaign (North Atlantic Waveguide and Downstream Impact Experiment, Schäfler et al. 2018) provide insights on vertical and horizontal distributions of moisture within storm systems, which can complement modelling studies.

The second scientific challenge posed in the Introduction is regional projections of the water cycle and future hydrometeorological extremes. Whan et al. (2020) studied intensity and frequency of atmospheric rivers affecting Norway in a future climate using the high spatial-resolution simulations of EC-Earth, that are also used in this thesis (see Chapter 2). They found that by the end of the century (2094-2098, RCP4.5) Norway will likely experience more intense and more frequent AR events (Whan et al., 2020), resulting in more precipitation. An additional result was that precipitation will likely fall more often as rain instead of snow, increasing the probability of flooding in winter and autumn (Whan et al., 2020). More intense ARs are expected as rising temperatures lead to more moisture in the atmosphere (thermodynamic effect), and similar intensifications of ARs are reported to affect other regions (Ramos et al., 2015; Gao et al., 2016b). However, the dynamic part is uncertain, resulting in the question if changes in the location and extend of ARs influence the location of landfall (Payne et al., 2020). This uncertainty in the large-scale circulation in future projections, are, among others, one reason for the uncertainty in regional projections. An approach to deal with these uncertainties, recently gaining attention, is to provide storylines on the tales of possible future weather events (Hazeleger et al., 2015). Within these storylines one explains the physics involved in the scenario of a selected extreme event, touching upon the imagination of users, although not quantifying the probability of such a storyline/event, and thus avoiding the challenging question how dynamics will change towards the future (Shepherd et al., 2018; Trenberth et al., 2015). These storylines are especially useful for the communication of high impact events with stakeholders. An example in the case of an atmospheric river is provided by Schaller et al. (2020), who communicated the story/modelling effort of an atmospheric river impacting the coast of Norway, along the expected modelling chain of global regional and flood-forecast modelling, as mentioned in the previous paragraph.

7.2.2 Blocking and land-atmosphere interactions

Another example of a storyline approach was given by Wehrli et al. (2020) who studied the extremely dry summer of 2018 over western Europe under different warming scenarios and a scenario with no human imprint. All simulations were nudged towards the dynamical situation of 2018. They found maximum temperatures over 40°C in the future scenarios (Wehrli et al., 2020). Such a study provides insightful information that helps understanding risk and consequences of similar events in a future climate. Regarding

process understanding, the first scientific challenge posed in the Introduction, we studied the moisture sources of western Europe during the drought of 2018, results are given in Box 7.1.

Within the research presented in this thesis, the dry summer of 2018 was investigated in terms of moisture sources of the Rhine basin, and compared to another extremely dry summer of 2003 (Chapter 5). The related research question reads: **What are the anomalous moisture sources of the drought over the Rhine basin in summer 2003 and 2018?** We found interesting differences for the 2003 and 2018 moisture sources of the Rhine, and thereby the importance of the large-scale drivers and local land-atmosphere interactions. In 2018, the synoptic situation with persistent blocking was more favourable to result in drought over the Rhine basin compared to 2003. For 2003, the positive precipitation temperature feedback enhanced the drought at the end of summer (Fischer et al., 2007b). Liu et al. (2020) also observed strong soil moisture-temperature coupling during the 2003 heatwave, and a weaker coupling in 2018. The amplification of drought through drought propagation can be studied using moisture tracking, as is done for North America by Herrera-Estrada et al. (2019). The propagation of the heatwave in 2018 was studied by Spensberger et al. (2020) who found no recycling of heat from the heatwave in July over Scandinavia to the heatwave in central Europe in August. In contrast, for the Russian mega-heatwave in 2010 heat advection from upwind areas is shown to play a role in the amplification of the heatwave (Schumacher et al., 2019). So far, advection of heat and moisture are often studied separately. However, when transport of heat and moisture are investigated simultaneously, links between the energy and water cycle might lead to deeper insights in the mechanisms and developments of droughts and heatwaves.

The second key scientific challenge on regional projections, raises the question how moisture sources of the Rhine basin are projected to change in future summers. As pronounced warming is undoubtedly occurring now and in the future, heatwaves will become more likely (Schär et al., 2004; Meehl and Tebaldi, 2004), and droughts probably more frequent (Seneviratne et al., 2010; Trenberth et al., 2014). Here we reflect upon the ability to simulate the synoptic situation (blocking) and land-atmosphere interactions affecting drought in western Europe, and how it will change to the future.

It has been, and remains, a challenge to correctly simulate mid-latitude atmospheric blockings in global climate models (Davini and D'Andrea, 2016). There is a historical tendency of models to underestimate the frequency of blocking (Woollings, 2010), whereas not much studies focused on persistency of blocking. Schiemann et al. (2020) investigated blocking with a new suite of high-resolution climate models, part of CMIP6-HighResMIP. They found that a resolution increase of 100 to 20 km benefits blocking frequency, although does not affect blocking persistency (Schiemann et al., 2020). In regards to climate change, the frequency and persistency of summer blockings projected towards the future is highly uncertain (Huguenin et al., 2020). Kennedy et al. (2016) finds no changes in blocking over

western Europe, while Masato et al. (2013) shows a small decrease in blocking frequency. Blockings over western Europe are related to a larger-scale pattern representing high-amplitude stationary Rossby wave-trains. Those high-amplitude waves with wavenumber 7 result in co-occurring droughts over western Europe and North America, and increased in frequency and persistence over recent decades (Kornhuber et al., 2019). However, it is not clear if this increase is related to climate change or multidecadal variability (Kornhuber et al., 2020; Mann et al., 2017). Also, the mechanisms of the occurrence of this pattern are unclear. Remote forcing from the tropics, from the Arctic and resonance in the jet stream have been reported (Cohen et al., 2014; Petoukhov et al., 2013). These mechanisms may all play a role and interact with each other. To summarize, signals in future changes in blockings and wave-7 pattern remain uncertain, as western Europe has a low signal-to-noise ratio (Woollings, 2010), which makes it more difficult to identify trend versus multi-decadal variability (Deser et al., 2012).

While the future dynamics of the atmosphere are very uncertain in models, observations and theory, the thermodynamic future changes are fairly robust (Shepherd, 2016). A valid related question is therefore how much future precipitation changes can be attributed to changes in circulation (dynamics) and or changes in global warming and land-atmosphere interactions (thermodynamics). We find in Chapter 5 that in the case of 2003 and 2018 the anomalous moisture sources were mostly explained by anomalous wind, thus anomalous dynamics, but we have not assessed trends. Van Oldenborgh et al. (2009) concludes that past rising temperatures over western Europe are not linearly related to shifts in atmospheric circulation, indicating that soil moisture depletion is important. Linden et al. (2019) studied soil drying over western Europe towards the future, and concludes that both anomalous circulation patterns and local feedbacks are responsible for a decrease in soil moisture (reduction in rainfall), and that both processes are better represented with higher resolution climate models. Fischer et al. (2007a) performed climate experiments with and without coupling of the land-surface and concludes that land-atmosphere coupling plays an important role for the evolution of the investigated heat waves both through local and remote effects. Thus soil moisture temperature and soil moisture precipitation feedbacks are shown to be important in droughts (Seneviratne et al., 2010), however the suggestion that droughts intensify and propagate via land-atmosphere feedbacks is not yet well understood (Miralles et al., 2019). In Chapter 5, we find the effect of soil moisture depletion in the Rhine basin indirectly, via a decrease of recycled moisture throughout the 2003 summer season. This only indicates local feedbacks over the Rhine basin, while it is well possible that soil moisture can have larger-scale non-local impact, as is suggested in literature (Fischer et al., 2007b; Haarsma et al., 2009; Pal and Eltahir, 2003). We can only find indications as soil moisture data and surface fluxes in reanalysis products may not be reliable.

Box 7.1: Moisture sources of western Europe during the 2018 summer drought

The persistence of high-pressure systems during summer 2018 also affected the atmospheric transport of moisture toward western Europe. Here, we identified the moisture sources for western Europe during the 2018 summer drought with the use of the Eulerian offline tracking tool WAM-2layers (Van der Ent et al., 2010, 2014). This tool was run using ERA-Interim reanalysis data (Dee et al., 2011) for May–August, and results were compared against tracking results for the long-term (1979–2018) summer mean. Precipitation over western Europe (region indicated with grey lines in Figure 7.1) was tracked backward in time to determine where this water originally evaporated (i.e. the moisture sources). The moisture sources during 2018 were determined to be much more of continental origin and less of oceanic compared to climatology. During most of the summer, a high-pressure system was located over western Europe/southern Scandinavia (see 500-hPa height anomalies in Figure 7.1), which redirected storms that normally result in precipitation over western Europe toward the southern Alps and south eastern Europe. As a result, less moisture was transported from the Atlantic Ocean toward western Europe. Precipitation that fell over the northern Alps (within the tracking region) in 2018 was mainly recycled from within the basin or originated from eastern Europe following the anomalous anti-cyclonic flow. Conversely, in southern Scandinavia, where the drought was strongest, moisture recycling over land was almost half of what it typically is in summer. The evaporation recycling ratio over southern Scandinavia was 6% in 2018 compared to 10% for the base period, which indicates that the drought there self-intensified due to positive soil moisture–evaporation–atmosphere feedbacks.

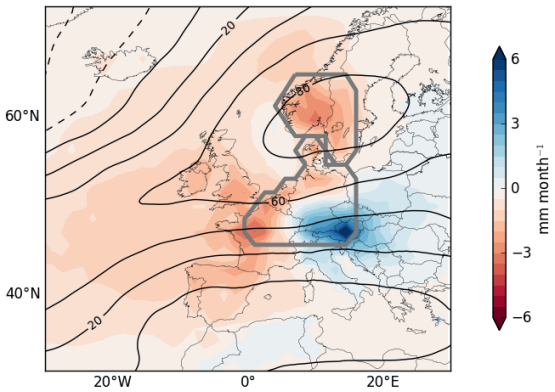

Figure 7.1: Absolute moisture source anomalies for western Europe (region indicated with grey contour lines) in mm month^{-1} (shading) and anomaly of geopotential height at 500 hPa in meters (contours). Anomalies indicate the difference between 2018 and the climatology from 1979-2018.

The information in this Box was a contribution to State of the Climate 2018 (Rosner et al., 2019).

Based on the findings given above, we expect that the exceptional droughts as 2003 and 2018 will happen more frequently due to rising temperatures. This insists an increased likelihood of anomalous moisture sources such as in 2003 and 2018 in the future. Rhine's moisture sources in summer will thus probably depend less on moisture transported from the North Atlantic, and other oceanic regions, and more on moisture sources over land. Consequently, local and land recycling will become more important in a future climate for the Rhine. This will make the basin more vulnerable for land-use changes and soil drying, thus soil-moisture climate feedbacks.

7.3 Modelling practices

So far, we discussed the two scientific challenges along two main mechanisms of (lack of) moisture transport: atmospheric rivers and blockings. However, the research performed in this thesis also focuses on understanding, and the ability of models to capture, the seasonal water cycle and its projections (Chapter 4 and 6). Further ideas, and embedding of, different modelling practices on understanding and projecting the seasonal water cycle are discussed below, going from moisture tracking to atmospheric and hydrologic modelling.

7.3.1 Moisture tracking

In Chapter 4, the WAM-2layers tracking model is adapted to perform tracking with the global climate simulations from EC-Earth (validation thereof is presented in Chapter 2), to determine the moisture sources of the Mississippi basin in present and future climate. These results are based on one climate model and one tracking model. Validation of moisture tracking results is difficult, as there are no observations available. The best verification possibility is found in isotope research, as stable water isotopes provide useful information on the origin of water, and oceanic and terrestrial sources can be distinguished. However, stable water isotope research does not provide a climatology of moisture sources for the large Mississippi River Basin. In Box 7.2 Mississippi's moisture sources studied in Chapter 4 are compared to the sources of the Mississippi found by other studies, using different datasets and moisture tracking methods. From this validation we learn that by combining different datasets and atmospheric moisture tracking tools, resulting moisture sources can differ substantially. This indicates that careful interpretation of moisture sources is needed. Further comparisons between different climate models and different tracking models will provide further insights.

The main research question of Chapter 4 reads: **How is the modelled atmospheric water budget over the Mississippi River basin (with a focus on its moisture sources) projected to change in the future?** We found a clear seasonal cycle in the moisture sources, with more recycling of moisture within the basin during summer

and more transport of moisture from the ocean toward the basin in winter. In future winters, increased evaporation over the oceans contributes to increased precipitation over the Mississippi basin. A decrease in moisture sources in future summers indicates that the moisture sources of the Mississippi basin become less local in a future climate. This implies less local dependence of changes in land-use within the basin, and increased dependence on water management and governance on the regional scale. Similar results with increased evaporation over the oceans are expected to lead to increased future winter precipitation in the Rhine basin.

Keune and Miralles (2019) proposed a 'watershed precipitation recycling network' to assess the vulnerability of freshwater resources between catchments in Europe, as is also done between countries (Keys et al., 2017). Their results suggest that changes in land-use affecting evaporation might propagate downwind and affect freshwater availability elsewhere. This application is part of the 'application list' of identifying 'the origin and fate of moisture' presented by Link et al. (2020), including a publicly available dataset demonstrating 'the fate of evaporation', i.e. the regions where precipitation occurs for a selected grid cell. Other applications for this dataset, and moisture tracking in general, are listed and incorporate understanding precipitation changes and trends, its inter-annual variability, and extreme weather events (Link et al., 2020). What is new in the study of Chapter 4 is that we apply tracking to future climate simulations, and we show in this thesis the added value of moisture tracking on understanding large-scale transport processes, such as blockings, and the seasonal water cycle. Summarized, atmospheric moisture tracking can provide insights in large-scale circulation, land-atmosphere interactions and water availability and sustainability, thereby emphasizing the intrinsic connection between atmosphere and hydrology. In my view, these fields should be more integrated, and moisture tracking tools are a good way to achieve this.

7.3.2 Atmosphere

In this thesis, we used atmospheric reanalysis data for process understanding of transport mechanisms and for validation. To investigate the effects of increased model resolution, and to analyse future projections of the water cycle, simulations of one climate model were used. In order to investigate the hypothesis that increased model resolution improves the representation of the hydrological cycle, we posed in Chapter 6 the main question: **Can we improve the simulated hydrological cycle over the Rhine and Mississippi basin by increasing the resolution of climate- and hydrological model?** This was studied using simulations with high and low resolutions from one climate model forcing a high and low resolution hydrological model. Concerning the atmospheric part, we found that increased resolution resulted in improved representation of precipitation over the Rhine basin. However, no improvements were found for the Mississippi basin, likely because the spatial resolutions are still to small to resolve convection.

Box 7.2: Validation of Mississippi's moisture sources

Here we validate the moisture sources of the Mississippi River Basin (Chapter 4) by comparing the results with other studies that determined the moisture sources of the Mississippi River Basin. Figure 7.2a shows the moisture sources determined in Chapter 4 (Figure 4.4, averaging over all seasons). Figure 7.2b shows Mississippi's moisture sources based on the NCEP reanalysis dataset from 1979 until 2014 and the quasi-isentropic back trajectory (QIBT) model (Dirmeyer and Brubaker, 2007). These results are published on the following website: `http://cola.gmu.edu/wcr`, and provided by Paul Dirmeyer after personal communication. Figure 7.2c shows the moisture sources of the Mississippi basin based on MERRA reanalysis from 1979 until 2008, using the same quasi-isentropic back trajectory (QIBT, data obtained after personal communication with Paul Dirmeyer).

Although the region where the moisture sources originate is comparable between the datasets and methods, there are very distinct differences in the amount of moisture source contributions. While in our study moisture sources are largest over the Gulf of Mexico and Gulf of California, these contributions are minor using NCEP data and the QIBT tracking, especially over the Gulf of California. This is partly due to the low resolution of 1.9° of the (old) reanalysis data, thereby not resolving the narrow water body of the Gulf of California. Using a more recent reanalysis dataset with the same moisture tracking technique (QIBT), shows different results (Figure 7.2c), more comparable to the sources found in this thesis. We expect overestimations in our study from the Gulf of California, due to overestimations in the specific humidity profiles using the interpolation technique (as described in Chapter 2). To summarize, different datasets and tracking techniques show distinct differences when comparing the moisture sources of the Mississippi basin. More tracking inter-comparison studies, using multiple climate model simulations and different tracking techniques is recommended to get a better feeling for the uncertainty around moisture sources.

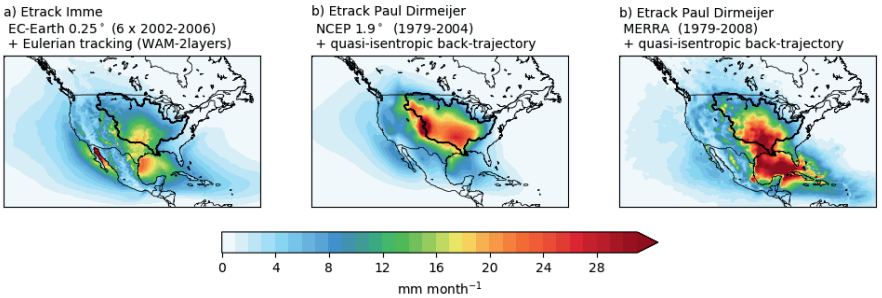

Figure 7.2: Moisture sources of the Mississippi for a) 30-years of simulations with EC-Earth and the Eulerian tracking model WAM-2layers, b) simulations with NCEP reanalysis 1.9° (1979-2004) using the quasi-isentropic back-trajectory model and c) simulations with MERRA reanalysis (1979-2008) and the quasi-isentropic back-trajectory model.

These results are based on simulations of one climate model, and thus depending on the specific physics and parameterizations used in that model. At the time the research was conducted, not many other climate simulations were available at such high resolution (Davini et al. 2017b; Delworth et al. 2012; Schiemann et al. 2018, and more references within Haarsma et al. 2016) as used in this study. However, with the availability of the CMIP6 high resolution simulations as part of the PRIMAVERA project, we are now able to verify the results found in this thesis among a diverse set of high-resolution climate simulations.

In Chapter 6, we approach the research question from a global modelling approach, and thereby investigate the benefits of increased model resolution. However, this does not mean that increasing the resolution of global climate models is the only 'way forward' to enhance our process understanding and improve modelling of regional water cycles. Similar questions as addressed in this thesis can be studied from a regional perspective. The European Coordinated Regional Downscaling Experiment (EURO-CORDEX) seeks to advance regional climate science (Jacob et al., 2020), and similar communities exist around the globe. Through dynamical and empirical-statistical downscaling more detailed simulations at the European level are provided, although depending on the boundary conditions of low resolution global climate models. In the evaluation of precipitation by Demory et al. (2020) the high-resolution global climate simulations (25-50 km) from PRIMAVERA are compared to the CORDEX regional climate simulations (12-50 km) over Europe. The effect of increasing resolution from 50 km to 12 km is small outside mountainous and coastal regions (Demory et al., 2020). This is a promising result indicating that high resolution global climate simulations can provide similar information as regional models, but then on a global scale. Or, differently framed, it indicates that both simulations are equally wrong when the driving physics act at even smaller scales, as what we hypothesize is the case for the bias in global simulations of (convective) precipitation over the Mississippi basin (Benedict et al., 2019b). What has potential in my opinion is that these high-resolution global models can be used as boundary conditions for higher resolutions regional models, going towards cloud permitting resolutions (cloud permitting models (CPMs), Liu et al. (2017) for North America and Prein et al. (2013) for the Alps). This cycle of increased resolution GCMs, providing better boundaries for RCMs and CPMs, will continue with increasing computational power (although with limits), and provides promising datasets to work with in the future. A challenge therein is to store and work with the large amounts of data involved, and process them in an efficient and transparent way, rather requiring programming and coding skills than meteorological knowledge.

Depending on the hypothesis or research question, another way forward to invest computational resources and improve process understanding is by creating large ensembles. Large ensembles are needed when one wants to study internal variability in relation to climate change (Deser et al., 2012). Uncertainty in climate projections arise from three main

factors: emission-scenario uncertainty, model-response uncertainty and natural variability (Hawkins and Sutton, 2009; Tebaldi and Knutti, 2007). The last mentioned uncertainty is addressed when using large ensembles. Model-response uncertainty can be validated when model results are compared, and modelling practices are improved. The use of large-ensembles in this thesis would improve our knowledge, also in terms of moisture sources, on the internal variability of moisture transport mechanism such as atmospheric rivers and blockings, and would provide more robust results in terms of extreme precipitation and flooding (when large ensembles of climate models forcing hydrological models are created, such as in Van der Wiel et al. 2019). To study moisture sources in large ensembles, atmospheric data at multiple levels in the atmosphere is required with a sub-daily timestep (6-hourly), which is often not available.

The last 'way forward' to enhance our understanding on regional water cycles from a modelling perspective, is to increase model complexity. Throughout this thesis we make use of atmosphere only simulations with the global climate model EC-Earth. Active coupling to the ocean however, is already quite common in high resolution models, and is shown to improve the development of storms (Takatama et al., 2012), and thereby moisture transport. Also surface fluxes are expected to become more realistic with an active coupling between ocean and atmosphere, especially in regions where storms develop (Kelly et al., 2010; Takatama et al., 2012). Although including ocean circulation and sea ice is already common in climate models, interactions with aerosols, carbon and nutrients as nitrogen are only included in so-called earth system models. By including complex interactions between for example water and carbon, or urban areas and their environment, simulations of the climate system become more realistic. However, one could also argue that with more conceptual models specific processes and their sensitivity can be better tested, while with a model including many complex interactions difficulties arise in assessing direct and indirect feedbacks.

In light of this research, increasing model complexity by coupling atmosphere and hydrology is relevant. A current limitation of land-surface models is that they often do not contain a routing module, i.e. that surface runoff is not translated to river runoff. When this last step is provided, river runoff can be directly simulated with global climate models, instead of running an additional hydrological model (as done in Chapter 6). This gives opportunities for model validation, as an integrated discharge response is a better observed variable then precipitation over mountainous areas where observations are sparse. Furthermore, a two-way coupling of atmosphere and hydrology also allows for direct feedbacks in land-atmosphere interactions. For example, extensive irrigation, if included in land-surface models, is shown to impact the regional climate (Puma and Cook, 2010; Thiery et al., 2020) and atmospheric water cycle (de Vrese et al., 2016). These interactions become even more relevant when dry regions get drier (Held and Soden, 2006) and the pressure on irrigation increases. Another interesting example of interactions between hydrology and climate, is how changes in land-use might affect the regional circulation.

Planting trees increases the latent heat flux which might influence precipitation elsewhere, depending on the circulation. In a system with direct interactions between the land and the atmosphere, and flexibility in changing land-use is enabled, moisture tracking can provide answers to the effect of regreening by planting trees, or the effect of deforestation on the climate (Khanna et al., 2017). Such studies need model interactions between vegetation and the atmosphere, where incorporating land-use changes also quests for high spatial resolution simulations.

7.3.3 Hydrology

In Chapter 6 of this thesis, a global hydrological model at low (~50 km) and high resolution (~5 km) is used to study the benefits of increased spatial resolution in simulating discharge over the Rhine and Mississippi basins. The global hydrological model W3RA is run with the original resolution of 50 km, which is the common resolution of current global hydrological models (Beck et al., 2016; Haddeland et al., 2011; Schellekens et al., 2016). To run the model at higher resolution, we remapped the parameters from the high to the low resolution, except for orography and vegetation which are known at high-resolution. Using this approach to increase the resolution of the model, no substantial improvements in discharge were found (Benedict et al., 2019b), although a discussion on the challenging field of hydrological modelling at multiple scales was triggered (Benedict et al., 2017). These challenges arise around model parameterizations, as many parameters are uncertain and non-physical (Melsen et al., 2016), and difficult to transfer across time and spatial scales. We show that our approach to deal with parameterizations across scales, simply remapping the parameters, does not result in improved discharge simulations and is probably not the best way forward. Different approaches on dealing with parameters in hydrological modelling across scales are taken. One way is to connect physical processes to landscape indications, allowing regionalization without further calibration (Samaniego et al., 2010; Gao et al., 2014a, 2016a). Such an approach was also taken by Imhoff et al. (2020) who combined point-scale (pedo)transfer functions with high spatial and temporal modelling for the Rhine basin. Almost all parameters were scaled over multiple resolutions (ranging from 4.8 to 1.2 km), while fluxes remain constant, and without any further calibration. With this method consistent parameter fields over various resolutions can be obtained. Besides, increasing the resolution of a hydrological model potentially requires the addition of different hydrological processes, which become relevant at higher resolutions. An example is for instance subsurface lateral flows, which are not considered in the simulations in Chapter 6, but are considered in the kilometer-scale simulations by Imhoff et al. (2020). These adaptations in parameters and included processes mainly strive for better results in simulated discharge. However, the correct simulation of other hydrologic variables such as soil moisture and snow pack can also be crucial. For example, in the case of a region affected by extreme precipitation from an atmospheric river, hydrological antecedent conditions affect the risk on flooding (Schaller et al., 2020).

7.4 Closing remarks

In the mid-latitudes, warm and cold fronts determine the transport of moisture and energy, resulting in convergence of moisture and precipitation over the continents. It is in these mid-latitude land regions where society is affected by the variations in weather, and thus the water cycle. Pressing issues related to the water cycle are among others food production, the availability of freshwater resources, and disasters related to extreme events. In this thesis moisture transport in the mid-latitudes is investigated for three distinct geographical areas, on various time and spatial scales, from a meteorological and hydrological perspective.

When I started this PhD research, I envisioned myself studying changes in precipitation and discharge in major river basins in the mid-latitudes using simulations of the climate under present and future conditions. While this partly became reality, I realised along the way that the correct understanding, and modelling, of the water cycle in the present climate is already challenging, and crucial, in itself. For example, modelled precipitation over the Mississippi basin showed deviations from the observed seasonal cycle (Benedict et al., 2019b), and the variability in basin-averaged precipitation compared to other models was quite substantial (Benedict et al., 2020). Other large-scale processes such as blocking are still very difficult to simulate, although new results with high resolution models look promising (Schiemann et al., 2020). When linking meteorology to impacts on land, new uncertainties arise related to land-atmosphere feedbacks and simulations of (global) hydrology. To further understand those processes, more basic research on moisture transport and how it impacts society is needed (Bony et al., 2013; Marotzke et al., 2017). Luckily, in the current era with advances in computer power and new observing techniques, exciting opportunities arise to gain further insights on how moisture is distributed in the atmosphere and on land.

Also, regional projections of climate change are crucial to prepare society for changes ahead (Stocker et al., 2013). These regional projections of the water-cycle mostly come with large uncertainties, due to internal variabilities, and because future changes in the large-scale circulation, such as the storm-track, are uncertain. This uncertainty in the large-scale circulation occurs mainly because different drivers of change can act in opposite directions (Shepherd, 2019). On the other hand, future changes related to thermodynamics are quite robust (Shepherd, 2014), following the laws of thermodynamics. An illustrative example is the occurrence of heatwaves in a future climate, which are projected to occur more frequently due to increased temperatures (thermodynamics), while the changes in circulation affecting heatwaves remain uncertain (Palmer, 2013). As advances in understanding of the changes in dynamics progress slowly (Bony et al., 2013), one can argue that many future climate projections can also be extrapolated from known thermodynamic theory (Clausius-Clapeyron) combined with a good understanding of the present climate. More concrete, I suggest instead of running a plethora of climate models

using many future scenario's, rather spent efforts into enhanced process understanding of present climate, and to invest computer power to build the best models we can (Jakob, 2014; Palmer and Stevens, 2019). This view is in agreement with the statement from Bony et al. (2013) that "The confidence in our predictions will remain disproportionately dependent on the development of understanding".

Finally, to advance our understanding of the water cycle I believe combined efforts in the field of climate science, meteorology, and hydrology are needed. Besides that combining these fields provides a very diverse topic to work on, the water cycle inherently asks for different perspectives and approaches. Only by continuing to bridge between the field of climate, weather and water we are able to advance our understanding and improve projections on extremes such as floods and droughts.

References

Albergel, C., Dutra, E., Munier, S., Calvet, J.-C., Munoz-Sabater, J., Rosnay, P. d., and Balsamo, G.: ERA-5 and ERA-Interim driven ISBA land surface model simulations: which one performs better?, Hydrology and Earth System Sciences, 22, 3515–3532, 2018.

Algarra, I., Eiras-Barca, J., Miguez-Macho, G., Nieto, R., and Gimeno, L.: On the assessment of the moisture transport by the Great Plains low-level jet, Earth System Dynamics, 10, 107–119, 2019.

Allen, M. R. and Ingram, W. J.: Constraints on future changes in climate and the hydrologic cycle, Nature, 419, 224, 2002.

Azad, R. and Sorteberg, A.: Extreme daily precipitation in coastal western Norway and the link to atmospheric rivers, Journal of Geophysical Research: Atmospheres, 122, 2080–2095, 2017.

Baatsen, M., Haarsma, R. J., Van Delden, A. J., and de Vries, H.: Severe Autumn storms in future Western Europe with a warmer Atlantic Ocean, Climate Dynamics, 45, 949–964, 2015.

Bader, M. and Roach, W.: Orographic rainfall in warm sectors of depressions, Quarterly Journal of the Royal Meteorological Society, 103, 269–280, 1977.

Balsamo, G., Beljaars, A., Scipal, K., Viterbo, P., van den Hurk, B., Hirschi, M., and Betts, A. K.: A revised hydrology for the ECMWF model: Verification from field site to terrestrial water storage and impact in the Integrated Forecast System, Journal of Hydrometeorology, 10, 623–643, 2009.

Balsamo, G., Boussetta, S., Lopez, P., and Ferranti, L.: Evaluation of ERA-Interim and ERA-Interim-GPCP-rescaled precipitation over the USA, ERA report series, 5, 10 pp., ECMWF, Reading, 2010.

Balsamo, G., Albergel, C., Beljaars, A., Boussetta, S., Cloke, H., Dee, D., Dutra, E., Muñoz-Sabater, J., Pappenberger, F., de Rosnay, P., and others: ERA-Interim/Land: a global land water resources dataset, Hydrol. Earth Syst. Sci., 10, 14–705, 2013.

Bauer, P., Thorpe, A., and Brunet, G.: The quiet revolution of numerical weather prediction, Nature, 525, 47–55, 2015.

Beck, H. E., van Dijk, A. I. J. M., de Roo, A., Miralles, D. G., McVicar, T. R., Schellekens, J., and Bruijnzeel, L. A.: Global-scale regionalization of hydrologic model parameters, Water Resources Research, 52, 3599–3622, 2016.

Beck, H. E., van Dijk, A. I., de Roo, A., Dutra, E., Fink, G., Orth, R., and Schellekens, J.: Global evaluation of runoff from 10 state-of-the-art hydrological models, Hydrology and Earth System Sciences, 21, 1812–2116, 2017.

Beck, H. E., Pan, M., Roy, T., Weedon, G. P., Pappenberger, F., Dijk, A. I. J. M. v., Huffman, G. J., Adler, R. F., and Wood, E. F.: Daily evaluation of 26 precipitation datasets using Stage-IV gauge-radar data for the CONUS, Hydrology and Earth System Sciences, 23, 207–224, 2019.

Benedict, I., van Heerwaarden, C. C., Weerts, A. H., and Hazeleger, W.: An evaluation of the importance

of spatial resolution in a global climate and hydrological model based on the Rhine and Mississippi, Hydrol. Earth Syst. Sci. Discuss., 2017.

Benedict, I., Ødemark, K., Nipen, T., and Moore, R.: Large-scale flow patterns associated with extreme precipitation and atmospheric rivers over Norway, Monthly Weather Review, 147, 1415–1428, 2019a.

Benedict, I., van Heerwaarden, C. C., Weerts, A. H., and Hazeleger, W.: The benefits of spatial resolution increase in global simulations of the hydrological cycle evaluated for the Rhine and Mississippi basins, Hydrol. Earth Syst. Sci., 23, 1779–1800, 2019b.

Benedict, I., van Heerwaarden, C. C., van der Ent, R. J., Weerts, A. H., and Hazeleger, W.: Decline in Terrestrial Moisture Sources of the Mississippi River Basin in a Future Climate, Journal of Hydrometeorology, 21, 299–316, 2020.

Beniston, M.: The 2003 heat wave in Europe: A shape of things to come? An analysis based on Swiss climatological data and model simulations, Geophysical Research Letters, 31, 2004.

Benton, G. S., Blackburn, R. T., and Snead, V. O.: The role of the atmosphere in the hydrologic cycle, Eos, Transactions American Geophysical Union, 31, 61–73, 1950.

Berghuijs, W. R., Woods, R. A., Hutton, C. J., and Sivapalan, M.: Dominant flood generating mechanisms across the United States, Geophysical Research Letters, 43, 4382–4390, 2016.

Betts, A. K., Köhler, M., and Zhang, Y.: Comparison of river basin hydrometeorology in ERA-Interim and ERA-40 reanalyses with observations, Journal of Geophysical Research: Atmospheres, 114, 2009.

Biemans, H., Hutjes, R., Kabat, P., Strengers, B., Gerten, D., and Rost, S.: Effects of precipitation uncertainty on discharge calculations for main river basins, Journal of Hydrometeorology, 10, 1011–1025, 2009.

Bierkens, M. F. P., Bell, V. A., Burek, P., Chaney, N., Condon, L. E., David, C. H., de Roo, A., Döll, P., Drost, N., Famiglietti, J. S., Flörke, M., Gochis, D. J., Houser, P., Hut, R., Keune, J., Kollet, S., Maxwell, R. M., Reager, J. T., Samaniego, L., Sudicky, E., Sutanudjaja, E. H., van de Giesen, N., Winsemius, H., and Wood, E. F.: Hyper-resolution global hydrological modelling: what is next?: "Everywhere and locally relevant", Hydrological Processes, 29, 310–320, 2015.

Bisselink, B. and Dolman, A. J.: Precipitation Recycling: Moisture Sources over Europe using ERA-40 Data, Journal of Hydrometeorology, 9, 1073–1083, 2008.

Bisselink, B. and Dolman, A. J.: Recycling of moisture in Europe: contribution of evaporation to variability in very wet and dry years, Hydrology and Earth System Sciences, 13, 1685–1697, 2009.

Black, E. and Sutton, R.: The influence of oceanic conditions on the hot European summer of 2003, Climate Dynamics, 28, 53–66, 2007.

Black, E., Blackburn, M., Harrison, G., Hoskins, B., and Methven, J.: Factors contributing to the summer 2003 European heatwave, Weather, 59, 217–223, 2004.

Blackmon, M. L.: A climatological spectral study of the 500 mb geopotential height of the Northern Hemisphere, Journal of the Atmospheric Sciences, 33, 1607–1623, 1976.

Bony, S., Stevens, B., Held, I. H., Mitchell, J. F., Dufresne, J.-L., Emanuel, K. A., Friedlingstein, P., Griffies, S., and Senior, C.: Carbon dioxide and climate: Perspectives on a scientific assessment, in: Climate Science for Serving Society, pp. 391–413, Springer, 2013.

Bony, S., Stevens, B., Frierson, D. M., Jakob, C., Kageyama, M., Pincus, R., Shepherd, T. G., Sherwood, S. C., Siebesma, A. P., Sobel, A. H., et al.: Clouds, circulation and climate sensitivity, Nature Geoscience, 8, 261–268, 2015.

Bosilovich, M. G. and Chern, J.-D.: Simulation of water sources and precipitation recycling for the MacKenzie, Mississippi, and Amazon River basins, Journal of Hydrometeorology, 7, 312–329, 2006.

Bosilovich, M. G. and Schubert, S. D.: Precipitation recycling over the central United States diagnosed from the GEOS-1 data assimilation system, Journal of Hydrometeorology, 2, 26–35, 2001.

Bosilovich, M. G. and Schubert, S. D.: Water vapor tracers as diagnostics of the regional hydrologic cycle, Journal of Hydrometeorology, 3, 149–165, 2002.

Brands, S., Gutiérrez, J., and San-Martín, D.: Twentieth-century atmospheric river activity along the west coasts of Europe and North America: algorithm formulation, reanalysis uncertainty and links to atmospheric circulation patterns, Climate Dynamics, 48, 2771–2795, 2017.

Browning, K. and Pardoe, C.: Structure of low-level jet streams ahead of mid-latitude cold fronts, Quarterly Journal of the Royal Meteorological Society, 99, 619–638, 1973.

Brubaker, K. L., Entekhabi, D., and Eagleson, P.: Estimation of continental precipitation recycling, Journal of Climate, 6, 1077–1089, 1993.

Brubaker, K. L., Dirmeyer, P. A., Sudradjat, A., Levy, B. S., and Bernal, F.: A 36-yr climatological description of the evaporative sources of warm-season precipitation in the Mississippi River basin, Journal of Hydrometeorology, 2, 537–557, 2001.

Cassou, C., Terray, L., and Phillips, A. S.: Tropical Atlantic Influence on European Heat Waves, Journal of Climate, 18, 2805–2811, 2005.

Chang, E. K. M., Guo, Y., and Xia, X.: CMIP5 multimodel ensemble projection of storm track change under global warming: CMIP5 model-projected storm track change, Journal of Geophysical Research: Atmospheres, 117, n/a–n/a, 2012.

Chen, M., Shi, W., Xie, P., Silva, V. B., Kousky, V. E., Wayne Higgins, R., and Janowiak, J. E.: Assessing objective techniques for gauge-based analyses of global daily precipitation, Journal of Geophysical Research: Atmospheres, 113, 2008.

Cohen, J., Screen, J. A., Furtado, J. C., Barlow, M., Whittleston, D., Coumou, D., Francis, J., Dethloff, K., Entekhabi, D., Overland, J., et al.: Recent Arctic amplification and extreme mid-latitude weather, Nature geoscience, 7, 627–637, 2014.

Cook, K. H., Vizy, E. K., Launer, Z. S., and Patricola, C. M.: Springtime intensification of the Great Plains low-level jet and Midwest precipitation in GCM simulations of the twenty-first century, Journal of Climate, 21, 6321–6340, 2008.

Dacre, H. F., Clark, P. A., Martinez-Alvarado, O., Stringer, M. A., and Lavers, D. A.: How do atmospheric rivers form?, Bulletin of the American Meteorological Society, 96, 1243–1255, 2015.

Davini, P. and D'Andrea, F.: Northern Hemisphere atmospheric blocking representation in global climate models: Twenty years of improvements?, Journal of Climate, 29, 8823–8840, 2016.

Davini, P., Corti, S., D'Andrea, F., Rivière, G., and von Hardenberg, J.: Improved Winter European Atmospheric Blocking Frequencies in High-Resolution Global Climate Simulations, Journal of Advances in Modeling Earth Systems, 9, 2615–2634, 2017a.

Davini, P., Von Hardenberg, J., Corti, S., Christensen, H. M., Juricke, S., Subramanian, A., Watson, P. A., Weisheimer, A., and Palmer, T. N.: Climate SPHINX: evaluating the impact of resolution and stochastic physics parameterisations in the EC-Earth global climate model, Geoscientific Model Development, 10, 1383–1402, 2017b.

de Vrese, P., Hagemann, S., and Claussen, M.: Asian irrigation, African rain: Remote impacts of irrigation, Geophysical Research Letters, 43, 3737–3745, 2016.

De Vries, H., Woollings, T., Anstey, J., Haarsma, R. J., and Hazeleger, W.: Atmospheric blocking and its relation to jet changes in a future climate, Climate Dynamics, 41, 2643–2654, 2013.

Dee, D., Uppala, S., Simmons, A., Berrisford, P., Poli, P., Kobayashi, S., Andrae, U., Balmaseda, M.,

Balsamo, G., Bauer, P., et al.: The ERA-Interim reanalysis: Configuration and performance of the data assimilation system, Quart. J. Roy. Meteor. Soc., 137, 553–597, 2011.

Delworth, T. L., Rosati, A., Anderson, W., Adcroft, A. J., Balaji, V., Benson, R., Dixon, K., Griffies, S. M., Lee, H.-C., Pacanowski, R. C., et al.: Simulated climate and climate change in the GFDL CM2.5 high-resolution coupled climate model, Journal of Climate, 25, 2755–2781, 2012.

Demory, M.-E., Vidale, P. L., Roberts, M. J., Berrisford, P., Strachan, J., Schiemann, R., and Mizielinski, M. S.: The role of horizontal resolution in simulating drivers of the global hydrological cycle, Climate Dynamics, 42, 2201–2225, 2014.

Demory, M.-E., Berthou, S., Sørland, S. L., Roberts, M. J., Beyerle, U., Seddon, J., Haarsma, R., Schär, C., Christensen, O. B., Fealy, R., et al.: Can high-resolution GCMs reach the level of information provided by 12–50 km CORDEX RCMs in terms of daily precipitation distribution?, Geoscientific Model Development Discussions, pp. 1–33, 2020.

Deser, C., Phillips, A., Bourdette, V., and Teng, H.: Uncertainty in climate change projections: the role of internal variability, Climate Dynamics, 38, 527–546, 2012.

Dettinger, M.: Climate change, atmospheric rivers, and floods in California–a multimodel analysis of storm frequency and magnitude changes, JAWRA Journal of the American Water Resources Association, 47, 514–523, 2011.

Dirmeyer, P. A. and Brubaker, K. L.: Contrasting evaporative moisture sources during the drought of 1988 and the flood of 1993, Journal of Geophysical Research: Atmospheres, 104, 19 383–19 397, 1999.

Dirmeyer, P. A. and Brubaker, K. L.: Characterization of the global hydrologic cycle from a back-trajectory analysis of atmospheric water vapor, Journal of Hydrometeorology, 8, 20–37, 2007.

Dirmeyer, P. A. and Kinter, J. L.: Floods over the US Midwest: A regional water cycle perspective, Journal of Hydrometeorology, 11, 1172–1181, 2010.

Dirmeyer, P. A., Brubaker, K. L., and DelSole, T.: Import and export of atmospheric water vapor between nations, Journal of hydrology, 365, 11–22, 2009.

Disse, M. and Engel, H.: Flood events in the Rhine basin: genesis, influences and mitigation, Natural Hazards, 23, 271–290, 2001.

Döll, P., Douville, H., Güntner, A., Müller Schmied, H., and Wada, Y.: Modelling Freshwater Resources at the Global Scale: Challenges and Prospects, Surveys in Geophysics, 37, 195–221, 2016.

Dominguez, F., Kumar, P., Liang, X.-Z., and Ting, M.: Impact of Atmospheric Moisture Storage on Precipitation Recycling, Journal of Climate, 19, 1513–1530, 2006.

Drouard, M. and Woollings, T.: Contrasting Mechanisms of Summer Blocking Over Western Eurasia, Geophysical Research Letters, 45, 12,040–12,048, 2018.

Drouard, M., Kornhuber, K., and Woollings, T.: Disentangling Dynamic Contributions to Summer 2018 Anomalous Weather Over Europe, Geophysical Research Letters, 46, 12 537–12 546, 2019.

Duffy, P., Govindasamy, B., Iorio, J., Milovich, J., Sperber, K., Taylor, K., Wehner, M., and Thompson, S.: High-resolution simulations of global climate, part 1: present climate, Climate Dynamics, 21, 371–390, 2003.

Eagleson, P. S.: The emergence of global-scale hydrology, Water Resources Research, 22, 6S–14S, 1986.

Efron, B. and Tibshirani, R. J.: An introduction to the bootstrap, CRC press, 1994.

Fekete, B. M., Vörösmarty, C. J., Roads, J. O., and Willmott, C. J.: Uncertainties in precipitation and their impacts on runoff estimates, Journal of Climate, 17, 294–304, 2004.

Fekete, B. M., Looser, U., Pietroniro, A., and Robarts, R. D.: Rationale for monitoring discharge on the

ground, Journal of Hydrometeorology, 13, 1977–1986, 2012.

Ferguson, C., Pan, M., and Oki, T.: The effect of global warming on future water availability: CMIP5 synthesis, Water Resources Research, 54, 7791–7819, 2018.

Ferranti, L. and Viterbo, P.: The European Summer of 2003: Sensitivity to Soil Water Initial Conditions, Journal of Climate, 19, 3659–3680, 2006.

Findell, K. L., Keys, P. W., van der Ent, R. J., Lintner, B. R., Berg, A., and Krasting, J. P.: Rising Temperatures Increase Importance of Oceanic Evaporation as a Source for Continental Precipitation, Journal of Climate, 32, 7713–7726, 2019.

Fischer, E. M., Seneviratne, S. I., Lüthi, D., and Schär, C.: Contribution of land-atmosphere coupling to recent European summer heat waves, Geophysical Research Letters, 34, 2007a.

Fischer, E. M., Seneviratne, S. I., Vidale, P. L., Lüthi, D., and Schär, C.: Soil Moisture–Atmosphere Interactions during the 2003 European Summer Heat Wave, Journal of Climate, 20, 5081–5099, 2007b.

Fleig, A. K., Tallaksen, L. M., Hisdal, H., and Hannah, D. M.: Regional hydrological drought in north-western Europe: linking a new Regional Drought Area Index with weather types, Hydrological Processes, 25, 1163–1179, 2011.

Folland, C. K., Knight, J., Linderholm, H. W., Fereday, D., Ineson, S., and Hurrell, J. W.: The Summer North Atlantic Oscillation: Past, Present, and Future, Journal of Climate, 22, 1082–1103, 2009.

Fowler, H. J., Blenkinsop, S., and Tebaldi, C.: Linking climate change modelling to impacts studies: recent advances in downscaling techniques for hydrological modelling, International Journal of Climatology, 27, 1547–1578, 2007.

Gao, H., Hrachowitz, M., Fenicia, F., Gharari, S., and Savenije, H.: Testing the realism of a topography driven model (FLEX-Topo) in the nested catchments of the Upper Heihe, China., Hydrology & Earth System Sciences, 18, 1895–1915, 2014a.

Gao, H., Hrachowitz, M., Schymanski, S., Fenicia, F., Sriwongsitanon, N., and Savenije, H.: Climate controls how ecosystems size the root zone storage capacity at catchment scale, Geophysical Research Letters, 41, 7916–7923, 2014b.

Gao, H., Hrachowitz, M., Sriwongsitanon, N., Fenicia, F., Gharari, S., and Savenije, H. H.: Accounting for the influence of vegetation and landscape improves model transferability in a tropical savannah region, Water Resources Research, 52, 7999–8022, 2016a.

Gao, Y., Lu, J., and Leung, L. R.: Uncertainties in projecting future changes in atmospheric rivers and their impacts on heavy precipitation over Europe, Journal of Climate, 29, 6711–6726, 2016b.

Gimeno, L., Stohl, A., Trigo, R. M., Dominguez, F., Yoshimura, K., Yu, L., Drumond, A., Durán-Quesada, A. M., and Nieto, R.: Oceanic and terrestrial sources of continental precipitation, Reviews of Geophysics, 50, 2012.

Gimeno, L., Nieto, R., Drumond, A., Castillo, R., and Trigo, R.: Influence of the intensification of the major oceanic moisture sources on continental precipitation, Geophysical Research Letters, 40, 1443–1450, 2013.

Gimeno, L., Vázquez, M., Eiras-Barca, J., Sorí, R., Stojanovic, M., Algarra, I., Nieto, R., Ramos, A. M., Durán-Quesada, A. M., and Dominguez, F.: Recent progress on the sources of continental precipitation as revealed by moisture transport analysis, Earth-Science Reviews, 201, 103 070, 2020.

GRDC: GRDC in the Bundesanstalt fuer Gewaesserkunde, Tech. rep., 56068 Koblenz, Germany, http://grdc.bafg.de, 2007.

Guo, L., van der Ent, R., Klingaman, N., Demory, M., Vidale, P., Turner, A., Stephan, C., and Chevuturi, A.: Moisture sources for East Asian precipitation: mean seasonal cycle and interannual variability, J.

Hydrometeor., in press, 2019.

Haarsma, R. J., Selten, F., Hurk, B. v., Hazeleger, W., and Wang, X.: Drier Mediterranean soils due to greenhouse warming bring easterly winds over summertime central Europe, Geophysical Research Letters, 36, 2009.

Haarsma, R. J., Hazeleger, W., Severijns, C., de Vries, H., Sterl, A., Bintanja, R., van Oldenborgh, G. J., and van den Brink, H. W.: More hurricanes to hit western Europe due to global warming, Geophysical Research Letters, 40, 1783–1788, 2013.

Haarsma, R. J., Roberts, M. J., Vidale, P. L., Senior, C. A., Bellucci, A., Bao, Q., Chang, P., Corti, S., Fučkar, N. S., Guemas, V., et al.: High resolution model intercomparison project (HighResMIP v1.0) for CMIP6, Geoscientific Model Development, 9, 4185–4208, 2016.

Haddeland, I., Clark, D. B., Franssen, W., Ludwig, F., Voß, F., Arnell, N. W., Bertrand, N., Best, M., Folwell, S., Gerten, D., Gomes, S., Gosling, S. N., Hagemann, S., Hanasaki, N., Harding, R., Heinke, J., Kabat, P., Koirala, S., Oki, T., Polcher, J., Stacke, T., Viterbo, P., Weedon, G. P., and Yeh, P.: Multimodel Estimate of the Global Terrestrial Water Balance: Setup and First Results, Journal of Hydrometeorology, 12, 869–884, 2011.

Hannah, D. M., Demuth, S., van Lanen, H. A., Looser, U., Prudhomme, C., Rees, G., Stahl, K., and Tallaksen, L. M.: Large-scale river flow archives: importance, current status and future needs, Hydrological Processes, 25, 1191–1200, 2011.

Harr, P. A., Anwender, D., and Jones, S. C.: Predictability associated with the downstream impacts of the extratropical transition of tropical cyclones: Methodology and a case study of Typhoon Nabi (2005), Mon. Wea. Rev., 136, 3205–3225, 2008.

Harrold, T.: Mechanisms influencing the distribution of precipitation within baroclinic disturbances, Quarterly Journal of the Royal Meteorological Society, 99, 232–251, 1973.

Hawkins, E. and Sutton, R.: The potential to narrow uncertainty in regional climate predictions, Bulletin of the American Meteorological Society, 90, 1095–1108, 2009.

Haylock, M. R., Hofstra, N., Klein Tank, A. M. G., Klok, E. J., Jones, P. D., and New, M.: A European daily high-resolution gridded data set of surface temperature and precipitation for 1950–2006, Journal of Geophysical Research, 113, 2008.

Hazeleger, W., Severijns, C., Semmler, T., Ştefănescu, S., Yang, S., Wang, X., Wyser, K., Dutra, E., Baldasano, J. M., Bintanja, R., Bougeault, P., Caballero, R., Ekman, A. M. L., Christensen, J. H., van den Hurk, B., Jimenez, P., Jones, C., Kållberg, P., Koenigk, T., McGrath, R., Miranda, P., Van Noije, T., Palmer, T., Parodi, J. A., Schmith, T., Selten, F., Storelvmo, T., Sterl, A., Tapamo, H., Vancoppenolle, M., Viterbo, P., and Willén, U.: EC-Earth: A Seamless Earth-System Prediction Approach in Action, Bulletin of the American Meteorological Society, 91, 1357–1363, 2010.

Hazeleger, W., Wang, X., Severijns, C., Ştefănescu, S., Bintanja, R., Sterl, A., Wyser, K., Semmler, T., Yang, S., Van den Hurk, B., et al.: EC-Earth V2.2: description and validation of a new seamless earth system prediction model, Climate dynamics, 39, 2611–2629, 2012.

Hazeleger, W., van den Hurk, B., Min, E., van Oldenborgh, G., Petersen, A., Stainforth, D., Vasileiadou, E., and Smith, L.: Tales of future weather, Nature Climate Change, 5, 107–113, 2015.

Hegdahl, T. J., Engeland, K., Müller, M., and Sillmann, J.: An event-based approach to explore selected present and future Atmospheric River induced floods in western Norway, Journal of Hydrometeorology, 2020.

Hegnauer, M., Beersma, J. J., van den Boogaard, H. F. P., Buishand, T. A., and Passchier, R. H.: Publications, presentations and other activities Generator of Rainfall and Discharge Extremes (GRADE) for the Rhine and Meuse basins; Final report of GRADE 2.0 2014, 2014.

Heikkilä, U. and Sorteberg, A.: Characteristics of autumn-winter extreme precipitation on the Norwegian west coast identified by cluster analysis, Climate Dyn., 39, 929–939, 2012.

Held, I. M. and Soden, B. J.: Robust responses of the hydrological cycle to global warming, Journal of Climate, 19, 5686–5699, 2006.

Helfand, H. M. and Schubert, S. D.: Climatology of the simulated Great Plains low-level jet and its contribution to the continental moisture budget of the United States, Journal of Climate, 8, 784–806, 1995.

Henn, B., Newman, A. J., Livneh, B., Daly, C., and Lundquist, J. D.: An assessment of differences in gridded precipitation datasets in complex terrain, Journal of Hydrology, 2017.

Herrera-Estrada, J. E., Martinez, J. A., Dominguez, F., Findell, K. L., Wood, E. F., and Sheffield, J.: Reduced moisture transport linked to drought propagation across North America, Geophysical Research Letters, 46, 5243–5253, 2019.

Hersbach, H., Bell, B., Berrisford, P., Hirahara, S., Horányi, A., Muñoz-Sabater, J., Nicolas, J., Peubey, C., Radu, R., Schepers, D., et al.: The ERA5 global reanalysis, Quarterly Journal of the Royal Meteorological Society, 2020.

Higgins, R., Yao, Y., Yarosh, E., Janowiak, J. E., and Mo, K.: Influence of the Great Plains low-level jet on summertime precipitation and moisture transport over the central United States, Journal of Climate, 10, 481–507, 1997.

Higgins, R.W., W. S. E. Y. and Joyce., R.: Improved United States Precipitation Quality Control System and Analysis, NCEP/Climate Prediction Center ATLAS No. 7, 40 pp., Camp Springs, MD 20746, USA, 2000.

Hodges, K. I., Lee, R. W., and Bengtsson, L.: A comparison of extratropical cyclones in recent reanalyses ERA-Interim, NASA MERRA, NCEP CFSR, and JRA-25, Journal of Climate, 24, 4888–4906, 2011.

Hofstra, N., Haylock, M., New, M., and Jones, P. D.: Testing E-OBS European high-resolution gridded data set of daily precipitation and surface temperature, Journal of Geophysical Research, 114, 2009.

Hohenegger, C., Brockhaus, P., Bretherton, C. S., and Schär, C.: The soil moisture–precipitation feedback in simulations with explicit and parameterized convection, Journal of Climate, 22, 5003–5020, 2009.

Hoskins, B. J. and Valdes, P. J.: On the existence of storm-tracks, Journal of the atmospheric sciences, 47, 1854–1864, 1990.

Hoyos, I., Dominguez, F., Cañón-Barriga, J., Martínez, J., Nieto, R., Gimeno, L., and Dirmeyer, P.: Moisture origin and transport processes in Colombia, northern South America, Climate dynamics, 50, 971–990, 2018.

Hrachowitz, M., Savenije, H., Blöschl, G., McDonnell, J., Sivapalan, M., Pomeroy, J., Arheimer, B., Blume, T., Clark, M., Ehret, U., and others: A decade of Predictions in Ungauged Basins (PUB)—a review, Hydrological sciences journal, 58, 1198–1255, 2013.

Hu, H., Dominguez, F., Wang, Z., Lavers, D. A., Zhang, G., and Ralph, F. M.: Linking atmospheric river hydrological impacts on the US West Coast to Rossby wave breaking, Journal of Climate, 30, 3381–3399, 2017.

Huguenin, M. F., Fischer, E. M., Kotlarski, S., Scherrer, S. C., Schwierz, C., and Knutti, R.: Lack of Change in the Projected Frequency and Persistence of Atmospheric Circulation Types Over Central Europe, Geophysical Research Letters, 47, e2019GL086 132, 2020.

Imhoff, R., van Verseveld, W., van Osnabrugge, B., and Weerts, A.: Scaling point-scale (pedo) transfer functions to seamless large-domain parameter estimates for high-resolution distributed hydrologic modeling: An example for the Rhine river, Water Resources Research, 56, e2019WR026 807, 2020.

Ionita, M., Nagavciuc, V., and Guan, B.: Rivers in the sky, flooding on the ground, Hydrol. Earth Syst. Sci. Discuss, 2020.

Iorio, J. P., Duffy, P. B., Govindasamy, B., Thompson, S. L., Khairoutdinov, M., and Randall, D.: Effects of model resolution and subgrid-scale physics on the simulation of precipitation in the continental United States, Climate Dynamics, 23, 243–258, 2004.

Jacob, D., Petersen, J., Eggert, B., Alias, A., Christensen, O. B., Bouwer, L. M., Braun, A., Colette, A., Déqué, M., Georgievski, G., et al.: EURO-CORDEX: new high-resolution climate change projections for European impact research, Regional Environmental Change, 14, 563–578, 2014.

Jacob, D., Teichmann, C., Sobolowski, S., Katragkou, E., Anders, I., Belda, M., Benestad, R., Boberg, F., Buonomo, E., Cardoso, R. M., et al.: Regional climate downscaling over Europe: perspectives from the EURO-CORDEX community, Regional Environmental Change, 20, 2020.

Jakob, C.: Going back to basics, Nature Climate Change, 4, 1042–1045, 2014.

Jung, T., Miller, M., Palmer, T., Towers, P., Wedi, N., Achuthavarier, D., Adams, J., Altshuler, E., Cash, B., Kinter Iii, J., et al.: High-resolution global climate simulations with the ECMWF model in Project Athena: Experimental design, model climate, and seasonal forecast skill, Journal of Climate, 25, 3155–3172, 2012.

Kelly, K. A., Small, R. J., Samelson, R., Qiu, B., Joyce, T. M., Kwon, Y.-O., and Cronin, M. F.: Western boundary currents and frontal air–sea interaction: Gulf Stream and Kuroshio Extension, Journal of Climate, 23, 5644–5667, 2010.

Kennedy, D., Parker, T., Woollings, T., Harvey, B., and Shaffrey, L.: The response of high-impact blocking weather systems to climate change, Geophysical Research Letters, 43, 7250–7258, 2016.

Keune, J. and Miralles, D.: A precipitation recycling network to assess freshwater vulnerability: Challenging the watershed convention, Water resources research, 55, 9947–9961, 2019.

Kew, S. F., Selten, F. M., Lenderink, G., and Hazeleger, W.: Robust assessment of future changes in extreme precipitation over the Rhine basin using a GCM, Hydrology and Earth System Sciences, 15, 1157–1166, 2011.

Keys, P. W., Wang-Erlandsson, L., Gordon, L. J., Galaz, V., and Ebbesson, J.: Approaching moisture recycling governance, Global Environmental Change, 45, 15–23, 2017.

Khanna, J., Medvigy, D., Fueglistaler, S., and Walko, R.: Regional dry-season climate changes due to three decades of Amazonian deforestation, Nature Climate Change, 7, 200–204, 2017.

Klok, E. and Klein Tank, A.: Updated and extended European dataset of daily climate observations, International Journal of Climatology: A Journal of the Royal Meteorological Society, 29, 1182–1191, 2009.

Knippertz, P. and Wernli, H.: A Lagrangian climatology of tropical moisture exports to the Northern Hemispheric extratropics, J. Climate, 23, 987–1003, 2010.

Knoche, H. R. and Kunstmann, H.: Tracking atmospheric water pathways by direct evaporation tagging: A case study for West Africa, Journal of Geophysical Research: Atmospheres, 118, 12–345, 2013.

Knutti, R., Furrer, R., Tebaldi, C., Cermak, J., and Meehl, G. A.: Challenges in combining projections from multiple climate models, Journal of Climate, 23, 2739–2758, 2010.

Kornhuber, K., Petoukhov, V., Karoly, D., Petri, S., Rahmstorf, S., and Coumou, D.: Summertime Planetary Wave Resonance in the Northern and Southern Hemispheres, Journal of Climate, 30, 6133–6150, 2017.

Kornhuber, K., Osprey, S., Coumou, D., Petri, S., Petoukhov, V., Rahmstorf, S., and Gray, L.: Extreme weather events in early summer 2018 connected by a recurrent hemispheric wave-7 pattern,

Environmental Research Letters, 14, 054 002, 2019.

Kornhuber, K., Coumou, D., Vogel, E., Lesk, C., Donges, J. F., Lehmann, J., and Horton, R. M.: Amplified Rossby waves enhance risk of concurrent heatwaves in major breadbasket regions, Nature Climate Change, 10, 48–53, 2020.

Koster, R. D., Dirmeyer, P. A., Guo, Z., Bonan, G., Chan, E., Cox, P., Gordon, C., Kanae, S., Kowalczyk, E., Lawrence, D., et al.: Regions of strong coupling between soil moisture and precipitation, Science, 305, 1138–1140, 2004.

Kramer, N., Mens, M., Beersma, J., and Kielen, N.: Hoe extreem was de droogte van 2018?, H2O, 2019.

Lavers, D., Prudhomme, C., and Hannah, D. M.: European precipitation connections with large-scale mean sea-level pressure (MSLP) fields, Hydrological Sciences Journal, 58, 310–327, 2013.

Lavers, D. A. and Villarini, G.: The nexus between atmospheric rivers and extreme precipitation across Europe, Geophys. Res. Lett., 40, 3259–3264, 2013.

Lavers, D. A., Allan, R. P., Wood, E. F., Villarini, G., Brayshaw, D. J., and Wade, A. J.: Winter floods in Britain are connected to atmospheric rivers, Geophys. Res. Lett., 38, 2011.

Läderach, A. and Sodemann, H.: A revised picture of the atmospheric moisture residence time, Geophysical Research Letters, 43, 924–933, 2016.

Leung, L. R. and Qian, Y.: Atmospheric rivers induced heavy precipitation and flooding in the western US simulated by the WRF regional climate model, Geophys. Res. Lett., 36, L03 820, 2009.

Linden, E. C. v. d., Haarsma, R. J., and Schrier, G. v. d.: Impact of climate model resolution on soil moisture projections in central-western Europe, Hydrology and Earth System Sciences, 23, 191–206, 2019.

Link, A., Ent, R. v. d., Berger, M., Eisner, S., and Finkbeiner, M.: The fate of land evaporation–A global dataset, Earth System Science Data Discussions, pp. 1–22, 2020.

Liu, C., Ikeda, K., Rasmussen, R., Barlage, M., Newman, A. J., Prein, A. F., Chen, F., Chen, L., Clark, M., Dai, A., et al.: Continental-scale convection-permitting modeling of the current and future climate of North America, Climate Dynamics, 49, 71–95, 2017.

Liu, X., He, B., Guo, L., Huang, L., and Chen, D.: Similarities and Differences in the Mechanisms Causing the European Summer Heatwaves in 2003, 2010, and 2018, Earth's Future, 8, e2019EF001 386, 2020.

Lorenz, D. J. and DeWeaver, E. T.: Tropopause height and zonal wind response to global warming in the IPCC scenario integrations, Journal of Geophysical Research: Atmospheres, 112, 2007.

Lundquist, J. D., Hughes, M., Henn, B., Gutmann, E. D., Livneh, B., Dozier, J., and Neiman, P.: High-Elevation Precipitation Patterns: Using Snow Measurements to Assess Daily Gridded Datasets across the Sierra Nevada, California, Journal of Hydrometeorology, 16, 1773–1792, 2015.

Lussana, C., Saloranta, T., Skaugen, T., Magnusson, J., Tveito, O. E., and Andersen, J.: seNorge2 daily precipitation, an observational gridded dataset over Norway from 1957 to the present day, Earth System Science Data, 10, 235, 2018.

Manganello, J. V., Hodges, K. I., Kinter III, J. L., Cash, B. A., Marx, L., Jung, T., Achuthavarier, D., Adams, J. M., Altshuler, E. L., Huang, B., et al.: Tropical cyclone climatology in a 10-km global atmospheric GCM: toward weather-resolving climate modeling, Journal of Climate, 25, 3867–3893, 2012.

Mann, M. E., Rahmstorf, S., Kornhuber, K., Steinman, B. A., Miller, S. K., and Coumou, D.: Influence of Anthropogenic Climate Change on Planetary Wave Resonance and Extreme Weather Events, Scientific Reports, 7, 45 242, 2017.

Maraun, D., Shepherd, T. G., Widmann, M., Zappa, G., Walton, D., Gutiérrez, J. M., Hagemann, S., Richter, I., Soares, P. M., Hall, A., et al.: Towards process-informed bias correction of climate change simulations, Nature Climate Change, 7, 764, 2017.

Marotzke, J., Jakob, C., Bony, S., Dirmeyer, P. A., O'Gorman, P. A., Hawkins, E., Perkins-Kirkpatrick, S., Le Quere, C., Nowicki, S., Paulavets, K., et al.: Climate research must sharpen its view, Nature Climate Change, 7, 89–91, 2017.

Martens, B., Miralles, D. G., Lievens, H., van der Schalie, R., de Jeu, R. A. M., Férnandez-Prieto, D., Beck, H. E., Dorigo, W. A., and Verhoest, N. E. C.: GLEAM v3: satellite-based land evaporation and root-zone soil moisture, Geoscientific Model Development, pp. 1–36, 2016.

Masato, G., Hoskins, B. J., and Woollings, T.: Winter and Summer Northern Hemisphere Blocking in CMIP5 Models, Journal of Climate, 26, 7044–7059, 2013.

McCabe, G. J., Hay, L. E., and Clark, M. P.: Rain-on-snow events in the western United States, Bulletin of the American Meteorological Society, 88, 319–328, 2007.

McTaggart-Cowan, R., Gyakum, J. R., and Moore, R. W.: The Baroclinic Moisture Flux, Mon. Wea. Rev., 145, 25–47, 2017.

Meehl, G. A. and Tebaldi, C.: More Intense, More Frequent, and Longer Lasting Heat Waves in the 21st Century, Science, 305, 994–997, 2004.

Meehl, G. A., Moss, R., Taylor, K. E., Eyring, V., Stouffer, R. J., Bony, S., and Stevens, B.: Climate model intercomparisons: preparing for the next phase, Eos, Transactions American Geophysical Union, 95, 77–78, 2014.

Melsen, L., Teuling, A., Torfs, P., Zappa, M., Mizukami, N., Clark, M., and Uijlenhoet, R.: Representation of spatial and temporal variability in large-domain hydrological models: case study for a mesoscale pre-Alpine basin, Hydrol. Earth Syst. Sci., 20, 2207–2226, 2016.

Miralles, D. G., Gentine, P., Seneviratne, S. I., and Teuling, A. J.: Land–atmospheric feedbacks during droughts and heatwaves: state of the science and current challenges, Annals of the New York Academy of Sciences, 1436, 19–35, 2019.

Moezzi, M., Janda, K. B., and Rotmann, S.: Using stories, narratives, and storytelling in energy and climate change research, Energy Research & Social Science, 31, 1–10, 2017.

Monteith, J. L. et al.: Evaporation and environment, in: Symp. Soc. Exp. Biol, vol. 19, p. 4, 1965.

Murakami, H., Vecchi, G. A., Underwood, S., Delworth, T. L., Wittenberg, A. T., Anderson, W. G., Chen, J.-H., Gudgel, R. G., Harris, L. M., Lin, S.-J., et al.: Simulation and prediction of category 4 and 5 hurricanes in the high-resolution GFDL HiFLOR coupled climate model, Journal of Climate, 28, 9058–9079, 2015.

Nakicenovic, N., Alcamo, J., Grubler, A., Riahi, K., Roehrl, R., Rogner, H.-H., and Victor, N.: Special report on emissions scenarios (SRES), a special report of Working Group III of the intergovernmental panel on climate change, Cambridge University Press, 2000.

Pal, J. S. and Eltahir, E. A. B.: A feedback mechanism between soil-moisture distribution and storm tracks, Quarterly Journal of the Royal Meteorological Society, 129, 2279–2297, 2003.

Palmer, T.: Climate extremes and the role of dynamics, Proceedings of the National Academy of Sciences, 110, 5281–5282, 2013.

Palmer, T. and Stevens, B.: The scientific challenge of understanding and estimating climate change, Proceedings of the National Academy of Sciences, 116, 24 390–24 395, 2019.

Payne, A. E., Demory, M.-E., Leung, L. R., Ramos, A. M., Shields, C. A., Rutz, J. J., Siler, N., Villarini, G., Hall, A., and Ralph, F. M.: Responses and impacts of atmospheric rivers to climate change, Nature

Reviews Earth & Environment, pp. 1–15, 2020.

Pelly, J. L. and Hoskins, B. J.: A new perspective on blocking, Journal of the Atmospheric Sciences, 60, 743–755, 2003.

Petoukhov, V., Rahmstorf, S., Petri, S., and Schellnhuber, H. J.: Quasiresonant amplification of planetary waves and recent Northern Hemisphere weather extremes, Proceedings of the National Academy of Sciences, 110, 5336–5341, 2013.

Pfahl, S. and Wernli, H.: Quantifying the relevance of atmospheric blocking for co-located temperature extremes in the Northern Hemisphere on (sub-)daily time scales, Geophysical Research Letters, 39, 2012.

Photiadou, C. S., Weerts, A. H., and van den Hurk, B. J. J. M.: Evaluation of two precipitation data sets for the Rhine River using streamflow simulations, Hydrology and Earth System Sciences, 15, 3355–3366, 2011.

Pinto, J. G., Gómara, I., Masato, G., Dacre, H. F., Woollings, T., and Caballero, R.: Large-scale dynamics associated with clustering of extratropical cyclones affecting Western Europe, Journal of Geophysical Research: Atmospheres, 119, 13–704, 2014.

Poli, P., Hersbach, H., Dee, D. P., Berrisford, P., Simmons, A. J., Vitart, F., Laloyaux, P., Tan, D. G., Peubey, C., Thépaut, J.-N., et al.: ERA-20C: An atmospheric reanalysis of the twentieth century, Journal of Climate, 29, 4083–4097, 2016.

Prein, A., Gobiet, A., Suklitsch, M., Truhetz, H., Awan, N., Keuler, K., and Georgievski, G.: Added value of convection permitting seasonal simulations, Climate Dynamics, 41, 2655–2677, 2013.

Prein, A. F. and Gobiet, A.: Impacts of uncertainties in European gridded precipitation observations on regional climate analysis, International Journal of Climatology, 37, 305–327, 2017.

Prein, A. F., Liu, C., Ikeda, K., Bullock, R., Rasmussen, R. M., Holland, G. J., and Clark, M.: Simulating North American mesoscale convective systems with a convection-permitting climate model, Climate Dynamics, pp. 1–16, 2017.

Priestley, C. H. B. and Taylor, R.: On the assessment of surface heat flux and evaporation using large-scale parameters, Monthly Weather Review, 100, 81–92, 1972.

Puma, M. and Cook, B.: Effects of irrigation on global climate during the 20th century, Journal of Geophysical Research: Atmospheres, 115, 2010.

Ralph, F. and Dettinger, M.: Storms, floods, and the science of atmospheric rivers, Eos, Transactions American Geophysical Union, 92, 265–266, 2011.

Ralph, F. M., Neiman, P. J., and Wick, G. A.: Satellite and CALJET aircraft observations of atmospheric rivers over the eastern North Pacific Ocean during the winter of 1997/98, Mon. Wea. Rev., 132, 1721–1745, 2004.

Ralph, F. M., Neiman, P. J., Wick, G. A., Gutman, S. I., Dettinger, M. D., Cayan, D. R., and White, A. B.: Flooding on California's Russian River: Role of atmospheric rivers, Geophys. Res. Lett., 33, 2006.

Ralph, F. M., Neiman, P. J., Kiladis, G. N., Weickmann, K., and Reynolds, D. W.: A multi-scale observational case study of a Pacific atmospheric river exhibiting tropical-extratropical connections and a mesoscale frontal wave, Mon. Wea. Rev., 139, 1169–1189, 2010.

Ramos, A. M., Trigo, R. M., Liberato, M. L., and Tomé, R.: Daily precipitation extreme events in the Iberian Peninsula and its association with atmospheric rivers, Journal of Hydrometeorology, 16, 579–597, 2015.

Rex, D. F.: Blocking action in the middle troposphere and its effect upon regional climate, Tellus, 2,

275–301, 1950.

Richman, M. B.: Rotation of principal components, Journal of climatology, 6, 293–335, 1986.

Rogelj, J., Meinshausen, M., and Knutti, R.: Global warming under old and new scenarios using IPCC climate sensitivity range estimates, Nature Climate Change, 2, 248, 2012.

Rosner, B., Benedict, I., Van Heerwaarden, C., Weerts, A., Hazeleger, W., Bissoli, P., and Trachte, K.: Sidebar 7.3: The long heat wave and drought in Europe in 2018, in: State of the Climate in 2018, 100 (9), pp. S222–S223, Bull. Amer. Meteor. Soc., URL doi:10.1175/2019BAMSStateoftheClimate.1., 2019.

Roy, T., Martinez, J. A., Herrera-Estrada, J. E., Zhang, Y., Dominguez, F., Berg, A., Ek, M., and Wood, E. F.: Role of Moisture Transport and Recycling in Characterizing Droughts: Perspectives from Two Recent U.S. Droughts and the CFSv2 System, Journal of Hydrometeorology, 20, 139–154, 2018.

Rutz, J. J., Steenburgh, W. J., and Ralph, F. M.: Climatological characteristics of atmospheric rivers and their inland penetration over the western United States, Mon. Wea. Rev., 142, 905–921, 2014.

Samaniego, L., Kumar, R., and Attinger, S.: Multiscale parameter regionalization of a grid-based hydrologic model at the mesoscale, Water Resources Research, 46, 2010.

Scaife, A. A., Copsey, D., Gordon, C., Harris, C., Hinton, T., Keeley, S., O'Neill, A., Roberts, M., and Williams, K.: Improved Atlantic winter blocking in a climate model, Geophysical Research Letters, 38, 2011.

Schäfler, A., Craig, G., Wernli, H., Arbogast, P., Doyle, J. D., McTaggart-Cowan, R., Methven, J., Rivière, G., Ament, F., Boettcher, M., et al.: The North Atlantic waveguide and downstream impact experiment, Bulletin of the American Meteorological Society, 99, 1607–1637, 2018.

Schaller, N., Sillmann, J., Müller, M., Haarsma, R., Hazeleger, W., Hegdahl, T. J., Kelder, T., van den Oord, G., Weerts, A., and Whan, K.: The role of spatial and temporal model resolution in a flood event storyline approach in western Norway, Weather and Climate Extremes, p. 100259, 2020.

Schellekens, J.: wflow Documentation, 2012.

Schellekens, J., Dutra, E., Martínez-de la Torre, A., Balsamo, G., van Dijk, A., Sperna Weiland, F., Minvielle, M., Calvet, J.-C., Decharme, B., Eisner, S., Fink, G., Flörke, M., Peßenteiner, S., van Beek, R., Polcher, J., Beck, H., Orth, R., Calton, B., Burke, S., Dorigo, W., and Weedon, G. P.: A global water resources ensemble of hydrological models: the eartH2Observe Tier-1 dataset, Earth System Science Data Discussions, pp. 1–35, 2016.

Schiemann, R., Demory, M.-E., Shaffrey, L. C., Strachan, J., Vidale, P. L., Mizielinski, M. S., Roberts, M. J., Matsueda, M., Wehner, M. F., and Jung, T.: The Resolution Sensitivity of Northern Hemisphere Blocking in Four 25-km Atmospheric Global Circulation Models, Journal of Climate, 30, 337–358, 2016.

Schiemann, R., Vidale, P. L., Shaffrey, L. C., Johnson, S. J., Roberts, M. J., Demory, M.-E., Mizielinski, M. S., and Strachan, J.: Mean and extreme precipitation over European river basins better simulated in a 25km AGCM, Hydrology and Earth System Sciences, 22, 3933–3950, 2018.

Schiemann, R., Athanasiadis, P., Barriopedro, D., Doblas-Reyes, F., Lohmann, K., Roberts, M. J., Sein, D. V., Roberts, C. D., Terray, L., and Vidale, P. L.: Northern Hemisphere blocking simulation in current climate models: evaluating progress from the Climate Model Intercomparison Project Phase 5 to 6 and sensitivity to resolution, Weather and Climate Dynamics, 1, 277–292, 2020.

Schär, C. and Jendritzky, G.: Hot news from summer 2003, Nature, 432, 559–560, 2004.

Schär, C., Vidale, P. L., Lüthi, D., Frei, C., Häberli, C., Liniger, M. A., and Appenzeller, C.: The role of increasing temperature variability in European summer heatwaves, Nature, 427, 332–336, 2004.

Schumacher, D. L., Keune, J., Van Heerwaarden, C. C., de Arellano, J. V.-G., Teuling, A. J., and

Miralles, D. G.: Amplification of mega-heatwaves through heat torrents fuelled by upwind drought, Nature Geoscience, 12, 712–717, 2019.

Seager, R. and Henderson, N.: Diagnostic computation of moisture budgets in the ERA-Interim reanalysis with reference to analysis of CMIP-archived atmospheric model data, Journal of Climate, 26, 7876–7901, 2013.

Seager, R., Ting, M., Held, I., Kushnir, Y., Lu, J., Vecchi, G., Huang, H.-P., Harnik, N., Leetmaa, A., Lau, N.-C., et al.: Model projections of an imminent transition to a more arid climate in southwestern North America, Science, 316, 1181–1184, 2007.

Seager, R., Naik, N., and Vecchi, G. A.: Thermodynamic and dynamic mechanisms for large-scale changes in the hydrological cycle in response to global warming, Journal of Climate, 23, 4651–4668, 2010.

Seager, R., Ting, M., Li, C., Naik, N., Cook, B., Nakamura, J., and Liu, H.: Projections of declining surface-water availability for the southwestern United States, Nature Climate Change, 3, 482, 2013.

Seager, R., Neelin, D., Simpson, I., Liu, H., Henderson, N., Shaw, T., Kushnir, Y., Ting, M., and Cook, B.: Dynamical and thermodynamical causes of large-scale changes in the hydrological cycle over North America in response to global warming, Journal of Climate, 27, 7921–7948, 2014.

Seneviratne, S. I., Corti, T., Davin, E. L., Hirschi, M., Jaeger, E. B., Lehner, I., Orlowsky, B., and Teuling, A. J.: Investigating soil moisture–climate interactions in a changing climate: A review, Earth-Science Reviews, 99, 125–161, 2010.

Shabalova, M. V., Deursen, W. P. A. v., and Buishand, T. A.: Assessing future discharge of the river Rhine using regional climate model integrations and a hydrological model, Climate Research, 23, 233–246, 2003.

Shaffrey, L. C., Stevens, I., Norton, W., Roberts, M., Vidale, P.-L., Harle, J., Jrrar, A., Stevens, D., Woodage, M. J., Demory, M.-E., et al.: UK HiGEM: The new UK high-resolution global environment model— Model description and basic evaluation, Journal of Climate, 22, 1861–1896, 2009.

Shaw, T., Baldwin, M., Barnes, E. A., Caballero, R., Garfinkel, C., Hwang, Y.-T., Li, C., O'Gorman, P., Rivière, G., Simpson, I., et al.: Storm track processes and the opposing influences of climate change, Nature Geoscience, 9, 656–664, 2016.

Shepherd, T. G.: Atmospheric circulation as a source of uncertainty in climate change projections, Nature Geoscience, 7, 703–708, 2014.

Shepherd, T. G.: A Common Framework for Approaches to Extreme Event Attribution, Current Climate Change Reports, 2, 28–38, 2016.

Shepherd, T. G.: Storyline approach to the construction of regional climate change information, Proceedings of the Royal Society A, 475, 20190 013, 2019.

Shepherd, T. G., Boyd, E., Calel, R. A., Chapman, S. C., Dessai, S., Dima-West, I. M., Fowler, H. J., James, R., Maraun, D., Martius, O., et al.: Storylines: an alternative approach to representing uncertainty in physical aspects of climate change, Climatic Change, 151, 555–571, 2018.

Sillmann, J., Thorarinsdottir, T., Keenlyside, N., Schaller, N., Alexander, L. V., Hegerl, G., Seneviratne, S. I., Vautard, R., Zhang, X., and Zwiers, F. W.: Understanding, modeling and predicting weather and climate extremes: Challenges and opportunities, Weather and Climate Extremes, 18, 65–74, 2017.

Singh, H. K., Bitz, C. M., Donohoe, A., Nusbaumer, J., and Noone, D. C.: A mathematical framework for analysis of water tracers. Part II: Understanding large-scale perturbations in the hydrological cycle due to CO2 doubling, Journal of Climate, 29, 6765–6782, 2016.

Sodemann, H. and Stohl, A.: Moisture Origin and Meridional Transport in Atmospheric Rivers and Their Association with Multiple Cyclones, Mon. Wea. Rev., 141, 2850–2868, 2013.

Sodemann, H., Schwierz, C., and Wernli, H.: Interannual variability of Greenland winter precipitation sources: Lagrangian moisture diagnostic and North Atlantic Oscillation influence, Journal of Geophysical Research: Atmospheres, 113, 2008.

Spensberger, C., Madonna, E., Boettcher, M., Grams, C., Papritz, L., Quinting, J., Röthlisberger, M., Sprenger, M., and Zschenderlein, P.: Dynamics of concurrent and sequential Central European and Scandinavian heatwaves, Quarterly Journal of the Royal Meteorological Society, 2020.

Sterl, A., Severijns, C., Dijkstra, H., Hazeleger, W., van Oldenborgh, G. J., van den Broeke, M., Burgers, G., van den Hurk, B., van Leeuwen, P. J., and van Velthoven, P.: When can we expect extremely high surface temperatures?, Geophysical Research Letters, 35, 2008.

Stocker, T. F., Qin, D., Plattner, G.-K., Tignor, M., Allen, S. K., Boschung, J., Nauels, A., Xia, Y., Bex, V., Midgley, P. M., et al.: Climate change 2013: The physical science basis, Contribution of working group I to the fifth assessment report of the intergovernmental panel on climate change, 1535, 2013.

Stohl, A. and James, P.: A Lagrangian Analysis of the Atmospheric Branch of the Global Water Cycle. Part II: Moisture Transports between Earth's Ocean Basins and River Catchments, Journal of Hydrometeorology, 6, 961–984, 2005.

Stohl, A., Forster, C., and Sodemann, H.: Remote sources of water vapor forming precipitation on the Norwegian west coast at 60 N –a tale of hurricanes and an atmospheric river, J. Geophys. Res.: Atmospheres (1984–2012), 113, 2008.

Stojanovic, M., Drumond, A., Nieto, R., and Gimeno, L.: Anomalies in Moisture Supply during the 2003 Drought Event in Europe: A Lagrangian Analysis, Water, 10, 467, 2018.

Stott, P. A., Stone, D. A., and Allen, M. R.: Human contribution to the European heatwave of 2003, Nature, 432, 610–614, 2004.

Stott, P. A., Allen, M., Christidis, N., Dole, R. M., Hoerling, M., Huntingford, C., Pall, P., Perlwitz, J., and Stone, D.: Attribution of weather and climate-related events, in: Climate Science for Serving Society, pp. 307–337, Springer, 2013.

Strachan, J., Vidale, P. L., Hodges, K., Roberts, M., and Demory, M.-E.: Investigating global tropical cyclone activity with a hierarchy of AGCMs: The role of model resolution, Journal of Climate, 26, 133–152, 2013.

Sutanudjaja, E., Van Beek, L., Drost, N., de Graaf, I., De Jong, K., Peßenteiner, S., Straatsma, M., Wada, Y., Wanders, N., Wisser, D., and others: PCR-GLOBWB 2.0: A 5 arc-minute global hydrological and water resources model, Geoscientific Model Development, 11, 2429–2453, 2018.

Szczypta, C., Decharme, B., Carrer, D., Calvet, J.-C., Lafont, S., Somot, S., Faroux, S., and Martin, E.: Impact of precipitation and land biophysical variables on the simulated discharge of European and Mediterranean rivers, Hydrology and Earth System Sciences, 16, 3351–3370, 2012.

Takatama, K., Minobe, S., Inatsu, M., and Small, R. J.: Diagnostics for near-surface wind convergence/divergence response to the Gulf Stream in a regional atmospheric model, Atmospheric Science Letters, 13, 16–21, 2012.

Tang, Y., Winkler, J., Zhong, S., Bian, X., Doubler, D., Yu, L., and Walters, C.: Future changes in the climatology of the Great Plains low-level jet derived from fine resolution multi-model simulations, Scientific reports, 7, 1–10, 2017.

Taylor, C. M., de Jeu, R. A., Guichard, F., Harris, P. P., and Dorigo, W. A.: Afternoon rain more likely over drier soils, Nature, 489, 423, 2012a.

Taylor, K. E., Stouffer, R. J., and Meehl, G. A.: An overview of CMIP5 and the experiment design, Bulletin of the American Meteorological Society, 93, 485–498, 2012b.

Tebaldi, C. and Knutti, R.: The use of the multi-model ensemble in probabilistic climate projections, Philosophical transactions of the royal society A: mathematical, physical and engineering sciences, 365, 2053–2075, 2007.

Thiery, W., Visser, A. J., Fischer, E. M., Hauser, M., Hirsch, A. L., Lawrence, D. M., Lejeune, Q., Davin, E. L., and Seneviratne, S. I.: Warming of hot extremes alleviated by expanding irrigation, Nature communications, 11, 1–7, 2020.

Thorncroft, C., Hoskins, B., and McIntyre, M.: Two paradigms of baroclinic-wave life-cycle behaviour, Quart. J. Roy. Meteor. Soc., 119, 17–55, 1993.

Toreti, A., Belward, A., Perez-Dominguez, I., Naumann, G., Luterbacher, J., Cronie, O., Seguini, L., Manfron, G., Lopez-Lozano, R., Baruth, B., Berg, M. v. d., Dentener, F., Ceglar, A., Chatzopoulos, T., and Zampieri, M.: The Exceptional 2018 European Water Seesaw Calls for Action on Adaptation, Earth's Future, 7, 652–663, 2019.

Trenberth, K. E.: Climate diagnostics from global analyses: Conservation of mass in ECMWF analyses, Journal of Climate, 4, 707–722, 1991.

Trenberth, K. E.: Atmospheric Moisture Residence Times and Cycling: Implications for Rainfall Rates and Climate Change, Climatic Change, 39, 667–694, 1998.

Trenberth, K. E.: Changes in precipitation with climate change, Climate Research, 47, 123–138, 2011.

Trenberth, K. E., Dai, A., Rasmussen, R. M., and Parsons, D. B.: The changing character of precipitation, Bulletin of the American Meteorological Society, 84, 1205–1218, 2003.

Trenberth, K. E., Fasullo, J. T., and Mackaro, J.: Atmospheric moisture transports from ocean to land and global energy flows in reanalyses, Journal of Climate, 24, 4907–4924, 2011.

Trenberth, K. E., Dai, A., Van Der Schrier, G., Jones, P. D., Barichivich, J., Briffa, K. R., and Sheffield, J.: Global warming and changes in drought, Nature Climate Change, 4, 17–22, 2014.

Trenberth, K. E., Fasullo, J. T., and Shepherd, T. G.: Attribution of climate extreme events, Nature Climate Change, 5, 725–730, 2015.

Turco, M., Zollo, A., Ronchi, C., Luigi, C. D., and Mercogliano, P.: Assessing gridded observations for daily precipitation extremes in the Alps with a focus on northwest Italy, Natural Hazards and Earth System Sciences, 13, 1457–1468, 2013.

Ulbrich, U. and Fink, A.: The January 1995 flood in Germany: meteorological versus hydrological causes, Physics and Chemistry of the Earth, 20, 439–444, 1995.

Ummenhofer, C. C., Seo, H., Kwon, Y.-O., Parfitt, R., Brands, S., and Joyce, T. M.: Emerging European winter precipitation pattern linked to atmospheric circulation changes over the North Atlantic region in recent decades, Geophysical Research Letters, 44, 8557–8566, 2017.

Uvo, C. B.: Analysis and regionalization of northern European winter precipitation based on its relationship with the North Atlantic Oscillation, Int. J. Climatol., 23, 1185–1194, 2003.

Van den Hurk, B., Viterbo, P., Beljaars, A., and Betts, A.: Online validation of the ERA40 surface scheme, ECMWF Tech. Mem, 295, 42, 2000.

Van den Hurk, B. J., Viterbo, P., and Los, S. O.: Impact of leaf area index seasonality on the annual land surface evaporation in a global circulation model, Journal of Geophysical Research: Atmospheres, 108, 2003.

Van der Ent, R., Wang-Erlandsson, L., Keys, P. W., and Savenije, H.: Contrasting roles of interception and transpiration in the hydrological cycle–Part 2: Moisture recycling, Earth System Dynamics, 5, 471–489, 2014.

Van der Ent, R. J.: A new view on the hydrological cycle over continents, Ph.D. thesis, Delft University of Technology, Delft, doi: http://dx.doi.org/10.4233/uuid:0ab824ee-6956-4cc3-b530-3245ab4f32be, 2014.

Van der Ent, R. J. and Tuinenburg, O. A.: The residence time of water in the atmosphere revisited, Hydrology and Earth System Sciences, 21, 779–790, 2017.

Van der Ent, R. J., Savenije, H. H., Schaefli, B., and Steele-Dunne, S. C.: Origin and fate of atmospheric moisture over continents, Water Resources Research, 46, 2010.

Van der Ent, R. J., T. O. A. K. H.-R. K. H. and Savenije, H. H. G.: Should we use a simple or complex model for moisture recycling and atmospheric moisture tracking?, Hydrol. Earth Syst. Sci., 17, 4869-4884, https://doi.org/10.5194/hess-17-4869-2013, 2013.

van der Wiel, K., Kapnick, S. B., van Oldenborgh, G. J., Whan, K., Philip, S., Vecchi, G. A., Singh, R. K., Arrighi, J., and Cullen, H.: Rapid attribution of the August 2016 flood-inducing extreme precipitation in south Louisiana to climate change, Hydrol. Earth Syst. Sci. Discuss., 2016, 1–40, 2016a.

van der Wiel, K., Kapnick, S. B., Vecchi, G. A., Cooke, W. F., Delworth, T. L., Jia, L., Murakami, H., Underwood, S., and Zeng, F.: The Resolution Dependence of Contiguous U.S. Precipitation Extremes in Response to CO2 Forcing, Journal of Climate, 29, 7991–8012, 2016b.

Van der Wiel, K., Kapnick, S. B., Vecchi, G. A., Smith, J. A., Milly, P. C., and Jia, L.: 100-Year Lower Mississippi Floods in a Global Climate Model: Characteristics and Future Changes, Journal of Hydrometeorology, 19, 1547–1563, 2018.

Van der Wiel, K., Wanders, N., Selten, F., and Bierkens, M.: Added value of large ensemble simulations for assessing extreme river discharge in a 2C warmer world, Geophysical Research Letters, 46, 2093–2102, 2019.

Van Dijk, A.: The Australian water resources assessment system, Version 0.5, 3, 2010a.

Van Dijk, A.: Climate and terrain factors explaining streamflow response and recession in Axustralian catchments, Hydrology and Earth System Sciences, 14, 159, 2010b.

Van Dijk, A. and Renzullo, L. J.: Water resource monitoring systems and the role of satellite observations, Hydrology and Earth System Sciences, 15, 39–55, 2011.

Van Dijk, A. I. J. M.: AWRA Technical Report 3, Landscape Model (version 0.5) Technical Description, Tech. rep., WIRADA/CSIRO Water for a Healthy Country Flagship, Canberra, 2010c.

van Dijk, A. I. J. M., Peña-Arancibia, J. L., Wood, E. F., Sheffield, J., and Beck, H. E.: Global analysis of seasonal streamflow predictability using an ensemble prediction system and observations from 6192 small catchments worldwide: Global Analysis of Seasonal Streamflow Predictability, Water Resources Research, 49, 2729–2746, 2013.

van Haren, R., van Oldenborgh, G. J., Lenderink, G., and Hazeleger, W.: Evaluation of modeled changes in extreme precipitation in Europe and the Rhine basin, Environmental Research Letters, 8, 014 053, 2013.

Van Haren, R., Haarsma, R. J., Van Oldenborgh, G. J., and Hazeleger, W.: Resolution Dependence of European Precipitation in a State-of-the-Art Atmospheric General Circulation Model, Journal of Climate, 28, 5134–5149, 2015.

Van Heerwaarden, C. C., de Arellano, J. V.-G., and Teuling, A. J.: Land-atmosphere coupling explains the link between pan evaporation and actual evapotranspiration trends in a changing climate, Geophysical Research Letters, 37, 2010.

Van Oldenborgh, G. J., Drijfhout, S., van Ulden, A., Haarsma, R., Sterl, A., Severijns, C., Hazeleger, W., and Dijkstra, H.: Western Europe is warming much faster than expected, Clim. Past, p. 12, 2009.

Van Osnabrugge, B., Weerts, A., and Uijlenhoet, R.: genRE: A Method to Extend Gridded Precipitation

Climatology Data Sets in Near Real-Time for Hydrological Forecasting Purposes, Water Resources Research, 53, 9284–9303, 2017.

Van Vuuren, D. P., Edmonds, J., Kainuma, M., Riahi, K., Thomson, A., Hibbard, K., Hurtt, G. C., Kram, T., Krey, V., Lamarque, J.-F., et al.: The representative concentration pathways: an overview, Climatic Change, 109, 5, 2011.

Vannière, B., Demory, M.-E., Vidale, P. L., Schiemann, R., Roberts, M. J., Roberts, C. D., Matsueda, M., Terray, L., Koenigk, T., and Senan, R.: Multi-model evaluation of the sensitivity of the global energy budget and hydrological cycle to resolution, Climate Dynamics, 52, 6817–6846, 2018.

Viterbo, P. and Beljaars, A. C. M.: An Improved Land Surface Parameterization Scheme in the ECMWF Model and Its Validation, Journal of Climate, 8, 2716–2748, 1995.

Vogel, M. M., Zscheischler, J., Wartenburger, R., Dee, D., and Seneviratne, S. I.: Concurrent 2018 Hot Extremes Across Northern Hemisphere Due to Human-Induced Climate Change, Earth's Future, 7, 692–703, 2019.

Wang, K. and Dickinson, R. E.: A review of global terrestrial evapotranspiration: Observation, modeling, climatology, and climatic variability, Reviews of Geophysics, 50, 2012.

Wang-Erlandsson, L., Bastiaanssen, W. G., Gao, H., Jagermeyr, J., Senay, G. B., Van Dijk, A., Guerschman, J. P., Keys, P. W., Gordon, L. J., and Savenije, H. H.: Global root zone storage capacity from satellite-based evaporation, Hydrol. Earth Syst. Sci., 20, 1459–1481, 2016.

Wehner, M. F., Smith, R. L., Bala, G., and Duffy, P.: The effect of horizontal resolution on simulation of very extreme US precipitation events in a global atmosphere model, Climate Dynamics, 34, 241–247, 2010.

Wehrli, K., Guillod, B. P., Hauser, M., Leclair, M., and Seneviratne, S. I.: Identifying Key Driving Processes of Major Recent Heat Waves, Journal of Geophysical Research: Atmospheres, 124, 11 746–11 765, 2019.

Wehrli, K., Hauser, M., and Seneviratne, S. I.: Storylines of the 2018 Northern Hemisphere heat wave at pre-industrial and higher global warming levels, Earth Syst. Dynam. Discuss., 2020.

Weijenborg, C. and Spengler, T.: Diabatic heating as a pathway for cyclone clustering encompassing the extreme storm Dagmar, Geophysical Research Letters, 47, e2019GL085 777, 2020.

Wernli, H.: A Lagrangian-based analysis of extratropical cyclones. II: A detailed case-study, Quarterly Journal of the Royal Meteorological Society, 123, 1677–1706, 1997.

Whan, K., Sillmann, J., Schaller, N., and Haarsma, R.: Future changes in atmospheric rivers and extreme precipitation in Norway, Climate Dynamics, 54, 2071–2084, 2020.

Wick, G. A., Neiman, P. J., Ralph, F. M., and Hamill, T. M.: Evaluation of forecasts of the water vapor signature of atmospheric rivers in operational numerical weather prediction models, Wea. Forecasting, 28, 1337–1352, 2013.

Wood, A. W., Leung, L. R., Sridhar, V., and Lettenmaier, D.: Hydrologic implications of dynamical and statistical approaches to downscaling climate model outputs, Climatic Change, 62, 189–216, 2004.

Wood, E. F., Roundy, J. K., Troy, T. J., van Beek, L. P. H., Bierkens, M. F. P., Blyth, E., de Roo, A., Döll, P., Ek, M., Famiglietti, J., Gochis, D., van de Giesen, N., Houser, P., Jaffé, P. R., Kollet, S., Lehner, B., Lettenmaier, D. P., Peters-Lidard, C., Sivapalan, M., Sheffield, J., Wade, A., and Whitehead, P.: Hyperresolution global land surface modeling: Meeting a grand challenge for monitoring Earth's terrestrial water, Water Resources Research, 47, 2011.

Woollings, T.: Dynamical influences on European climate: an uncertain future, Philosophical Transactions of the Royal Society A: Mathematical, Physical and Engineering Sciences, 368, 3733–3756,

2010.

Zangvil, A., Portis, D. H., and Lamb, P. J.: Investigation of the Large-Scale Atmospheric Moisture Field over the Midwestern United States in relation to Summer Precipitation. Part I: Relationships between Moisture Budget Components on Different Timescales, Journal of Climate, 14, 582–597, 2001.

Zangvil, A., Portis, D. H., and Lamb, P. J.: Investigation of the Large-Scale Atmospheric Moisture Field over the Midwestern United States in Relation to Summer Precipitation. Part II: Recycling of Local Evapotranspiration and Association with Soil Moisture and Crop Yields, Journal of Climate, 17, 3283–3301, 2004.

Zappa, G. and Shepherd, T. G.: Storylines of atmospheric circulation change for European regional climate impact assessment, Journal of Climate, 30, 6561–6577, 2017.

Zappa, G., Shaffrey, L. C., Hodges, K. I., Sansom, P. G., and Stephenson, D. B.: A multimodel assessment of future projections of North Atlantic and European extratropical cyclones in the CMIP5 climate models, Journal of Climate, 26, 5846–5862, 2013.

Zhu, Y. and Newell, R. E.: A proposed algorithm for moisture fluxes from atmospheric rivers, Monthly Weather Review, 126, 725–735, 1998.

Dankwoord

"Werken en feesten vormt schoone geesten"
- motto Johanna Westerdijk (eerste vrouwelijke hoogleraar in Nederland)

De afgelopen jaren heb ik met veel plezier en vrijheid onderzoek kunnen doen en daar is deze thesis het resultaat van. Betaald krijgen om een boekje te maken over iets wat je interessant vindt is best wel cool, en mede mogelijk gemaakt door een fijn begeleidingsteam en een goede werksfeer op de vakgroep. Als sociaal persoon is het soms ook best pittig om in je eentje aan een project te werken, en ik ben blij dat ik de nodige afleiding heb gehad door onderwijs, maar ook door mijn leuke leven buiten werk. Iedereen die daar aan heeft bijgedragen (en bijdraagt), zowel aan het 'werken' als aan het 'feesten', wil ik graag bedanken!

Tijdens mijn sollicitatie was mijn belangrijkste vraag wie mij van dag tot dag zou begeleiden, en ik had het niet beter kunnen treffen dan met jou Chiel! Naast de enorme inhoudelijke en technische hulp, wist je ook op de goede momenten een keer extra te vragen hoe het ging. De 'Atmospheric Dynamics'-maanden november en december waren hectisch, maar vooral heel leuk. Bedankt voor het vertrouwen om mij gewoon voor de klas te zetten. Ik hoop (en weet) dat ik voor tips, of gewoon een praatje, bij je binnen kan blijven lopen. Daarnaast had ik twee promotors van verschillende vakgroepen, die met enige (on)regelmaat in Wageningen waren. Dit klinkt misschien als een ingewikkelde constructie, maar zo heb ik het bijna nooit ervaren. Bedankt Wilco, voor het bewaren van overzicht en de sturing, en dat je regelde dat ik een dag per week op het KNMI kon zitten. Bedankt Albrecht, voor je nuchterheid, door jou heeft dit boekje een duidelijke structuur, en elk hoofdstuk een experimentele set-up. De eerste zin van dit proefschrift (heb je 'm al gelezen?) bevat de woorden *weather*, *water* en *climate*. Chiel, Albrecht en Wilco, het was een luxe om zoveel kennis bij elkaar te hebben. Daarnaast heeft het feit dat jullie nooit je eigen onderwerp hebben gepusht, maar wel altijd betrokken waren, ervoor gezorgd dat ik mijn PhD onderzoek een eigen draai kon geven en met veel plezier kon uitvoeren. Ik vind het jammer dat de vrijdag meetings nu verleden tijd zijn.

Ola Jordi, thanks for introducing me to science during my BSc thesis and never losing interest. I really enjoy all chats, coffees and dinners with you (when is the next canoe tour?). Bedankt Kees voor alle technische hulp in het begin, de secretaresses voor de administratie, en Gert-Jan voor het onwijs snel beantwoorden van al mijn vragen over onderwijs in het laatste jaar. Ik wil ook graag mijn co-auteurs Eveline en Ruud bedanken voor de leuke samenwerking. Thanks to Karianne, Rich and Thomas for the work on Chapter 3. It was not easy to finish the work with a distance, but I am very proud that we made it.

Dank aan de studenten die ik kon begeleiden met hun thesis, of die op een andere manier zorg(d)en voor een dynamische werksfeer, door jullie is het werken op de universiteit zo leuk! I also like to take the opportunity here to be thankful for the organisation of summer schools, workshops and conferences that I was able to attend. Learning from peers, and getting a broader perspective on your field of research in a dynamic setting at a nice location, were for me the most joyfull experiences during my PhD.

When working from home, it becomes even more clear how valuable a good working atmosphere and nice colleagues are. Thanks to everyone at MAQ for the chats over coffee, lunch or at other circumstances. Special thanks to all PhDs for creating good vibes, and helping me out with my random questions I regularly disturbed you with. Special thanks to Peter for the nice chats, and commenting all my figures when you passed by my screen. Thanks to Aris, Auke and Sony for the tennis. 'Work' and 'party' can also be a good combination as shown by Anja, Alba, Stijn, Xabi and more. Thanks for all the good times during dinners and drinks outside work, I hope they will continue! Also a shout out to the inspiring ladies in room A.113, in which I am sure more good office time will follow. Bedankt Anna-Lena, voor de gezelligheid op het KNMI. Ik wil ook de andere KNMI'ers (Karin, Emma, Folmer en meer) bedanken voor de interesse en gezelligheid als ik er was.

Tien jaar geleden begon mijn studententijd in Wageningen, waar ik naast een top studie en studententijd vooral heel veel leuke mensen heb ontmoet. Meiden van de studie, jullie zijn stuk voor stuk stoer en intelligent. Het was fijn om PhD-zaken met jullie te delen, maar het is nog veel fijner om met jullie op pad te zijn. Dat er nog maar veel gezamenlijke activiteiten mogen volgen! Bedankt Merel en Anne dat jullie mijn paranimfen zijn. Vivien, Mirthe, Ileen, Dorith; bedankt voor de gezelligheid in Utrecht, en jullie support. Daarvoor ook dank aan Sieg, Bar, Sol en de andere meiden van FV. En dan nog de meiden die mij al het langst kennen, en waarschijnlijk het minst goed weten wat ik doe. Bilouten, met jullie is het altijd weer goed. Ik vind het heerlijk om vriendinnen te hebben die met zoveel diverse dingen bezig zijn.

Dan als laatste mijn familie, en vooral papa en mama, bedankt voor alle goede zorgen! Bente, je bent een echte 'voorbeeld'-zus, iets waar ik vroeger misschien niet altijd blij mee was, maar nu alleen maar heel trots op ben. Paul, het leven met jou is fijn en leuk, en daar ben ik je heel dankbaar voor. Dat we nog maar veel mogen meemaken samen!

Imme
Utrecht, September 2020

About the author

"If you want to master something, teach it"
- Richard Feynman

This quote very much relates to my vision, and favorite way of working. You can read as many papers as you want, but at the end only if you talk about, or teach a topic to another you will really learn it, especially if it is on a topic of your interest. Besides, teaching provides interaction, which I really enjoy.
I started studying Soil, Water and Atmosphere in 2010 in Wageningen, driven by my interest in geography and physics. During my bachelor I followed courses at the University of Utrecht to learn more on ocean dynamics and river morphology. As I mostly enjoyed the topics of meteorology and hydrology, I continued with the Master Earth and Environment in these directions. In autumn 2013, I went for a semester abroad to follow courses on meteorology and oceanography at the Geophysical Institute of the University of Bergen. My master thesis work was conducted at Deltares in Delft, where I studied the impact of a changing climate on river discharge. During my studies I worked as student assistant for the Meteorology and Air Quality group, developing teaching material and assisting with courses. For my internship I went back to Norway, studying extreme precipitation along the Norwegian coast (see Chapter 3), although located inland at the Meteorological Institute in Oslo. In April 2016 I continued working on the topics of hydrology, large-scale meteorology and climate by starting the PhD project presented in this thesis. During my PhD I assisted with the course Atmospheric Dynamics, and lectured in the course Introduction Atmosphere. I continue my interest in education with a lecturer position at the Meteorology and Air Quality group in Wageningen.


Imme with the Rhine and Mississippi Rivers.

List of publications

Benedict, I., Ødemark, K., Nipen, T., and Moore, R.: Large-scale flow patterns associated with extreme precipitation and atmospheric rivers over Norway, Monthly Weather Review, 147, 1415–1428, 2019a

Benedict, I., van Heerwaarden, C. C., Weerts, A. H., and Hazeleger, W.: The benefits of spatial resolution increase in global simulations of the hydrological cycle evaluated for the Rhine and Mississippi basins, Hydrol. Earth Syst. Sci., 23, 1779–1800, 2019b

Benedict, I., van Heerwaarden, C. C., van der Ent, R. J., Weerts, A. H., and Hazeleger, W.: Decline in Terrestrial Moisture Sources of the Mississippi River Basin in a Future Climate, Journal of Hydrometeorology, 21, 299–316, 2020

Benedict, I., van Heerwaarden, C. C., Van der Linden, E. C., Weerts, A. H., & Hazeleger, W.: Anomalous moisture sources of the Rhine basin during the extremely dry summers of 2003 and 2018, *Under review.*

Rosner, B., Benedict, I., Van Heerwaarden, C., Weerts, A., Hazeleger, W., Bissoli, P., and Trachte, K.: Sidebar 7.3: The long heat wave and drought in Europe in 2018, in: State of the Climate in 2018, 100 (9), pp. S222-S223, Bull. Amer. Meteor. Soc.

Van Heerwaarden, C. C., Mol, W.B., Veerman, M.A., Benedict, I., Heusinkveld, B.G., Knap. W.H., Kazadzis, S., Kouremeti, N. & Fiedler, S.: COVID-19 lockdown contribution to spring surface solar irradiance record in Western Europe, *Under review*, *preprint available at:* https://arxiv.org/pdf/2008.13497.pdf.

Van Galen, L., Hartogensis, O.K., Benedict, I., Steeneveld, G.J., Teaching Weather Forecasting Class in the 2020s, *To be submitted.*

Netherlands Research School for the
Socio-Economic and Natural Sciences of the Environment

D I P L O M A

for specialised PhD training

The Netherlands research school for the
Socio-Economic and Natural Sciences of the Environment
(SENSE) declares that

Imme Bo Benedict

born on 26 August 1992, in Breda, The Netherlands

has successfully fulfilled all requirements of the
educational PhD programme of SENSE.

Wageningen, 20 November 2020

Chair of the SENSE board

Prof. dr. Martin Wassen

The SENSE Director

Prof. Philipp Pattberg

The SENSE Research School has been accredited by the Royal Netherlands Academy of Arts and Sciences (KNAW)

KONINKLIJKE NEDERLANDSE
AKADEMIE VAN WETENSCHAPPEN

The SENSE Research School declares that **Imme Bo Benedict** has successfully fulfilled all requirements of the educational PhD programme of SENSE with a work load of 42.2 EC, including the following activities:

SENSE PhD Courses

- Environmental research in context (2016)
- Research in context activity: 'Organising workshop for stakeholders and presenting my research at a WUR alumni event, and on the yearly organised Deltacongres' (2016-2020)

Other PhD and Advanced MSc Course

- 16th Swiss Climate Summer School "High-resolution climate: observations, models and projections", Center for Climate Systems Modeling (2017)
- Parametrization of subgrid physical processes, ECMWF, United Kingdom (2018)
- Towards regional information to improve our understanding on weather, water, and climate extreme events, YESS-YHS Early Career Researcher Workshop, Canmore (2018)
- Advanced Climate Dynamics Course "The Anthropocene", University of Bergen (2019)
- Scientific writing , Wageningen Graduate Schools (2016)
- Exploring teaching outside academia, Wageningen Graduate Schools (2017)
- Teaching and supervising Thesis students, Wageningen Graduate Schools (2017)
- Brain training, Wageningen Graduate Schools (2018)
- Brain based teaching, Wageningen University (2018)

Management and Didactic Skills Training

- Supervising two BSc student with thesis (2017)
- Supervising two MSc students with thesis (2018-2019)
- Assisting in MSc course 'Atmospheric Dynamics' (2017-2019)
- Lecturing in the BSc course 'Introduction Atmosphere' (2018-2020)

Oral Presentations

- **Invited talk**: *Atmospheric rivers, large scale pre-conditioning and extreme precipitation over Norway*. Norwegian Meteorological Institute, 20 September 2016, Oslo, Norway
- *Evaluating the importance of horizontal resolution in global climate and hydrological models for the Rhine and Mississippi.* EGU, 24-28 April 2017, Vienna, Austria
- ***Invited talk**: Understanding Mississippi's moisture sources in present and future climate.* Deltares, 18 March 2019, Delft, The Netherlands
- *Mississippi's moisture sources shift from land to ocean in a future climate*. EGU, 7-12 April 2019, Vienna, Austria

SENSE coordinator PhD education

Dr. ir. Peter Vermeulen

This research received funding from the Netherlands Organization for Scientific Research (NWO) for project 869.15.004.

Financial support from Wageningen University for printing this thesis is gratefully acknowledged.

Cover design by Imme Bo Benedict and ProefschriftMaken
Shading shows specific humidity at 850 hPa from ERA5 re-analysis data at 14th of September 2005 07:00.

Thesis printed by ProefschriftMaken